



**UNIVERSITE DE CERGY-PONTOISE**  
**ECOLE DOCTORALE : SCIENCES ET INGENIERIE**  
**Spécialité : Sciences de la Terre et de l'univers**

# **THESE**

Présentée pour l'obtention du grade de

**Docteur Co-tutelle de l'université de Cergy-Pontoise  
et National Taiwan University**

par

**Yu-Min CHOU**

**MINÉRALOGIE ET PROPRIÉTÉS MAGNÉTIQUES DE LA ZONE  
DE GLISSEMENT DU SÉISME DE CHI-CHI, 1999 ( $M_w$  7,6)  
ET LEURS IMPLICATIONS**

Thèse réalisée à National Taiwan University et à l'Université Cergy-Pontoise  
Soutenue le vendredi 14 Decembre 2012 devant le jury composé de :

|                 |  |                      |
|-----------------|--|----------------------|
| Eric FERRÉ      | Pr. South Illinois University, USA                         | Rapporteur           |
| Kuo-Fong MA     | Pr. National Central University, Taiwan                    | Rapporteur           |
| Teh-Quei LEE    | Dr. Academia Sinica, Taiwan                                | Examineur            |
| Yen-Fang SONG   | Dr. National Synchrotron Radiation Research Center, Taiwan | Examineur            |
| Chao-Song LIN   | Pr. National Taiwan University, Taiwan                     | Examineur            |
| Christian DAVID | Pr. Université Cergy-Pontoise                              | Examineur            |
| Charles AUBOURG | Pr. Université de Pau et des Pays de l'Adour               | CoDirecteur de thèse |
| Sheng-Rong SONG | Pr. National Taiwan University, Taiwan                     | CoDirecteur de thèse |

# 國立臺灣大學博士學位論文

## 口試委員會審定書

### 1999 集集地震( $M_w$ 7.6)滑動帶礦物學與 磁學性質之研究與應用

### Mineralogy and Magnetic Properties of the 1999 Chi-Chi Earthquake ( $M_w$ 7.6) Slip Zone and their Implications

本論文係周祐民君 (D95224003) 在國立臺灣大學地質科學系、所完成之博士學位論文，於民國 101 年 12 月 14 日承下列考試委員審查通過及口試及格，特此證明

口試委員：



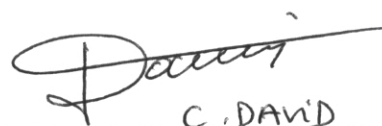
(簽名)

(指導教授)



ERIC C. FERRE

宋艷芳



C. DAVID

林柏松





## Acknowledgement

In first, I would like to thank God. He created this beautiful Earth, which is complex and mysterious for human to understand. We are infinitesimal in this universe!

In my life, I have to thank my parents! They support and encourage me to pursue my dream, let me finish my PhD degree without disturbance. I LOVE YOU!

I would like to thank Pr. Sheng-Rong Song and Pr. Charles Aubourg as my co-supervisors. They gave me a right direction and a lot of suggestions for my research.

I also thank Pr. Kuo-Fong Ma and Pr. Eric Ferré as my reporters of thesis, Pr. Christian David, Dr. The-Quei Lee, Dr. Yen-Fang Song, and Pr. Chao-Song Lin as juries of defense. I thank Pr. Anne-Marie Boullier, Pr. En-Chao Yeh, Pr. Ming-Kuan Wang, Pr. Jean-Pierre Pozzi, Dr. France Lagroix, Pr. Laurent Louis, Dr. Fabien Humbert, Dr. Li-Wei Kuo, Dr. Tung-Ming Tsao, Dr. Chun-Jay Wang, Mr. Chao-Chi Chen, Mr. Kung-Chen Yeh, and Mr. Yi-Ming Chen helped me to accomplish my lab measurements and thesis writing. I would like to thank all the members in Pr. Song's laboratory and the members in Cergy. Thanks for accompany with me during the long trip of PhD study.

The National Science Council of Taiwan under grants NSC 96-2627-M-002-011 and NSC 97- 2627-M-213-001 with a TEC contribution number supported this research. Eiffel excellence scholarship program (EGIDE, France) and the Graduate Student Study Abroad Program (NSC, Taiwan) also supported me for my finance in France.

## 致謝

首先我要感謝上帝創造了這個美麗的地球，在世界上有太多奧秘是人類永遠無法瞭解的，越深入科學研究越感受到人類的渺小。

在這六年半的博士求學期間，首先我要感謝父母給與我的支持與包容，讓我能夠無後顧之憂完成研究，也完成了許多的夢想！我愛你們！

能夠完成這本不算太薄論文，最需要感謝宋聖榮教授的指導，給我一個這麼好的研究題目，在整個研究過程中研究方向討論、儀器使用、經費支與內容修改，更重要的是引領我申請法國政府提供的艾菲爾雙博士學位獎學金與國科會博士千里馬計畫，使我能到法國賽吉蓬圖瓦茲大學進行研究兩年攻讀雙博士學位，也感謝 Charles Aubourg 教授共同指導我的博士論文，讓我學到許多研究方法與邏

輯思考，打開我許多眼界，接觸到法國博士生與教授間亦師亦友的關係，帶我融入法國文化。

感謝中研院李德貴老師從我大四進古地磁實驗室，十多年來永遠很有耐心地教導我，除了在學術研究外，也很關心我的未來規劃，畢業前沒有讓老師失望找到女朋友！感謝慈祥的 Anne-Marie Boullier 教授與其丈夫 Jimmy 在法國對我的照顧，研究上給我許多重要意見與經費支持。感謝同步輻射中心宋艷芳博士、台大農化系王明光教授與台大材料所林招松教授擔任我的論文指導委員，給予我論文許多建議。感謝中央大學地科系馬國鳳教授擔任我論文審查委員，給我許多建議。感謝賽吉蓬圖瓦茲大學 Christian David 教授在法國給予我許多幫助，特地來台灣擔任我的口試委員。感謝美國南伊利諾大學地質系 Eric Ferré 教授特地擔任我的口試委員，給我在斷層磁學研究上許多精闢的建議。感謝葉恩肇學長，在 TCDP 計畫與斷層研究上的帶領與討論，協助我進行採樣。感謝農化系曹崇銘博士帶領我作實驗，給我許多鼓勵。感謝中研院助理陳朝志在古地磁實驗室十多年來協助我測量打拼！感謝中研院助理葉光晟協助我切樣品，以及打羽球兼人生顧問。感謝 IPGP 磁學實驗室 France Lagroix 博士在 MPMS 量測給我許多幫助。感謝同步輻射中心陳一銘先生與王俊杰博士，在 TXM 實驗給我許多的幫助。感謝台大材料系陳輔澤博士在 TEM 實驗的幫助。感謝 Laurent Louis 博士在研究與生活上給我很多的幫助。感謝 Fabien Humbert 博士一起在法國打拼我們的博士論文！

在法國感謝最要感謝我的叔叔鄧柄權給我的照顧，讓我更瞭解法國文化。感謝彩霞姐與老克，讓我認識了主耶穌，成為我一生最大的祝福。感謝陪我兩年到處奔馳的小紅 Opel Corsa 1.5 TD，每天順暢地載我到學校，免去風吹雨打日曬外加罷工誤點跳軌施工髒亂的 SNCF RER A 線。感謝 Rueil-Malmaison 音樂院 André Gilbert 教授耐心地指導我上低音號演奏，我出差時還叮嚀我要帶樂器去練(雖然都沒帶過)，並獲得業餘演奏文憑，感謝 Savigny-sur-Orge 音樂院校長 Gérard Léclerc 校長讓我加入管樂團，給我音樂會獨奏的機會。也感謝在拉威爾音樂宿舍一起快樂生活的朋友們，彥傑、邦豪、子傑、左興、慧豐、威廷、海婷、愉諄、奕如、品輝....等人，讓我的生活多采多姿！感謝松山教會這個大家庭，牧師、師母、信怡阿姊、瓊瑤姐、莉敏姐、貴恆哥、伶智姐、我的好弟兄冠冠、撒母耳小組的組員們....等人族繁不及被載給我的許多禱告與祝福！

感謝研究室的力維學長、小 P 學姊、一起打拼的昱銘、詠忠、艾琦、聖元、黃琳、乙嘉、佩竹、琇錦、峻鳴、玉嵐、浩渝、斑斑、春妤、頭大、小黃、幃幃、衡之的參與及各種幫助陪伴。

最後要感謝佳穎，在我論文最後衝刺的一年，給我許多支持鼓勵與禱告！還與佳恬&媽咪全家一起熬夜幾天製作口試的卡片～！給我完成學業邁向人生新開始的強大動力！呱呱呱！

## 中文摘要

當地震發生時，斷層泥中之主要滑動面產生物理與化學轉變，導致斷層泥中之礦物發生礦物相改變與新礦物生成。斷層泥中含有磁性礦物，可經由斷層滑動產生之摩擦熱與液體的作用而生成。因此在地震發生的過程中，斷層泥具有獲得磁性紀錄的能力，可用來作為判定地震滑動帶的工具。此外經由分析受地震作用而改變與新生成的磁性礦物，可進一步回推地震時斷層泥中之物理與化學變化過程。

本研究利用台灣車籠埔斷層深鑽計劃中 B 井所連續取得之岩芯樣品，包含 1999 年規模 7.6 集集地震之車籠埔斷層主要滑動帶斷層泥，進行岩石磁學與古地磁學研究分析。此外本研究亦採集車籠埔斷層地表破裂帶之斷層泥進行奈米粒子分析。

本論文第一部份利用古地磁學方法分析指出，深度 1,136 公尺斷層帶(亦稱 FZB1136)之斷層泥之古地磁記錄方向與現今地磁場方向相符，而其他斷層帶與圍岩之記錄不符，判斷 FZB1136 為集集地震主要滑動帶，此外由岩石磁學結果，可指出集集地震在此斷層泥中主要滑動面之位置。此斷層泥中獲得殘磁記錄之主要磁性礦物為磁鐵礦與針鐵礦，磁鐵礦主要分佈於主要滑動面，而針鐵礦分佈於整個斷層泥之中。本研究提出一斷層泥在地震過程中重新磁化模式：(一) 殘磁記錄在地震間隔時期保存 (二) 地震時殘磁記錄消失 (三) 在地震之後斷層泥中液體冷卻過程中獲得地磁場記錄。

本論文第二部份，利用顯微觀察與岩石磁學方法，分析 FZB1136 斷層帶和錦水頁岩中黃鐵礦與磁性礦物之關係。錦水頁岩中可發現許多微球狀黃鐵礦與自形黃鐵礦，磁性礦物以磁鐵礦、硫複鐵礦與細顆粒磁黃鐵礦為主。在斷層泥中黃鐵礦數量較圍岩減少許多，主要磁性礦物為針鐵礦、磁黃鐵礦與部份氧化磁鐵礦。此三種磁性礦物為地震後所新生成，磁硫鐵礦成因可能為黃鐵礦在多次地震過程中，受摩擦熱高溫（溫度高於攝氏五百度）分解形成。針鐵礦成因推論因為集集地震後，造成之熱液（溫度高於攝氏三百五十度）於降溫過程中所形成，此熱液亦可解釋磁鐵礦部份氧化與磁黃鐵礦逆轉化為黃鐵礦之成因。這些新生成之磁性礦物可提供研究沈積岩中斷層帶，於地震過程產生物理化學變化之指標。

本論文第三部份，分析 FZB1136 斷層帶之磁學參數，可觀察到斷層帶中之磁感率最高值與等溫殘磁最高值，具有約四公分之偏移，磁感率最高值位於主要滑動面，而等溫殘磁最高值則位於斷層帶中央。然而此兩磁性參數皆為磁性礦物豐度指標，斷層帶中主要磁性礦物為針鐵礦與磁鐵礦，此兩礦物之磁學特性不同

且分佈範圍不同，可能為造成此兩磁性豐度參數偏移之原因。本研究利用針鐵礦與磁鐵礦分佈模型，利用其磁學特性參數不同，模擬計算斷層帶之磁感率與等溫殘磁分佈曲線，此模式計算出磁鐵礦在主要滑動面的最大豐度值約為 300 ppmv，而針鐵礦在斷層帶中央最大豐度約為 1%。

本論文第四部份，為判斷地震斷層滑動摩擦造成斷層泥粒子破裂之最小粒徑，用以協助斷層滑動破裂能估算，本研究採樣集集地震車籠埔斷層地表破裂面斷層泥，分離不同顆粒大小粒子至奈米粒徑，使用同步輻射 X-光粉末繞射儀與穿透式電子顯微鏡進行分析觀察礦物相與產狀。斷層泥主要礦物成份為石英、長石、澎潤石、伊萊石、綠泥石與高嶺石，而粒徑小於 100 奈米之粒子礦物組成為石英、澎潤石與伊萊石，然而在粒徑 1 至 25 奈米之粒子無石英存在，只含有澎潤石與伊萊石。澎潤石與伊萊石在此露頭環境條件下易風化新生成，石英則為穩定不易改變，因此石英可作為地震摩擦破碎指標，此斷層泥中破裂能估算之最小粒徑可至約 25 奈米。

本論文第五部份，為 FZB1194 與 FZB1243 兩斷層帶之磁學分析初步結果。此兩斷層帶中各含有一層黑色硬質塊，然而在 FZB1136 中並不含此層。此兩斷層帶之古地磁學記錄，皆具有一磁極正向與反向記錄，然而殘磁是由許多分向量所重疊構成，無法完全的分離每個分向量。反向磁極記錄成因有幾個可能性：(一) 車籠埔斷層帶活動年代早於 78 萬年 (二) 地震發生在古地磁場漂移期 (三) 磁性礦物殘磁自反轉；未來需更進一步研究確定成因。由此兩斷層帶磁學參數分析結果中，可觀察到與 FZB1136 相同之磁感率最高值與等溫殘磁最高值偏移現象，顯示在此兩斷層帶中亦有不同磁性礦物豐度分佈變化。此兩斷層帶中主要磁性礦物種類為磁鐵礦與針鐵礦，然而與 FZB1136 具有幾點不同：(一) 斷層泥中無單一分向量古地磁記錄 (二) 此兩斷層帶中存有超順磁性磁性顆粒存在 (三) 此兩斷層帶僅有部份 FZB1243 含有磁黃鐵礦。由這些現象顯示，此兩斷層帶所記錄之地震規模可能小於 FZB1136 所記錄之地震規模 7.6 集集地震。

關鍵字：車籠埔斷層、集集地震、車籠埔斷層深鑽計劃、岩石磁學、磁性礦物、磁鐵礦、磁黃鐵礦、針鐵礦、奈米粒子、石英

## Résumé

Lors d'un tremblement de terre, les transformations physiques et chimiques qui surviennent le long d'une zone de glissement vont conduire à l'altération et à la formation de minéraux. Les zones de glissement sismique contiennent des minéraux ferromagnétiques, qui peuvent être hérités ou bien formés sous l'action combinée de la chaleur frictionnelle et par l'action chimique des fluides. Ainsi, la gouge a le potentiel d'enregistrer le champ magnétique local pendant un tremblement de terre. Il s'agit là d'une nouvelle méthode pour identifier les zones de glissement de tremblements de terre. En outre, les minéraux magnétiques initiaux, altérés, et néoformés peuvent être utilisés comme traceurs de certains processus physico-chimiques répétitifs.

Dans cette étude, nous étudions le magnétisme des roches et l'enregistrement paléomagnétique de la gouge de faille active de Chelungpu qui contient, entre autres, la principale zone de glissement du tremblement de terre de Chi-Chi ( $M_w$  7.6, 1999, Taiwan). Nous avons bénéficié pour cette étude d'échantillons non altérés provenant des carottes du forage B Taiwan Chelungpu-Fault Drilling Project (TCDP). Nous avons également échantillonné la faille de Chelungpu à l'affleurement pour une caractérisation des nanoparticules. Cette caractérisation vise à estimer l'énergie de fracture dans la gouge de faille.

Dans la première partie de cette thèse, nous étudions l'enregistrement paléomagnétique dans les zones de gouges, dont la gouge de 0.16 m d'épaisseur portant la zone de glissement sismique de Chi-Chi à 1,136 m de profondeur (étiqueté FZB1136). Les paramètres magnétiques ont permis de localiser précisément la zone de glissement sismique de Chi-Chi. Une composante parallèle au dipôle magnétique moderne du champ magnétique terrestre est identifiée dans FZB1136 mais pas dans les roches encaissantes, ni dans les deux autres zones de failles adjacentes. L'enregistrement de cette composante est porté essentiellement par deux minéraux magnétiques; la magnétite dans la zone de glissement principale, et la goethite néoformée ailleurs dans la gouge. Nous suggérons que l'identification d'un enregistrement magnétique stable porté par la goethite néoformée pourrait être une signature de friction liée au processus de chauffage dans la zone de glissement sismique.

Dans la deuxième partie de la thèse, nous étudions la pyrite et les minéraux magnétiques dans la gouge FZB1136. Dans la formation Chinshui, qui est caractérisée

par une alternance de silt et de grès fins, les framboïdes de pyrite de différentes tailles ainsi que des pyrites automorphes isolés sont observés. L'assemblage de minéraux magnétique comprend: la magnétite stœchiométrique avec une très forte proportion de minéraux nanométriques, la greigite, et probablement la pyrrhotite infra micrométrique. Dans la gouge, la concentration de la pyrite est beaucoup plus faible que dans la formation Chinshui. L'assemblage des minéraux magnétiques est constitué de la goethite, de la pyrrhotite supra micrométrique, et de la magnétite partiellement oxydée. La pyrrhotite et la goethite sont néoformées. Nous proposons que la pyrrhotite se forme à partir d'une décomposition à haute température de la pyrite ( $>500^{\circ}\text{C}$ ) lors de la production de chaleur frictionnelle co-sismique. Nous suggérons que la goethite, se forme à partir de fluides chauds ( $>350^{\circ}\text{C}$ ) chaude co-sismiques en liaison avec le séisme de Chi-Chi en 1999. Les températures de fluide élevées peuvent aussi expliquer la modification partielle de la magnétite et l'altération rétrograde de certaine pyrrhotite en pyrite. Nous suggérons que la caractérisation de minéraux néoformés magnétiques peut fournir des informations importantes pour l'étude des zones de glissement du tremblement de terre dans les sédiments dérivés de gouge de faille.

Dans la troisième partie de la thèse, nous tentons de comprendre le décalage de 40 mm entre le pic de susceptibilité magnétique et le pic de rémanence magnétique. Nous précisons la distribution de la goethite et de la magnétite dans la gouge en analysant les paramètres magnétiques. La susceptibilité magnétique maximum est localisée le long de la zone de glissement principale de Chi-Chi. Les principaux minéraux magnétiques identifiés sont la magnétite et la goethite, qui possèdent des paramètres magnétiques différents. Une modélisation numérique nous permet de proposer que les maximums de la concentration de la magnétite et de la goethite correspondent au maximum de la susceptibilité magnétique et de la rémanence magnétique, respectivement. En modélisant les concentrations de ces deux minéraux magnétiques, nous expliquons de façon satisfaisante les profils de la susceptibilité magnétique et de la rémanence magnétique. Cette modélisation indique que  $\sim 300$  ppmv de magnétite sont formés dans la zone de glissement principale et sa surface de contact principale. De même,  $\sim 1\%$  de goethite est formé dans le centre de la gouge, où les fluides sont plus riches en fer. Nous proposons que la magnétite et la goethite sont formés et modifiés au cours des cycles sismiques.

Dans la quatrième partie de cette thèse, nous proposons de déterminer les grains nanométriques dans une gouge de faille de Chelungpu. Des fractions

granulométriques ont été analysées par diffraction des rayons X au synchrotron et par microscopie électronique à transmission. Les minéraux les plus importants de gouge sont le quartz, le plagioclase, la smectite, l'illite, la chlorite et la kaolinite. La composition minérale des particules <100 nm sont le quartz, la smectite, et l'illite. Cependant, il y a seulement de la smectite et de l'illite sans quartz dans les fractions de 1 à 25 nm. Nous proposons que le quartz est le minéral index associé à une fracture co-sismique et la taille de grain minimale est de 25 nm. Les nanoparticules de smectite et d'illite pourraient être associée à l'érosion de la gouge à l'affleurement.

Dans la cinquième partie de cette thèse, nous présentons des résultats préliminaires des analyses magnétiques des gouges FZB1194 et FZB1243. Ces deux zones abritent une gouge centimétrique très sombre (black material disk, BMD) qui n'est présente dans la gouge FZB1136. Dans ces deux gouges, l'enregistrement paléomagnétique indique la présence de composantes stables avec des polarités normales et inverses. Cependant, ces composantes semblent résulter d'un recouvrement de plusieurs composantes, que l'analyse paléomagnétique n'a pas permis de séparer clairement. La polarité inverse pourrait avoir plusieurs origines: 1) un âge de la faille de Chelungpu supérieur à 780 ka, 2) activité sismique pendant une excursion paléomagnétique, 3) une auto-inversion d'origine minérale. Il existe des points communs entre ces deux gouges et la gouge FZB1136. Un décalage entre le pic de rémanence et de susceptibilité est observé, ce qui pourrait traduire des concentrations de minéraux magnétiques variables dans la gouge. La magnétite, mais surtout la goethite sont observées systématiquement dans les deux gouges. En revanche, trois observations fondamentales marquent une différence avec la gouge FZB1136: 1) l'absence d'une composante paléomagnétique unique, homogène dans toute la gouge, 2) la préservation de nanominéraux magnétique dans la gouge, 3) l'absence de pyrrhotite, qui pourrait être un indicateur de haute température de chaleur frictionnelle. Ces différences suggèrent que les événements sismiques enregistrés dans ces deux gouges ont eu une magnitude plus faible que celle enregistré dans la gouge FZB1136. FZB1243 présente aussi l'enregistrement de deux polarités.

Mots-clés: faille de Chelungpu, gouge, minéral magnétique, magnétisme, Taiwan Chelungpu-Fault Drilling Project, magnétite, goethite, pyrrhotite, nanoparticules, quartz

## Abstract

During an earthquake, the physical and chemical transformations along a slip zone lead to alteration and formation of minerals within the gouge layer of a mature fault zone. The gouge contains ferromagnetic minerals, which could be formed under the combined action of friction heat and fluid. Thus, gouge has the capacity to behave as a magnetic recorder during an earthquake. This may constitute an efficient way to identify earthquake slip zones. Besides, altered and neoformed magnetic minerals can be used as tracers of some earthquake processes. In this study, we investigate the rock magnetism and paleomagnetism of the Chelungpu Fault gouge that hosts the principal slip zone of the Chi-Chi earthquake ( $M_w$  7.6, 1999, Taiwan) using Taiwan Chelungpu-Fault Drilling Project (TCDP) hole-B core samples. We also took a Chelungpu fault outcrop sample for identification of nanoparticle, which associated with fracture energy estimation in fault gouge.

In the first part of this thesis, we studied the rock magnetism and paleomagnetism of the 0.16 m thick gouge at 1,136 m depth (labeled FZB1136). The rock magnetic investigation pinpoints precisely the location of the Chi-Chi mm-thick principal slip zone. A modern magnetic dipole of Earth magnetic field is recovered throughout this gouge but not in the wall rocks nor in the two other adjacent fault zones. This magnetic record resides essentially in two magnetic minerals; magnetite in the principal slip zone, and neoformed goethite elsewhere in the gouge. We propose a model where the magnetic record: 1) is preserved during inter-seismic time, 2) is erased during co-seismic time and 3) is imprinted during post-seismic time when fluids cooled down. We suggest that the identification of a stable magnetic record carried by neoformed goethite may be a signature of friction-heating processes in the seismic slip zone.

In the second part of the thesis, we investigate pyrite and magnetic minerals within the host Chinshui siltstone and the FZB1136 gouge. In the Chinshui siltstone, pyrite framboids of various sizes and euhedral pyrite are observed. The magnetic mineral assemblage comprises stoichiometric magnetite, greigite, and fine-grained pyrrhotite. The pyrite content is generally lower in the gouge compared to the wall rock. The magnetic mineral assemblage in the gouge consists of goethite, pyrrhotite, and partially oxidized magnetite. The pyrrhotite, goethite and some magnetite are neoformed. Pyrrhotite likely formed from high temperature decomposition of pyrite ( $>500^\circ\text{C}$ ) generated during co-seismic slip of repeated earthquakes. Goethite is



inferred to have formed from hot aqueous co-seismic fluid ( $>350^{\circ}\text{C}$ ) in association with the 1999 Chi-Chi seismic event. Elevated fluid temperatures can also explain the partial alteration of magnetite and the retrograde alteration of some pyrrhotite to pyrite. We suggest that characterization of neoformed magnetic minerals can provide important information for studying earthquake slip zones in sediment-derived fault gouge.

In the third part of the thesis, we aimed to model the observed 40 mm shift between the maximum of magnetic susceptibility and the maximum of magnetic remanence. The result of the model suggests that the maximum of the concentration of magnetite and goethite correspond to the maximum of magnetic susceptibility and magnetic remanence, respectively. By modeling the concentrations of these two magnetic minerals, we explain satisfactorily the profiles of magnetic susceptibility and remanence. This modeling indicates that  $\sim 300$  ppmv of magnetite formed in the principal slip zone and its main contact area. Similarly,  $\sim 1\%$  of goethite is formed in the center of the gouge, where the fluids are more enriched in iron. We propose that the magnetite and goethite are formed and altered during successive seismic cycles.

In the fourth part of the thesis, we determined the ultrafine nano-scale grains of the Chelungpu fault gouge. The particle size range was analyzed using the synchrotron X-ray diffraction and observed through transmission electron microscopy. The minerals of gouge are predominantly composed of quartz, plagioclase, smectite, illite, chlorite, and kaolinite. The mineral association of  $<100$  nm particles are quartz, smectite, and illite. However, there are only smectite and illite without quartz in the 1 to 25 nm fractions. We propose that quartz is the index mineral associated with co-seismic fracture and the minimum grain size is 25 nm. The smectite and illite nano-particles may be associated with weathering process of gouge at shallow or surface conditions.

In the fifth part of this thesis, we show the preliminary results of magnetic analysis of FZB1194 and FZB1243. These two fault zones have a very dark centimeter black material disk (BMD) that is not present in the FZB1136. In both fault zone, the paleomagnetic record indicates the presence of stable components with normal and reverse polarities. However, these components appear to result from an overlap of several contributions, which the analysis did not separate properly. The identification of opposite polarity, could have several origins: 1) an age of Chelungpu fault greater than 780 ka, 2) earthquake occurring during paleomagnetic excursion, 3) self-reversal processes of magnetic mineral. There are similarities

between these two fault zones and FZB1136. A shift between the peak of remanence and susceptibility is observed, which may reflect varying concentrations of magnetic minerals in the gouge. Magnetite and goethite are found ubiquitously in both fault zones. However, three observations mark a fundamental difference with FZB1136: 1) the absence of a homogeneous single component paleomagnetic throughout the gouge, 2) the preservation of magnetic nano-grains in FZB1194 and FZB1243, 3) the absence of pyrrhotite, which could be an indicator of high temperature transformation. We suggest that seismic events recorded in these two fault zones had a magnitude lower than that recorded in the FZB1136 (Chi-Chi,  $M_w$  7.6).

Keywords: Chelungpu Fault, gouge, magnetic mineral, magnetism, Taiwan Chelungpu-fault Drilling Project, magnetite, goethite, pyrrhotite, nanoparticle, quartz



# Contents

|  |       |
|--|-------|
| 口試委員審定書 .....  | i     |
| 致謝 (Acknowledgement) .....   | ii    |
| 中文摘要 (Abstract in Chinese)I .....  | iv    |
| Résumé (Abstract in French) .....  | vi    |
| Abstract .....   | ix    |
| Contents .....   | xii   |
| List of figures .....  | xv    |
| List of tables .....   | xxiii |
| <b>Chapter 1 Introduction</b> .....  | 1     |
| 1.1 Taiwan Chelungpu fault and the 1999 Chi-Chi earthquake ( $M_w$ 7.6) .....  | 1     |
| 1.2 Taiwan Chelungpu fault drilling project (TCDP) .....   | 2     |
| 1.2.1 FZB1136 .....  | 2     |
| 1.2.2 FZB1194 .....  | 3     |
| 1.2.3 FZB1243 .....  | 3     |
| 1.3 Previous research of TCDP .....  | 4     |
| 1.3.1 Magnetic studies of fault rocks .....  | 4     |
| 1.3.1.1 Paleomagnetism .....   | 4     |
| 1.3.1.2 Magnetic mineralogy of TCDP .....  | 5     |
| 1.3.2 Previous research of fracture energy estimation in TCDP .....  | 6     |
| 1.4 Objectives and Importance .....  | 6     |
| 1.4.1 Identify the Chi-Chi slip zone .....   | 6     |
| 1.4.2 Identify magnetic minerals within fault gouge .....  | 7     |
| 1.4.3 Identify the smallest nano-metric grains within gouge which were<br>formed by fracture during earthquake ..... | 7     |
| 1.5 Scheme of this study .....   | 8     |
| <b>Chapter 2 An earthquake slip zone is a magnetic recorder</b> .....  | 25    |
| 2.1 Introduction .....   | 25    |
| 2.2 Methods .....  | 25    |
| 2.3 Results .....  | 26    |
| 2.4 Discussion and conclusions .....   | 27    |

|                  |  |    |
|------------------|--|----|
| <b>Chapter 3</b> | <b>Pyrite alteration and neoformed magnetic minerals in the fault zone of the Chi-Chi earthquake (<math>m_w</math> 7.6, 1999): evidence for frictional heating and co-seismic fluids</b> | 38 |
| 3.1              | Introduction   | 38 |
| 3.2              | Geologic setting   | 39 |
| 3.3              | Sampling and methods   | 40 |
| 3.4              | Results  | 42 |
| 3.4.1            | Reflected-light polarizing microscopy  | 42 |
| 3.4.2            | SEM observation  | 42 |
| 3.4.3            | Transmission microscopy  | 43 |
| 3.4.4            | Magnetic properties  | 44 |
| 3.5              | Discussion   | 46 |
| 3.5.1            | Iron sulfides  | 46 |
| 3.5.2            | Magnetite  | 48 |
| 3.5.3            | Goethite   | 50 |
| 3.5.4            | Implications for identification of earthquake slip zones   | 50 |
| 3.6              | Conclusions  | 51 |
| <b>Chapter 4</b> | <b>Quantitative Modeling of the Newly Formed Magnetic Minerals in the fault gouge of the 1999 Chi-Chi Earthquake (<math>M_w</math> 7.6), Taiwan</b>                                      | 62 |
| 4.1              | Introduction   | 62 |
| 4.2              | Sampling and methods   | 64 |
| 4.3              | Rock magnetism   | 65 |
| 4.4              | Model  | 66 |
| 4.5              | Discussion and conclusions   | 69 |
| <b>Chapter 5</b> | <b>Nano-particle Analysis of Fault Gouge in the Chelungpu Fault outcrop of Taiwan</b>  | 79 |
| 5.1              | Introduction   | 79 |
| 5.2              | Geological setting and sampling  | 80 |
| 5.3              | Methods  | 81 |
| 5.3.1            | Separation of Fault Particles in Different Particle Size   | 81 |
| 5.3.2            | XRD and TEM analysis   | 82 |
| 5.4              | Results  | 82 |
| 5.4.1            | Synchrotron XRD  | 83 |

|  |            |
|--|------------|
| 5.4.2 TEM .....  | 83         |
| 5.5 Discussion .....   | 83         |
| 5.6 Conclusions .....  | 85         |
| <b>Chapter 6 Preliminary result of FZB1194 and FZB1243 .....</b> | <b>96</b>  |
| 6.1 Analyses of FZB1194 .....                                    | 96         |
| 6.2 Analyses of FZB1243 .....                                    | 97         |
| 6.3 Discussion and conclusions .....                             | 98         |
| 6.3.1 Paleomagnetic records .....                                | 98         |
| 6.3.2 Large magnitude vs. small magnitude .....                  | 99         |
| <b>Chapter 7 Conclusions .....</b>                               | <b>109</b> |
| <b>Chapter 8 Perspectives .....</b>                              | <b>111</b> |
| <b>References .....</b>  | <b>114</b> |
| <b>Appendix .....</b>  | <b>130</b> |



## List of Figures

|  |    |
|--|----|
| Fig. 1-1. Schematic block-diagram illustrating the lithospheric structure of Taiwan (Figure from <i>Angelier et al.</i> , 2001). .....   | 10 |
| Fig. 1-2. Map of active faults and background seismicity distribution in Taiwan. The hypocentre of 1999 Chi-Chi earthquake is located at centre Taiwan (120.81°E, 23.86°N) (Modified from <i>Ma et al.</i> , 1999). .....  | 11 |
| Fig. 1-3. GPS records of 1999 Chi-Chi earthquake show that the large slip velocity was observed about 3.0-4.5 m/s with 8-12 m displacements and low level of high-frequency radiation in the northern part of Chelungpu fault. But in the southern part, the slip velocity is 0.5-2 m/s with 3-4 m displacements (Figure from <i>Ma et al.</i> , 2003). .....  | 12 |
| Fig. 1-4. Correlation of three major fault zones within Chelungpu fault system between TCDP Hole A and Hole B (Figure from <i>Hirono et al.</i> , 2007). .....   | 13 |
| Fig. 1-5. (A) Fault zone description, X-ray CT images, and photos of FZB1136. The white frame corresponds to the locations of polished sections. (B) In the collage of SEM images from the polished sections, two yellow lines are the boundaries between gray gouge zone (GGZ) and the black gouge zone (BGZ). The yellow asterisks indicate clay-clast aggregates (CCAs). The double green dashed line is the Chi-Chi principal slip zone (PSZ). (C) The SEM image of the 3 mm-thick Chi-Chi PSZ shows very fine-grained ultracataclasite (after <i>Boullier et al.</i> , 2009; <i>Hirono et al.</i> , 2007a). ..... | 14 |
| Fig. 1-6. Fault zone description, X-ray CT images, and photos of FZB1194 (Figure from <i>Hirono et al.</i> , 2007a). .....   | 15 |
| Fig. 1-7. Fault zone description, X-ray CT images, and photos of FZB1243 (Figure from <i>Hirono et al.</i> , 2007a). .....   | 16 |
| Fig. 1-8. Photo of pseudotachylytes, which is found in an exposure of the Skeeter fault, USA (Figure from <i>Kirkpatrick et al.</i> , 2009). .....   | 17 |
| Fig. 1-9. Examples of pseudotachylytes in granite and pattern of magnetic susceptibility (Figure from <i>Ferré et al.</i> , 2012). .....   | 18 |
| Fig. 1-10. 2-D thermal conductivity model for a pseudotachylite vein ( <i>Peacock</i> , 1990; Figure from <i>Ferré et al.</i> , 2005). A 20 mm-thick pseudotachylite vein and thermal  |    |

|  |    |
|--|----|
| transfer from slip zone to host-rock is assumed. The melt temperature is assumed to be 1000°C while the host-rock is assumed to be at 100°C. Ten seconds after slipping, the vein edge has cooled down below the magnetite Curie temperature of 580°C and block the thermoremanent magnetization (TRM) of Earth's magnetic field. ....   | 19 |
| Fig. 1-11. Reflected light microscopy image of a black fault gouge in the thin section of Nojima fault, Japan (Figure from <i>Nakamura et al.</i> , 2001). Black arrows show the shear plane. White arrows indicate fine goethite grains, which are ~5 µm or less in diameter and formed euhedral sharp. ....  | 20 |
| Fig. 1-12. The illustration of earthquake lightnings (EQL) predicted characteristics of NRM in fault plane (Modified from <i>Ferré et al.</i> , 2005). (A) An electrical current related to EQL along the fault plane could make a magnetic field perpendicular to the plane. (B) The fault rock could be expected to acquire a magnetization perpendicular to the fault plane. .... | 21 |
| Fig. 1-13. Continuous in situ and non-destructive measurement, which were by using the Multi-Sensor Core Logger (MSCL) system in TCDP hole B has shown that three major fault zones are characterized by an increase in the magnetic susceptibility (Figure from <i>Hirono et al.</i> , 2006). ....  | 22 |
| Fig. 1-14. A schematic diagram of high-speed frictional testing machine (Figure from <i>Fukuchi et al.</i> , 2005). ....   | 23 |
| Fig. 1-15. Schematic plot of re-magnetization within a fault gouge during an earthquake. The physical/chemical alteration process (e.g. conduction and evolution of frictional heating along fault plane (after <i>Fukuchi et al.</i> , 2005)) could re-magnetize the magnetic minerals within gouge to attain new remanent magnetization of earth magnetic field. ....              | 24 |
| Fig. 1-16. The TEM image and particle size distribution for estimation of fracture energy between (A) <i>Chester et al.</i> (2005) and (B) <i>Ma et al.</i> (2006). The low-cut of finest particle size is 1.6 nm of <i>Chester et al.</i> (2005) and 50 nm of <i>Ma et al.</i> (2005). ....   | 25 |
| Fig. 2-1. Locations, major fault zones and paleomagnetic records. (A) A geological map showing the epicenter of Chi-Chi earthquake ( $M_w$ 7.6, 1999) and the Taiwan Chelungpu-fault Drilling Program (TCDP) drilling site at 120.73916°E, 24.20083°N (Modified from <i>Ma et al.</i> , 2006). FZB stands for Fault Zone of hole   |    |

B. (B) A Schematic log of the borehole showing the three major fault zones of the Chelungpu fault within the Chinshui Formation. (C) Equal-area stereo-plot displaying the Chelungpu fault plane and the mean paleomagnetic components recorded in the three fault zones and wall rock. Due to the orientation of the borehole B, there is an error of  $\pm 20^\circ$  in declination for all paleomagnetic component. This error is indicated for the FZB1136 gouge component. We plot the orientation of an expected earthquake lightning (EQL) according to the model of *Ferré et al.* (2005) with  $20^\circ$  error in orientation. The black (open) symbols correspond to the downward (upward) hemisphere. The cross indicates the 1999 international geomagnetic reference field (IGRF) dipole magnetic vector ( $D = 0.2^\circ$ ,  $I = 29.7^\circ$ ). The wall rock's main component lies away from the modern magnetic field ( $D = 322^\circ$ ,  $I = 48^\circ$ ,  $\kappa = 99$ ,  $\alpha_{95} = 4^\circ$ ; range 10–80 mT). The FZB1136 gouge component ( $D = 348^\circ$ ,  $I = 48^\circ$ ,  $\kappa = 140$ ,  $\alpha_{95} = 2^\circ$ ) is the closest to the modern magnetic field and statistically different from a hypothetical EQL. Within the FZB1194 gouge, normal and reverse components are southerly oriented ( $D = 235^\circ$ ,  $I = 27^\circ$ ,  $\kappa = 110$ ,  $\alpha_{95} = 8^\circ$  and  $D = 154^\circ$ ,  $I = -52^\circ$ ,  $\kappa = 144$ ,  $\alpha_{95} = 5^\circ$ ), respectively. Within the FZB1243 gouge, normal and reverse components are also oriented southerly ( $D = 125^\circ$ ,  $I = 11^\circ$ ,  $\kappa = 189$ ,  $\alpha_{95} = 4^\circ$  and  $D = 125^\circ$ ,  $I = -10.0^\circ$ ,  $\kappa = 280$ ,  $\alpha_{95} = 3^\circ$ ), respectively. (D) The natural remanent magnetization (NRM) orthogonal plot of FZB1136 gouge (depth 1,136.33 m). Open (black) circles represent projection of the vector along the vertical (horizontal) plane. (E) Curves of normalized NRM intensity of FZB1136 and wall rock. ....32

Fig. 2-2. Photo of one U-channel in this study. The U-channel is a plastic box of 2 cm  $\times$  2 cm with  $\sim 20$  cm long. ....33

Fig. 2-3. The 755 SRM cryogenic magnetometer manufactured by 2G Enterprises in the magnetic shielding room at the Institute of Earth Sciences, Academia Sinica, Taiwan. ....34

Fig. 2-4. The stepwise heating temperature is from 100°C up to 600°C by using the MMTD80 thermal demagnetizer. ....35

Fig. 2-5. The IRM of the samples was acquired from 25 mT up to 950 mT by using a 2G cryogenic magnetometer. ....36

Fig. 2-6. NRM thermal demagnetization, TXM photo, and S-ratio. (A) The NRM thermal demagnetization for a gouge sample (depth of 1,136.34 m) and the



Chi-Chi's principal slip zone (PSZ) (depth of 1,136.38 m) within FZB1136. In the gouge, there is a break-in-slope near 150 °C where ~80% of the NRM is lost. The remaining part of the NRM has a maximum unblocking temperature close to 580°C. In the Chi-Chi's PSZ, the maximum unblocking temperature is close to 580°C. (B) The TXM photo from a 15 mm thick polished-section collected from a gouge within FZB136. Scattered elongated dense minerals with a low aspect ratio 2:25 and maximum length of 5 mm are likely to be goethite. (C) The S-ratio profile along the U-channel. The lowest value of the S-ratio (magnetically hard) is located at a depth of 1,136.30 m, near the center of the gouge and corresponds to the highest concentration in goethite. The Chi-Chi's PSZ is marked by an enhancement of the S-ratio, which is consistent with a larger contribution of magnetite. ....37

Fig. 2-7. The magnetic record cycle of a fault gouge. 1) During an inter-seismic period, the magnetic record of an old earthquake is preserved within the fault gouge through geological times. 2) During a co-seismic period, the gouge acts as a magnetic eraser. At the PSZ and baked contact the temperature elevation and chemical degradation lead to the partial-to-complete demagnetization of the gouge. The co-seismic hot fluids probably demagnetized the former goethite. 3) During a post-seismic period, the gouge acts as a magnetic recorder. Cooling of the gouge or fluids leads to a thermo-remnant magnetization (TRM) imprint. Neoformed minerals resulting from any form of chemical processes, including cooling, carry a chemical-remnant magnetization (CRM). ....38

Fig. 3-1. Geological setting of the TCDP borehole (modified from *Yeh et al.* [2007]). (A) Schematic geological map of western Taiwan with the location of the TCDP site (red star, 120.73916°E, 24.20083°N) on the northern part of the Chelungpu fault. The focal mechanism of the Chi-Chi main shock is located at the hypocentre of the 1999 Chi-Chi earthquake (128.81°E, 23.86°N). (B) Geological cross-section through the TCDP site. The Chelungpu fault is located within the Chinshui Formation. ....53

Fig. 3-2. Images of the cores and samples from TCDP Hole B. (A) Half-core image for the depth interval from 1,133.33 to 1,138.63 m. The blue arrows and frame indicate the sample locations. (B) Half-core image of the FZB1136 fault zone at a depth of 1,136.22~1,136.43 m; the white frame corresponds to the locations of

polished sections. The green dashed line frames the Chi-Chi principal slip zone (PSZ) (*Boullier et al.*, 2009). (C) Collage of SEM images from the polished sections. Red circles indicate sample positions for TXM analysis. The yellow lines are the boundaries between deformed sediments (DFS) and the gouge zone (BGZ). The yellow stars indicate clay-clast aggregates (CCAs, see *Boullier et al.* (2009)). The double yellow dashed line is an ancient slip zone (ASZ) and the double green dashed line is the Chi-Chi PSZ (after *Boullier et al.* (2009)). ....54

Fig. 3-3. Back-scattered SEM images with EDS results. (A) Large iron sulfide aggregates that contain framboidal pyrite ( $\text{FeS}_2$ ) within the deformed sediments (S1 in Figure 2C). Some parts of the aggregate are greigite ( $\text{Fe}_3\text{S}_4$ ). (B) Large iron sulfide aggregates that contain framboidal pyrite with micro-fractures and shears in the deformed sediments (S2 in Figure 2C). (C) Pyrite grain in the gouge (S3 in Figure 2C). The framboidal  $\text{FeS}$  core (pyrrhotite, which is a replacement of a framboidal pyrite) has an  $\text{FeS}_2$  rim. The photos on the right were obtained using reflected-light microscopy (P: polarized reflected; L: light reflected); pyrite is dark and pyrrhotite is light under polarized light. (D) Large cluster of pyrite grains mixed with quartz (S4 in Figure 2C). (E) Small pyrite grains (bright back-scattered grains, smaller than  $5\text{ }\mu\text{m}$ , one is  $\sim 20\text{ }\mu\text{m}$ ) and quartz grains within the Chi-Chi PSZ (S8 in Figure 2C). (F) Detail of Figure 3E: fractured pyrite grain within the PSZ (S8 in Figure 2C). (G) Image of the Chi-Chi PSZ (S8 in Figure 2C). (H) Pyrite grain ( $3\text{ }\mu\text{m}$ ) within the Chi-Chi PSZ (S8 in Figure 2C). .....55

Fig. 3-4. 2-D and 3-D images acquired for TXM observations. (A) Sediment at a depth of 1,134.04 m in TCDP hole B (M1 in Figure 2A). (B) Deformed sediment at a depth of 1,136.25 m (S10 in Figure 2C). (C) Gouge at a depth of 1,136.33 m (S11 in Figure 2C). (D) Gouge close to the PSZ at a depth of 1,136.38 m (S12 in Figure 2C). .....56

Fig. 3-5. Low temperature magnetic measurements (inset: relative values of RT-SIRM) from 10 to 300 K and FORC diagrams. (A) Wall rock sample (M1 in Figure 2A). (B) Deformed sediment sample (M2 in Figure 2C). (C) Gouge sample (M3 in Figure 2C). (D) ASZ sample (M4 in Figure 2C). (E) PSZ sample (M5 in Figure 2C). (F) FORC diagram for wall rock sample (field 0–100 mT). (G) FORC diagram for deformed sediment sample (field 0–100 mT). (H) and (I) FORC diagrams for samples from fault gouge (field 0–100 mT). .....57

|   |    |
|---|----|
| Fig. 3-6. Warming-cooling RT-SIRM cycle from 300 to 400 K (127°C), which is close to the Néel temperature of goethite (120°C). (A) For a wall rock sample, less than 25% of the RT-SIRM is lost at 400 K. (B) For a gouge sample, about ~50% of the RT-SIRM is lost at 400 K. This indicates neoformation of a significant concentration of goethite in the fault gouge. ....   | 58 |
| Fig. 3-7. Cooling-warming RT-SIRM cycle from 10 to 50 K. A reversible magnetic transition at 35 K for the PSZ sample indicates that pyrrhotite is fine-grained and close to 1 $\mu\text{m}$ in size ( $h/c$ ratio = 0.96) (see <i>Dekkers et al.</i> (1989)). ....  | 59 |
| Fig. 3-8. Eh-pH diagrams for fluid temperatures of 300°C and 100°C. The model parameters are: $a_{\text{SO}_4^{2-}} = 10^{-2}$ , $a_{\text{Cl}^-} = 10^{-2}$ , $a_{\text{Fe}^{2+}} = 10^{-4}$ (higher iron concentration). The pressure used is 30 MPa, which is equivalent to lithostatic pressure at a depth of 1,100 m. Note that at higher temperatures the pyrrhotite field exists at strong reducing conditions in a pH range of 5.3-8.2. As temperature decreases, the pyrite field expands and pyrrhotite alters to pyrite. ....  | 60 |
| Fig. 4-1. (A) SEM image observation of FZB1136. The yellow line indicates the boundary of deformed sediments (DFS) and gouge, and dash red lines show the range of the 1999 Chi-Chi earthquake PSZ. (B) Normalized magnetic susceptibility and (C) normalized $\text{IRM}_{\text{IT}}$ of FZB1136 U-channel measurements. The blue arrow line at 1,136.34 m is the location of Sample A at the $\text{IRM}_{\text{IT}}$ peak ( $\sim 1 \times 10^{-2} \text{ Am}^2/\text{kg}$ ). The red arrow line at 1,136.38 m (PSZ) is the location of Sample B at the magnetic susceptibility peak (600 $\mu\text{SI}$ ). The green arrow line at 1,136.41 m is the location of Sample C at the deformed sediments. .... | 72 |
| Fig. 4-2. Photo of Bartington MS3 magnetic susceptibility system mounted on the ASC auto-tracking rail in Institute of Earth Sciences, Academia Sinica, Taiwan .....  | 73 |
| Fig. 4-3. Low temperature analyses result of samples. (A) LT-SIRM warming curves (B) RT-SIRM cooling curves. ....   | 74 |
| Fig. 4-4. (A) Thermal demagnetization of natural remanent magnetization (NRM). (B) IRM acquisition curves up to 2.5 T. The locations of Sample A, Sample B, and Sample C are specified in Fig. 4-1. ....  | 75 |
| Fig. 4-5. Thermal demagnetization of gouge sample located near the deformed sediments and of gouge sample located at gouge center after applying 1.2 T RT-SIRM. ....  | 76 |

- Fig. 4-6. (A) Model of magnetite and goethite assemblage curves in a 20 cm U-channel. Blue line is relative to the magnetite concentration. Red line is relative to the goethite concentration. Green dash line is magnetic susceptibility contribution of paramagnetic minerals ( $\chi_{para}$ ). Yellow line is magnetic susceptibility contribution of SP minerals ( $\chi_{SP}$ ). (B)(C) The comparison between U-channel results (red line) and our best-fit curves (blue line) of normalized magnetic susceptibility ( $\chi$ ) and SIRM, respectively. The  $R^2$  value of normalized magnetic susceptibility ( $\chi$ ) model is 0.981 and of SIRM is 0.986. .... 77
- Fig. 4-7. The concentration curves of (A) magnetite and (B) goethite, which were calculated from our model by using the magnetic susceptibility and the remanence. .... 78
- Fig. 5-1. Geological setting of sampling location in Wu-Feng, center Taiwan (Modified from *Huang et al.*, 2001). (A) Geological map of Wu-Feng with Chelungpu fault and the Chi-Chi earthquake fault rupture. (B) Geological cross section passing the sampling location. .... 87
- Fig. 5-2. Block black gouge sample of Chelungpu fault outcrop. It contains very fine grains. .... 88
- Fig. 5-3. Photo of Hitachi CR21 refrigerated centrifuge (Hitachi High-Technologies Corp., Tokyo, Japan). .... 89
- Fig. 5-4. Schematic diagram of an automated ultrafiltration device (AUD) for nanoparticle separation (*Tsao et al.*, 2009). .... 90
- Fig. 5-5. Flow chart for dispersion and separation of fault gouge nanoparticles. .... 91
- Fig. 5-6. Synchrotron XRD results of different grain size particles. .... 92-93
- Fig. 5-7. TEM photos of <100 nm grains. (A)(B) Platy pieces, lath-like fractions, and rounded grains are observed. Some ultrafine grains (<10 nm) could be found. (C) Image of a rounded grain with electron diffraction and EDX analysis. .... 94
- Fig. 6-1. The magnetic properties of FZB1194 U-channel show the shift between the maximum of remanence and magnetic susceptibility. The S-ratio value of upper deformed sediments and black material disk is lower (~0.93) than gouge and deformed sediments (0.97-0.98). .... 101
- Fig. 6-2. LT-SIRM warming curves of FZB1194 samples show that the Verwey transition (120 K) is well identified in all samples. The drop of LT-SIRM between 10 K and 35 K is large (>99%) for deformed sediments and is smaller

|  |     |
|--|-----|
| for gouge. But this drop is limited (<1%) for black material disk. ....  | 102 |
| Fig. 6-3. RT-SIRM cooling curves of FZB1194 samples provide subtle Morin transition (240 K) in all samples. The Verwey transition (120 K) is not visible in black material disk and some black gouge samples. The cooling increasing at about 10% from 300 K to 150 K is attribute to the presence of goethite, this increasing is found within all samples. The increases from 100 K to 10 K as the P-behavior of SP pyrrhotite signature could be found in gray gouge and some black gouge samples. However, for black material disk and some black gouge samples, the P-behavior is weak and the 35 K transition is unclear. .... | 103 |
| Fig. 6-4. The TXM image of FZB1194 black material disk shows numerous elongated dense minerals (aspect ratio 2:25; maximum length 5 $\mu\text{m}$ ). ....  | 104 |
| Fig. 6-5. The magnetic properties of FZB1243 U-channel show the maximum of the remanence and the magnetic susceptibility curves are shifted. S-ratio value of upper deformed sediments is 0.80~0.85 and from black material disk to whole black gouge is 0.80~0.82. ....   | 105 |
| Fig. 6-6. LT-SIRM warming curves of FZB1243 samples show that the Verwey transition (120 K) is well identified in deformed sediments and some black gouge samples, but is not visible in black material disk and some black gouge samples. The drop between 10 K and 35 K is large (>99%) for deformed sediments and is smaller for black gouge samples (<6%). But this drop is limited (<1%) for black material disk. ....  | 106 |
| Fig. 6-7. RT-SIRM cooling curves of FZB1243 samples show subtle Morin transition (240 K) in all samples. The Verwey transition (120 K) is not visible in black material disk and some black gouge samples. The cooling increasing at about 10% from 300 K to 150 K is found within all samples. The increases from 100 K to 10 K as the P-behavior of SP pyrrhotite signature could be found in gray gouge and some black gouge samples. However, for black material disk and some black gouge samples, the P-behavior is weak and the 35 K transition is unclear. ...   | 107 |
| Fig. 6-8. Range and total slip (~0.3 km) of Chelungpu Chinshui detachment. (after Yue <i>et al.</i> , 2005). ....  | 108 |
| Fig. 8-1. SEM photo of pyrite alteration from a creep gouge from the Jura mountain (Azaruk & Aubourg, unpublished work). ....  | 113 |

## List of Tables

|  |    |
|--|----|
| Table 3-1: Sample depths and measurements made in this study. ....         | 61 |
| Table 5-1: Synchrotron XRD results of different grain size fractions. .... | 95 |



## Chapter 1. Introduction

### 1.1 Taiwan Chelungpu fault and 1999 Chi-Chi earthquake

The Taiwan Island is located at the convergent boundary between the Eurasian Continent Plate and the Philippine Sea Plate (Fig. 1-1). Taiwan is also located at the join between the Ryukyu trench and the Luzon arc system. The Philippine Sea Plate is moving with a speed of 56~82 mm/year in the N306°E~N322°E azimuth and is colliding with the Eurasian Plate margin (*Yu et al.*, 1997). The South China Sea of the Eurasian Continent Plate is subducting beneath the Philippine Sea Plate in the south Taiwan. The Philippine Sea Plate is also subducting beneath the Eurasian Continent Plate in the northeast Taiwan. This cross collision between two subduction systems results in active faulting, numerous earthquakes, crust uplifting, and crustal deformation within the Taiwan mountain belt.

Taiwan is divided into several geological regions, from west to east; the Costal Plain, the Western Foothills, the Central Range, the Longitudinal Valley, and the Coastal Range (*Ho*, 1988). Along the belt between the Costal Plain and the Western Foothills, several fault systems occur around this active seismic region, including the Shuilikeng, Shuangtung, Chelungpu, and Changhua faults, which are the most active regions in Taiwan.

The Chelungpu thrust fault zone is one of the major active faults in the western Taiwan thrust belt. Originally, it was characterized as the Chinshui Formation thrusting on the Toukashan Formation in the Taichung Basin (*Chang*, 1971). This fault is considered as an active fault due to its distinct geomorphic feature (*Bonilla*, 1977).

The largest earthquake ( $M_w$  7.6) during the last 100 years in Taiwan took place on 21 September 1999, near the town of Chi-Chi in central Taiwan (Fig. 1-2, hypocenter 120.81°E, 23.86°N, depth ~10 km, *Ma et al.*, 1999; *Kao and Chen*, 2000), which caused many casualties (2,321 deaths, ~10,000 injured) and destruction (more than 100,000 buildings were damaged or destroyed). During this earthquake, the surface rupture closely followed the ~85 km Chelungpu fault (*Chen et al.*, 2002). In the northern part, the large slip velocity was observed about 3.0-4.5 m/s with 8-12 m displacements and low level of high-frequency radiation. But in the southern part, the slip velocity was 0.5-2 m/s with 3-4 m displacements by records of GPS data (Fig.

1-3, *Ma et al.*, 2003). The average slip duration (rise time) is 7.2 sec (*Chen et al.*, 2003). According to elastohydrodynamic lubrication model (*Brodsky and Kanamori*, 2001), this kind of slip behaviour could be explained by fluid pressurization in a fluidized gouge during slip (*Ma et al.*, 2003).

## **1.2 Taiwan Chelungpu Fault Drilling Project (TCDP)**

The Taiwan Chelungpu-fault Drilling Project (TCDP) started in 2004. The drilling site is located at 120.73916°E, 24.20083°N near the town of DaKeng, central Taiwan, 2 km east of the surface rupture of the Chi-Chi earthquake. Surface structures around the drilling site were constrained by high-resolution shallow seismic reflection. These investigations suggested that the Chelungpu fault was a bedding-parallel thrust in the Chinshui Formation and that the Chi-Chi rupture is at a depth of about 1,200 m below the drilling site (*Wang et al.*, 2002, 2004). This project drilled two vertical holes 40 m apart, Hole-A to a depth of 2,003.0 m into the Kueichulin Formation (passing through the Sanyi fault zone) and Hole-B to a depth of 1,352.6 m (*Yeh et al.*, 2007).

From Hole-A, three major fault zones were found within the Pliocene Chinshui Formation at depths about 1,111, 1,153, and 1,222 m, respectively. From the Hole-B core, three major fault zones were also found within the Chinshui Formation at depths of about 1,136, 1,194 and 1,243 m, respectively (*Hirono et al.*, 2007; *Hung et al.*, 2007; *Song et al.*, 2007; *Yeh et al.*, 2007). The three major fault zones FZA1111 (fault zone in Hole-A, at depth 1,111 m), FZA1153, and FZA1222, may correspond to FZB1136 (fault zone in Hole-B, at depth 1,136 m), FZB1194, and FZB1243, respectively. By calculating the relative depth difference from the horizontal distance between the holes, the angle and dip of the fault zones are 35°, 45°, and 30° (Fig. 1-4, *Hirono et al.*, 2007a). On the basis of the correlation of fault zones in Hole A and Hole B, the Chelungpu fault system may display a duplex structure (*Hirono et al.*, 2008).

### **1.2.1 FZB1136**

The following subzones within FZB1136 were described from top to bottom: upper fracture-damaged zone (1,134.40 – 1,134.93 m), upper breccia zone (1,134.93 – 1,136.22 m), upper gray fault gouge (also called deformed sediments)



(1,136.22 – 1,136.26 m), black fault gouge (1,136.26 – 1,136.40 m), lower gray fault gouge (1,136.40 – 1,136.46 m), lower breccia zone (1,136.46 – 1,136.70 m), and lower fracture-damaged zone (1,136.70 – 1,137.90 m) (Fig. 1-5A, after *Hirono et al.*, 2007a).

The micro scale observation of FZB1136 reveals a complex architecture, with the stack of tens of slip zones (*Boullier et al.*, 2009). A detailed SEM analysis shows a 3 mm-thick layer of very fine-grained ultracataclasite that is not fractured (Fig. 1-5B, C). It is located at 2 cm above the bottom of black gouge zone, and was considered as the principal slip zone of Chi-Chi earthquake by *Boullier et al.* (2009). The SEM observation underlines the nature of the ‘gray gouge’. It is actually not a gouge, but a layer of deformed sediments where bedding can still be identified. For that reason, we decided to abandon the term ‘gray gouge’ and we use instead ‘deformed sediments’. One of the most interesting features of Boullier’s work is the discovery of clay-clast aggregates (CCAs) within the compacted gouge layers (Fig. 1-5B; after *Boullier et al.*, 2009). The CCAs are believed to form with fluid pressurization within the gouge (*Boutareaud et al.*, 2008, 2010). To date, no evidence of melting has been yet documented in the gouge.

### 1.2.2 FZB1194

The description of FZB1194 observed from top to bottom were upper fracture-damaged zone (1,194.00 – 1,194.73 m), black material disk (1,194.73 – 1,194.75 m), black fault gouge (1,194.75 – 1,194.81 m), deformed sediments (1,194.81 – 1,194.84 m), black fault gouge (1,194.84 – 1,194.87 m), deformed sediments (1,194.87 – 1,195.13 m), breccia zone (1,195.13 – 1,195.50 m), and lower fracture-damaged zone (1,195.50 – 1,197.25 m) (Fig. 1-6, after *Hirono et al.*, 2007a). It appears, therefore, that this 14-cm thick gouge hosts a 2 cm-thick layer of black material disk where evidence of partial melting has been suggested (*Otsuki et al.*, 2009). The two layers of gouge are separated by a layer of 3 cm-thick deformed sediments. This fault zone, as a whole, differs notably from the FZB1136.

### 1.2.3 FZB1243

Similarities between this fault zone and FZB1194 are evident. Subdivisions observed from top to bottom are upper fracture-damaged zone (1,242.70 – 1,243.33

m), upper deformed sediments (1,243.33 – 1,243.38 m), black material disk (1,243.38 – 1,243.40 m), black fault gouge (1,243.40 – 1,243.50 m), lower deformed sediments (1,243.50 – 1,243.60 m), and lower fracture-damaged zone (1,243.60 – 1,244.30 m) (Fig. 1-7, after *Hirono et al.*, 2007a). So again, a 2 cm-thick layer of black material disk is observed here.

### **1.3 Previous Research**

The targets of fault zone investigation have been focused on the energy budget of an earthquake include heat contribution and estimate the fracture. In this study, we propose a short review of the magnetic properties and mineralogy of pseudotachylyte and gouge.

#### **1.3.1 Magnetic studies of fault rocks**

##### **1.3.1.1 Paleomagnetism**

Fault-related pseudotachylytes are dark fine-grained to glassy rocks, which form by frictional melting during seismic slip along fault planes as earthquake fossils (Fig. 1-8) (e.g., *Philpotts*, 1964; *Sibson*, 1975; *Spray*, 1987; *Magloughlin*, 1992; *Di Toro and Pennacchioni*, 2004; *Andersen and Austrheim*, 2006; *Lin*, 2008; *Kirkpatrick et al.*, 2009). Several magnetic investigations of fault rocks focused on pseudotachylytes. The pseudotachylyte layer generally shows a high magnetic susceptibility (Fig. 1-9) and strong natural remanent magnetization (NRM) (typically  $>200 \text{ Am}^2/\text{kg}$ , *Ferré et al.*, 2005). The NRM originates from single domain (SD) to pseudo single domain (PSD) ferromagnetic minerals (e.g., *Piper*, 1981; *Piper and Poppleton*, 1988; *Enomoto and Zheng*, 1998; *Enomoto et al.*, 2001; *Nakamura and Nagahama*, 2001; *Nakamura et al.*, 2002; *Fukuchi*, 2003; *Ferré et al.*, 2005; *Nakamura and Iyeda*, 2005; *Molina Garza et al.*, 2009; *Ferré et al.*, 2012).

The magnetization acquisition processes could be 1) a thermal remanent magnetization (TRM) acquired during cooling of the pseudotachylyte melt (Fig. 1-10) (e.g., *Piper*, 1981; *Piper and Poppleton*, 1988; *Nakamura et al.*, 2002; *Ferré et al.*, 2005), 2) a chemical remanent magnetization (CRM) carried by neoformed magnetic minerals (Fig. 1-11) (e.g., *Hailwood et al.*, 1992; *Nakamura and Nagahama*, 2001; *Fukuchi*, 2003; *Fukuchi et al.*, 2005; *Molina Garza et al.*, 2009), 3) an isothermal remanent magnetization (IRM) occurred by earthquake lightning (EQL) during

earthquakes near the fault plane (Fig. 1-12) (e.g., *Enomoto and Zheng*, 1998; *Enomoto et al.*, 2001; *Ferré et al.*, 2005). In sediments-derived gouge, there are no published studies that report paleomagnetic record. However, *Hailwood et al.* (1992) used the paleomagnetic record to date the fault movement from clay-rich fault gouge, which originated from meta-sedimentary rocks. Besides, *Nakamura et al.* (2008) studied the paleomagnetic record of fault gouges of TCDP boreholes. They observed stable components and attempted to relate them to EQL processes.

#### **1.3.1.2 Magnetic mineralogy of TCDP**

Several rock magnetic studies related to TCDP gouges have been published (*Hirono et al.*, 2006; *Mishima et al.*, 2006; *Tanikawa et al.*, 2007, 2008; *Mishima et al.*, 2009). Continuous in situ and non-destructive measurement of the magnetic susceptibility in TCDP hole B has shown that three major fault zones are characterized by an increase in the magnetic susceptibility (Fig. 1-13, *Hirono et al.*, 2006). The initial aim of these studies was to explain the origin of the peak of magnetic susceptibility. It was soon established that the main magnetic mineral is magnetite, more or less oxidized into maghemite. *Tanikawa et al.* (2007; 2008) reported that thermally and mechanically induced formation of ferrimagnetic minerals might have caused a magnetic susceptibility anomaly as being due to the neoformed ferrimagnetic iron oxydes induced by frictional heat as experimentally reproduced during high-speed frictional test (Fig. 1-14) (e.g., *Nakamura et al.*, 2002; *Fukuchi et al.*, 2005). The most recent study by *Mishima et al.* (2006, 2009) is also the most complete, as it combined high-temperature investigation (>300K), low-temperature investigation (10K to 300K), and hysteresis loops. They proposed that formation of magnetite or maghemite by thermal decomposition of paramagnetic minerals could be the cause of the high magnetic susceptibility of the black material disks and fault gouge, which have experienced temperatures of at least 400°C. However, in the following chapter, we have discovered the presence of goethite and pyrrhotite, while *Mishima et al.* (2006, 2009) didn't report. The main reason for this is that they did not used the monitoring of the cooling of an artificial magnetic remanence imparted at 300K. This procedure allowed us to detect goethite and pyrrhotite.

### 1.3.2 Previous research of fracture energy estimation in TCDP

In order to better estimate fracture energy in the energy budget of earthquakes, *Ma et al.* (2006) calculated the grain-size distribution in the principal slip zone of FZA1111 by microscope observations. By comparison, they concluded that the contribution of gouge surface energy to the earthquake breakdown work is quantified to be 6 per cent, which is higher than the less than 1% value obtained on mature gouge of San Andreas Fault system by *Chester et al.* (2005) and *Rockwell et al.* (2009).

### 1.4 Objectives and Importance

The three major fault zones of Chelungpu fault system in TCDP are not parallel in the bedding of Chinshui Formation. The dip angle of the first fault zone is 35°, the second is 45° and the third is 30° (*Hirono et al.*, 2007a). The relationship and occasion of those three fault zones are still unknown. Different dip angle maybe point out that each fault zone was formed by different stress event or the rock character is disparity. Thus, it's important for us to analyze the rock properties. The magnetic properties of fault zones could give us some valuable information.

#### 1.4.1 Identify the Chi-Chi slip zone

One of the most important target of TCDP is the finding of the 1999 Chi-Chi slip zone, however there are three major fault zones of Chelungpu fault system in borehole samples. It's difficult to distinguish which fault zone belong to 1999 Chi-Chi event from image observation or chemical/physical analyses. We could only conjecture that the first fault zone - FZA1111 (correlate to FZB1136) hosts the slip zone of the 1999 Chi-Chi earthquake from thermal anomaly (*Kano et al.*, 2006), geophysical logging measurements (*Ma et al.*, 2006; *Hung et al.*, 2007; *Song et al.*, 2007a; *Wu et al.*, 2007). However, we still don't have strong evidence of the answer. The physical/chemical alteration (e.g. frictional heating, fluid interactions, etc.) of fault gouge during an earthquake could re-magnetize the magnetic minerals within gouge to attain new remanent magnetization of earth magnetic field (Figure 1-14). The magnetic field direction of earth drifts with time. Thus, the most recent fault slip zone could record the 1999 earth magnetic field direction in central Taiwan. Perhaps, the paleomagnetic record of fault gouge acquired during earthquake could give us a

chance to find the answer.

#### **1.4.2 Identify magnetic minerals within fault gouge**

Anomalous high magnetic susceptibilities were found in the three major fault zones (Figure 1-13) (*Hirono et al.*, 2006). The frictional heating (*Hirono et al.*, 2007; *Kano et al.*, 2007; *Mishima et al.*, 2006, 2009; *Kuo et al.*, 2009, 2011), thermal pressurization (*Ishikawa et al.*, 2008; *Boullier et al.*, 2009), and co-seismic hot fluid (*Ishikawa et al.*, 2008) were reported within TCDP fault gouges. Those effects could cause rock-fluid interactions, also include magnetic minerals alterations; therefore, change the value of magnetic susceptibility. There are some researches of the magnetic properties (*Mishima et al.*, 2006, 2009; *Tanikawa et al.*, 2007), but the species of new produced mineral and the courses of magnetic mineral changes during earthquake are still unclear. The assemblage of magnetic minerals could also provide us tracks of physical/chemical alteration within fault gouge.

#### **1.4.3 Identify the smallest nano-metric grains within gouge which were formed by fracture during earthquake**

During a fault slipping, gouge particles will be milling into smaller fractions and changing particle size distribution. The grain size of ultrafine fractions within fault gouge could approach the nanometer scale (*Wilson et al.*, 2005). *Chester et al.* (2005) observed the finest particle size is 1.6 nm within Punchbowl fault gouge as the lower cut-off for estimation of fracture energy. *Ma et al.* (2006) observed the fault gouge of TCDP at depth 1,111 m in Hole-A. They used grain sizes larger than 50 nm as lower cut-off for estimation of fracture energy, cause of the TEM image of grain sizes less than 50 nm shows rounded shapes. Therefore, they considered those grains <50 nm might be formed by chemical precipitation rather than fracturing. However, the TEM image of *Chester et al.* (2005) also shows rounded shapes of ultrafine grains; the image of *Ma et al.* (2006) shows very fine grain around several nm in diameter (Fig. 1-15). In addition, the very fine grains have larger surface area than coarse grains and could provide high percentage within total fracture energy significantly. Thus, to determine the lower cut-off grain sizes is important for fracture energy calculation. The nanoparticles (<100 nm) within fault gouge could be the key point of fracture energy estimation.

### 1.5 *Scheme of this study*

In chapter 1 of this study, an introduction of the 1999 Chi-Chi earthquake ( $M_w$  7.6), the Taiwan Chelungpu-fault Drilling Project (TCDP), the previous studies related to the earthquake and the fault zone researches will be briefly summarized. Also the purpose and the scheme of this study are presented.

The major work on identifying the Chi-Chi slip zone is shown in chapter 2. Fault gouge materials from three different fault zones of the core of TCDP Hole- B sampled by U-channels were subjected to analyze their paleomagnetic records and compare to the present day Earth magnetic dipole field in center Taiwan. In addition, some rock magnetic analyses were also analyzed for understanding the major magnetic carriers acquired the co- and/or post- seismic remanent magnetizations, which preserved in the Chi-Chi slip zone. And a simple model to explain the magnetic recording processes during a large earthquake was proposed.

A pyrite dissolution phenomenon has been reported (*Hirono et al.*, 2008). Also different magnetic minerals within the Chi-Chi slip zone have been found and described in chapter 2. To further understand the chemical/physical alteration processes about the magnetic minerals, in chapter 3, microscope observations and some further magnetic analytical results were used and discussed.

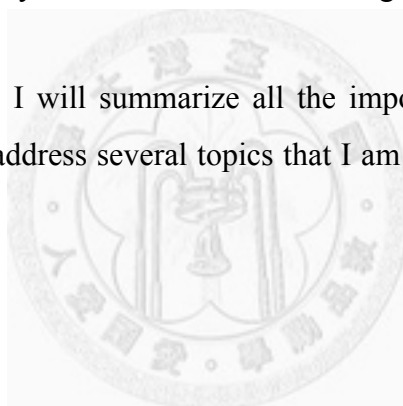
Magnetic properties of the Chi-Chi slip zone showed an offset between magnetic susceptibility and saturated isothermal remanent magnetization (SIRM). Generally, these two parameters all show the variation of the abundance of the magnetic minerals. Usually their variation trends are quite consistent, but why the offset occurred in our results is quite interesting. To figure out this offset, in chapter 4, a quantitative model of magnetic properties was developed after ruled out the affection of the superparamagnetic grains. The construction of the magnetic mineral assemblage thus was set up in the Chi-Chi slip zone. This method could also support us a new view of the neoformed magnetic minerals during post-seismic periods.

To estimate the energy budget of an earthquake is a very important topic and attracts the researchers to work on it. It is known that the fracturing processes during earthquake could ground the gouge materials, including magnetic minerals, to become much finer grain sizes. The much finer grains are found implies that the higher energy budget of the earthquake would have. Thus, in chapter 5, we tried to

identify the smallest nano-metric grains within the fault gouge, which were formed by fracture during the Chi-Chi earthquake. But the rest fault gouge material from the two cores of the TCDP boreholes after distributed to several different studies is quite limited, which is not enough for our planning analyses. Therefore, an additional larger amount gouge sample taken from a surface outcrop of the Chelungpu fault slipped during the Chi-Chi earthquake was used for the purpose of identifying the possible cutoff limit of the nano-particles.

The major analyses of this study were focused on the Chi-Chi slip zone (FZB1136) of the TCDP Hole-B. However, some preliminary studies of the other two major fault zones, FZB1194 and FZB1243 were also carried out on their magnetic properties for the purpose of delimiting the major fault zone of the Chi-Chi earthquake. These results have shown many important points. Thus, in chapter 6, I prefer to present these obtained results and try to address some interesting topics for the future further studies.

Finally, in chapter 7, I will summarize all the important results of this study. And in the chapter 8, I'll address several topics that I am interesting to study in near future.



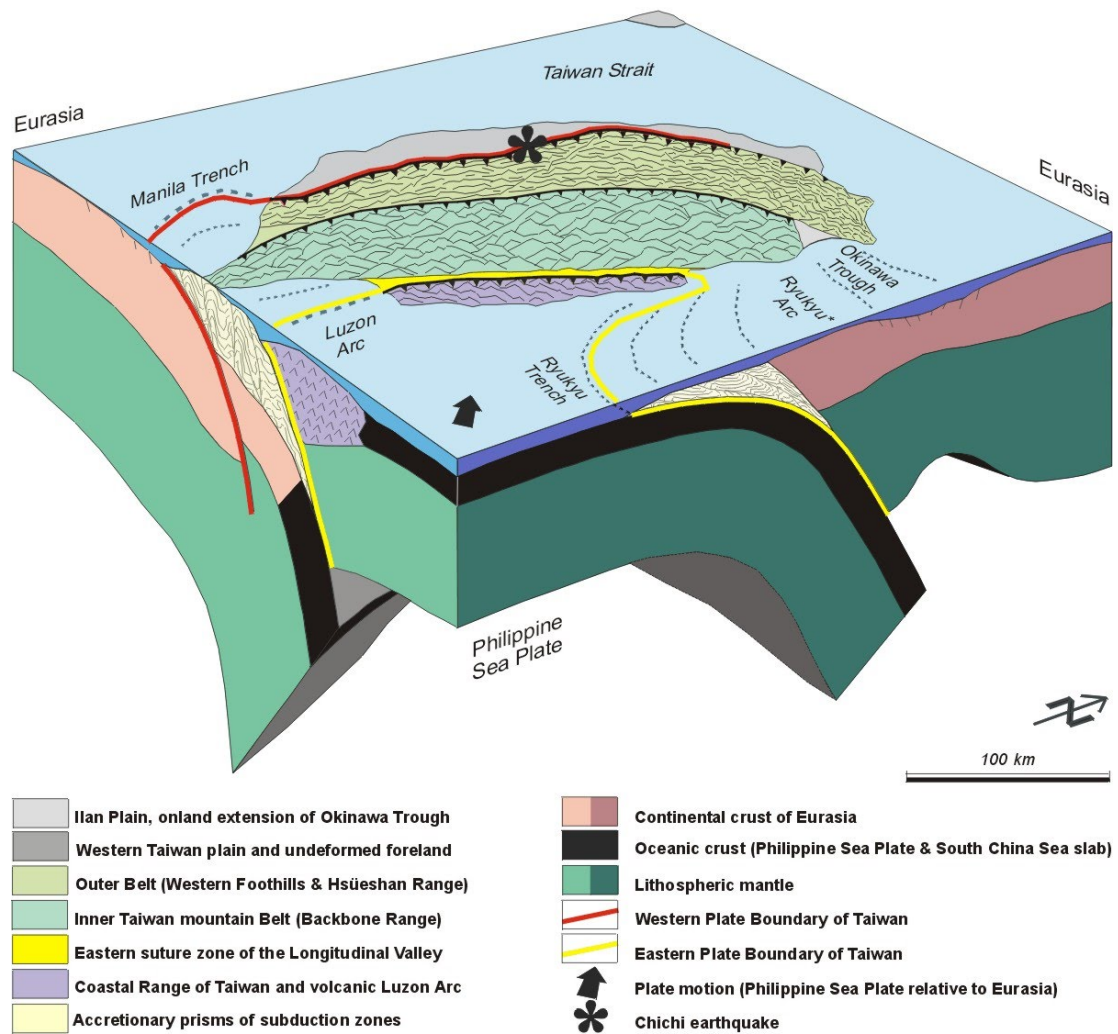


Fig. 1-1: Schematic block-diagram illustrating the lithospheric structure of Taiwan (Figure from *Angelier et al.*, 2001).



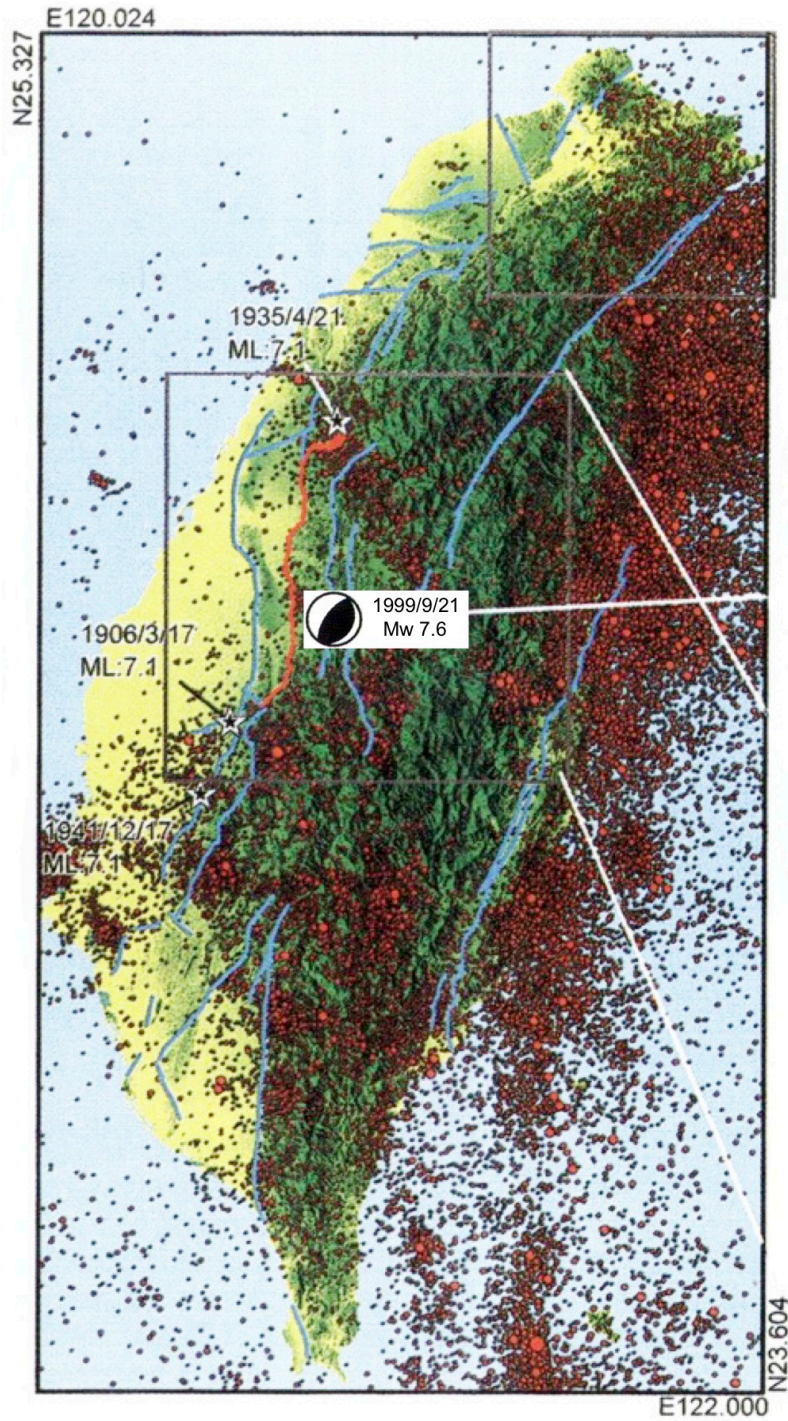


Fig. 1-2: Map of active faults and background seismicity distribution in Taiwan. The hypocentre of the 1999 Chi-Chi earthquake is located near the centre of Taiwan (120.81°E, 23.86°N) (Modified from *Ma et al.*, 1999).

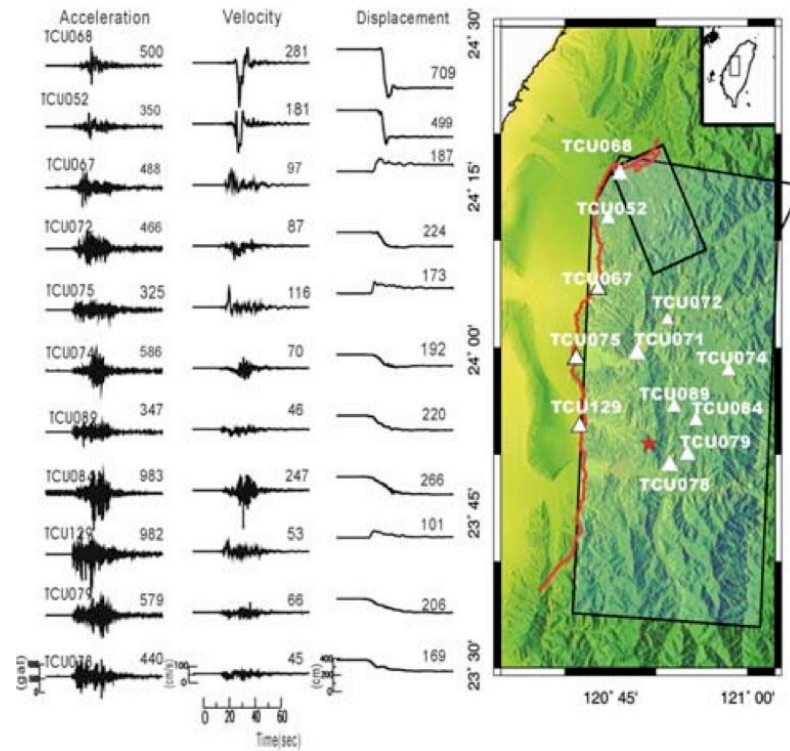


Fig. 1-3: GPS records of 1999 Chi-Chi earthquake show that the large slip velocity was observed about 3.0-4.5 m/s with 8-12 m displacements and low level of high-frequency radiation in the northern part of Chelungpu fault. But in the southern part, the slip velocity is 0.5-2 m/s with 3-4 m displacements (Figure from *Ma et al.*, 2003).

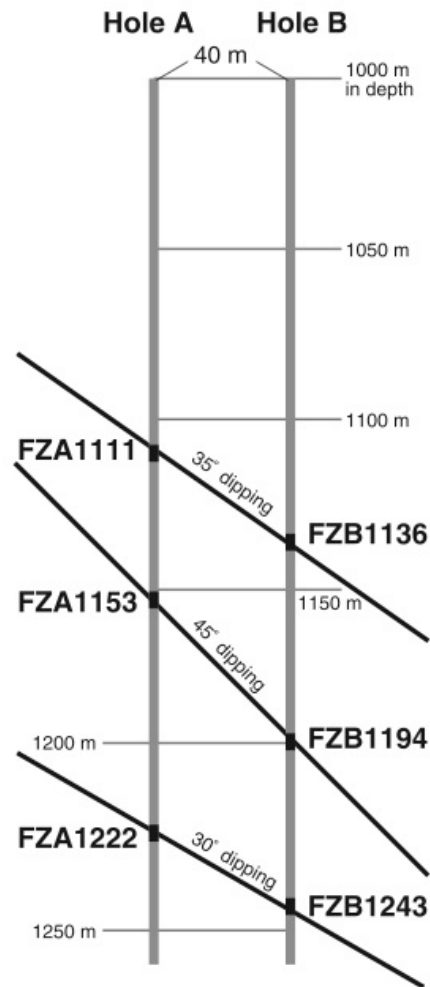


Fig. 1-4: Correlation of three major fault zones within Chelungpu fault system between TCDP Hole A and Hole B (Figure from *Hirono et al.*, 2007a).

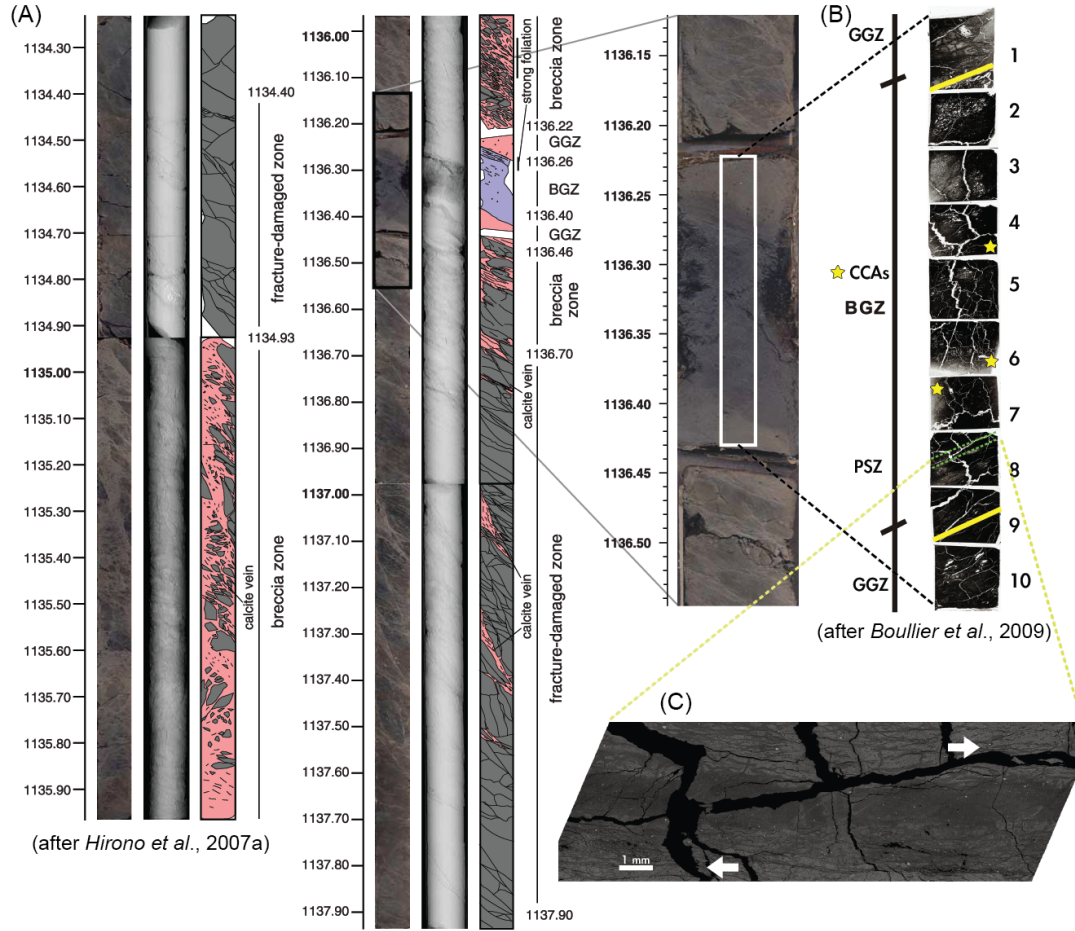


Fig. 1-5: (A) Fault zone description, X-ray CT images, and photos of FZB1136. The white frame corresponds to the locations of polished sections (after *Hirono et al.*, 2007a). (B) In the collage of SEM images from the polished sections, two yellow lines are the boundaries between gray gouge zone (GGZ) and the black gouge zone (BGZ). The yellow asterisks indicate clay-clast aggregates (CCAs). The double green dashed line is the Chi-Chi principal slip zone (PSZ) (after *Boullier et al.*, 2009). (C) This SEM image illustrates of the 3 mm-thick Chi-Chi PSZ. One can observed a dark layer with little fracturation, S-C plane and evidence for fluid circulation.



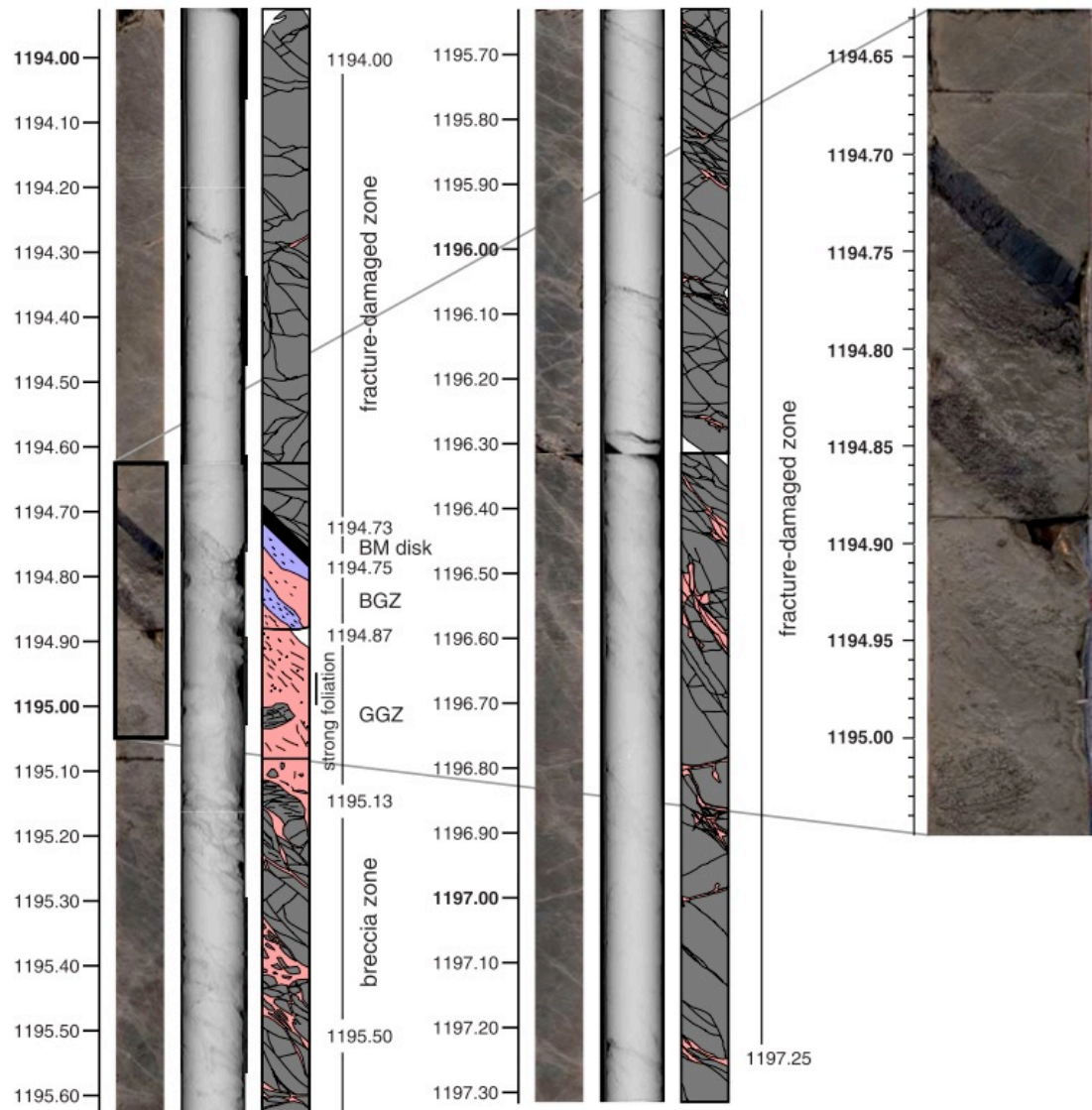


Fig. 1-6: Fault zone description, X-ray CT images, and photos of FZB1194 (Figure from *Hirono et al.*, 2007a).

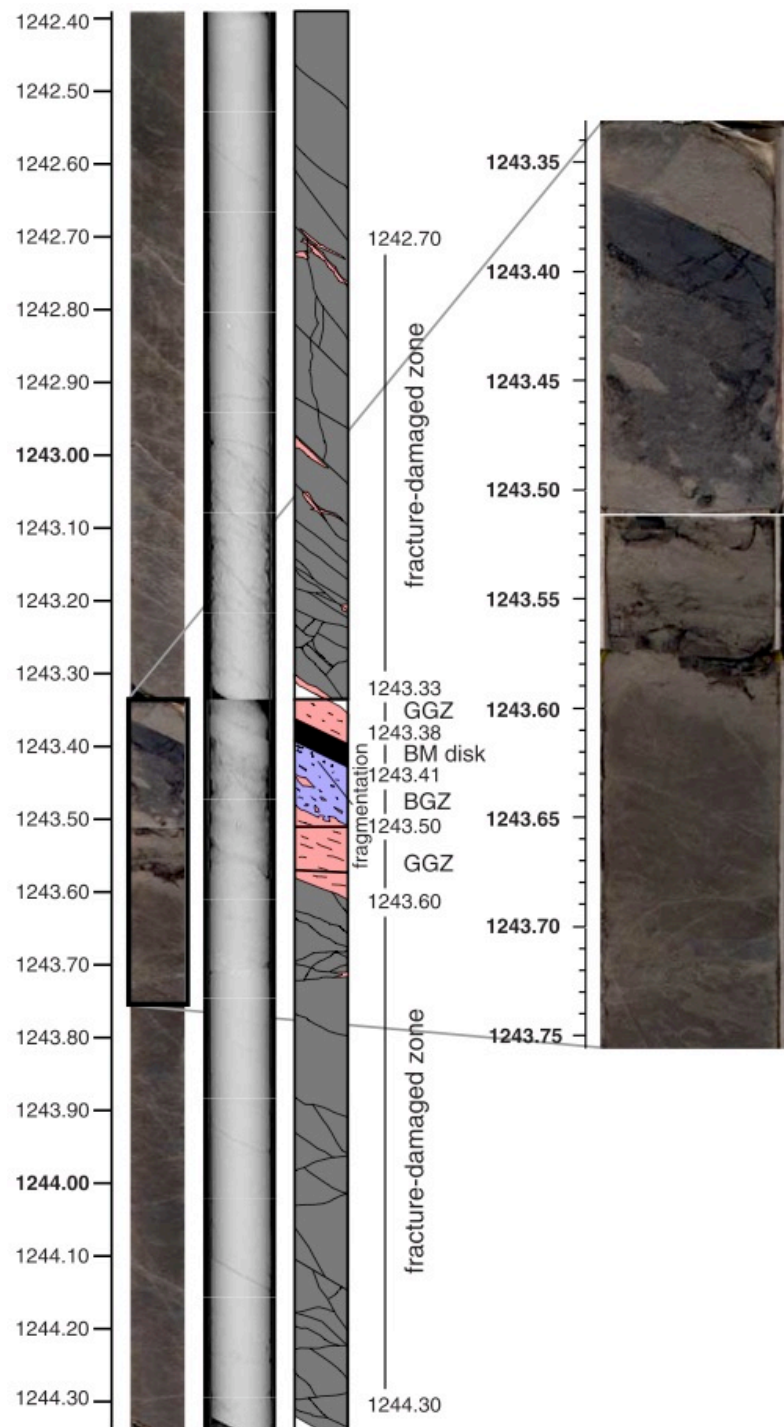


Fig. 1-7: Fault zone description, X-ray CT images, and photos of FZB1243 (Figure from *Hirono et al.*, 2007a).



Fig. 1-8: Photo of pseudotachylytes, which is found in an exposure of the Skeeter fault, USA (Figure from *Kirkpatrick et al.*, 2009).



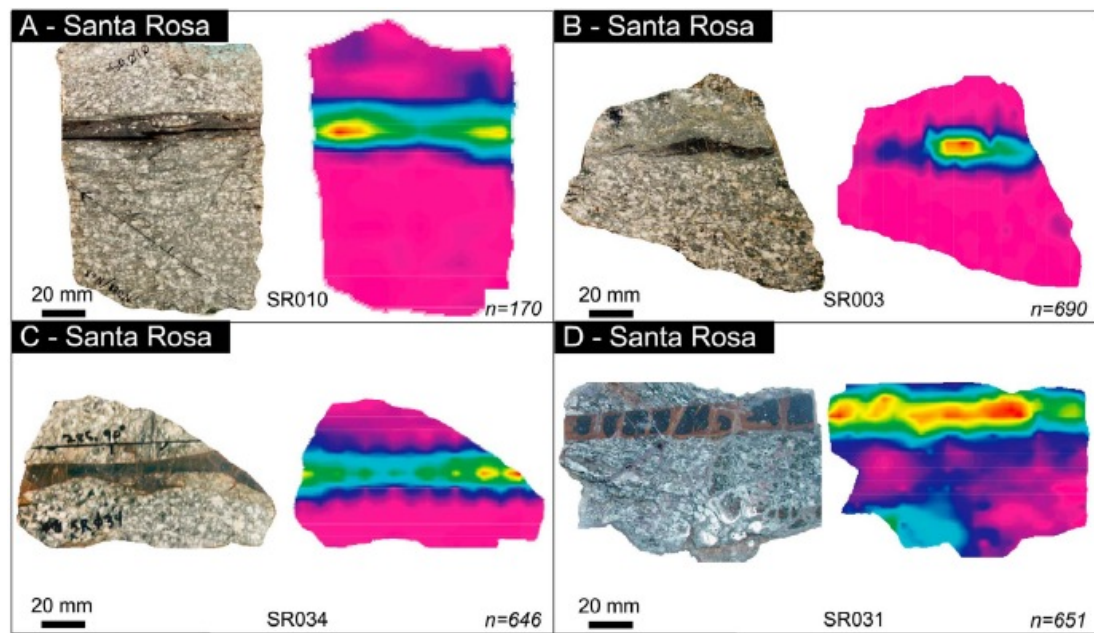


Fig. 1-9: Examples of pseudotachylytes in granite and pattern of magnetic susceptibility (Figure from *Ferré et al.*, 2012).



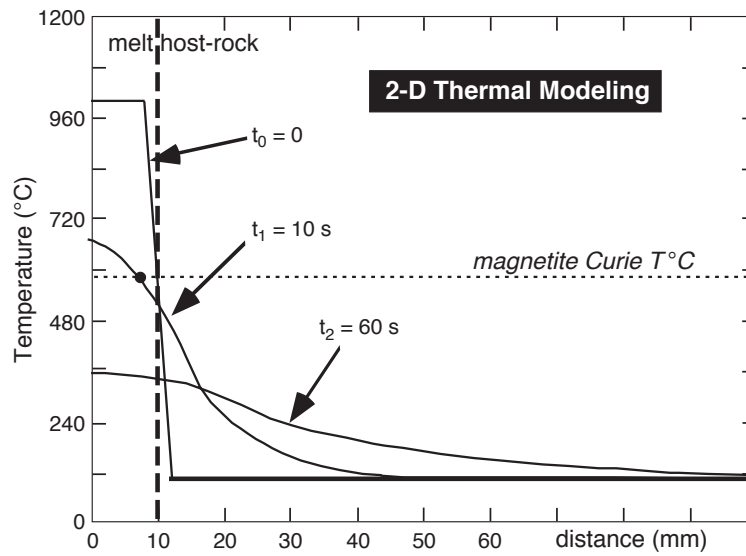


Fig. 1-10: 2-D thermal conductivity model for a pseudotachylite vein (*Peacock, 1990*; Figure from *Ferré et al., 2005*). A 20 mm-thick pseudotachylite vein and thermal transfer from slip zone to host-rock is assumed. The melt temperature is assumed to be 1000°C while the host-rock is assumed to be at 100°C. Ten seconds after slipping, the vein edge has cooled down below the magnetite Curie temperature of 580°C and block the thermoremanent magnetization (TRM) of Earth's magnetic field.

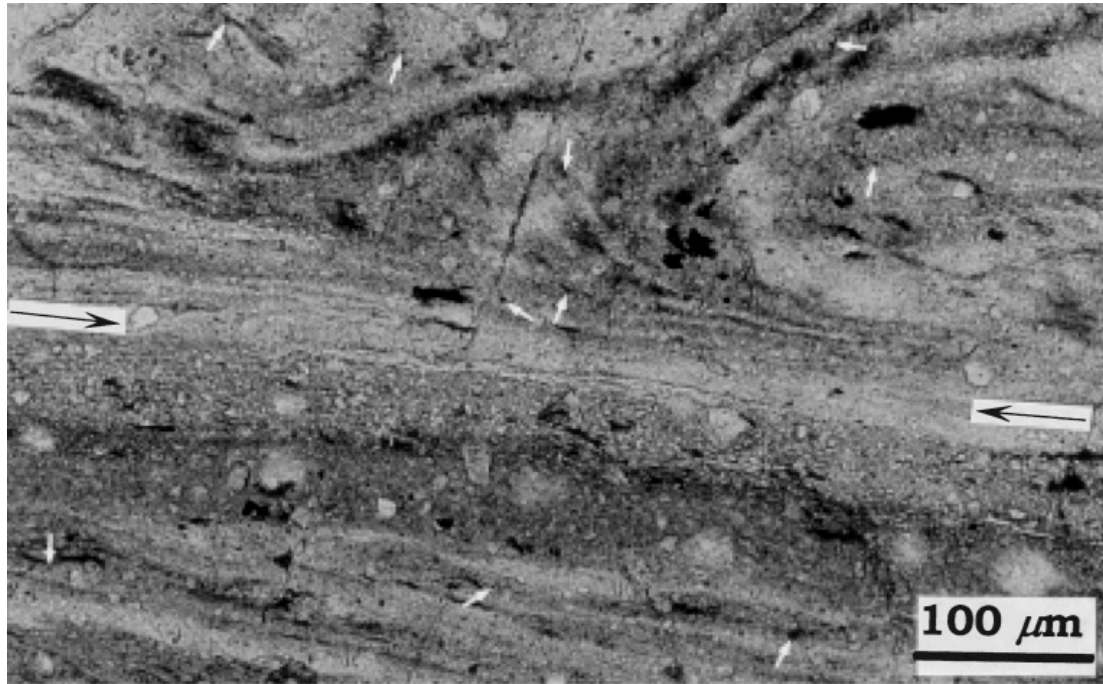


Fig. 1-11: Reflected light microscopy image of a black fault gouge in the thin section of Nojima fault, Japan (Figure from *Nakamura et al.*, 2001). Black arrows show the shear plane. White arrows indicate fine goethite grains, which are  $\sim 5 \mu\text{m}$  or less in diameter and formed euhedral sharp.

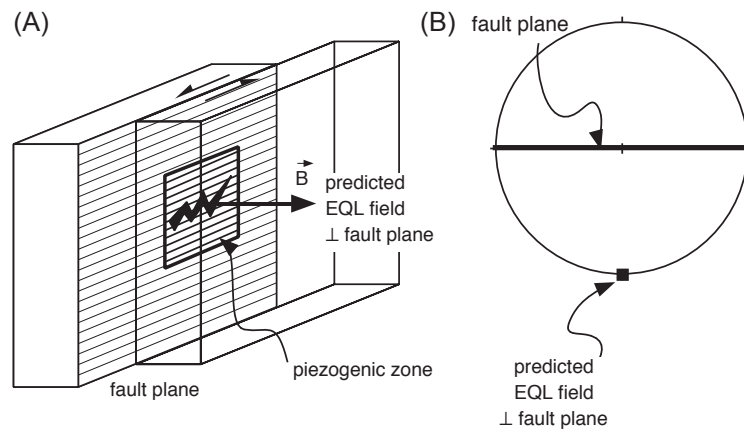


Fig. 1-12: The illustration of earthquake lightnings (EQL) predicted characteristics of NRM in fault plane (Modified from *Ferré et al.*, 2005). (A) An electrical current related to EQL along the fault plane could make a magnetic field perpendicular to the plane. (B) The fault rock could be expected to acquire a magnetization perpendicular to the fault plane.



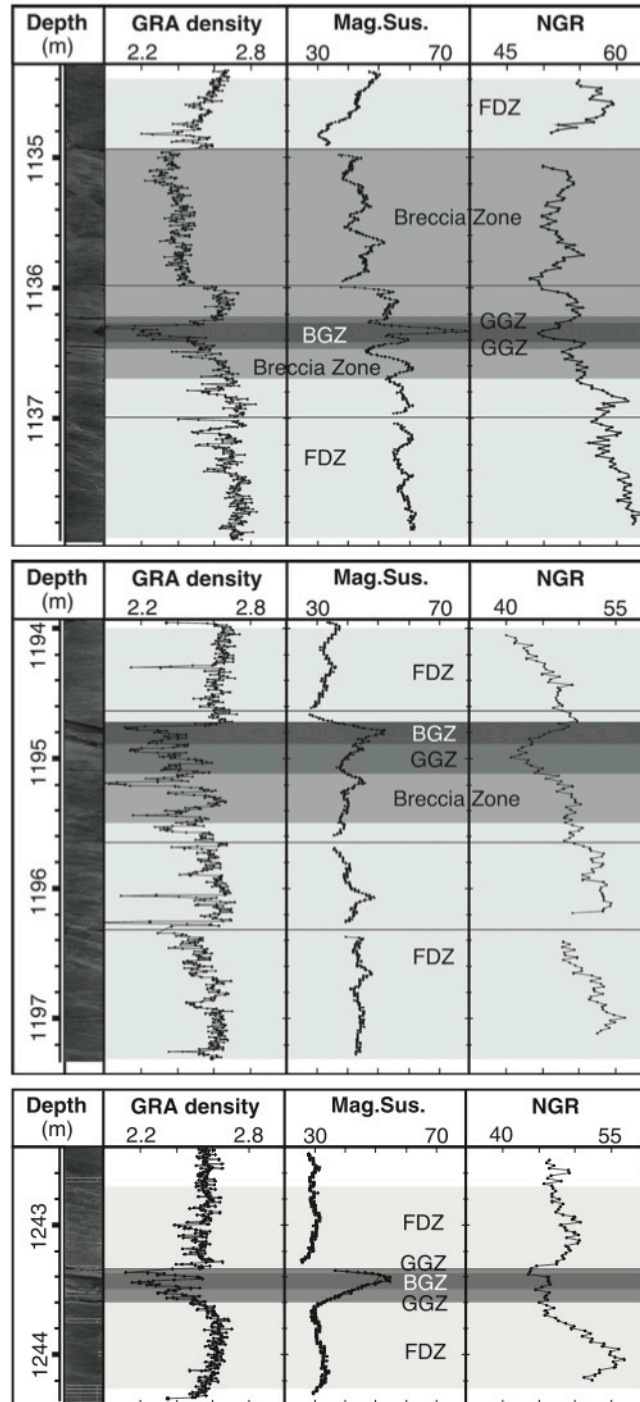


Fig. 1-13: Continuous in situ and non-destructive measurement, which were by using the Multi-Sensor Core Logger (MSCL) system in TCDP hole B has shown that three major fault zones are characterized by an increase in the magnetic susceptibility (Figure from *Hirono et al.*, 2006).

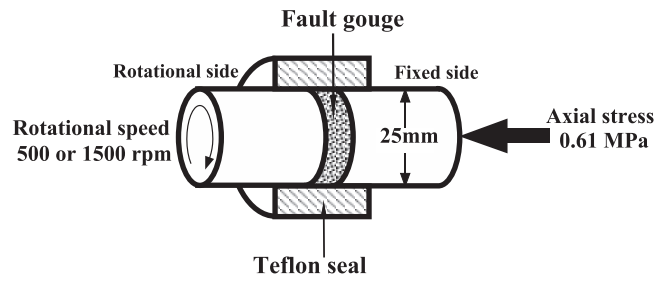


Fig. 1-14: A schematic diagram of high-speed frictional testing machine (Figure from *Fukuchi et al.*, 2005).



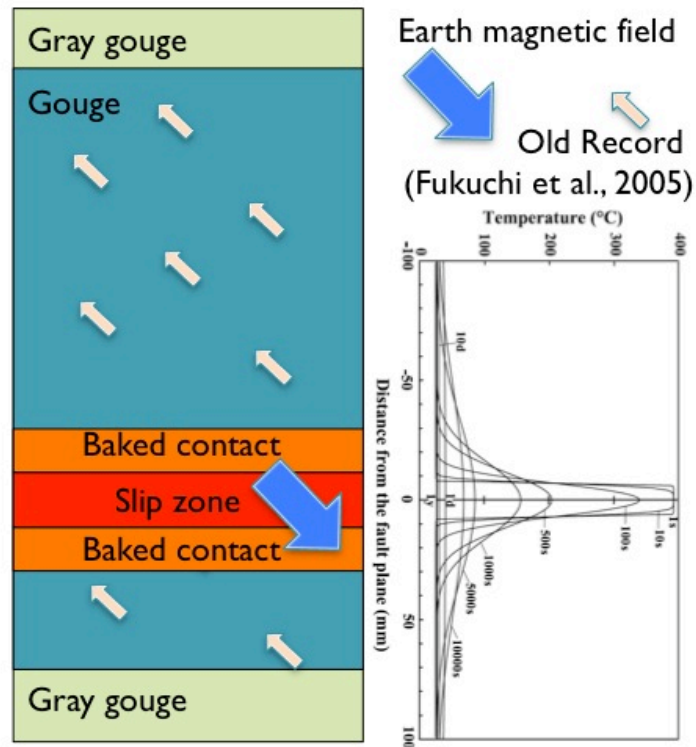


Fig. 1-15: Schematic plot of re-magnetization within a fault gouge during an earthquake. The physical/chemical alteration process (e.g. conduction and evolution of frictional heating along fault plane (after *Fukuchi et al.*, 2005)) could re-magnetize the magnetic minerals within gouge to attain new remanent magnetization of earth magnetic field.

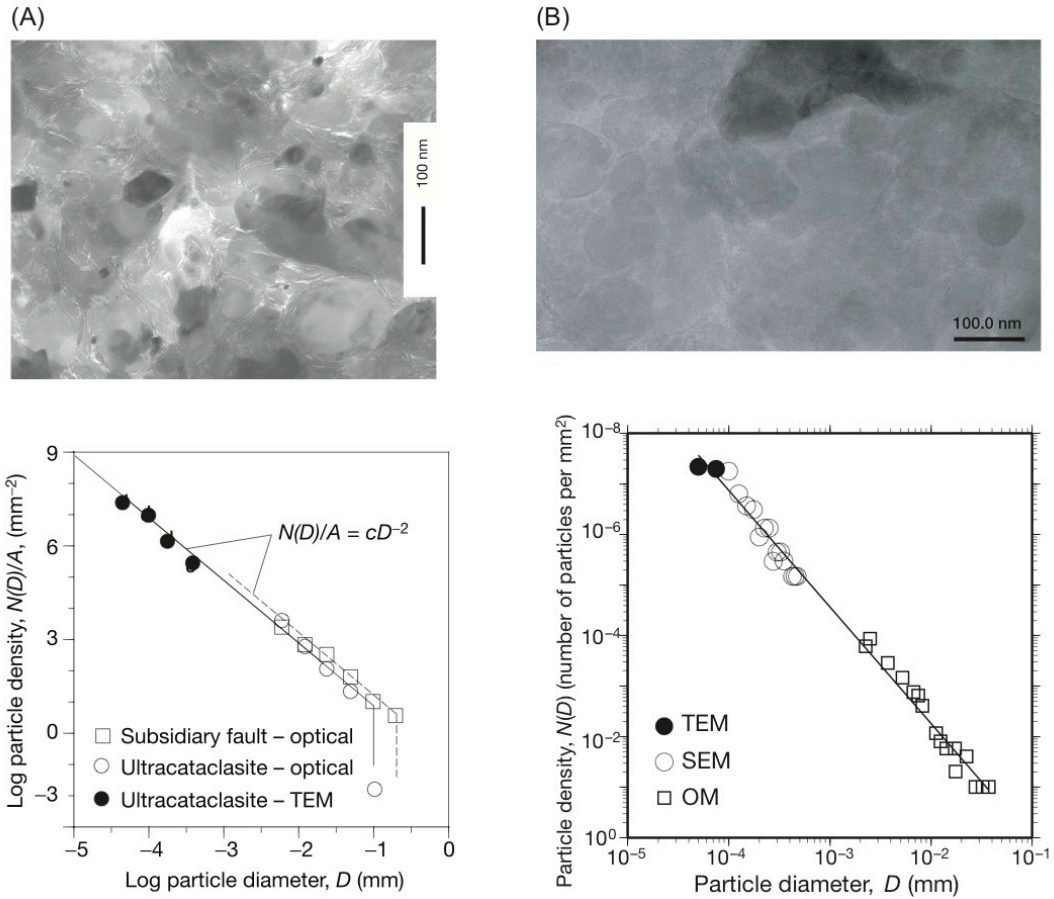


Fig. 1-16: The TEM image and particle size distribution for estimation of fracture energy between (A) *Chester et al.* (2005) and (B) *Ma et al.* (2006). The low-cut of finest particle size is 1.6 nm of *Chester et al.* (2005) and 50 nm of *Ma et al.* (2005).

## Chapter 2. An earthquake slip zone is a magnetic recorder (Geology, published)

### 2.1 Introduction

The Chi-Chi earthquake ( $M_w$  7.6, 21 September 1999) is the largest inland earthquake to hit Taiwan during the past century. The ~85 km rupture along the Chelungpu thrust extends from the north to the south (Figure 2-1A). Five years after the earthquake, two boreholes (holes A and B, 40 m apart, Taiwan Chelungpu-fault Drilling Project [TCDP]; <http://www.rcep.dpri.kyoto-u.ac.jp/~mori/ChelungpuDrilling/>) were drilled through ~2 km of alternating sandstones and siltstones of early Pliocene age. The boreholes provided fresh and unaltered material suitable for paleomagnetic investigation. In hole B, three fault zones, labeled FZB1136, FZB1194, and FZB1243 have been identified within the Chinshui Formation using core observations and physical property measurements (Hirono *et al.*, 2007) (Fig. 2-1B). From an independent data set, it was proposed that the 16 cm thick gouge of FZB1136 contained the principal slip zone (PSZ) of the Chi-Chi earthquake at 1136.38 m (Boullier *et al.*, 2009). The Chi-Chi PSZ accommodated a co-seismic displacement of ~8 m with a maximum 3 m/s velocity (Ma *et al.*, 2006). To explain some characteristics of the low friction in the northern part of the fault rupture, several authors have inferred the role of fluids and thermal pressurization processes (Boullier *et al.*, 2009; Ishikawa *et al.*, 2008). Mishima *et al.* (2009) reported evidence of neoformed magnetite ( $\text{Fe}_3\text{O}_4$ ) in Chelungpu gouges possibly due to temperature elevation >400 °C. Assuming that magnetite formed by nucleation-growth process, we expect that magnetite has the capability to record durably Earth's magnetic field. To check the existence of this record, we present a paleomagnetic and rock magnetic investigation of the three major fault zones within TCDP hole B. We identify for the first time a magnetic record that is directly related to a large-magnitude earthquake. This magnetic record is carried by magnetite within the PSZ and neoformed goethite in the entire gouge.

### 2.2 Methods

In 2008, U-channels (plastic boxes 2 cm × 2 cm, ~20 cm long, Fig. 2-2) were used to contain core samples from the working half of TCDP hole B within the gouge layers of the three fault zones, FZB1136 (1,136.22–1,136.43 m), FZB1194 (1,194.67–1,194.89 m), and FZB1243 (1,243.33–1,243.51 m). One U-channel sample was from the wall rock of the Pliocene siltstones of the Chinshui Formation (1,133.55–1,133.69



m). The U-channels were oriented geographically, with an error  $<20^\circ$ , using the bedding orientation (dip  $30^\circ$  toward N105°E; *Wu et al.*, 2008; *Yeh et al.*, 2007). The natural remanent magnetization (NRM) of each U-channel was analyzed in the automated stepwise alternating-field demagnetization process (up to 100 mT) using a 755 SRM cryogenic magnetometer manufactured by 2G Enterprises (Fig. 2-3). The residual field inside the shielded room was  $<500$  nT. A principal component analysis was used to infer paleomagnetic components. The mean vector was averaged out using Fisher statistics (*Fisher*, 1953). The stable paleomagnetic components are characterized by declination (D), inclination (I), distribution parameter ( $\kappa$ ), and the angle of confidence at the 95% level ( $\alpha_{95}$ ). To obtain complementary information on the NRM, we performed thermal demagnetization of nonoriented core fragments ( $<5$  mm). Each sample was put in an oriented glass container and was fixed by glass fiber. The stepwise heating temperature is from  $100^\circ\text{C}$  up to  $600^\circ\text{C}$  by using MMTD80 thermal demagnetizer (Figure 2-4). The remanent magnetization was measured by 2G Enterprises after each heating step. The S-ratio profile was measured along each U-channel. The S-ratio ( $\text{IRM}_{-0.3\text{T}}/\text{IRM}_{+1\text{T}}$ , where IRM is the isothermal remanent magnetization) is a proxy of magnetic coercivity (*Thompson and Oldfield*, 1986). The IRM of the samples was acquired by using a 2G cryogenic magnetometer (Fig. 2-5). It is measured at room temperature with a magnetic field applied first with 1 T, and second in the opposite direction with -0.3 T. In practice, an S-ratio close to 1 is an indication of magnetically soft minerals, such as magnetite. Its decrease points to the presence of magnetically hard minerals such as goethite and hematite. A transmission X-ray microscope image was obtained from a  $15\text{ }\mu\text{m}$  thick gouge sample of FZB1136 using the Beamline 01B1 from the National Synchrotron Radiation Research Center (NSRRC) in Taiwan.

### 2.3 Results

Within the Chinshui Formation, the NRM carries multiple paleomagnetic components, with a main component of normal polarity (Fig. 2-1C). Its  $\sim 40^\circ$  counterclockwise deviation from the modern dipole implies that this component is not a modern record. In comparison to the wall rock, the analysis of the FZB1136 gouge reveals a stable and single characteristic remanent magnetization of normal polarity, throughout its 16 cm thick layer (Fig. 2-1D). This component is close to the 1999 international geomagnetic reference field (IGRF) from central Taiwan (Fig. 2-1C). It resides essentially in hard coercive minerals because  $\sim 60\%$  of the NRM remains after

100 mT alternating-field demagnetization (Fig. 2-1E). The thermal demagnetization of core fragments reveals a linear decrease of NRM without evidence of secondary components. This is confirmed by the analysis of directional data (not shown). The analysis of the FZB1194 and FZB1243 gouges revealed multiple paleomagnetic components with both normal and reverse magnetic polarities (Fig. 2-1C). These components are oriented in a southern direction and away from the 1999 IGRF magnetic dipole field. After comparing the paleomagnetic results within the three fault zones and the wall rock, it is proposed that the single component observed throughout the FZB1136 gouge is the most recent magnetic record, and more than likely contemporaneous with the 1999 Chi-Chi seismic event. Information is provided on the magnetic carriers of the FZB1136 gouge using the unblocking temperature spectrum of NRM (Fig. 2-6A), transmission X-ray microscope observations (Fig. 2-6B), and the magnetic coercivity parameters (Fig. 2-6C). Within the gouge, the principal maximum unblocking temperature is close to 120°C (Fig. 2-6A) and is consistent with the Néel temperature of goethite ( $\alpha$ -FeOOH,  $T_N = 120^\circ\text{C}$ ), a magnetically hard antiferromagnet (*Hunt et al.*, 1995). Transmission X-ray microscopy reveals the occurrence of scattered, elongated (<5  $\mu\text{m}$  long) and dense grains in the gouge, which are likely goethite (Fig. 2-6B). Within the Chi-Chi PSZ (1,136.38 m; *Boullier et al.*, 2009), the maximum unblocking temperature is close to 580°C (Fig. 2-6A), which is the Curie temperature of magnetite ( $\text{Fe}_3\text{O}_4$ ), a magnetically soft ferromagnet (*Hunt et al.*, 1995). Thus, the single paleomagnetic component of Chi-Chi PSZ resides, essentially, in magnetite. The record of coercivity parameters (S-ratio) pinpoints the relative contribution of magnetite and goethite within the FZB1136 gouge (Fig. 2-6C). The S-ratio profile shows one relative minimum (magnetically hard) at 1,136.30 m and one maximum (magnetically soft) within the Chi-Chi PSZ. The S-ratio profile is consistent with a larger distribution of goethite in the center of the gouge layer, and a larger distribution of magnetite in the Chi-Chi PSZ. It shows that the S-ratio profile is an index to identify the most recent PSZ in the Chi-Chi gouge.

## 2.4 Discussion and conclusions

From these observations, a model of the paleomagnetic record is proposed for FZB1136. We proffer three main types of magnetization that are acquired within the slip zones during an earthquake: (1) a thermoremanent magnetization (TRM) acquired post-seismically on the cooling of the slip zone (*Ferré et al.*, 2005), (2) a chemical

remanent magnetization (CRM) acquired post-seismically and carried by neoformed magnetic minerals (*Nakamura et al.*, 2002), and (3) an isothermal remanent magnetization (IRM) acquired co-seismically during earthquake lightning (EQL) (*Ferré et al.*, 2005). An EQL magnetization would be perpendicular to the fault plane (*Ferré et al.*, 2005), which is not the case for the component of magnetization within the Chi-Chi gouge (Fig. 2-1C). Thus, we propose that EQL may be excluded as a magnetization process, and only thermal-related and chemical-related magnetic records are considered in the FZB1136 gouge. Because the magnetic carriers of the magnetic record are different, we have to distinguish scenarios in the Chi-Chi PSZ and in the rest of the gouge. A temperature elevation due to frictional heating is expected during a co-seismic slip (*Rice*, 2006). Frictional heating depends on the fault slip rate, displacement, friction coefficient, normal stress, and physical properties of the fault rocks. The ultimate phase of this process involves melting, with the formation of pseudotachylytes (*Di Toro et al.*, 2006). The temperature peaks in the gouge and the Chi-Chi PSZ are still being debated, but generally, a lower limit of 400°C is accepted (*Boullier et al.*, 2009; *Mishima et al.*, 2009). The PSZ cooling lasts only tens of seconds, and the thermal aureole extends less than the width of the PSZ (*Kano et al.*, 2006). Upon cooling, a TRM is imprinted in the magnetic minerals contained in the PSZ and the baked contact. Within the 16 cm of gouge that carries the stable paleomagnetic component, only the millimeter-thick heated layers on both sides of the Chi-Chi PSZ have the potential to carry a friction-induced TRM. Experimental heating of the FZB1136 gouge showed that magnetite formed above 400°C (*Mishima et al.*, 2009). It is therefore proposed that the paleomagnetic record of the Chi-Chi PSZ and baked contact is partly a TRM carried by former magnetic minerals and partly a CRM carried by neoformed magnetite. The paleomagnetic record in the 16 cm gouge is essentially carried by goethite, and other processes of magnetization should be viewed apart from the Chi-Chi PSZ and baked contact. To date, this is the first time that goethite has been reported in the Chelungpu fault. *Nakamura and Nagahama* (2001) observed similar, ~5 µm, goethite within the Nojima fault gouge (Japan). They suggested that the goethite growth postdates the grain alignment of silicate minerals. Within the FZB1136, scattered ~5 µm elongated goethite could be observed, which supports the theory that goethite growth postdates the broad texture of gouge (Fig. 2-6B). In order to crystallize, goethite requires water, temperature <200°C, and low pH and iron (*Cornell and Schwertmann*, 2003). Therefore, the goethite attests to the presence of water in FZB1136. Recent

geochemical investigations in the FZB1136 gouge suggest the presence of pore fluids with a minimum temperature of 350°C (*Ishikawa et al.*, 2008). It is then possible that goethite formed upon the cooling of the pore fluids. The source of iron could possibly be brought about by the dissolution of iron sulfide in the FZB1136 gouge (*Yeh et al.*, 2007). The dissolution of pyrite not only releases  $\text{Fe}^{2+}$  and  $\text{SO}_4^{2-}$  ions but also decreases the fluid's pH (*Nakamura and Nagahama*, 2001). It is therefore suggested that goethite is formed post-seismically within a few days of the earthquake's occurrence. Upon growing larger than the  $\sim 1800 \text{ nm}^3$  blocking volume (minimum volume for recording remanent magnetization; *Cornell and Schwertmann*, 2003), the goethite acquires a CRM. The recovery of a single-component record from within the FZB1136 gouge, unlike adjacent fault zones, implies the partial or complete removal of the magnetic records of ancient slip zones. It remains to be proven whether this behavior is related to earthquakes of large magnitudes (e.g.,  $M_w > 7$ ). The post-seismic magnetic record is instantaneous in the geological time scale, but it has the potential to survive for millions or even billions of years (*Néel*, 1955). Thus, the fault gouge can retain the magnetic record during inter-seismic time. It is suggested that the fault gouge magnetic record is a record of the latest earthquake event if only a single component is recovered, as in the case of the Chi-Chi gouge. If several components are detected, as in the fault zones FZB1194 and FZB1243, it is possible that the components overlap each other due to perturbation. Therefore, we propose the following scenario of a cycle of magnetic record during a large earthquake similar to Chi-Chi (Fig. 2-7).

1. During inter-seismic periods, the magnetic record of the latest large earthquake is preserved within the fault gouge.
2. During the co-seismic period, the gouge acts essentially as a magnetic eraser. Both the temperature elevation above the unblocking temperature of magnetic minerals and the chemical degradation of these minerals lead to the partial-to-complete demagnetization of the gouge. The exact mechanisms remain to be definitively determined, but in the Chi-Chi gouge, the  $>350^\circ\text{C}$  hot fluids (*Ishikawa et al.*, 2008) have probably demagnetized the former goethite.
3. During the post-seismic period, the gouge acts as a magnetic recorder. The cooling of the gouge and/or fluids leads to a TRM imprint. Similarly, neoformed minerals resulting from any form of chemical process have the potential to carry a CRM. If confirmed by further studies, this proposed

seismic cycle of magnetic records opens new horizons for paleoseismology as well as for PSZ identification and dating. To identify a PSZ, methods based on microscopy (*Boullier et al.*, 2009), geochemistry (*Hirano et al.*, 2008), or physical properties (*Wu et al.*, 2007) are not one-to-one because several PSZs may stack together in the gouge.

In this study, the Chi-Chi gouge layer was identified using the orientation of the magnetic record; the location of the millimeter-thick Chi-Chi PSZ was pinpointed using rock magnetism characteristics. This constitutes a new, fast, and nondestructive way to find the most recent PSZ.



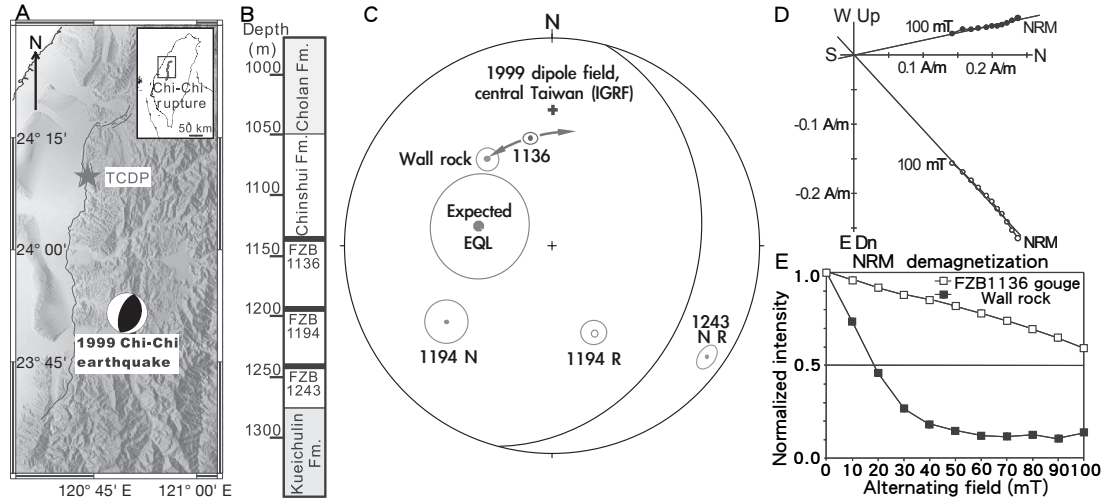


Fig. 2-1: Locations, major fault zones and paleomagnetic records. (A) A geological map showing the epicenter of Chi-Chi earthquake (M<sub>w</sub> 7.6, 1999) and the Taiwan Chelungpu-fault Drilling Program (TCDP) drilling site at 120.73916°E, 24.20083°N (Modified from *Ma et al.*, 2006). FZB stands for Fault Zone of hole B. (B) A Schematic log of the borehole showing the three major fault zones of the Chelungpu fault within the Chinshui Formation. (C) Equal-area stereo-plot displaying the Chelungpu fault plane and the mean paleomagnetic components recorded in the three fault zones and wall rock. Due to the orientation of the borehole B, there is an error of  $\pm 20^\circ$  in declination for all paleomagnetic component. This error is indicated for the FZB1136 gouge component. We plot the orientation of an expected earthquake lightning (EQL) according to the model of *Ferré et al.* (2005) with  $20^\circ$  error in orientation. The black (open) symbols correspond to the downward (upward) hemisphere. The cross indicates the 1999 international geomagnetic reference field (IGRF) dipole magnetic vector ( $D = 0.2^\circ$ ,  $I = 29.7^\circ$ ). The wall rock's main component lies away from the modern magnetic field ( $D = 322^\circ$ ,  $I = 48^\circ$ ,  $\kappa = 99$ ,  $\alpha_{95} = 4^\circ$ ; range 10–80 mT). The FZB1136 gouge component ( $D = 348^\circ$ ,  $I = 48^\circ$ ,  $\kappa = 140$ ,  $\alpha_{95} = 2^\circ$ ) is the closest to the modern magnetic field and statistically different from a hypothetical EQL. Within the FZB1194 gouge, normal and reverse components are southerly oriented ( $D = 235^\circ$ ,  $I = 27^\circ$ ,  $\kappa = 110$ ,  $\alpha_{95} = 8^\circ$  and  $D = 154^\circ$ ,  $I = -52^\circ$ ,  $\kappa = 144$ ,  $\alpha_{95} = 5^\circ$ ), respectively. Within the FZB1243 gouge, normal and reverse components are also oriented southerly ( $D = 125^\circ$ ,  $I = 11^\circ$ ,  $\kappa = 189$ ,  $\alpha_{95} = 4^\circ$  and  $D = 125^\circ$ ,  $I = -10.0^\circ$ ,  $\kappa = 280$ ,  $\alpha_{95} = 3^\circ$ ), respectively. (D) The natural remanent magnetization (NRM) orthogonal plot of FZB1136 gouge (depth 1,136.33 m). Open (black) circles represent projection of the vector along the vertical (horizontal) plane. (E) Curves of normalized NRM intensity of FZB1136 and wall rock.



Fig. 2-2: Photo of one U-channel in this study. The U-channel is a plastic box of 2 cm  $\times$  2 cm with  $\sim$ 20 cm long.



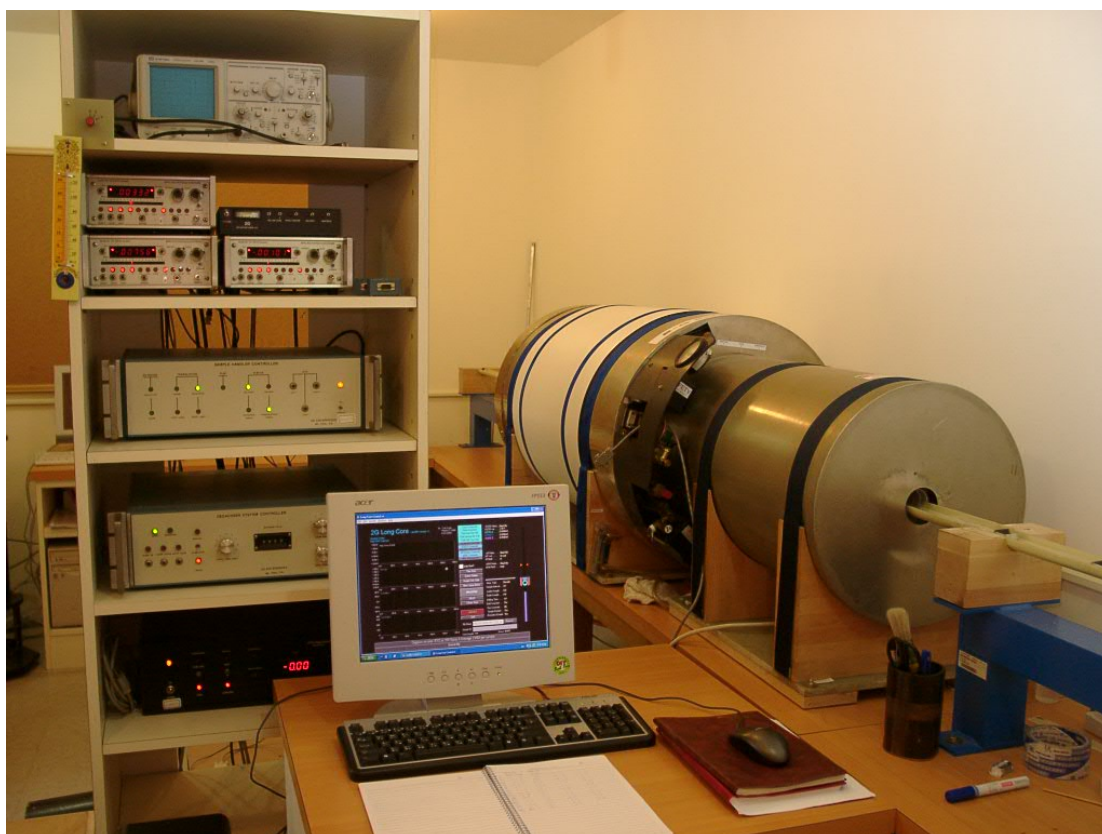


Fig. 2-3: The 755 SRM cryogenic magnetometer manufactured by 2G Enterprises in the magnetic shielding room at the Institute of Earth Sciences, Academia Sinica, Taiwan.





Fig. 2-4: The stepwise heating temperature is from 100°C up to 600°C by using the MMTD80 thermal demagnetizer.



Fig. 2-5: The IRM of the samples was acquired from 25 mT up to 950 mT by using a 2G cryogenic magnetometer.

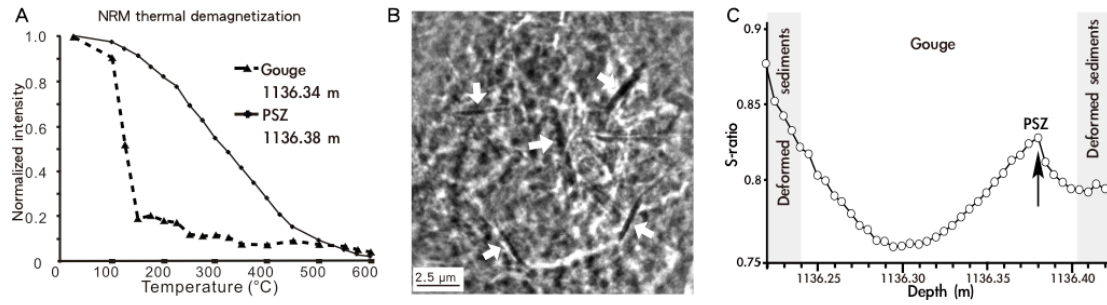


Fig. 2-6: NRM thermal demagnetization, TXM photo, and S-ratio. (A) The NRM thermal demagnetization for a gouge sample (depth of 1,136.34 m) and the Chi-Chi's principal slip zone (PSZ) (depth of 1,136.38 m) within FZB1136. In the gouge, there is a break-in-slope near 150°C where ~80% of the NRM is lost. The remaining part of the NRM has a maximum unblocking temperature close to 580°C. In the Chi-Chi's PSZ, the maximum unblocking temperature is close to 580°C. (B) The TXM photo from a 15 mm thick polished-section collected from a gouge within FZB1136. Scattered elongated dense minerals with a low aspect ratio 2:25 and maximum length of 5 mm are likely to be goethite. (C) The S-ratio profile along the U-channel. The lowest value of the S-ratio (magnetically hard) is located at a depth of 1,136.30 m, near the center of the gouge and corresponds to the highest concentration in goethite. The Chi-Chi's PSZ is marked by an enhancement of the S-ratio, which is consistent with a larger contribution of magnetite.

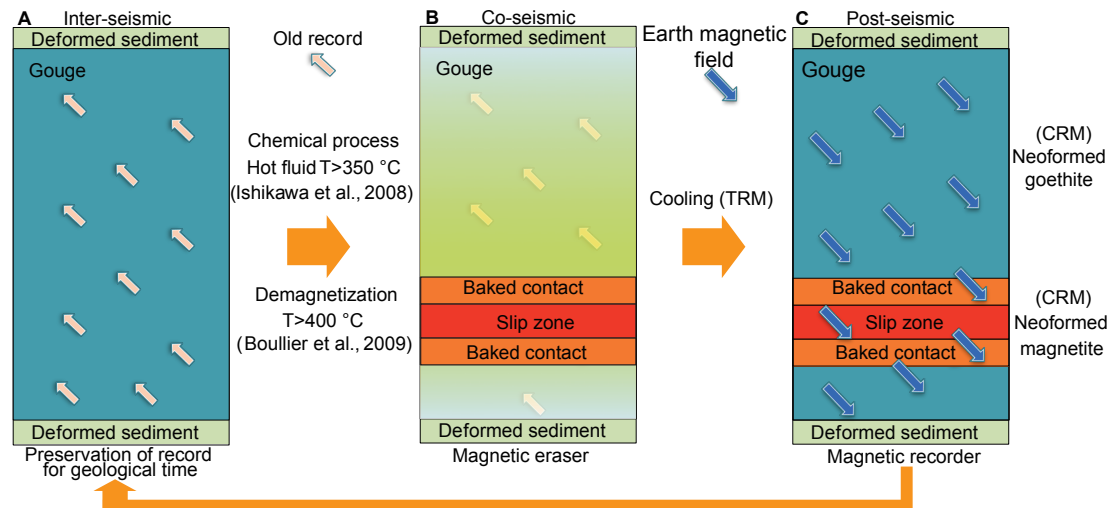


Fig. 2-7: The magnetic record cycle of a fault gouge. 1) During an inter-seismic period, the magnetic record of an old earthquake is preserved within the fault gouge through geological times. 2) During a co-seismic period, the gouge acts as a magnetic eraser. At the PSZ and baked contact the temperature elevation and chemical degradation lead to the partial-to-complete demagnetization of the gouge. The co-seismic hot fluids probably demagnetized the former goethite. 3) During a post-seismic period, the gouge acts as a magnetic recorder. Cooling of the gouge or fluids leads to a thermo-remanent magnetization (TRM) imprint. Neoformed minerals resulting from any form of chemical processes, including cooling, carry a chemical-remanent magnetization (CRM).

### **Chapter 3. Pyrite alteration and neoformed magnetic minerals in the fault zone of the Chi-Chi earthquake ( $M_w$ 7.6, 1999): Evidence for frictional heating and co-seismic fluids (Geochemistry, Geophysics, Geosystem, published)**

#### **3.1 Introduction**

High-friction fault slip zones formed during earthquakes or laboratory experiments have distinguishable textures and mineral characteristics (*Nakamura et al.*, 2002; *Fukuchi et al.*, 2005; *Tanikawa et al.*, 2007; *Boullier et al.*, 2009). In principle, characterization of slip zones may be relevant for assessing physical processes such as frictional heating, thermal pressurization, fracture energy, redox conditions, etc. In siliciclastic sedimentary environments, faults can develop within siltstones. These detrital rocks typically contain accessory minerals like siderite, iron oxides, and iron sulfides. Among these accessory minerals, pyrite ( $\text{FeS}_2$ ) is worthy of study across slip zones for several reasons: 1) it is common within fine-grained sediments with a concentration of about 1% (*Berner*, 1984); 2) it is easy to identify using optical microscopy or electron microscopy; 3) it generally has a euhedral morphology with well-calibrated size distributions (*Craig et al.*, 1998); 4) pyrite crystals often cluster in so-called framboids that are as large as tens of microns across (*Craig et al.*, 1998); 5) it alters rapidly with temperature and in the presence of certain fluids; and releases  $\text{SO}_4^{2-}$  and  $\text{Fe}^{2+}$  (*Jovanović*, 1989; *Music et al.*, 1992; *Lambert et al.*, 1998; *Pelovski and Petkova*, 1999; *Mayoral et al.*, 2002); 6) pyrite alteration lowers pH, which can result in dissolution of carbonate minerals that can then reprecipitate in the gouge (*Liu and Liu*, 2004).

In fault zones, magnetic minerals are of interest because magnetic susceptibility anomalies have been reported in gouge and pseudotachylites (*Nakamura et al.*, 2002; *Mishima et al.*, 2007; *Tanikawa et al.*, 2007; *Ferré et al.*, 2012). Similarly, *Nakamura et al.* (2002) and *Ferré et al.* (2005) suggested that magnetic minerals form during frictional melting associated with fault displacement during earthquakes. Generally, magnetic minerals are difficult to observe using optical or electron microscopy because of their low concentration (<0.1%) and small grain size (<1  $\mu\text{m}$ ). However, it is relatively easy to determine the nature, size and concentration of magnetic minerals using rock magnetic methods (e.g., *Hunt et al.*, 1995). Comparison between the magnetic mineral assemblage of wall rocks and fault gouge can help to determine the nature of neoformed magnetic minerals.

During the Chi-Chi earthquake ( $M_w$  7.6, 1999), a large ~80 km rupture occurred along the Chelungpu thrust (*Ma et al.*, 1999). The Chelungpu thrust propagates through the siliciclastic early Pliocene Chinshui Formation where pyrite framboids are initially present in the undeformed sediment (*Boullier et al.*, 2009). However, *Hirono et al.* (2008) reported a lack of pyrite in the gouge zone. Similarly, *Hirono et al.* (2007b) and *Ishikawa et al.* (2008) observed an abundance of  $SO_4^{2-}$  in the gouge zone and related it to pyrite dissolution. The gouge zone is also marked by a magnetic susceptibility peak due to the contribution of neoformed ferrimagnetic minerals (*Mishima et al.*, 2009). There is, therefore, an apparent correlation between the lack of pyrite and neoformed magnetic minerals that we would like to elucidate. Using unaltered samples from the Taiwan Chelungpu-fault Drilling Project (TCDP) Hole B borehole (*Hirono et al.*, 2007a; *Song et al.*, 2007a; *Yeh et al.*, 2007), we determined how pyrite alter with the gouge and established the magnetic mineralogy of the Chinshui Formation and the gouge that hosts the 1999 Chi-Chi principal slip zone. The peak temperature reached in the gouge during the Chi-Chi earthquake is still debated; however, we show that identification of neoformed magnetic minerals provides additional evidence to estimate peak temperature and the presence of co-seismic fluids.

### 3.2 Geologic setting

In Taiwan, one of the largest inland earthquakes ( $M_w = 7.6$ ) took place on 21 September 1999, near the town of Chi-Chi (hypocentre  $120.81^\circ$  E,  $23.86^\circ$  N, depth ~10 km (*Ma et al.*, 1999; *Kao and Chen*, 2000), which caused large-scale casualties (2,321 deaths, 10,000 injured) and destruction (more than 100,000 buildings were damaged or destroyed). During the 1999 Chi-Chi earthquake, the surface rupture closely followed the ~80 km Chelungpu fault, which is one of the most active faults in western Taiwan (*Chen et al.*, 2002). The Chelungpu fault system is an out-of-sequence thrust (Fig. 3-1A), which is part of the ramp of a ~20 km fault-bend-fold that is now largely eroded (*Yue et al.*, 2005; *Yeh et al.*, 2007). The TCDP was designed to drill two cores in DaKeng, central Taiwan (Fig. 3-1A, B) (*Yeh et al.*, 2007). Hole A (depth 2,003 m) and Hole B (depth 1,352.6 m) are separated by 40 m. At the location of the two boreholes, the estimated slip during the 1999 Chi-Chi earthquake is ~8 m (*Ma et al.*, 2003). Three major fault zones were identified within the Chinshui Formation (*Hirono et al.*, 2007a). From independent datasets, different authors proposed that the fault zone at 1,111 m depth and 1,136 m depth for Hole A

and B, respectively, contains the principal slip zone (PSZ) of the Chi-Chi earthquake (Kano *et al.*, 2006; Ma *et al.*, 2006; Song *et al.*, 2007a; Wu *et al.*, 2007; Chou *et al.*, 2012). Boullier *et al.* (2009) determined the location of the Chi-Chi PSZ by identifying a ~2 cm (Hole A) to 3 mm (Hole B) thick gouge layer. The PSZ differs from other ancient slip zones in that it has not been affected by any later compaction or deformation (veins, fractures, or shear zones). The PSZ at 1,136 m does not show evidence of melting (Boullier *et al.*, 2009).

The lower Pliocene Chinshui Formation (also called the Chinshui Shale) consists of alternating siltstones and ~10-cm-thick sandstones. Minerals in the siltstones are quartz, clays, and accessory minerals (feldspar, calcite) (Isaacs *et al.*, 2007). Clay minerals consist of an assemblage of illite, chlorite, and kaolinite with accessory smectite (Kuo *et al.*, 2009). Organic matter is present at a concentration of ~1% in the sediments, but its quantity is less than 0.7% in the fault zone (Ikehara *et al.*, 2007). Iron sulfides are common in the undeformed and deformed sediments (Boullier *et al.*, 2009). The Chinshui siltstones are unmetamorphosed with a recorded peak temperature due to modest burial of ~120°C based on vitrinite reflectance (Sakaguchi *et al.*, 2007).

### 3.3 Sampling and Methods

For this study, we sampled the Chinshui Formation in TCDP Hole B across the ~20-cm-thick fault zone (from 1,136.22 m to 1,136.43 m) together with wall rocks at different depths (Fig. 3-2A, B; samples are listed in Table 3-1). In addition, we analysed ten (2.5 cm × 2 cm) polished thin sections that were cut perpendicular to bedding within the fault plane (samples 1 to 10, Fig. 3-2C) that were thoroughly described by Boullier *et al.* (2009). These sections contain the boundaries between the gouge, the hanging wall, and the foot-wall deformed sediments. The deformed sediments were initially labelled ‘grey gouge’ principally because of their color (Hirono *et al.*, 2007a). However, within the ‘grey gouge’, bedding is preserved and thus the ‘grey gouge’ cannot be genetically related to gouge formation. To avoid confusion, we abandon the name ‘grey gouge’ in favor of ‘deformed sediments’ and we call gouge the ‘black gouge’ horizon. The ~16-cm-thick gouge, which is surrounded by deformed sediments, constitutes a horizon of gouges where the bedding or other sedimentary structures are no longer preserved. Some gouges are reworked and are interpreted as ancient slip zones (Boullier *et al.*, 2009). A 3-mm-thick level of gouge in thin section 8 (Fig. 3-2C) is not reworked and consists



of alternating clay-rich and clast-rich layers. *Boullier et al.* (2009) proposed that this slip zone was generated during the 1999 Chi-Chi event. Hereafter, it is referred to as the PSZ. From the 10 thin sections, we made scanning electron microscope (SEM) observations coupled with energy dispersive spectrometry (EDS) measurements and reflected-light polarizing microscope observations. We also made transmission X-ray microscopy (TXM) observations on 17 polished thick sections from the working section of TCDP Hole B core (Table 3-1). From these polished thick sections, we cut a few millimeter-long pieces and impregnated them with resin. Then, we cut each section into  $\sim 15\text{-}\mu\text{m}$ -thick samples for TXM observation. We obtained fourteen  $15\text{-}\mu\text{m}$ -thick samples from the fault zone, and three from the two parts of the hanging-wall and foot-wall deformed sediments (Fig. 3-2A, Table 3-1). For magnetic property measurements, we sampled hundreds of milligrams of rock powder within the  $\sim 20\text{-cm}$ -thick fault zone, including deformed sediments and gouge.

We used a LEO Stereoscan 440 SEM equipped with EDS (Analyzer EDX KEVEX SYGMA) for elemental analysis. The SEM was operated at 15 keV with 4 nA current. For TXM observation, we used the BL01B Beamline with 60 nm tomographic resolution at the National Synchrotron Radiation Research Center (NSRRC), Taiwan (*Yin et al.*, 2006; *Song et al.*, 2007b). A superconducting wavelength shifter source provides a measured photon flux of  $4.5 \times 10^{11}$  photons/s/0.1% bw in the energy range 5–20 keV. X-rays generated by a wavelength shifter are primarily focused at a charge-coupled detector by a toroidal focusing mirror with a focal ratio of nearly 1:1. A double crystal monochromator that exploits a pair of Ge (111) crystals selects X-rays of energy 8–11 keV. After the focusing mirror and double crystal monochromator, a capillary condenser further shapes the X-ray beam. The condenser intercepts the impinging X-rays and further focuses them onto the sample. The image of the sample is magnified with a zone plate. The field of view of the image is  $15 \times 15 \mu\text{m}^2$  for the first-order diffraction mode of the zone plate. The phase term can be retrieved by the Zernike's phase contrast method for imaging light materials. The phase ring positioned at the back focal plane of the zone plate results in a recording of the phase contrast images at the detector. By acquiring a series of two-dimensional (2-D) images with the sample rotated stepwise, three-dimensional (3-D) tomography datasets are reconstructed from 141 images from  $-70^\circ$  to  $+70^\circ$ . We scanned each sample over an area of  $2700 \mu\text{m}^2$ .

We also conducted a non-destructive magnetic investigation at room temperature (300 K) and at low temperature (10 to 300 K) to characterize the magnetic mineral



assemblage in the deformed sediments and gouge in the Chi-Chi fault zone. In a first set of experiments, we measured the low-temperature dependency of a saturation isothermal remanent magnetization (SIRM) using a Quantum Designs Magnetic Property Measurement System (MPMS) XL5 EverCool system at the Institute de Physique du Globe de Paris (IPGP), France. To impart an SIRM, a magnetic field of 2.5 T was applied, either at room temperature (RT-SIRM at 300 K) or at low temperature (LT-SIRM at 10 K). We monitored successively the cooling and the warming demagnetization curves of the RT-SIRM and the LT-SIRM. We refer to warming curves of LT-SIRM as ZFC (zero field cooled). During cooling of the RT-SIRM, a positive magnetic field of 5  $\mu$ T ( $\sim 1/10$  of the Earth's magnetic field) was applied to enable detection of a potential Néel transition. For samples M3, M4, and M5 (Table 3-1), we cycled the RT-SIRM during cooling and warming (cycling RT-SIRM). For this procedure, we removed the 5  $\mu$ T magnetic field, and the residual magnetic field in the MPMS was  $<0.1$   $\mu$ T. We measured  $\sim 400$  mg of rock powder sealed in a gel-cap. In a second set of experiments, we measured first-order reversal curves (FORCs) (Pike *et al.*, 1999; Roberts *et al.*, 2000) using a Princeton Measurement Corporation vibrating sample magnetometer located at the Institute for Rock Magnetism (Minneapolis, USA). We measured FORCs using an averaging time of 0.5 s and processed the data using the FORCinel software (Harrison and Feinberg, 2008).

### **3.4 Results**

#### **3.4.1 Reflected-light polarizing microscopy**

Inspection of thin sections using reflected-light polarizing microscopy indicates the presence of numerous framboids in the undeformed and deformed sediments. Complete extinction is observed for most of the framboids under polarized reflected-light, which suggests that they are isotropic minerals. The number of framboids decreases considerably from the deformed sediments to the gouge, where only a few reflective minerals ( $<25$   $\mu$ m) are observed. We did not observe magnetic minerals such as magnetite at the  $>1$   $\mu$ m scale.

#### **3.4.2 SEM observations**

In the deformed sediments close to the gouge, as well as in sediments from the hanging-wall and foot-wall, numerous large iron sulfide aggregates include framboids of various sizes (1-5  $\mu$ m) (Fig. 3-3A). EDS analysis reveals that euhedral crystals

within the framboids consist of pyrite ( $\text{FeS}_2$ ). The size of pyrite crystals ( $\sim 1\ \mu\text{m}$ ) is homogenous within framboids (Fig. 3-3A). Isolated euhedral pyrite grains, with variable sizes, are also observed. Small framboids ( $\sim 5\ \mu\text{m}$ ) consist of aggregates of  $\sim 100\ \text{nm}$  iron monosulfide grains ( $\text{FeS}$ ) (Fig. 3-3A).  $\text{FeS}$  framboids are commonly observed from similar sediments in Taiwan and elsewhere and are interpreted as greigite ( $\text{Fe}_3\text{S}_4$ ) framboids (Jiang *et al.*, 2001; Roberts and Weaver, 2005; Rowan and Roberts, 2006). In deformed sediments close to the gouge, some iron sulfide aggregates have been dismembered by shearing (Fig. 3-3B). From the pattern of shear planes, we identified a sense of shear that is consistent with the thrust orientation on the Chelungpu fault (Fig. 3-3B).

In the gouge (thin sections 2 to 9), we observed framboids of two types. Some framboids, with diameter of 5 to  $\sim 25\ \mu\text{m}$ , have a  $\text{FeS}$  core surrounded by a  $1\sim 10\ \mu\text{m}$   $\text{FeS}_2$  rim (Fig. 3-3C). Under reflected-light microscopy, the core remains bright and the rim is black (Fig. 3-3C inset). This observation suggests that the  $\text{FeS}$  core is not cubic, which excludes the possibility that it is greigite. The second type of framboid is observed 1 mm from the PSZ (thin section 8). It consists of  $\sim 100\ \mu\text{m}$  clusters of irregular-shaped pyrite crystals (Fig. 3-3D). This resembles intensely deformed overgrown sedimentary sulfides. Within the 1999 Chi-Chi PSZ (thin section 8), we never observed framboids. Instead, small overgrown sulfide aggregates ( $< 25\ \mu\text{m}$ ) are identified (Fig. 3-3H). We also observed fine ( $< 3\ \mu\text{m}$ ) pyrite grains scattered within the quartz and clay matrix (Fig. 3-3G, H).

### 3.4.3 Transmission X-ray Microscopy

TXM provides three-dimensional (3-D) images of framboids that complement our two-dimensional (2-D) SEM and reflected-light microscopy observations. Within hanging-wall (at a depth of 1,133.04 m) sediments, foot-wall (1,138.48 m) sediments, and deformed sediments (1,135.83 m) (Fig. 3-2A), framboids are common (Fig. 3-4A). Framboids are generally grouped in high concentrations in some parts of siltstones. This is probably a result of remineralization of large pieces of organic matter during early diagenesis (Roberts and Weaver, 2005). Typically, the diameter of the framboids is larger than  $10\ \mu\text{m}$ , and the grain size of each pyrite crystal within the framboids is close to  $1\ \mu\text{m}$ .

At a depth of 1,136.24 m in the borehole (thin section 2), a  $\sim 1\text{-cm}$ -thick layer of foliated gouge was identified by Boullier *et al.* (2009) (Fig. 3-2C). There, TXM observations reveal the occurrence of numerous framboids together with dense

spherical or cubic minerals (Fig. 3-4B). The framboids are not aggregates and are scattered throughout the gouge. Within the gouge and near the 1999 Chi-Chi PSZ (Fig. 3-4C, D), framboidal clusters are not observed. Instead, we observed 5 to 25  $\mu\text{m}$  individual spherical-like mineral aggregates (Fig. 3-4C) that probably correspond to the pyrite that we described in the gouge using SEM (Fig. 3-3C, D).

#### 3.4.4 Magnetic properties

Magnetic properties are comparable for the undeformed sediments (sample M1) and deformed sediments (sample M2) (Fig. 3-5A, B). A Verwey transition at 120 K is detected in RT-SIRM demagnetization curves (see derivatives in inset, Fig. 3-5) and in ZFC demagnetization curves. The Verwey transition indicates the occurrence of stoichiometric magnetite (*Özdemir and Dunlop, 1999*). An additional magnetic transition is detected near 35 K for both ZFC and RT-SIRM demagnetization curves. This  $\sim 35$  K transition is marked by a drop of one to two orders of magnitude of the LT-SIRM. The  $\sim 35$  K transition is less evident in RT-SIRM demagnetization curves, with a break in slope at about 80 K followed by an enhancement of remanence (Fig. 3-5A, B; see derivative). This behavior is similar to the P-behavior described by *Aubourg and Pozzi (2010)* and *Kars et al. (2011)*. The nature of P-behavior will be discussed later. We calculated the maximum concentration of magnetite by assuming that only magnetite contributes to the RT-SIRM at room temperature (300 K). The RT-SIRM at 300 K is less than  $10^{-3}$   $\text{Am}^2/\text{kg}$  for the different sediments that we measured. Taking the SIRM of magnetite as  $\sim 10$   $\text{Am}^2/\text{kg}$  (*Maher et al., 1999*), we infer a maximum concentration of magnetite of 100 ppmv (concentration in parts per million by volume =  $1 \times 10^6 \times \text{RT-SIRM}/\text{SIRM}_{\text{magnetite}}$ ). FORC diagrams are noisy due to the small concentration of ferrimagnetic grains with respect to the paramagnetic contribution (Fig. 3-5F, G), so high values of the smoothing factor (SF) were needed. The FORC diagrams are consistent with a distribution of weakly interacting single domain to superparamagnetic (SP) particles (e.g., *Pike et al., 2001*; *Rowan and Roberts, 2006*).

Gouge samples M3–M5 (Table 3-1) have different magnetic properties (Fig. 3-5C–E). From 300 K to 150 K, there is a regular increase of up to  $\sim 10\%$  of the RT-SIRM. This increase is diagnostic of goethite ( $\alpha\text{-FeOOH}$ ) (*Dekkers, 1989*; *Maher et al., 1999*; *Liu et al., 2006*). To check for the presence of goethite, we imparted a RT-SIRM at 300 K, and warmed it up to 400 K (Fig. 3-6), which is close to Néel temperature of goethite (120  $^{\circ}\text{C}$ , e.g., *Özdemir and Dunlop (1996)*). About  $\sim 50\%$  of

the RT-SIRM is then lost at 400 K, which indicates that goethite contributes a large part of the artificial remanence. In the host sediments, by comparison, the increase of RT-SIRM from 300 K to 150 K is limited to 1 to 2% and the drop from 300 K to 400 K is less than 25%. In the gouge, the Verwey transition is much less pronounced and is observed only during cooling of the RT-SIRM (Fig. 3-5D, E). The most notable difference is observed near 35 K. The ZFC curves do not undergo the one to two order magnitude remanence decrease at 35 K that is observed in host rock sediments. In addition, there is no P-behavior during cooling of the RT-SIRM. Instead, a ~35 K transition is characterized by a remanence drop despite application of a +5  $\mu$ T magnetic field in the MPMS. This transition is similar to the magnetic transition for >1  $\mu$ m pyrrhotite (*Dekkers et al.*, 1989; *Rochette et al.*, 1990). According to *Dekkers et al.* (1989), the degree of reversibility of this transition is an indication of grain size. When cycling the RT-SIRM for sample M5 (Fig. 3-7), we observed a reversible magnetic transition at 35 K, which indicates that pyrrhotite is fine-grained and close to 1  $\mu$ m in size (h/c ratio 0.96). We calculated the maximum concentrations of goethite, pyrrhotite, and magnetite in the studied samples. At room temperature, the RT-SIRM is  $< 10^{-2}$  Am<sup>2</sup>/kg for the different measured gouges. We assume that the contribution of goethite is about half of this value. Taking the SIRM of goethite as 0.05 Am<sup>2</sup>/kg (*Maher et al.*, 1999), we obtain a maximum concentration of several percent goethite (RT-SIRM/SIRM<sub>goethite</sub>). Assuming that the other half of the remanence is carried by pyrrhotite or magnetite, and assuming the SIRM of pyrrhotite as ~4.5 Am<sup>2</sup>/kg and of magnetite as ~10 Am<sup>2</sup>/kg (*Maher et al.*, 1999), we obtain a maximum concentration of pyrrhotite of less than 0.1% (concentration% = 100 x RT-SIRM/2SIRM<sub>pyrrhotite</sub>) and a maximum concentration of magnetite of less than 500 ppmv (concentration ppmv = 1 x 10<sup>6</sup> x RT-SIRM/2SIRM<sub>magnetite</sub>). This suggests that there is an enhanced concentration of ferrimagnetic minerals in the gouge. FORC diagrams for gouge (M3) and PSZ (M5) have a significant high-coercivity contribution (Fig. 3-5H, I). A coercivity peak at 90 mT is consistent with the presence of magnetically interacting pyrrhotite (*Wehland et al.*, 2005; *Roberts et al.*, 2006). Although goethite is identified using low-temperature remanence properties, we did not observe evidence of high-coercivities up to 500 mT in the FORC diagrams (data are not shown). We infer that the coercivity of this goethite is too high to contribute to the FORC distribution. *Rochette et al.* (2005) showed that natural goethite may not saturate even at fields up to 57 T.

### 3.5 Discussion

#### 3.5.1 Iron sulfides

Iron sulfide minerals are common in organic matter rich sedimentary rocks (Reimer, 1984; Tribovillard *et al.*, 2002; Maclean *et al.*, 2008). This is particularly true within Plio-Pleistocene sediments from Taiwan (Horng *et al.*, 1992, 1998; Jiang *et al.*, 2001) and within the Chinshui Formation, as confirmed by our observations. In these sediments, the iron sulfides typically form as framboids (Fig. 3-3A, 3-3B, 3-4A), but they can also appear as individual euhedral crystals. TXM inspection indicates that the framboids are not randomly scattered but are grouped as packs of tens of framboids in the sediments (Fig. 3-3A, 3-3B, 3-4A). SEM observations coupled with EDS analyses indicate that the framboids consist essentially of pyrite aggregates. However, small framboids ( $<0.1\ \mu\text{m}$ ) have an 'FeS' composition, and are likely greigite ( $\text{Fe}_3\text{S}_4$ ). Greigite often forms during early (Rowan *et al.*, 2009) or late (Rowan and Weaver, 2005) diagenesis and is probably preserved in the unmetamorphosed Chinshui Formation. In deformed sediments, the only form of alteration of pyrite that we observed is the development of shear planes (Fig. 3-3B). This is the first type of alteration of framboids that we detected in the deformed sediments. In the gouge, all micro-scale observations confirm the absence of well-preserved framboids.

The pyrite content decreases drastically from the host sediments to the gouge. Hirono *et al.* (2007b) and Ishikawa *et al.* (2008) reported an enhanced abundance of  $\text{SO}_4^{2-}$  in the gouge zone and related it to pyrite dissolution. Pyrite dissolution would release sulfate and would lower the pH of the immediately surrounding sediment (Roberts and Weaver, 2005). Low pH conditions in turn would favor dissolution of carbonate minerals. This could be an alternative explanation for the low inorganic carbon content in the gouge (Hirono *et al.*, 2008; Hamada *et al.*, 2009; Mishima *et al.*, 2009).

Hirono *et al.* (2008) reported a lack of pyrite in the gouge based on X-ray diffraction spectroscopy. Our observations contradict this view. In the gouge, we observe: 1) unusual small framboids ( $<25\ \mu\text{m}$ ) with  $\text{FeS}_2$  as a rim and FeS as a core (Fig. 3-3C), 2) detrital pyrite with irregular shapes (Fig. 3-3D, F), and 3) individual  $<2\ \mu\text{m}$  pyrite grains (Fig. 3-3G). Individual pyrite grains are observed within the whole gouge, including the Chi-Chi PSZ (Fig. 3-3E–H). However, framboids have not been observed in the Chi-Chi PSZ.

For the first time, we identified pyrrhotite in the gouge. This is based on the drop in remanence at  $\sim 35\ \text{K}$  in the RT-SIRM demagnetization curves (Fig. 3-7) which is a

diagnostic signature of  $>1\ \mu\text{m}$  pyrrhotite (*Dekkers et al.*, 1989; *Rochette et al.*, 1990). The quasi-reversible path of the pyrrhotite transition indicates that the size of pyrrhotite grains is close to  $1\ \mu\text{m}$  (*Dekkers et al.*, 1989). The distribution of coercivities around  $\sim 90\ \text{mT}$  (Fig. 3-5H, I) suggests that strongly interacting pyrrhotite dominates the magnetic assemblage of the gouge (*Wehland et al.*, 2005; *Roberts et al.*, 2006). Our magnetic observations along with SEM observations reveal the occurrence of unusual framboids with rims of  $\text{FeS}_2$  (pyrite) and cores of  $\text{FeS}$  (Fig. 3-3C). The  $\text{FeS}$  phase included in framboids is likely pyrrhotite, which is detected magnetically, because it has grain sizes between  $0.5$  and  $1\ \mu\text{m}$  and is not cubic (Fig. 3-3C). In addition, the strong magnetic interactions suggested by FORC diagrams can be explained by the tight grouping of pyrrhotite minerals enclosed in framboids. We never detected coarser  $>1\ \mu\text{m}$  pyrrhotite in the Chinshui siltstones. Additional low-temperature magnetic experiments performed by *Humbert et al.* (2012) confirm our observations. We therefore argue that the coarser  $>1\ \mu\text{m}$  pyrrhotite is not derived from the host rocks and that it was neoformed in the fault gouge.

The preservation of iron sulfides like pyrite and the neoformation of pyrrhotite in the fault gouge are consistent with several observations. First, iron sulfide neoformation attests to a reducing environment in the gouge. This is in agreement with geochemical observations in the gouge from FZB1136 (*Ishikawa et al.*, 2008). Second, the association of pyrite and pyrrhotite may imply heating and cooling during co-seismic and post-seismic processes. We assume that pyrrhotite formation is related to alteration of pyrite grains. *Chin et al.* (2005) observed that mechanical milling of pyrite under  $\text{CO}_2$ -rich conditions triggered pyrrhotite formation. This process is feasible in a gouge where milling is a common process. However, we infer the presence of large pyrrhotite grains ( $\sim 1\ \mu\text{m}$ ) grains in the FZB1136 gouge, which is supported by direct observations of framboid relics that have not been completely crushed (Fig. 3-3C). Therefore, we conclude that an additional process occurred. *Wang et al.* (2008) demonstrated that oxidation of pyrite to pyrrhotite or hematite can occur during short-term exposure to temperatures up to  $700^\circ\text{C}$  (heating rate:  $11^\circ\text{C}/\text{minute}$ ). With a similar heating rate, *Bhargava et al.* (2009) observed that heating of pyrite yields pyrrhotite at  $500^\circ\text{C}$  under inert conditions (pure  $\text{N}_2$  or Ar gas). This is consistent with the heating experiments of *Mayoral et al.* (2002) at  $500^\circ\text{C}$  with a higher heating rate ( $80^\circ\text{C}/\text{minute}$ ). When extrapolating these experimental results to our study, we suggest that elevated temperatures of  $>500^\circ\text{C}$  in the gouge triggered pyrrhotite formation at the expense of pyrite. The gouge is a stack of numerous slip

zones, and within each slip zone elevated temperatures are likely due to frictional processes (Boullier *et al.*, 2009). Even if there is no evidence of melting in the FZB1136 gouge (Hirono *et al.*, 2008; Boullier *et al.*, 2009), temperatures above 500°C are nevertheless possible in parts of the gouge, including the 1999 Chi-Chi PSZ. Therefore, we suggest that pyrrhotite formed at temperatures >500°C associated with repeated earthquakes.

A temperature above 350°C in the gouge has been proposed by several authors, based on geochemistry (Ishikawa *et al.*, 2008), carbonate alteration (Hirono *et al.*, 2008), vaporization of water during thermal pressurization (Boullier *et al.*, 2009), and formation of magnetic minerals (Hirono *et al.*, 2006; Tanikawa *et al.*, 2008; Mishima *et al.*, 2009). Ishikawa *et al.* (2008) suggested that the chemical characteristics of the gouge were produced by interaction with co-seismic aqueous fluids derived from sediment pore waters with temperatures up to 350°C. We calculated Eh-pH diagrams using the Geochemist's Workbench software and considered the stability of pyrite and pyrrhotite in an aqueous fluid within the gouge (Fig. 3-8). The pyrite stability field increases from 300 to 100°C at lower Eh conditions. The gouge appears to have formed under anoxic conditions based on microbial observations at 1,000 m depth in TCDP core Hole A (Wang *et al.*, 2007). We suggest that pyrite formed as a result of retrograde metamorphism. The presence of pyrite rims on pyrrhotite cores in the framboids (Fig. 3-3C) supports the retrograde metamorphism hypothesis. Only pyrrhotite on the surface of framboids will be affected by retrograde metamorphism, and the core of pyrrhotite will be preserved. If correct, this suggests that most pyrite in the gouge (Fig. 3-3E-H) resulted from retrograde metamorphism during cooling of co-seismic fluids from above 350°C.

### 3.5.2 Magnetite

Magnetite is present in the Chinshui Formation, and recognition of the Verwey transition (~120 K; Fig. 3-5A) implies the occurrence of stoichiometric magnetite with a maximum concentration of 100 ppmv. Mishima *et al.* (2009) also reported a low concentration of magnetite in the Chinshui siltstones. The marked ~35 K magnetic transition observed from ZFC demagnetization curves (Fig. 3-5), also observed by Mishima *et al.* (2009), could be explained by superparamagnetic (SP) grains, monoclinic pyrrhotite, siderite (FeCO<sub>3</sub>), and rhodochrosite (MnCO<sub>3</sub>) (Housen *et al.*, 1996; Kars *et al.*, 2011). It is well known that magnetite nanoparticles carry a remanence at low temperature (typically 10 K), and that they lose this remanence on

warming (*Hunt et al.*, 1995). *Mishima et al.* (2009) attributed this 35 K transition to SP grains in the Chinshui Formation. Although we agree with *Mishima et al.* (2009), from the same samples we observed development of a magnetic transition with a break-in-slope at ~35 K on RT-SIRM demagnetization curves (Fig. 3-5). *Aubourg and Pozzi* (2010) and *Kars et al.* (2011) observed the same behavior in unmetamorphosed claystones. They proposed that this magnetic transition, referred to as P-behavior, is due to a combination of a fine-grained pyrrhotite transition and an induced magnetization of unknown origin. We support this interpretation because of the strong similarity of low-temperature demagnetization curves (ZFC, RT-SIRM) of Chinshui Formation sedimentary rocks with those reported by *Aubourg and Pozzi* (2010) and *Kars et al.* (2011). If correct, the presence of stoichiometric fine-grained magnetite and fine-grained pyrrhotite of the Chinshui Formation is diagnostic of modest burial below 5 km (*Aubourg and Pozzi*, 2010; *Abdelmalak et al.*, 2011). This is consistent with a burial temperature of about 120°C, inferred from vitrinite reflectance data ( $R_0 \sim 0.8\%$ ) (*Sakaguchi et al.*, 2007).

The magnetic properties of gouge differ from those of the host sediments. In particular, we observe a weakening of the Verwey transition (Fig. 3-5C-E), which suggests that magnetite is partially oxidized (*Özdemir et al.*, 1993; *Cui et al.*, 1994; *Özdemir et al.*, 2002). The presence of co-seismic hot fluids in the gouge (*Ishikawa et al.*, 2009) constitutes a possible explanation for the partial alteration of magnetite, where magnetite could be oxidized to maghemite thereby causing weakening of the Verwey transition (*Özdemir et al.*, 1993; *Cui et al.*, 1994; *Özdemir et al.*, 2002). The absence of a large remanence drop between 10 K and 40 K in the ZFC demagnetization curves (Fig. 3-5A, B) implies that the grain size fraction of magnetite is essentially above the SP threshold size (~20 nm). Paradoxically, ultrafine-grained magnetic minerals present in the Chinshui Formation do not exist in the gouge, where grain size reduction by a milling process is likely. We interpret that the ultrafine fraction is altered chemically during repeated earthquakes. *Aubourg and Pozzi* (2010) showed that moderate heating up to 250°C promotes drastic reduction of the 35 K magnetic transition. We suggest, therefore, that the increased temperature in the gouge alters the ultrafine-grained fraction of magnetic minerals.

A fraction of magnetite could have been inherited from the Chinshui Formation. However, detrital magnetite is probably unlikely in sediments that have been extensively pyritized (*Rowan et al.*, 2009). Magnetite can form at elevated temperatures, by precipitation from frictional melts as observed in natural



pseudotachylites (*Ferré et al.*, 2005, 2012) or in experimental pseudotachylites (*Nakamura et al.*, 2002). Similar to pyrrhotite, we suggest that some magnetite formed during repeated earthquakes within the gouge.

### **3.5.3 Goethite**

The evolution of remanence on heating and cooling (Fig. 3-5C-E) also suggests the occurrence of goethite ( $\alpha$ -FeOOH) in the gouge. Recognition of goethite is important because it demonstrates the presence of fluid in the gouge. In a companion paper, we provided additional evidence for the occurrence of goethite (*Chou et al.*, 2012) and showed that the natural remanent magnetization in the gouge is carried essentially by goethite. We suggest that this magnetization record is contemporaneous with the 1999 Chi-Chi event. TXM tomography identified scattered 5  $\mu$ m goethite grains within the gouge. The remanence and TXM observations led *Chou et al.* (2012) to propose that goethite formed from cooling of co-seismic fluids within the gouge. Low pH conditions associated with pyrite alteration would favor goethite formation (*Schwertmann and Murad*, 1983; *Murad and Rojik*, 2003). In addition, *Nakamura and Hagahama* (2001) also observed 5  $\mu$ m goethite in the Nojima fault gouge from Japan. We therefore suggest that study of goethite in fault gouge is important to detect evidence of co-seismic fluids and could be an indicator of thermal pressurization.

### **3.5.4 Implications for identification of earthquake slip zones**

In sediment-derived fault gouge, endothermic dehydration reactions and the phase change from liquid water to steam can efficiently buffer the temperature within a fault (*Brantut et al.*, 2011). This is consistent with the scarcity of melts in sediment-derived fault gouge, as was observed in the FZB1136 gouge (*Boullier et al.*, 2009). Generally, recognition of clay-clast aggregates (CCA) (*Boullier et al.*, 2009) is good evidence of thermal pressurization processes, and, in turn, as a signature of earthquakes (*Boutareau et al.*, 2008). Identification of neoformed minerals can be an alternative indicator of limited temperature elevation and fluid interaction. In this regard, we suggest that at the time of pyrrhotite formation in the FZB1136 gouge, this implies a temperature above 500°C. Similarly, we suggest that goethite formation is an indication of thermal pressurization processes. In fold-and-thrust belts, thrusts similar to the Chelungpu fault are common and likely developed within clay-rich rocks. If pyrrhotite and goethite exist in the gouge, and not in the host rocks, then it can be inferred that temperature enhancement took place and that fluids infiltrated the

gouge.

### 3.6 Conclusions

The 16-cm-thick gouge zone intersected in the TCDP drill holes is a product of repeated earthquakes, including the Chi-Chi earthquake ( $M_w$  7.6, 1999), and has had a complex mechanical and thermal history. The wall rocks are made up of the Chinshui Formation, which contains several percent pyrite. The magnetic mineral assemblage of this formation is typical of unmetamorphosed sediments and consists essentially of nanometric stoichiometric magnetite. Micro-scale observations indicate that the concentration of pyrite framboids decreases considerably from the wall rock into the gouge. Pyrite alteration would cause a lowering of pH, and, in turn, would promote carbonate mineral dissolution. Beside pyrite alteration, we identify for the first time the occurrence of micrometric pyrrhotite in the fault gouge. The pyrrhotite likely formed at high temperatures ( $>500^\circ\text{C}$ ) at the expense of pyrite. Magnetite, which is also present in the gouge, is partially altered. We propose that pyrrhotite and some of the magnetite formed at elevated temperatures during frictional heating along the slip zones. The total concentration of pyrrhotite and magnetite is therefore a result of numerous earthquakes. In the gouge, we also identify neoformed goethite, which implies the presence of hot fluids ( $>350^\circ\text{C}$ ). On cooling, these hot fluids altered pyrrhotite into pyrite and magnetite into partially altered magnetite. Our results demonstrate that characterization of magnetic minerals provides a useful means of studying earthquake processes in faults.

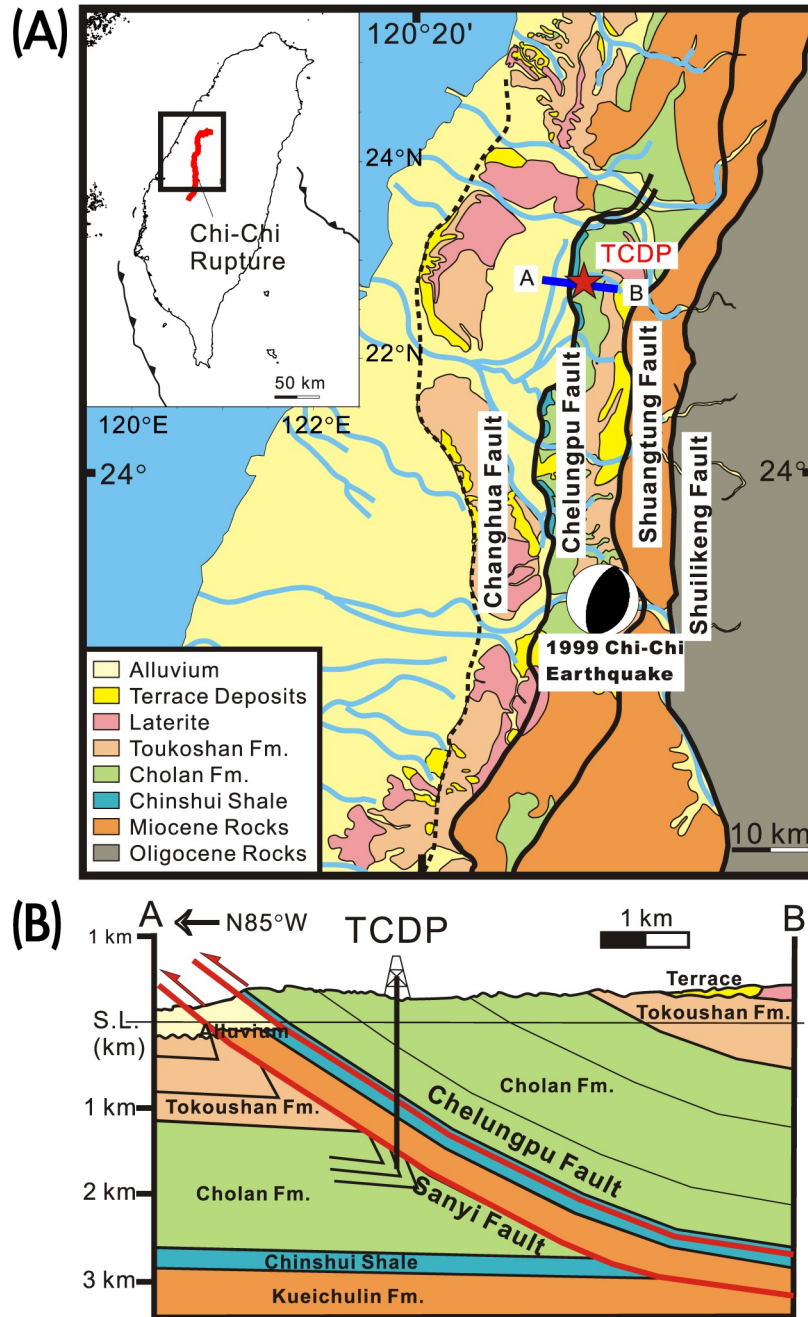


Fig. 3-1: Geological setting of the TCDP borehole (modified from *Yeh et al.* [2007]). (A) Schematic geological map of western Taiwan with the location of the TCDP site (red star, 120.73916°E, 24.20083°N) on the northern part of the Chelungpu fault. The focal mechanism of the Chi-Chi main shock is located at the hypocentre of the 1999 Chi-Chi earthquake (128.81°E, 23.86°N). (B) Geological cross-section through the TCDP site. The Chelungpu fault is located within the Chinshui Formation.

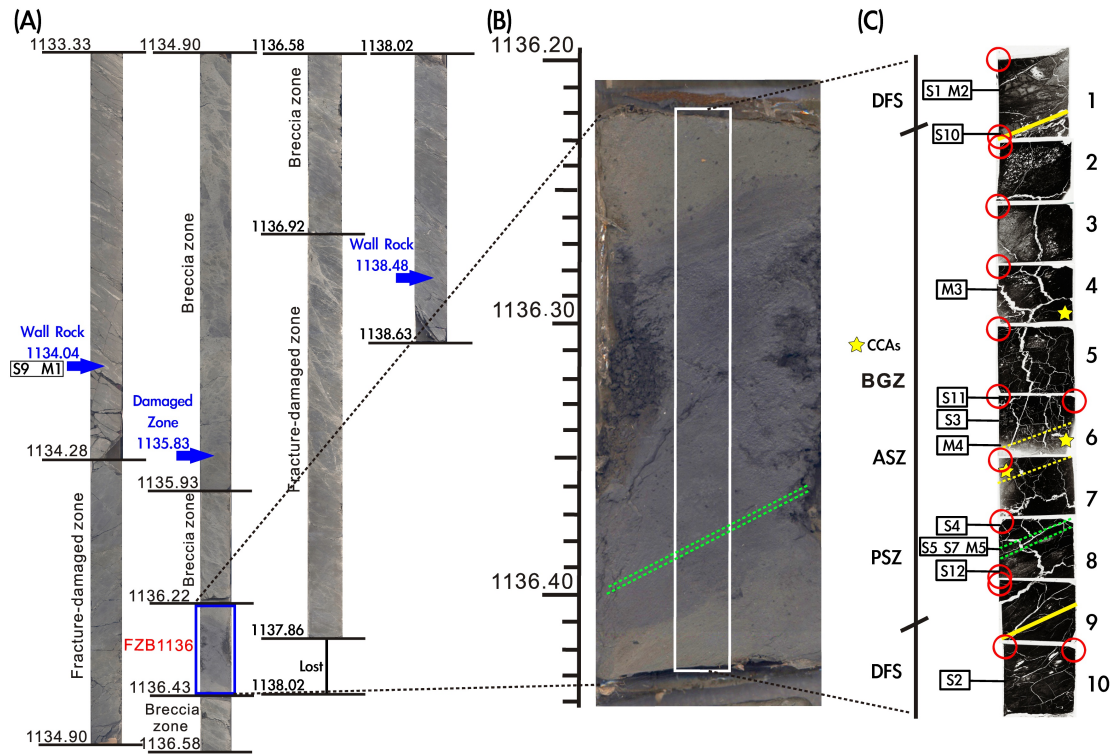


Fig. 3-2: Images of the cores and samples from TCDP Hole B. (A) Half-core image for the depth interval from 1,133.33 to 1,138.63 m. The blue arrows and frame indicate the sample locations. (B) Half-core image of the FZB1136 fault zone at a depth of 1,136.22~1,136.43 m; the white frame corresponds to the locations of polished sections. The green dashed line frames the Chi-Chi principal slip zone (PSZ) [Boullier *et al.*, 2009]. (C) Collage of SEM images from the polished sections. Red circles indicate sample positions for TXM analysis. The yellow lines are the boundaries between deformed sediments (DFS) and the gouge zone (BGZ). The yellow stars indicate clay-clast aggregates (CCAs, see Boullier *et al.* [2009]). The double yellow dashed line is an ancient slip zone (ASZ) and the double green dashed line is the Chi-Chi PSZ (after Boullier *et al.* [2009]).

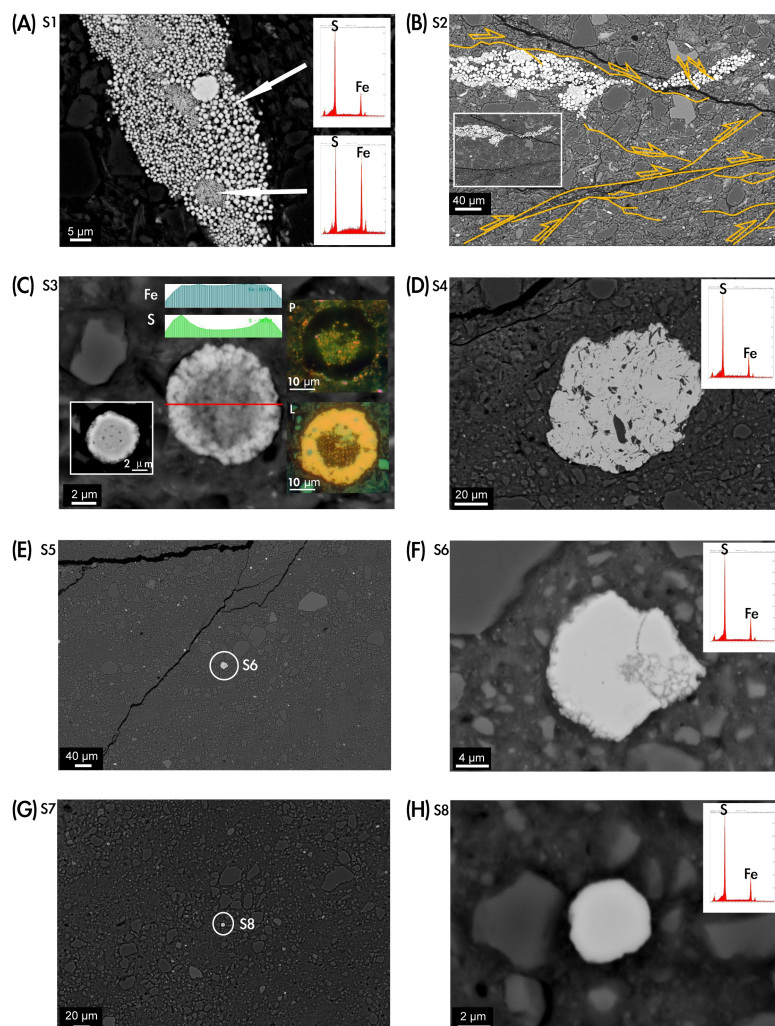


Fig. 3-3: Back-scattered SEM images with EDS results. (A) Large iron sulfide aggregates that contain framboidal pyrite ( $\text{FeS}_2$ ) within the deformed sediments (S1 in Figure 2C). Some parts of the aggregate are greigite ( $\text{Fe}_3\text{S}_4$ ). (B) Large iron sulfide aggregates that contain framboidal pyrite with micro-fractures and shears in the deformed sediments (S2 in Figure 2C). (C) Pyrite grain in the gouge (S3 in Figure 2C). The framboidal  $\text{FeS}$  core (pyrrhotite, which is a replacement of a framboidal pyrite) has an  $\text{FeS}_2$  rim. The photos on the right were obtained using reflected-light microscopy (P: polarized reflected; L: light reflected); pyrite is dark and pyrrhotite is light under polarized light. (D) Large cluster of pyrite grains mixed with quartz (S4 in Figure 2C). (E) Small pyrite grains (bright back-scattered grains, smaller than  $5\ \mu\text{m}$ , one is  $\sim 20\ \mu\text{m}$ ) and quartz grains within the Chi-Chi PSZ (S8 in Figure 2C). (F) Detail of Figure 3E: fractured pyrite grain within the PSZ (S8 in Figure 2C). (G) Image of the Chi-Chi PSZ (S8 in Figure 2C). (H) Pyrite grain ( $3\ \mu\text{m}$ ) within the Chi-Chi PSZ (S8 in Figure 2C).



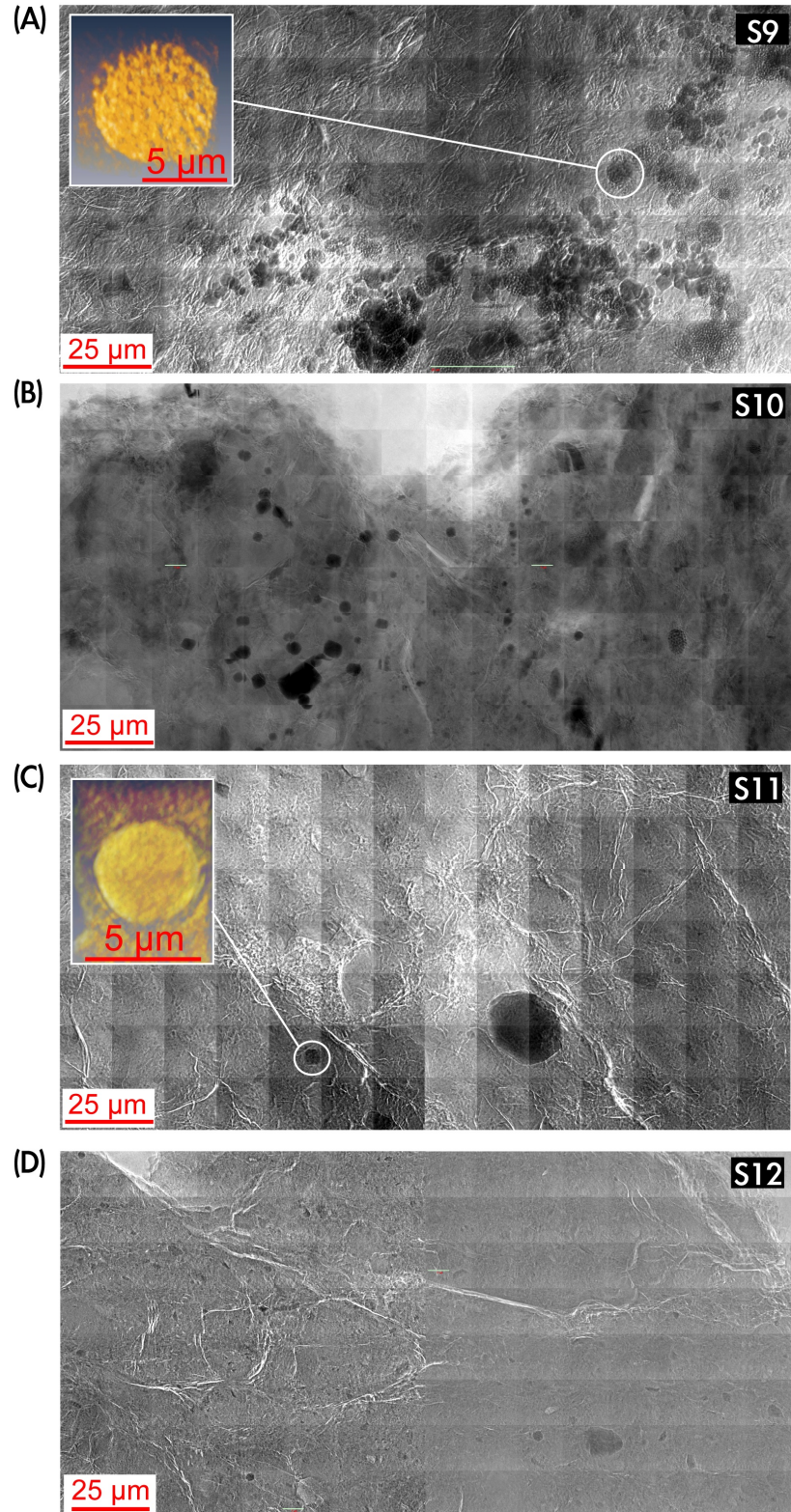


Fig. 3-4: 2-D and 3-D images acquired for TXM observations. (A) Sediment at a depth of 1,134.04 m in TCDP hole B (M1 in Figure 2A). (B) Deformed sediment at a depth of 1,136.25 m (S10 in Figure 2C). (C) Gouge at a depth of 1,136.33 m (S11 in Figure 2C). (D) Gouge close to the PSZ at a depth of 1,136.38 m (S12 in Figure 2C).

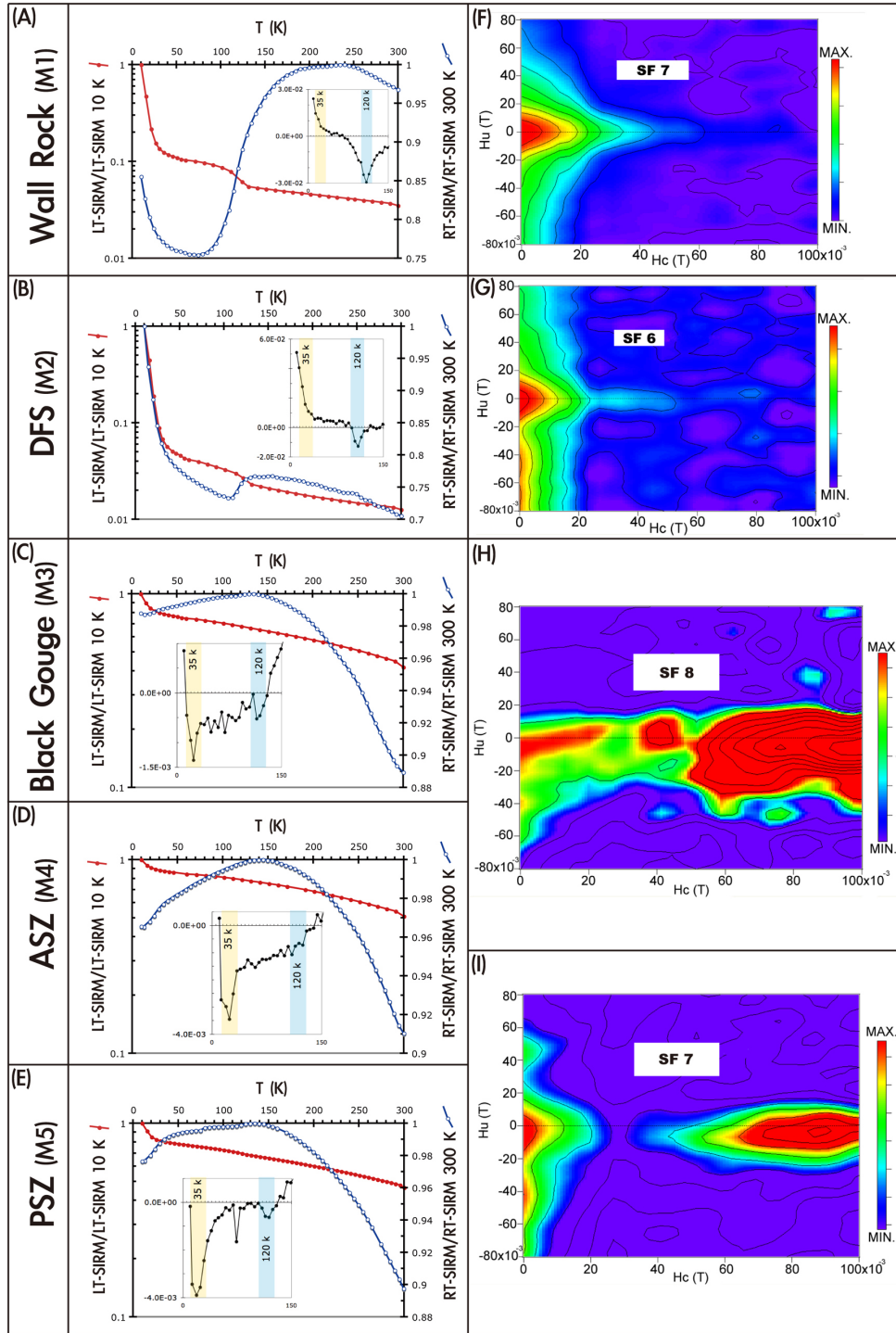


Fig. 3-5: Low temperature magnetic measurements (inset: relative values of RT-SIRM) from 10 to 300 K and FORC diagrams. (A) Wall rock sample (M1 in Figure 2A). (B) Deformed sediment sample (M2 in Figure 2C). (C) Gouge sample (M3 in Figure 2C). (D) ASZ sample (M4 in Figure 2C). (E) PSZ sample (M5 in Figure 2C). (F) FORC diagram for wall rock sample (field 0–100 mT). (G) FORC diagram for deformed sediment sample (field 0–100 mT). (H) and (I) FORC diagrams for samples from fault gouge (field 0–100 mT).

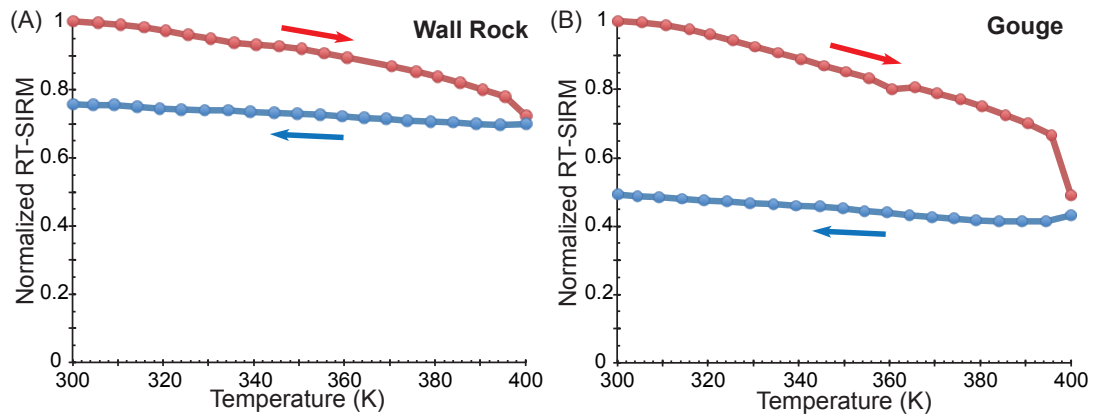


Fig. 3-6: Warming-cooling RT-SIRM cycle from 300 to 400 K (127°C), which is close to the Néel temperature of goethite (120°C). (A) For a wall rock sample, less than 25% of the RT-SIRM is lost at 400 K. (B) For a gouge sample, about ~50% of the RT-SIRM is lost at 400 K. This indicates neoformation of a significant concentration of goethite in the fault gouge.





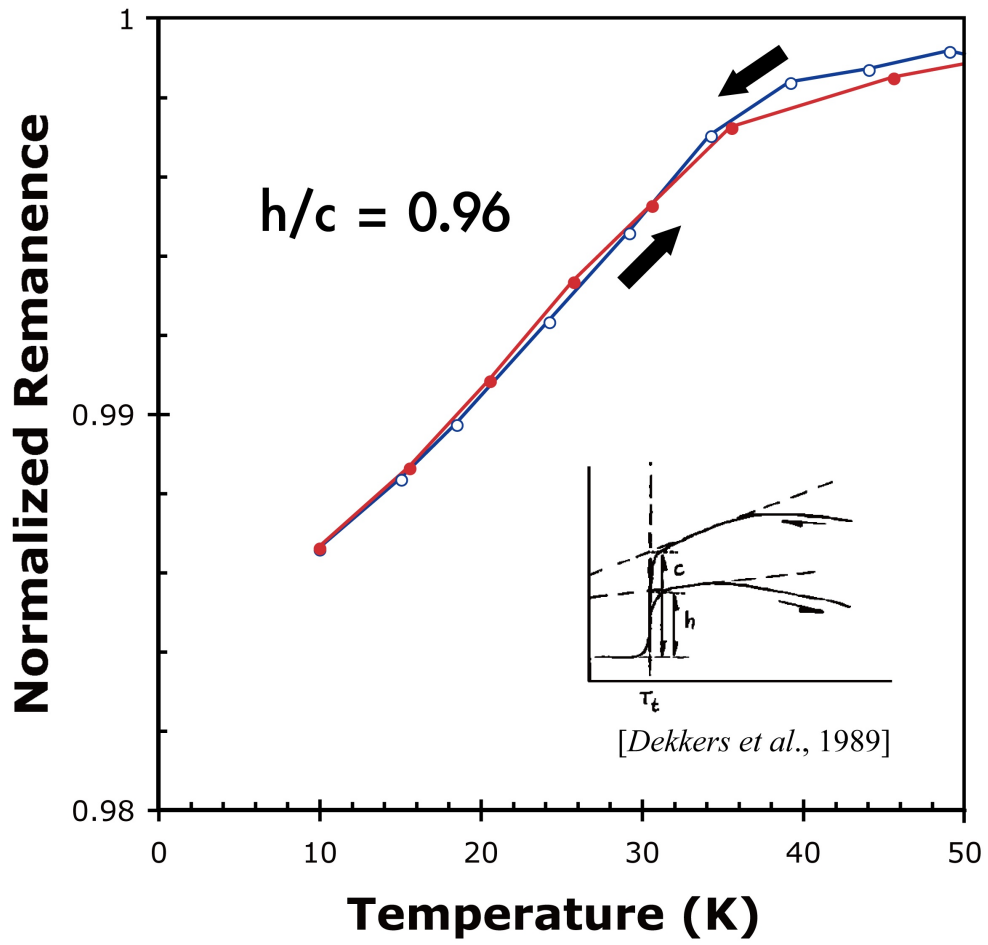


Fig. 3-7: Cooling–warming RT-SIRM cycle from 10 to 50 K. A reversible magnetic transition at 35 K for the PSZ sample indicates that pyrrhotite is fine-grained and close to 1  $\mu\text{m}$  in size ( $h/c$  ratio = 0.96) (see Dekkers et al. [1989]).

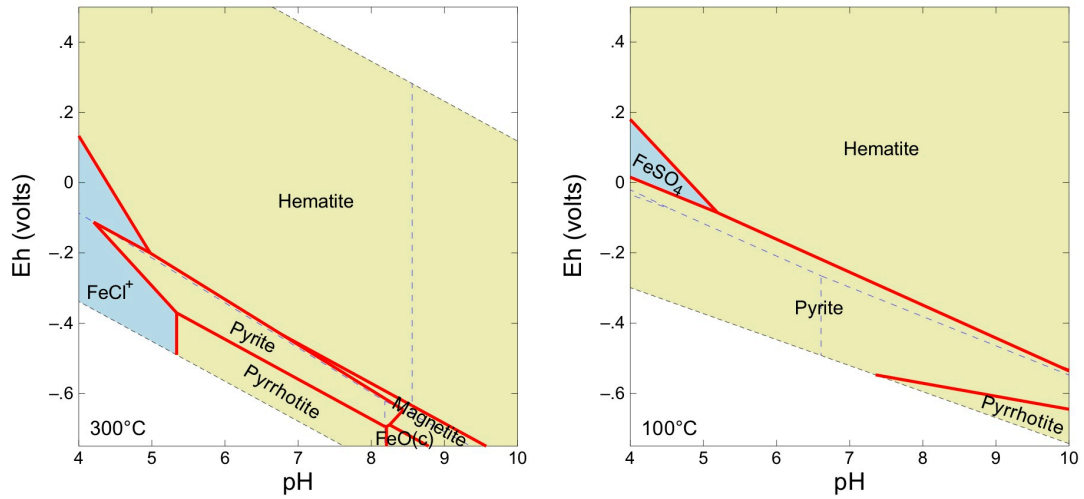


Fig. 3-8: Eh-pH diagrams for fluid temperatures of 300°C and 100°C. The model parameters are:  $a_{\text{SO}_4^{2-}} = 10^{-2}$ ,  $a_{\text{Cl}^-} = 10^{-2}$ ,  $a_{\text{Fe}^{2+}} = 10^{-4}$  (higher iron concentration). The pressure used is 30 MPa, which is equivalent to lithostatic pressure at a depth of 1,100 m. Note that at higher temperatures the pyrrhotite field exists at strong reducing conditions in a pH range of 5.3-8.2. As temperature decreases, the pyrite field expands and pyrrhotite alters to pyrite.

Table 3-1: Sample depths and measurements made in this study.

| Depth (m) | Location          | Number   | Measurements                 |
|-----------|-------------------|----------|------------------------------|
| 1134.04   | hanging wall rock | S9 M1    | MPMS, FORC, TXM              |
| 1135.83   | damaged zone      |          | TXM, RFM                     |
| 1136.22   | deformed sediment | S1 M2    | TXM, RFM, SEM, MPMS,<br>FORC |
| 1136.25   | black gouge       | S10      | TXM, RFM, SEM                |
| 1136.27   | black gouge       |          | TXM, RFM                     |
| 1136.29   | black gouge       | M3       | TXM, RFM, SEM, MPMS,<br>FORC |
| 1136.31   | black gouge       |          | TXM, RFM                     |
| 1136.33   | black gouge       | S3 S11   | TXM, RFM, SEM                |
| 1136.35   | ASZ               | M4       | TXM, RFM, SEM, MPMS,<br>FORC |
| 1136.37   | black gouge       | S4       | TXM, RFM, SEM                |
| 1136.38   | PSZ               | S5 S7 M5 | TXM, SEM, RFM, MPMS,<br>FORC |
| 1136.39   | black gouge       | S12      | TXM, RFM, SEM                |
| 1136.41   | deformed sediment |          | TXM, RFM, SEM                |
| 1138.48   | foot-wall rock    | S2       | TXM                          |

FORC: First-order reversal curve, MPMS: Magnetic property measurement system, RFM: Reflected-light microscope, SEM: Scanning electron microscope, TXM: Transmission X-ray microscope.

## **Chapter 4. Quantitative Modeling of the Newly Formed Magnetic Minerals in the fault gouge of the 1999 Chi-Chi Earthquake ( $M_w$ 7.6), Taiwan**

### **(Geophysical Journal International, submitted)**

#### **4.1 Introduction**

*Chou et al.* (2012) reported for the first time a stable paleomagnetic record parallel to the modern geomagnetic field in a sedimentary-derived gouge. As this 16 cm gouge hosts the 3-mm-thick principal slip zone (PSZ) of the 1999 Chi-Chi earthquake ( $M_w$  7.6), *Chou et al.* (2012) proposed that the paleomagnetic record took place during, or soon after the 1999 Chi-Chi earthquake. The discovery of co-to-post seismic magnetic record brings a possible way to provide dating constraints of active fault, as magnetic record is stable at the scale of geological time. Yet, the exact origin of magnetic minerals that carry this magnetization remains to demonstrate.

Thanks to the Taiwan Chelungpu-fault Drilling Project (TCDP), km-long boreholes drilled in 2005 provide fresh and unaltered continuous section of gouges within the active Chelungpu fault (*Song et al.* 2007; *Yeh et al.* 2007). This fault zone, labeled FZB1136 (fault zone in hole B, at depth 1,136 m), has been the matter of intense investigation, including geochemistry (*Hirono et al.* 2007; *Ishikawa et al.* 2008), petrophysics (*Boullier et al.* 2009; *Otsuki et al.* 2009), physical properties (*Mizoguchi et al.* 2008; *Tanikawa et al.* 2009), and paleomagnetism (*Chou et al.* 2012).

It was soon established that this gouge shows a distinguishable peak of magnetic susceptibility with respect to the surrounding Chinshui siltstone Formation. The Chinshui Formation has a background magnetic susceptibility  $\sim 300$   $\mu\text{SI}$  while the gouge can reach up to  $\sim 600$   $\mu\text{SI}$  (*Hirono et al.* 2006). The origin of this peak is still debated. It was first proposed that the increase in magnetic susceptibility might be related to mechanical reduction of grain (*Hirono et al.* 2006). Other hypotheses proposed the formation of magnetic minerals due to the chemical transformation of paramagnetic minerals (*Mishima et al.* 2006; *Tanikawa et al.* 2008; *Mishima et al.* 2009), the alteration of pyrite (*Chou et al.*, 2012b), or the precipitation during cooling of iron rich hot fluid (*Chou et al.* 2012). All of these hypotheses require modest to high temperature elevation in the range 350-500°C.

*Mishima et al.* (2009) proposed a detailed rock magnetic study of FZB1136

gouge and wall rocks. In particular, they used for the first time the low-temperature monitoring of remanence. Their studies revealed the occurrence of Verwey transition at 120 K in the Chinshui Formation, which is diagnostic of stoichiometric magnetite ( $\text{Fe}_3\text{O}_4$ ). In addition, they observed a huge drop of remanence between 10~35 K. These two signatures are not encountered in the sample gouge, which make them recognizable. *Mishima et al.* (2009) also indicated that the paramagnetic susceptibility, deduced from hysteresis curves, is stable ( $\sim 300 \mu\text{SI}$ ) through the entire gouge. They also observed that the magnetic susceptibility of Chinshui Formation is almost entirely carried by paramagnetic and superparamagnetic (SP) minerals, indicating therefore a minute amount of magnetite.

*Chou et al.* (2012) observed for the first time the presence of goethite ( $\alpha\text{-FeOOH}$ ) in relative abundance within the gouge. The identification of goethite was making possible because of the predominance of unblocking of temperature near  $120^\circ\text{C}$ , the Néel temperature of goethite. In addition, they observed elongated  $5 \mu\text{m}$  goethite using transmission X-ray microscopy. The euhedral shape of goethite is a clear indication of late growth within the gouge. A similar observation of neoformed goethite has been done by *Nakamura & Nagahama* (2001) in the Nojima fault, Japan. Of particular interest, the goethite carries a large portion of the characteristic remanent magnetization (ChRM). *Chou et al.* (2012) have suggested this goethite formed in response to post-seismic cooling of hot fluids ( $<350^\circ\text{C}$ , *Ishikawa et al.* 2008). Within the 3-mm-thick PSZ, *Chou et al.* (2012) observed that the ChRM is carried by magnetite and not by goethite. Magnetite is a magnetically soft mineral while goethite is a magnetically hard mineral. The dual distribution of goethite and magnetite within the gouge was confirmed by the analysis of the S-ratio, a proxy of magnetic hardness. From the profile of S-ratio, *Chou et al.* (2012) proposed that the maximum concentration of goethite takes place within the center of the gouge, while concentration of magnetite is maximum near the PSZ.

In this paper, we propose a new series of magnetic measurements to clarify the distribution of goethite and magnetite in the gouge FZB1136. To reflect a  $\sim 4 \text{ cm}$  offset between the peak of magnetic susceptibility and remanence to saturation along the 16 cm gouge, we propose a quantitative model that confirms that goethite and magnetite have a separate distribution within the gouge.

## 4.2 Sampling and methods

FZB1136 consists of a 16-cm-thick gouge zone framed by deformed sediments. The gouge derived from the alteration of the Pliocene Chinshui Formation, which consists of an alternating formation of sandstones, claystones and marls (*Song et al.* 2007; *Yeh et al.* 2007; *Boullier et al.* 2009). The gouge is composed of fine-grained fragments and rounded clasts (*Boullier et al.* 2009) and the major components are, by importance: quartz, plagioclase, feldspar, and clay minerals (*Kuo et al.* 2009). More than ten slip zones were identified within the FZB1136 gouge, including the 3-mm-thick Chi-Chi earthquake PSZ (Fig. 4-1A) (*Boullier et al.* 2009).

U-channels (plastic box of ~20 cm long and 2 × 2 cm large) were used as core samples from the working half of TCDP hole-B within the 16 cm gouge and deformed sediments of the FZB1136 (1,136.22–1,136.43 m). We collected discrete samples (several grams) to the following depths: 1136.34 m (Sample A, gouge), 1136.38 m (Sample B, PSZ), and 1136.41 m (Sample C, deformed sediments).

Magnetic susceptibility of the U-channel sample was first measured continuously every 0.5 cm with a Bartington MS3 magnetic susceptibility system mounted on an ASC auto-tracking rail (Fig. 4-2). Additional measurements of magnetic susceptibility have been performed on discrete samples with the MS3. The isothermal remanent magnetization (IRM) at 950mT (named  $IRM_{IT}$ ) was performed on U-channel using an impulse magnetizer (MMPM-10) and measured by a 755 SRM cryogenic magnetometer manufactured by 2G Enterprises. In addition, we performed stepwise acquisition of IRM up to 2.5 T of discrete samples by using a Magnetic Property Measurement System (MPMS) XL5 Ever Cool system at the Institute de Physique du Globe de Paris (IPGP), France.

We followed the cooling of a RT-SIRM (room temperature saturated isothermal remanent magnetization) acquired at 300 K and with the application of a magnetic field of 2.5T. On cooling, we applied a small magnetic field of 50  $\mu$ T applied upward. This procedure has been proposed by *Aubourg & Pozzi* (2008) in order to better elucidate a behavior <50 K named the P-behavior. Then a LT-SIRM (low temperature saturated isothermal remanent magnetization) is imparted at 10 K and its evolution is monitored on warming. We present the warming and cooling curves of ~0.5 g of discrete samples sealed in gel caps (Fig. 4-3). Finally, we performed thermal demagnetization of natural remanent magnetization and RT-SIRM of discrete

samples.

### 4.3 Rock Magnetism

The magnetic susceptibility profile of the U-channel sample displays 3 bumps at 1,136.26 m, 1,136.32 m, and 1,136.38 m, the latest being the most developed (Fig. 4-1B). Interestingly, the highest value (600  $\mu$ SI from discrete sample) is localized along the Chi-Chi PSZ. *Hirono et al.* (2006) reported higher susceptibility values ( $\sim$ 700  $\mu$ SI) but the peak is localized at about the middle of the gouge, while here we observed the maximum in the lowest part. The two profiles however cannot be compared. Here, we measured the gouge on a  $2 \times 2$  cm sample. By contrast, *Hirono et al.* (2006) measured the bulk half-borehole ( $\sim$ 10 cm of diameter). As the gouge has an angle of  $\sim 30^\circ$  with respect to the horizontal (*Yeh et al.* 2007), and the measurement was done with a ring-probe, the localization of the magnetic susceptibility peak is not well constrained in the profile presented by *Hirono et al.* (2006).

The  $IRM_{IT}$  curve shows a monotonous ‘hill’ trend with a maximum value ( $\sim 1 \times 10^{-2}$  Am<sup>2</sup>/kg) found at 1,136.34 m (Fig. 4-1C).  $IRM_{IT}$  varies by a factor of 5:1 as also reported by *Mishima et al.* (2009). When comparing the remanence and magnetic susceptibility profiles, it appears that the peak values are shifted by  $\sim$ 4 cm. As the two magnetic parameters are proxies of grain concentration (e.g. *Hunt et al.* 1995), the shift deserves attention, and this will be the main goal of our numerical modeling.

The analysis of low temperature on the remanence of discrete samples provides additional information on the nature of magnetic minerals. The warming curves of LT-SIRM are similar to those presented by *Mishima et al.* (2009) and *Chou et al.* (2012b) (Fig. 4-3A). The Verwey transition (120 K) is well identified in the deformed sediments, and is not visible in the gouge. The most relevant feature is the huge drop of LT-SIRM between 10 K and 35 K ( $>99\%$ ) for the deformed sediments while this drop is limited ( $<1\%$ ) for the gouge samples. The large drop of LT-SIRM is the signature of abundant superparamagnetic (SP) minerals (*Hunt et al.* 1995).

The cooling curves of RT-SIRM provide additional information (Fig. 4-3B). The deformed sediments present a well-developed Verwey transition (120 K) and a subtle Morin transition ( $\sim$ 240 K). Respectively, this indicates the occurrence of stoichiometric magnetite and some occurrence of hematite (Fe<sub>2</sub>O<sub>3</sub>). Two additional observations deserve attention: 1) the RT-SIRM upon cooling increases at about 20%

from room temperature to 150 K. This behavior is generally attributed to the presence of goethite (Dekkers, 1989). 2) Similarly, the RT-SIRM increases at about 90% from 100 K to 10 K. This trend is favored by the application of a small magnetic field upon cooling. Aubourg & Pozzi (2008) and Kars *et al.* (2011) refer this as a P-behavior. It is possibly diagnostic of SP pyrrhotite ( $\text{Fe}_7\text{S}_8$ ,  $<1\ \mu\text{m}$ ). Within the gouge, the RT-SIRM cooling curve is different. The Verwey transition is strongly attenuated, meaning that magnetite is partially oxidized (Özdemir *et al.* 1993; Cui *et al.* 1994; Özdemir *et al.* 2002). A Besnus transition at 35 K develops. This attests for the presence of monoclinic pyrrhotite (Dekkers *et al.* 1989; Rochette *et al.* 1990). The RT-SIRM increase from 300 K to 200 K supports the occurrence of goethite.

We show the thermal demagnetization of natural remanent magnetization of gouge samples, which carry the ChRM (Fig. 4-4A). As already pointed out by Chou *et al.* (2012), the unblocking spectrum temperature is different between the sample localized near the  $\text{IRM}_{1T}$  peak and the sample within the PSZ. For Sample A, the 80% drop of natural remanent magnetization is consistent with a large contribution by goethite for which Néel temperature is  $\sim 120^\circ\text{C}$ . For Sample B, the main contributor to natural remanent magnetization is magnetite for which Curie temperature is  $\sim 575^\circ\text{C}$ . In the deformed sediments (Sample C), the maximum unblocking temperature is near  $600^\circ\text{C}$  (Fig. 4-4A). This indicates that the major magnetic carrier is magnetite. Note the remaining  $\sim 5\%$  portion of NRM at  $600^\circ\text{C}$  for all samples. This suggests a minor contribution of hematite (Néel temperature  $\sim 675^\circ\text{C}$ ). The gouge samples which are located near the deformed sediments exhibit a little contribution of goethite, because only 20% of natural remanent magnetization is destroyed at  $150^\circ\text{C}$  (Fig. 4-5). The thermal demagnetization reveals that goethite has a maximum concentration near the center of the gouge and minimum concentration in the margin of the gouge. The magnetite concentration is maximum near the PSZ.

When monitoring the acquisition of IRM, we note that the deformed sediments (Sample C) is almost saturated at 300 mT (Fig. 4-4B), suggesting a major contribution of the magnetically soft magnetite. In contrast, samples of the gouge (Sample A and Sample B) reach a near saturation at 2 T. This confirms that the high coercivity goethite concentration is more predominant in the gouge.

#### 4.4 Model



The ~4 cm offset between the magnetic susceptibility peak and the  $IRM_{IT}$  peak (Fig. 4-1) will provide the ground of our model. We propose a model where we assume the contribution of hematite and pyrrhotite is negligible.

We calculate the magnetic susceptibility ( $\chi$ ) using:

$$\chi = C_M(x) \cdot C_M \cdot \chi_M + C_G(x) \cdot C_G \cdot \chi_G + C_O(x) \cdot \chi_O$$

Where M and G are magnetite and goethite, respectively.  $C(x)$  is the relative concentration along the profile (values between 0 and 1) and  $C_M$  is the concentration. The “O” stands for the contribution of other magnetic minerals like paramagnetic and SP minerals. Similarly, we calculate the saturated isothermal remanent magnetization using:

$$SIRM = C_M(x) \cdot C_M \cdot SIRM_M + C_G(x) \cdot C_G \cdot SIRM_G$$

$\chi$  and SIRM are averaged using a sliding window filter of 4 cm to simulate the measurement with the U-channel. We take intrinsic magnetic parameters of magnetite and goethite from *Maier et al.* (1999). The intrinsic SIRM are 9 and 0.05  $Am^2/kg$  for magnetite and goethite, respectively. The intrinsic  $\chi$  are 560 and 0.7  $\mu m^3/kg$  for magnetite and goethite, respectively. The ratio of  $\chi/SIRM$  is ~62 for magnetite and ~14 for goethite. The magnetic susceptibility profile of other minerals ( $\chi_O$ ) was based on Mishima’s data (2009) where it is reported a constant paramagnetic susceptibility within the gouge, and a steady decrease of ~30% of this value in the deformed sediments. We assume that the monotonous  $IRM_{IT}$  curve mimics the distribution of goethite concentration, with a maximum value close to the center of gouge. The SIRM at this depth is  $\sim 1 \times 10^{-2}$   $Am^2/kg$ . We assume that magnetite concentration is homogenous in the gouge, except in the PSZ and the presumed baked contact. The width of the PSZ is about 3 mm (*Boullier et al.* 2009) and the baked contact is about the thickness of the PSZ (*Hamada et al.* 2009). The best fit of our model consists in a linear decrease in concentration of magnetite for a thickness of 4 cm including PSZ and baked contact. For the maximum value of magnetic susceptibility, we used the value of 600  $\mu SI$ , inferred from discrete sample measurement within the PSZ.

We fit the concentration of goethite, magnetite, and  $\chi_O$  and compare the model with U-channel results to find the best fit by calculating minimum residual. Within the gouge, we have chosen at first a paramagnetic susceptibility ( $\chi_O$ ) of about half the maximum value observed at the PSZ. However, we never succeed in a good fit of magnetic susceptibility data. To fit the data, we had to take  $\chi_O$  as a quarter of the

maximum magnetic susceptibility (150  $\mu\text{SI}$ ), which is about half of the high-field magnetic susceptibility deduced from the hysteresis loops (*Mishima et al.* 2009). The difference with Mishima's data (2009) is probably due to the fact that the gouge has a significant portion of magnetically hard minerals like goethite. The high susceptibility of the magnetic field is probably more sensitive to hard minerals than weak magnetic field susceptibility can be. In the deformed sediments, by contrast, we take  $\chi_0$  at 485  $\mu\text{SI}$ , which is very close to the low-field magnetic susceptibility measured from the borehole (*Hirono et al.* 2007). *Mishima et al.* (2009) found lower values of high-field magnetic susceptibility (<300  $\mu\text{SI}$ ), but it ignores the contribution of SP minerals. In the deformed sediments, the large drop of LT-SIRM (Fig. 4-3A) indicates that a large portion of magnetic minerals is SP.

Our best model is shown in Fig. 4-6. The  $R^2$  value of normalized magnetic susceptibility ( $\chi$ ) model is 0.981 and of SIRM is 0.986. The calculation is provided in supplementary material. We model a shift of  $\sim 3$  cm between the peak of SIRM and  $\chi$ , which is close to the  $\sim 4$  cm shift observed in U-channel record. Our model indicates the presence of a break-in-slope in the magnetic susceptibility profile that marks the goethite maximum concentration. A break-in-slope is also observed in the U-channel record, although shifted by about  $\sim 1$  cm. This model fits satisfactorily with U-channel observation, and we thus conclude that the dual magnetic assemblage magnetite and goethite dominates the magnetic remanence and the magnetic susceptibility within the gouge.

This model allows calculating the concentration of magnetite and goethite. We plot the absolute concentration inferred from our model in Fig. 4-6. At the remanence peak, we infer a concentration of goethite of  $\sim 20\%$  using either magnetic susceptibility data or remanence. Such a high concentration of goethite is unlikely because XRD investigation failed to reveal this mineral (*Hirono et al.* 2007). This means that the concentration is near 1%. It is possible that pyrrhotite or hematite contribute in a significant way to the magnetic remanence. Therefore, we tested the contribution of goethite by performing a thermal demagnetization of the SIRM (Fig. 4-5). More than 90% of the SIRM is demagnetized below  $150^\circ\text{C}$ , indicating unambiguously that goethite is the major contributor to the magnetic remanence. Therefore, there is a need to reassess the intrinsic magnetic susceptibility and the magnetic remanence of the goethite. To account for the maximum concentration of

about 1% of the goethite, we must increase the initial magnetic parameters by an order of magnitude. The new values are  $\text{SIRM} = 0.5 \text{ Am}^2/\text{kg}$  and  $\chi = 7 \mu\text{m}^3/\text{kg}$  for the micrometric elongated goethite of the gouge. When comparing these values to those reported by *Peters & Dekkers* (2003) for a variety of natural goethites, it seems that the  $\chi$  deduced from our model is close to the largest measured values, but that the SIRM is higher for a factor of 5  $\mu\text{m}^3/\text{kg}$ . Taking these new values, the maximum concentration of goethite is 1.6 to 2.5% when using the magnetic susceptibility and magnetic remanence to saturation, respectively (Fig. 4-7B).

To calculate the maximum concentration of magnetite, we use the magnetic record along the PSZ. The maximum concentration is 180 to 267 ppmv when using the magnetic susceptibility and the magnetic remanence at saturation (Fig. 4-7A). These concentrations are close to the range of values proposed by *Mishima et al.* (2009). Elsewhere in the gouge, the concentration of magnetite is less than 30 ppmv, suggesting a decrease of one order of magnitude in concentration. In the deformed sediments, we make the distinction between magnetite above and below the blocking volume (SD-MD and SP, respectively). The SD-MD magnetite concentration is below 2 ppmv in the deformed sediments. By contrast, The SP magnetite concentration is about ~400 ppmv when assuming the SP susceptibility (~200  $\mu\text{SI}$ ) is dominantly carried by magnetite. We take the intrinsic susceptibility of SP magnetite at about 2 SI according to experimental data of *Heider et al.* (1996). Note that contribution of greigite ( $\text{Fe}_3\text{O}_4$ ) or fine pyrrhotite may complicate the calculation of this concentration.

#### 4.5 Discussion and conclusions

We propose a model which satisfactorily explains the shift of ~4 cm from the peak of magnetic susceptibility and remanence peak. We demonstrate this by taking different concentration profiles for goethite and magnetite. From our best fit, we infer three order of magnitude of magnetite concentration between the Chi-Chi PSZ (~200 ppmv), the gouge (~20 ppmv), and the deformed sediments (~2 ppmv) (Fig. 4-7A). This demonstrates the presence of neoformed magnetite in the gouge, and particularly within the PSZ and its baked contact. *Mishima et al.* (2009) and *Chou et al.* (2012b) suggested that magnetite formed during frictional processes. If it seems clear that the friction can cause new magnetic minerals, it is surprising that there is a concentration

gradient between the PSZ and the rest of the gouge. *Boullier et al.* (2009) reported the existence of tens of slip zone within the 16 cm gouge. If the magnetite was produced during friction, it makes sense to find a rather homogeneous concentration of magnetite in the gouge, rather than more localized on a single slip zone. We suggest two hypotheses. 1) Magnetite formed principally during large earthquakes. In this case, the Chi-Chi PSZ is probably unique and there is no other slip zone associated with large magnitude earthquakes in the FZB1136 gouge. 2) Magnetite formed during successive earthquakes has been altered during inter-seismic periods. We prefer the latter case because the analysis at low temperature (Fig. 4-3) shows a severe attenuation of Verwey transition, which might be an indication of partial oxidation of magnetite (*Özdemir et al.* 1993; *Cui et al.* 1994; *Özdemir et al.* 2002). The distribution of magnetite as shown in our model indicates that the maximum magnetic susceptibility marks the location of the most recent seismic slip zone in a gouge.

In the deformed sediments, the concentration of magnetite whose grain size is larger than the volume of blocking is very low (~2 ppmv). However, the concentration of SP magnetic minerals is larger by two orders of magnitude (~200 ppmv). Identification of SP minerals in sediments and not in the gouge was also observed by *Mishima et al.* (2009). The SP minerals come from sediments are probably altered during the earthquake and are no longer present in the gouge. However, the grinding process is likely to produce ultra-fine magnetic minerals, and it is rather surprising that no SP is observed in the gouge. We propose two hypotheses to explain this absence. 1) Hyper-fine minerals for products during milling are oxidized, just like sediments-derived SP. 2) Grain crushing is not sufficient to produce SP minerals. *Ma et al.* (2006) suggested that minerals <50 nm of the gouge are produced probably by chemical precipitation processes. If we stick to *Ma et al.* (2006) study, it is unlikely that SP minerals formed during the earthquake, since the sizes of these minerals are generally <50 nm.

The occurrence of goethite in the FZB1136 gouge was first discovered by *Chou et al.* (2012). According to these authors, the goethite was formed shortly after the Chi-Chi earthquake, probably due to the cooling of hot fluids. According to our model, the concentration of goethite reached about 1% in the middle of the gouge and has a V-shaped distribution (Fig. 4-7B). During the Chi-Chi earthquake, several studies (*Ishikawa et al.* 2008; *Boullier et al.* 2009) have suggested that the phenomena of

thermal pressurization had limited friction in the gouge. The presence of goethite confirms that fluids were present in the gouge in the earthquake. Our model suggests that these fluids were richer in iron in the center of the gouge on the edges.

From this study, it is concluded that the major constituents of magnetic minerals in FZB1136 gouge resides in magnetite and goethite. Our quantitative model of magnetic mineral assemblage simulates very well the profile of magnetic susceptibility and remanence, while explaining the shift of  $\sim 4$  cm between the maximum of these values. The magnetic susceptibility maximum corresponds to the maximum concentration of the magnetite and suggests that this maximum may mark the location of the most recent seismic slip zone. Similarly, the maximum remanence is associated with a higher concentration of goethite, and precise location of iron-rich fluids. We propose that the magnetite and goethite form, but also deteriorate during seismic cycles. When co-seismic to post-seismic phase, these two minerals form under the combined action of temperature and fluids on cooling. When inter-seismic phase, magnetite oxidizes. If this oxidation is verified by studies in other gouges, this implies that the maximum magnetic susceptibility is located along the most recent seismic slip zone. With respect to goethite, the latter may be altered under the action of fluids  $>300^{\circ}\text{C}$  during the co-seismic phase.

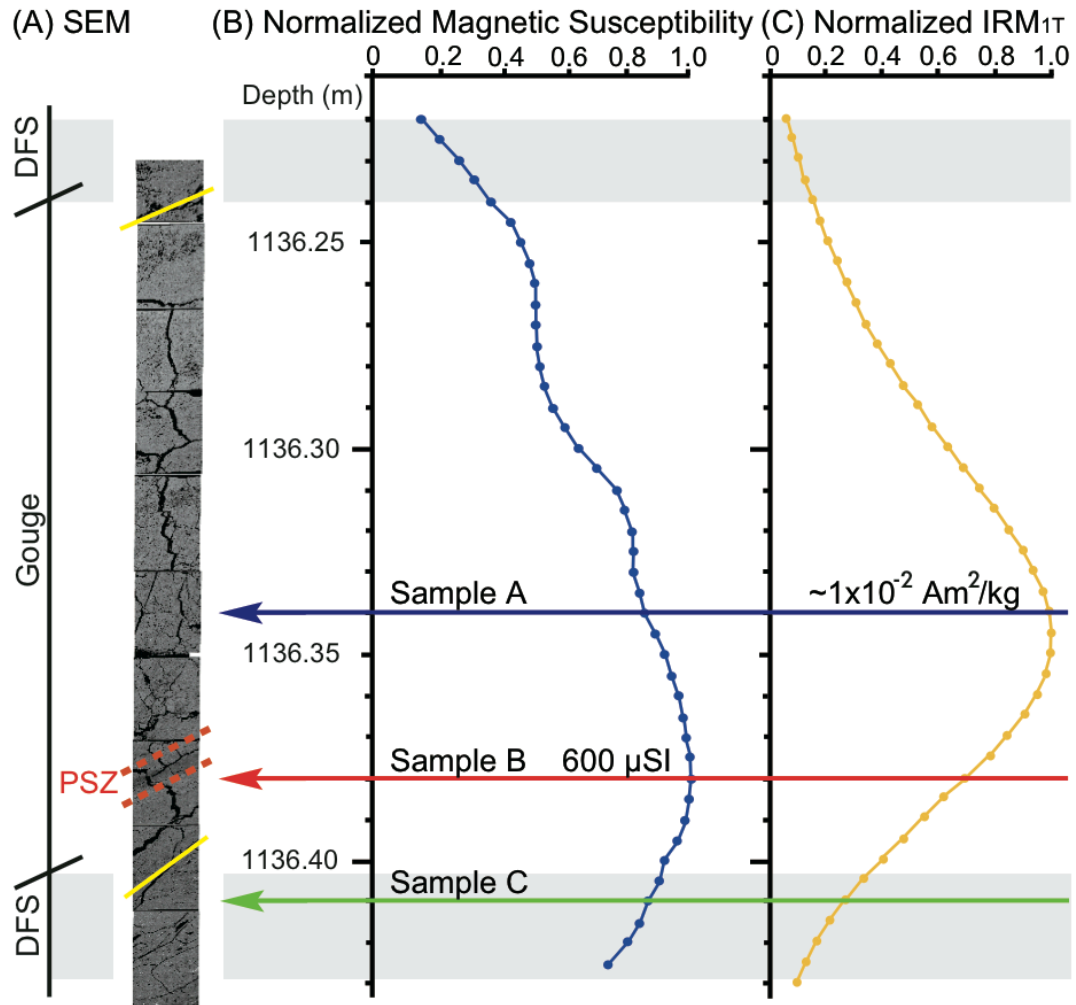


Fig. 4-1: (A) SEM image observation of FZB1136. The yellow line indicates the boundary of deformed sediments (DFS) and gouge, and dash red lines show the range of the 1999 Chi-Chi earthquake PSZ. (B) Normalized magnetic susceptibility and (C) normalized  $IRM_{1T}$  of FZB1136 U-channel measurements. The blue arrow line at 1,136.34 m is the location of Sample A at the  $IRM_{1T}$  peak ( $\sim 1 \times 10^{-2} Am^2/kg$ ). The red arrow line at 1,136.38 m (PSZ) is the location of Sample B at the magnetic susceptibility peak (600  $\mu SI$ ). The green arrow line at 1,136.41 m is the location of Sample C at the deformed sediments.



Fig. 4-2: Photo of Bartington MS3 magnetic susceptibility system mounted on an ASC auto-tracking rail in IES, Academia Sinica.

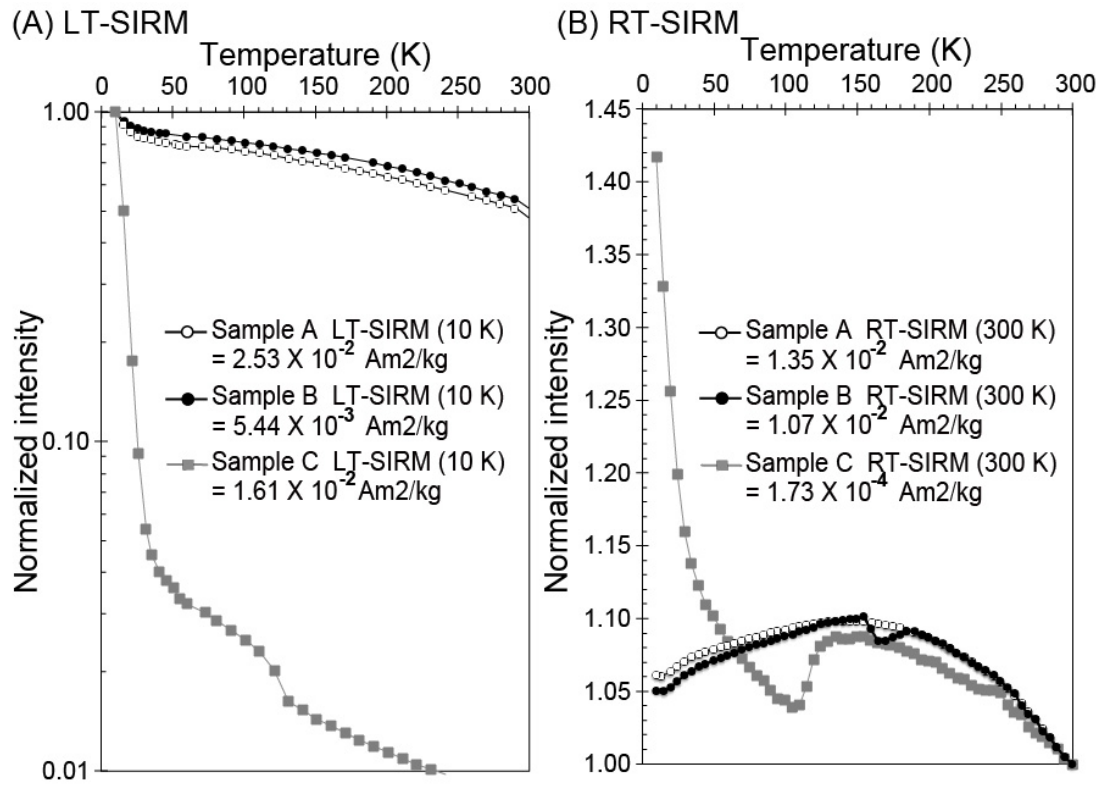


Fig. 4-3: Low temperature analyses result of samples. (A) LT-SIRM warming curves (B) RT-SIRM cooling curves.



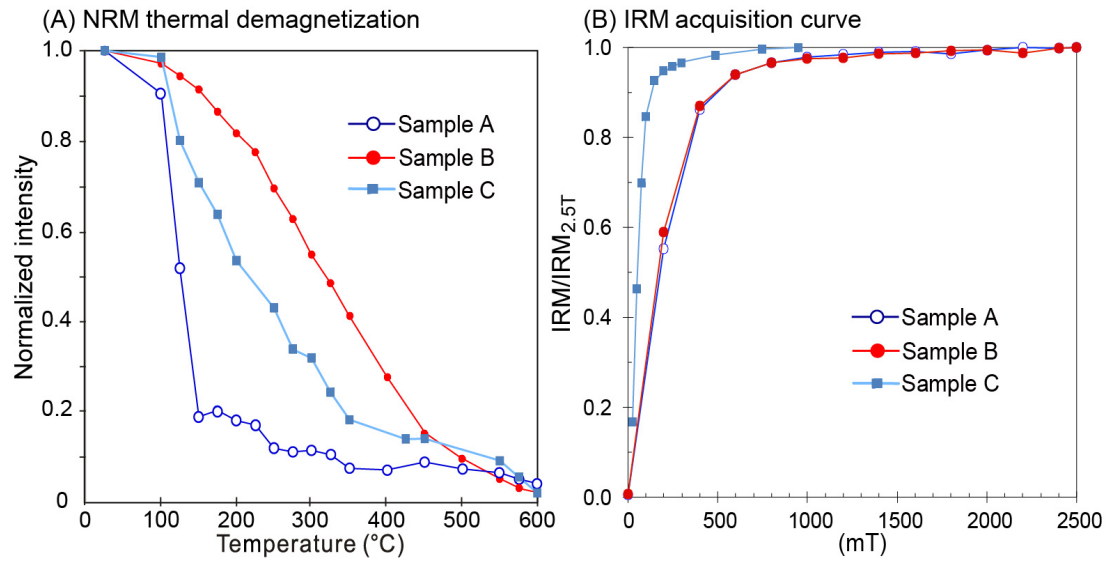


Fig. 4-4: (A) Thermal demagnetization of natural remanent magnetization (NRM). (B) IRM acquisition curves up to 2.5 T. The locations of Sample A, Sample B, and Sample C are specified in Fig. 4-1.



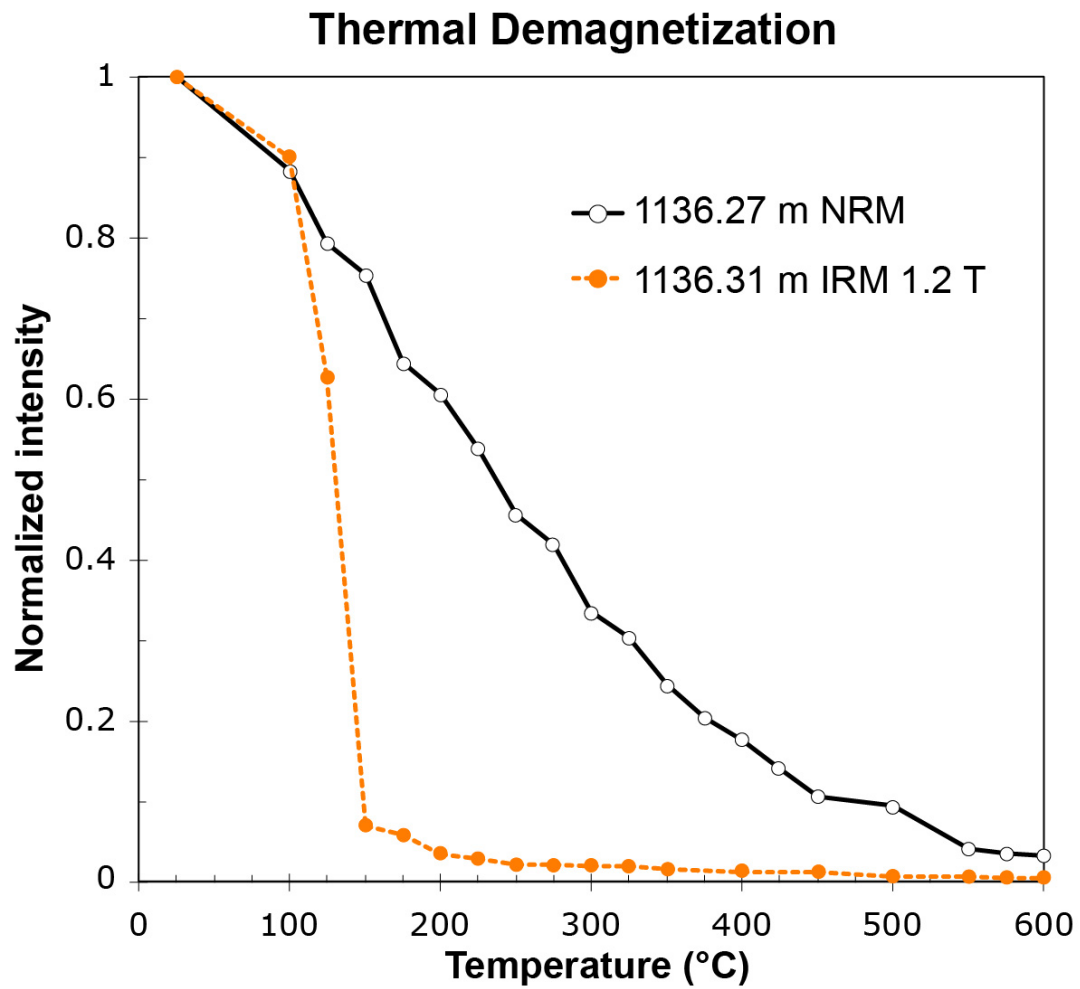


Fig. 4-5: Thermal demagnetization of gouge sample located near the deformed sediments and of gouge sample located at gouge center after applying 1.2 T RT-SIRM.

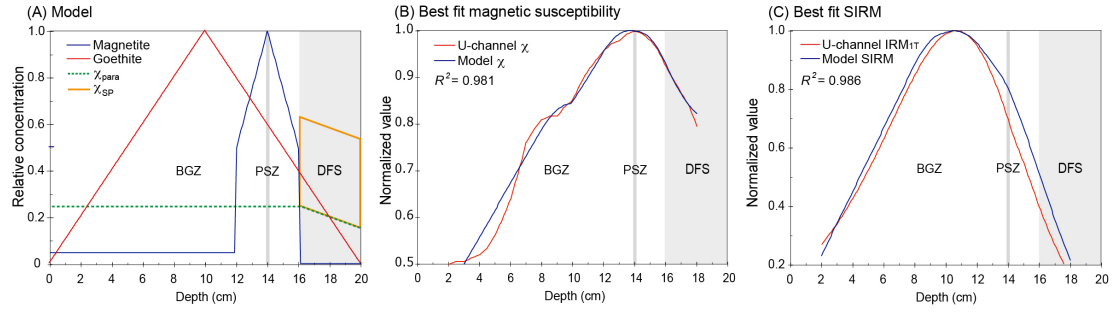


Fig. 4-6: (A) Model of magnetite and goethite assemblage curves in a 20 cm U-channel. Blue line is relative to the magnetite concentration. Red line is relative to the goethite concentration. Green dash line is magnetic susceptibility contribution of paramagnetic minerals ( $\chi_{para}$ ). Yellow line is magnetic susceptibility contribution of SP minerals ( $\chi_{SP}$ ). (B)(C) The comparison between U-channel results (red line) and our best-fit curves (blue line) of normalized magnetic susceptibility ( $\chi$ ) and SIRM, respectively. The  $R^2$  value of normalized magnetic susceptibility ( $\chi$ ) model is 0.981 and of SIRM is 0.986.



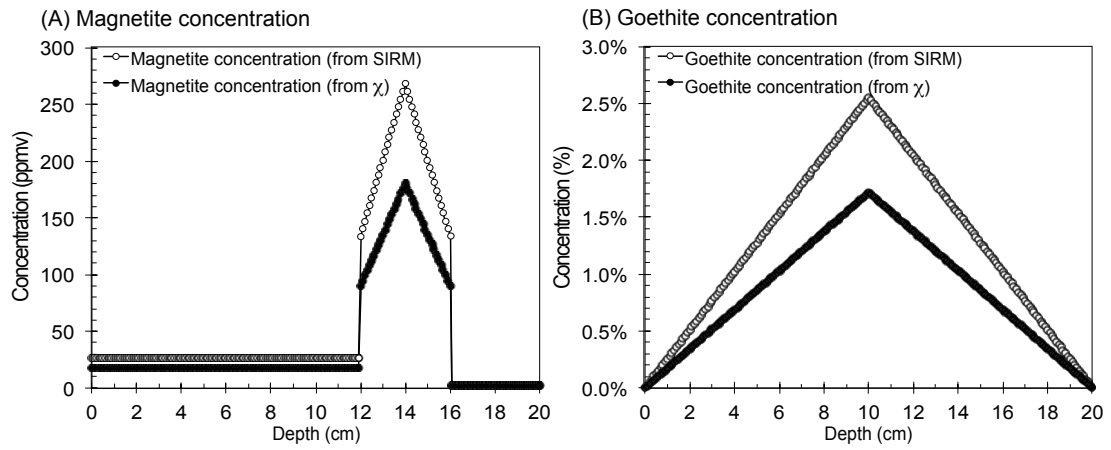


Fig. 4-7: The concentration curves of (A) magnetite and (B) goethite, which were calculated from our model by using the magnetic susceptibility and the remanence.



## **Chapter 5. Nano-particle Quartz (<50 nm) Investigation in the gouge of the Chelungpu Fault, Taiwan and Its Tectonic Implications**

### **(Tectonophysics, in prepared)**

#### **5.1 Introduction**

For studying the physical and chemical process of earthquake, gouge is a key to investigate the faulting mechanism. The total energy releases of fault zone during an earthquake are still unknown clearly (*Heaton, 1990; Kanamori, 1994; Kanamori and Heaton, 2000*). Fracture energy calculation has been reported from seismological and experimental rock deformation data (*Wong, 1982; Okubo and Dieterich, 1984; Guatteri et al., 2001; Rice et al., 2005; Abercrombie and Rice, 2005*). In the past, numerous studies reported that analysis of particle size distribution within ultrafine gouge to calculate total grain surface area by optical and electron microscopies, then to estimate the fracture energy associated with gouge formation (*Wilson et al., 2005; Chester et al., 2005; Ma et al., 2006*). During a fault slipping, gouge particles will be milling into smaller fractions to the nanometer scale (*Wilson et al., 2005*). *Chester et al. (2005)* observed the finest particle size being 1.6 nm within the Punchbowl fault gouge as the lower cut-off for fracture energy estimation. *Ma et al. (2006)* observed the gouge in the fault zone of Taiwan Chelungpu-fault Drilling Project (TCDP) at depth about 1 km. They used grain sizes larger than 50 nm as lower cut-off to estimate fracture energy, because the transmission electron microscope (TEM) image of grain sizes less than 50 nm shows rounded shapes. Therefore, they considered those grains <50 nm might be formed by chemical precipitation rather than fracturing. However, the TEM image of *Chester et al. (2005)* also shows rounded shapes in their ultrafine grains for calculation; the image of *Ma et al. (2006)* shows very fine grain around several nm in diameter, which did not consider for fracture energy. In addition, the very fine grains have larger surface area than coarse grains and could provide high percentage of total fracture energy significantly. Thus, to determine the lower cut-off grain sizes is important for fracture energy calculation.

In order to investigate the smallest grain sizes formed by fracture within ultrafine gouge, analysis of the finest mineral composition and grain size distribution are requisites. Nevertheless, nanoparticles generally aggregate to each other quickly or cling to large grain surface because of their surface reactivity at the nanometer scale and their relatively large surface area. Hence, how to collect nanoparticles in natural materials with high efficiency and in large quantities for analyses is a challenge. *Tsao*

*et al.* (2009a, b) developed an automated ultrafiltration device (AUD) for high efficient collection of nanoparticles, which had been proved to be more efficient than the conventional ultracentrifugation and syringe filtration methods. This device provides us a solution to nanoparticle collection from ultrafine gouge for further analysis.

In this study, we present a grain size separation of gouge sample from the 1999 Chi-Chi earthquake surface rupture. First, we separate different particle size ranging from 50  $\mu\text{m}$  to 1 nm by centrifuge and AUD. Second, we focus on the mineralogy by using synchrotron X-ray diffraction (XRD) and TEM. Lastly, we propose quartz is the index mineral associated with gouge formation and the low cut-off grain size is 25 nm. The smectite and illite nanoparticles could be associated with weather process of gouge at outcrop.

## 5.2 Geological setting and sampling

Taiwan is located at the boundary between the Eurasian Plate and the Philippine Sea Plate. The Philippine Sea Plate is moving toward W54°N at a speed around 80 mm per year (*Yu et al.*, 1997) and is impacting with the Eurasian continental margin. This substantial collision and uplifting between two subduction systems result in active faulting, enhance the development of numerous earthquakes and crustal deformation within Taiwan Island. Taiwan is generally subdivided into some geological regions, from west to east; they are the Coastal Plain, the Western Foothills, the Central Range, the Longitudinal Valley, and the Coastal Range (*Ho*, 1986). The most active region within Taiwan is along the belt between the Coastal Plain and the Western Foothills. There are several fault zones around this active seismic region, include Shuilikeng, Shuangtung, Chelungpu, and Changhua faults.

The Chelungpu fault zone was described as the Chinshui Formation overthrusting the Toukashan Formation in the southern Taichung Basin (*Chang*, 1971). This fault is a thrust fault of over 85 km in length and is a main boundary between the Plio-Pleistocene fold-and-thrust belt to the east and late Quaternary basin to the west. The fault is reasoning to have formed at the beginning of the Mid-Pleistocene, 0.7-0.5 Ma (*Chen et al.*, 2001).

The Chi-Chi earthquake ( $M_w$  7.6) took place to the central Taiwan on 21 September 1999. The hypocenteris was located near Chi-Chi town (120.81° E, 23.86° N, depth ~10 km, *Ma et al.*, 1999; *Kao and Chen*, 2000). The surface rupture was along the Chelungpu fault zone at about 85 km in length with large surface

deformation (*Ma et al.*, 1999; *Lee et al.*, 2002; *Angerlier et al.*, 2003). The surface deformation provides us a good opportunity to sample outcrop fault gouge of recent earthquake.

Our gouge sample was caught from the Chelungpu fault branch of the 1999 Chi-Chi earthquake surface rupture passes through Wu-Feng downtown in center Taiwan (Fig. 8.1.5-1). The hanging wall raised a height about 2.5 m in the campus of Kuang-Fu junior high school during the Chi-Chi earthquake. The sample investigated in this study is from the outcrop of Chi-Chi fault gouge, which is located at riverbed behind campus. The fault black gouge zone is up 15 cm wide and 60° in dip within the Chinshui Formation (siltstone). A block of black gouge was sampled for nanoparticle analyses (Fig. 5-2).

### 5.3 Methods

#### 5.3.1 Separation of Fault Particles in Different Particle Size

The sample was shattered into powder and put in room for air dry 2 weeks. After, the gouge powder was passed through a 300-mesh sieve (aperture 50 µm) to remove coarse fraction (>50 µm). Then the <50 µm size fraction (about 100 mg) was removed organic matter by H<sub>2</sub>O<sub>2</sub> under 70°C. Next, the <50 µm size fraction was divided into <2 µm size fraction by sedimentation according to Stokes' Law (*Tanner and Jackson*, 1947; *Williams et al.*, 1958; *Jackson*, 2005). The <2 µm size fraction was separated into different range by using centrifugation. The centrifugation time required to separate this fraction into the size range was calculated by the modified Stokes' equation

$$d = \sqrt{\frac{18\eta \ln(R_2/R_1)}{(\rho_s - \rho_w)\omega^2 t}} \quad (\text{Poretz, 1979; Ross and Morrison, 1988; McFadyen and}$$

*Fairhurst*, 1993; *Laidlaw and Steinmetz*, 2005).  $d$  is the particle diameter (cm),  $\eta$  is the viscosity coefficient of the liquid (g cm<sup>-1</sup>s<sup>-1</sup>),  $\rho_w$  is the density of the liquid (g cm<sup>-3</sup>),  $\rho_s$  is the particle density (g cm<sup>-3</sup>),  $R_1$  is the radius from the centrifugal center to the sample height inside the tube (cm),  $R_2$  is the radius from the centrifugal center to the sample bottom inside the tube (cm),  $\omega$  is angular velocity (rpm), and  $t$  is the ultracentrifugation time (sec). The fault gouge density was measured by pycnometer method; the average gouge density is 2.58 g cm<sup>-3</sup>.

The centrifugal steps were using a Hitachi CR21 refrigerated centrifuge (Fig. 5-3, Hitachi High-Technologies Corp., Tokyo, Japan), which had a R12A3 rotor with polycarbonate tubes (250 ml × 6) and settling sample height of 10 cm. For collecting

the 450-to-2000 nm size fractions, the suspension (<2000 nm size fractions) was centrifuged at  $980 \times g$  (3370 rpm) for 5 min by ultracentrifugation at 4°C. The settled particles were re-suspended in double deionized water (DDW) and were using ultrasonic dispersion at 170 W and 60 kHz for 1 min by NEY 300 Ultrasonic. The dispersed suspension was then repeatedly centrifuged and washed ten times by the same centrifugation and dispersion methods to rarefy the 450-to-2000 nm size fractions. We used the same process with different centrifuged speed and time for separating different particle size range (100-to-450 and 50-to-100) by using higher centrifugation velocity and time.

To collect the 25-to-50 nm fractions, <50 nm suspension was filtered by the AUD (Fig. 5-4) using 25 nm pore size Millipore membrane filter to separate <25 nm size fraction. After, the <25 nm suspension was filtered by the AUD using the Sigma ultrafiltration disk membrane (NMWL: 1000 Da-equivalent to 1 nm in diameter) to collect the size of 1-to-25 nm fractions.

The flow chart of separation methods, centrifuge velocity, and time for different particle size fracture collection is shown in Fig. 5-5.

### 5.3.2 XRD and TEM analysis

The synchrotron XRD could provide higher X-ray counts and a small size X-ray beam for a few samples. The synchrotron powder XRD patterns were analyzed at Wiggler Beamline BL17A W20 XRD with  $\lambda = 1.334431 \text{ \AA}$  of the National Synchrotron Radiation Research Center, Taiwan. It was operated at 1.5 GeV with a ring current of 300 mA using the top-up injection mode. The suspension was treated by frozen dry for collecting powder (non-orientated) for synchrotron XRD measurement. For observing the occurrence of the particle <100 nm fractures, images were taken by using a FEI Tecnai G2 T20TEM with energy dispersive X-ray spectrometer (EDX), which was operated accelerating voltage at 200 keV in the Department of materials science and engineering, National Taiwan University.

## 5.4 Results

This study focuses on observing the smallest particle-size fractions for understanding the mineralogy of nano-particles within the Chelungpu fault gouge, which were formed from fractured or precipitation by faulting process. In addition, to know the finest grain size of fractured particle by faulting.



### 5.4.1 Synchrotron XRD

The synchrotron XRD within the NSRRC provides higher resolution diffraction patterns; the analysis patterns of different particle size fractions are shown in Fig. 5-6. These diffraction patterns indicate the major minerals are quartz, plagioclase, smectite, illite, chlorite, and kaolinite. From results, we found quartz, plagioclase, smectite, illite, chlorite, and kaolinite in the 2-50  $\mu\text{m}$ ; quartz, plagioclase, smectite, illite, chlorite, and kaolinite in the 450~2000 nm; quartz, plagioclase, smectite, and illite in the 100~450 nm; quartz, smectite, and illite in the 50~100 nm; smectite, illite, and quartz in the 25~50 nm; smectite and illite in the 1~25 nm. The mineral categories of these different grain size intervals are listed in Table 5-1. Among, quartz is dominant mineral within the coarse grains (>450 nm); however, clay minerals are major components within fine grains (<100 nm). The peak intensity of clay increases largely as the reduction of grain size. Besides, chlorite, kaolinite and plagioclase were not found within the fractions <450 nm. The 3.34 Å diffraction peak could be an overlap of illite  $d(003)$  and quartz  $d(101)$ .

### 5.4.2 TEM

We concentrate on the fractures of grain size <100 nm which contain minerals of quartz, illite and smectite. The TEM images of <100 nm grains are shown in Fig. 5-7. Platy pieces, lath-like fractions, and rounded grains are observed (Fig. 5-7A, B). Platy pieces and lath-like fractions could be clay minerals as illite or smectite. Rounded grains seem be swathed by a cortex of clays. This kind of grains are likely clay-clast aggregates (CCA) which were reported by *Boutareaud et al.* (2008) and *Boullier et al.* (2009) within fault gouge. The rounded grain could be as quartz cause of hexagonal electron diffraction and the EDX analysis result shows that the Si and O are major components (Fig. 5-7C). Some ultrafine grains (<10 nm) could be found.

## 5.5 Discussion

The very fine grains formed by grinding have been reported in nature fault zones (~10-50 nm; *Chester et al.*, 2005; *Reches and Dewers*, 2005; *Wilson et al.*, 2005; *Ma et al.*, 2006), in mining induced fault zone (40 nm; *Olgaard and Brace*, 1983), and in deformation experiments on granite (10-30 nm; *Yund et al.*, 1990; *Heilbronner and Keulen*, 2006). In this study, the particles being smaller than 10 nm could also be found within nature fault gouge by TEM. The efficiency of nanoparticle collection technique by AUD provides us a new view to identify those very fine grains.

The mineral compositions of our gouge sample are coincidence with the gouge sample from TCDP deep-drilled core Hole-A fault zone at depth 1,111 m (*Kuo et al.*, 2009), by importance: quartz, plagioclase, illite, smectite, and kaolinite. For clay mineral analysis, *Hirono et al.* (2008) reported the black gouge of TCDP Hole-B at depth 1,136 m with the disappearance of kaolinite, lower relative abundances of smectite and chlorite, and large abundances of illite. They also suggested that the dehydroxylation of kaolinite and illitization of smectite occurred during co-seismic frictional heating within the gouge (*Hirono et al.* (2008)). *Kuo et al.* (2009) reported anomalies of clay mineral assemblage within the principal slip zone of the Chelungpu fault gouge as decline of illite, disappearance of kaolinite and chlorite, and increasing of smectite. *Kuo et al.* (2009) considered the pseudotachylyte has been occurred due to strong shear heating during the earthquake within the principal slip zone of gouge and altered to smectite quickly. In the Chelungpu fault gouge outcrop, we found the similar state as *Kuo et al.* (2009) rather than *Hirono et al.* (2008). Moreover, we could observe that the relative abundances of smectite and illite increases as grain size reduced, which were still found in the 1-25 nm fractions (Fig. 845-6). However, we don't have any evidence of pseudotachylyte exist in our gouge sample. Furthermore, because our gouge sample locates at surface outcrops and closes to riverbank, the weathering process could be another way to influence the clay mineral formation (*Kuo et al.*, 2012). Plagioclase is easy to alter as illite by weathering process (*Bétard et al.*, 2009) and could not be found in fine grains. Although clay minerals could also be grinded into small pieces during co-seismic time, we suggest that ultrafine grain clay minerals formed by chemical process rather than fracturing process.

Eliminating clay minerals, quartz is the most important target mineral. *Gibbs* (1967) reported that the minimum grain size of quartz is ~1 mm within the suspended solids at the mouth of Amazon River. The sedimentary environment of Chinshui Formation (siltstone) is shallow marine; the original grain size of quartz within the Chelungpu fault gouge could be around 1 mm. *Kendall* (1978) illustrated that a grain size limitation was ~1 mm occurred for particles under grinding in nature. Particles smaller than the grinding limitation were observed to deform plastically and change their shape and the grinding limitation of quartz is 0.9 mm for quartz (*Prasher*, 1987). Some experiences showed that quartz could be grinding to 30-50 nm in a stirred-media mill (*Chao et al.*, 1996; *Wang and Forssberg*, 2006). Grain size reduction in the fault zone is cause of cracked grains result from original fragmentation by rupturing (*Heilbronner and Keulen*, 2006; *Keulen et al.*, 2007,

*Sammis and King, 2007*). In this study, we observe rounded quartz grain of <50 nm in the gouge sample from both results of synchrotron XRD analysis and TEM observation (Fig. 5-6 and 5-7).

*Ma et al. (2006)* considered grain sizes less than 50 nm in fault gouge shows rounded shapes as formed by chemical precipitation. Quartz is easy to precipitate under lower pH (<6) (*Knauss and Wolery, 1988*); the overgrowths of authigenic quartz in different sediments and diagenetic environments have been reported (e.g., *Williams et al., 1985; Evans, 1990; Jakobsen et al., 2000; Oelkers et al., 2000*). However, we exclude the quartz precipitation in this study under lower pH cause of 1) the shallow marine sedimentary environment of Chinshui Formation, and 2) location at riverbank.

*Sammis et al. (2008)* discussed the limitation of the smallest nanoparticle size in fault zone rock is derived from the healing effect of nanoparticles by amplitude and duration of the temperature pulse during large earthquake. They showed the time required to double the grain size of quartz as a function of the original grain size for a range of temperature. Because the study sample is located at surface condition with low normal stress, the co-seismic temperature elevation could be not very high. The CCAs grains (Fig. 5-7) could an evidence of large slip at co-seismic velocity with thermal pressurization (*Boutareaud et al., 2008*). The absence of pseudotachylite exist in the study gouge sample also indicates the temperature not higher than 900°C (*Kuo et al., 2011*). Although we don't have any evidence about the experienced temperature in the gouge, we consult the estimated temperature in the range of 550-680°C by vitrinite reflectance analysis result in shallow hole sample of Chelungpu fault gouge (*Sakaguchi et al., 2007*). Even at the highest temperature of 680°C, a 10 nm quartz particle will double its size around 20 minutes. Thus, we exclude temperature effect to influence the grain size of nanometer quartz in the gouge.

## 5.6 Conclusion

The ultrafine nanoparticle is the key point to determine the low cut-off for seismic fracture energy estimating from the slip fault gouge. The gouge sample from the Chelungpu fault branch of the 1999 Chi-Chi earthquake ( $M_w$  7.6) surface rupture was separated into different particle sizes ranging from 50  $\mu\text{m}$  to 1 nm by centrifuge and AUD. The mineral results suggested that the formation of <100 nm nanoparticles of smectite and illite could be associated with weathering process. The quartz could

be the index mineral associated with earthquake fracture and the finest grain size is around 25 nm.



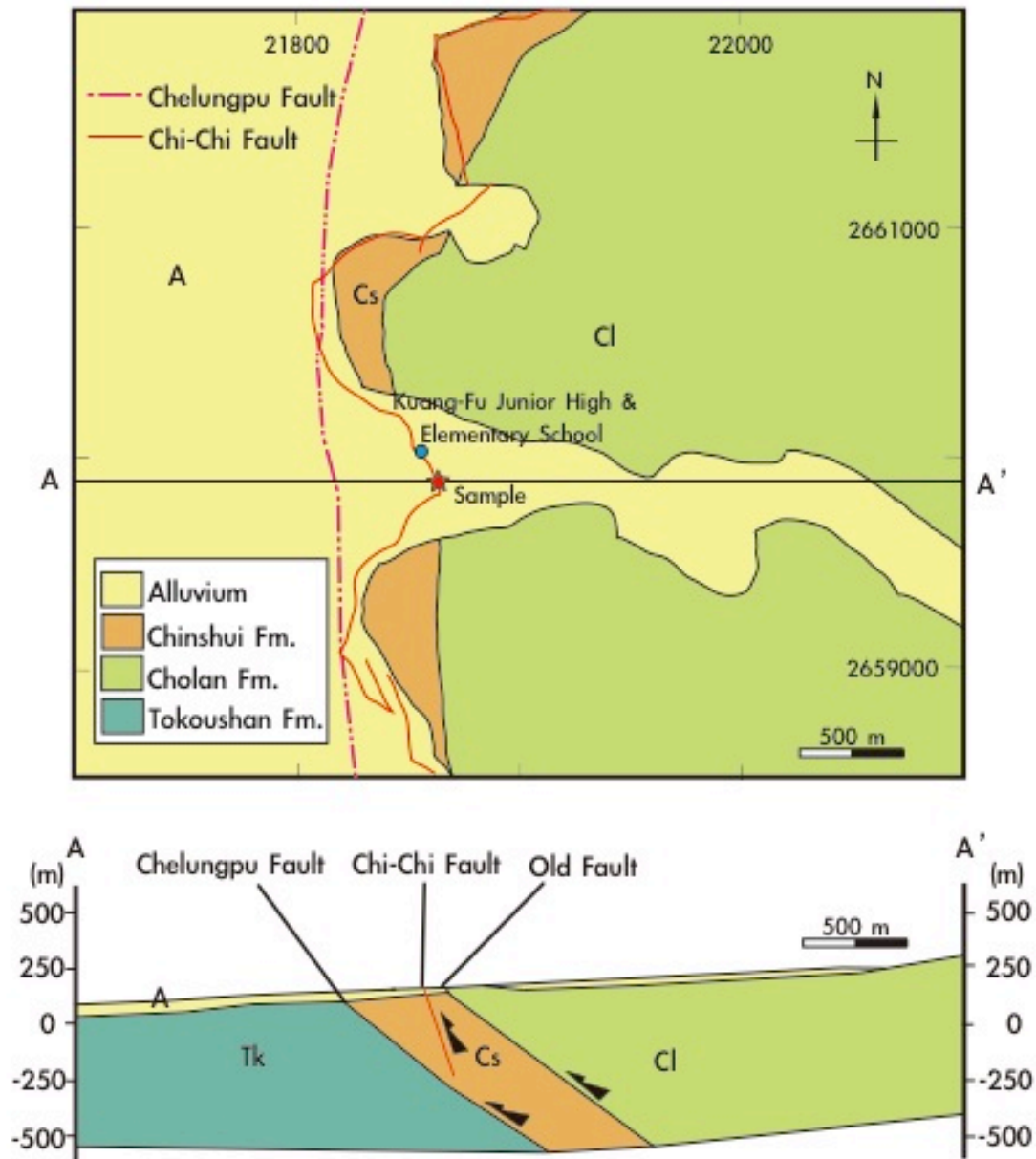


Fig. 5-1: Geological setting of sampling location in Wu-Feng, center Taiwan (Modified from *Huang et al.*, 2001). (A) Geological map of Wu-Feng with Chelungpu fault and the Chi-Chi earthquake fault rupture. (B) Geological cross section passing the sampling location.



Fig. 5-2: Block black gouge sample of Chelungpu fault outcrop. It contains very fine grains.

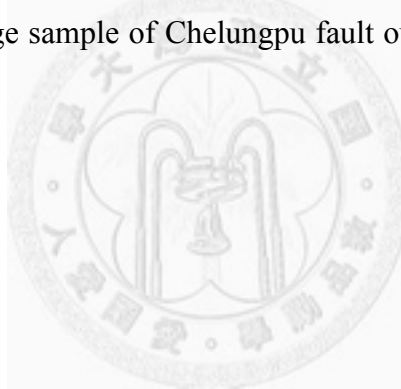
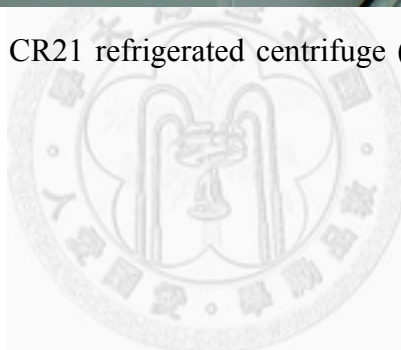






Fig. 5-3: Photo of Hitachi CR21 refrigerated centrifuge (Hitachi High-Technologies Corp., Tokyo, Japan).



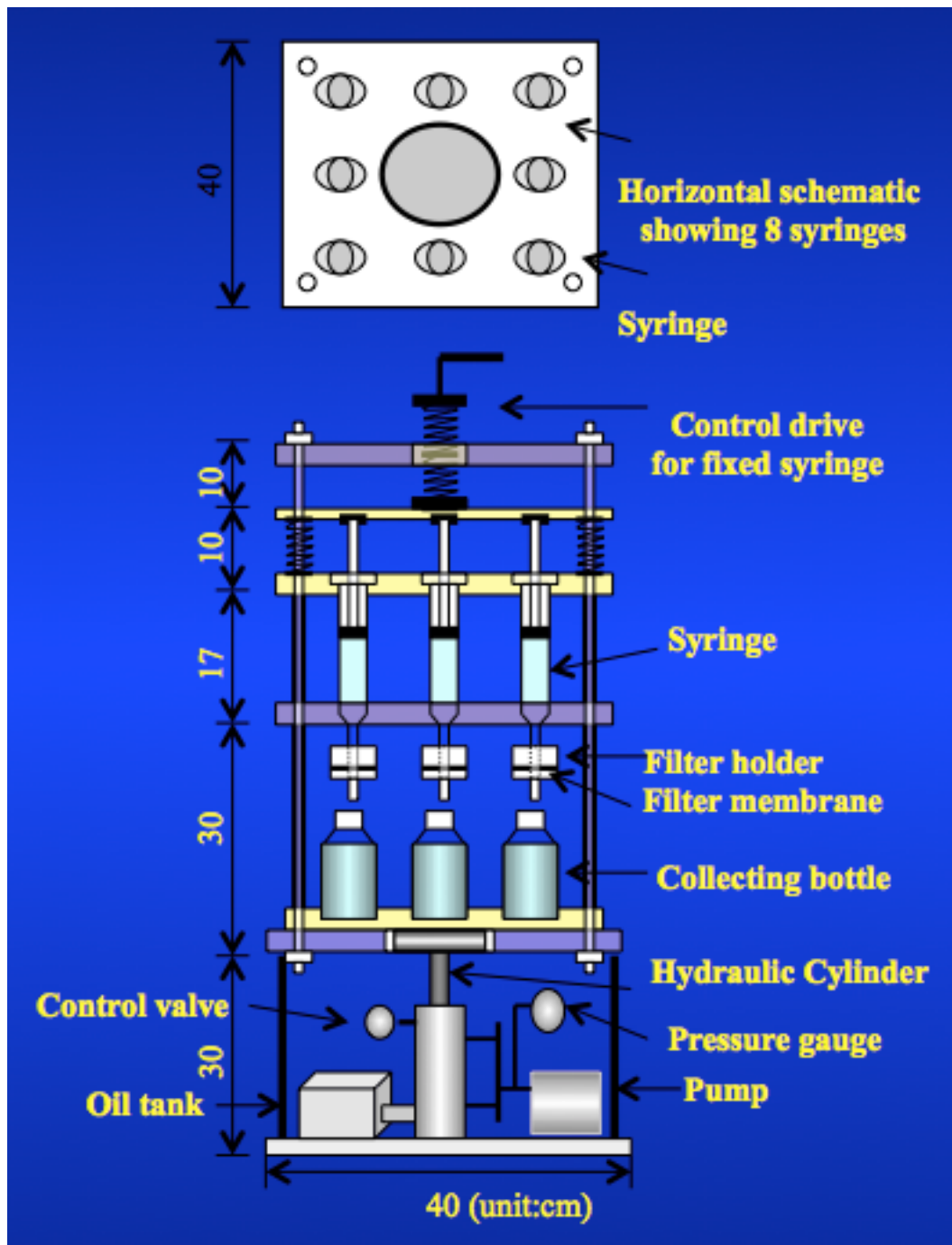


Fig. 5-4: Schematic diagram of an automated ultrafiltration device (AUD) for nanoparticle separation (Tsao *et al.*, 2009a).



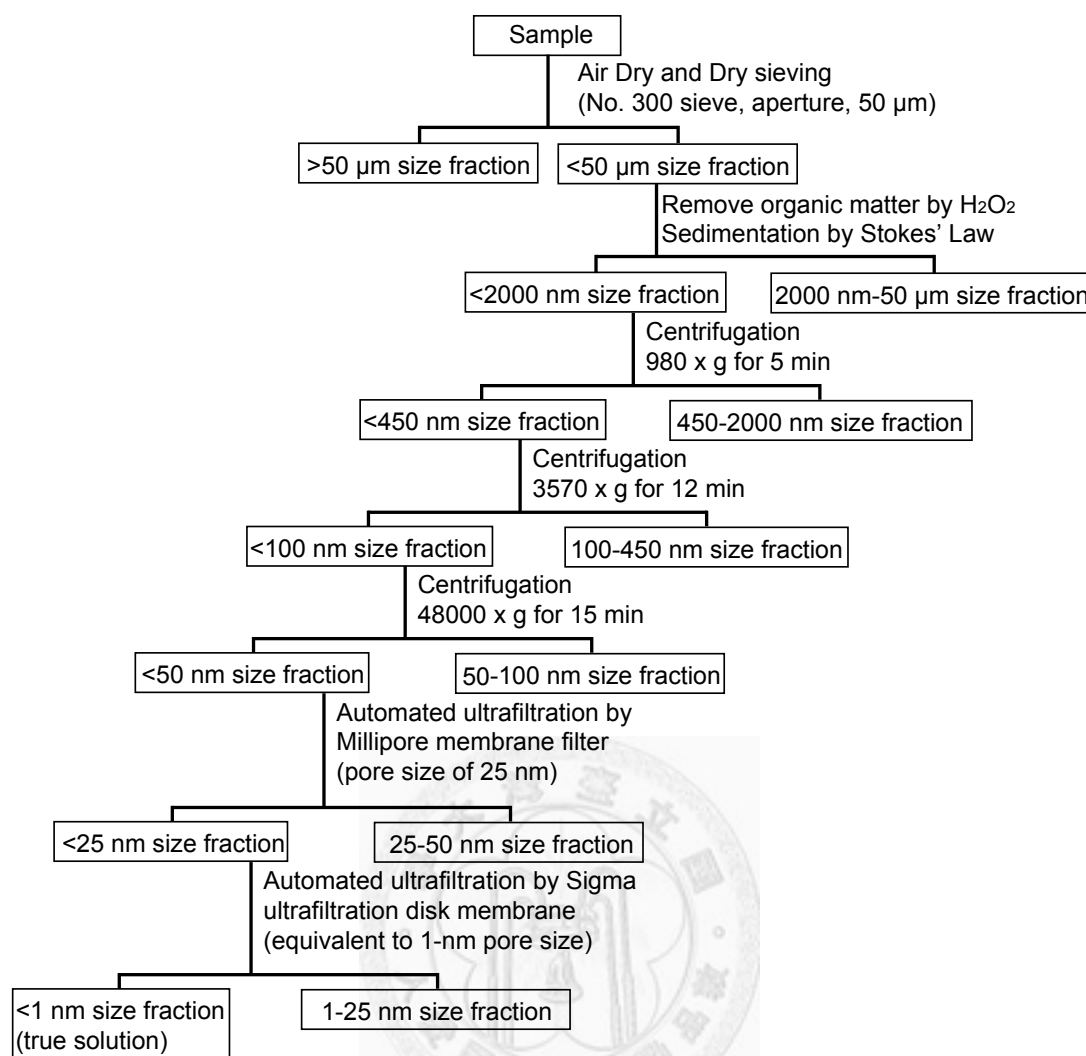
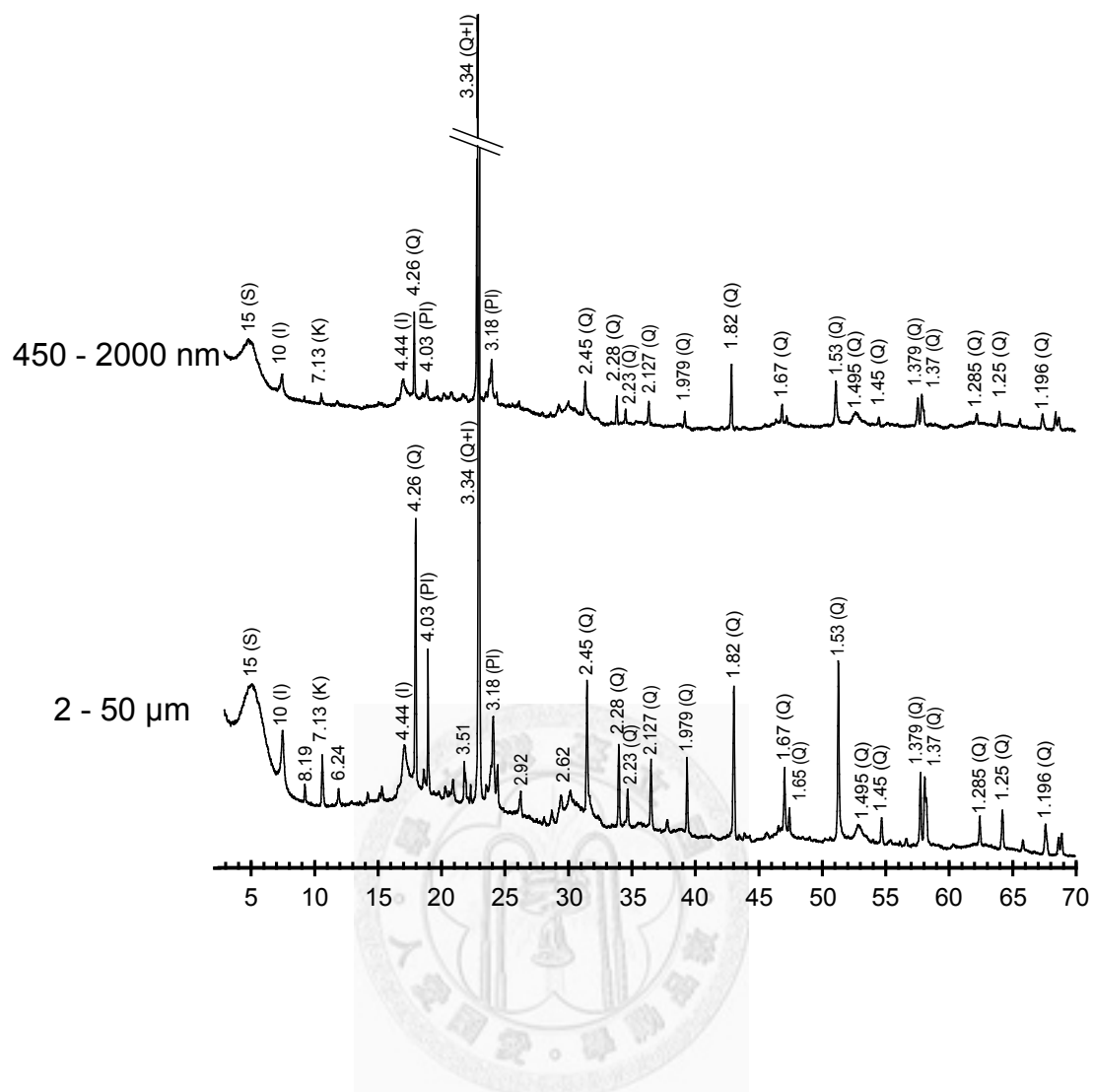


Fig. 5-5: Flow chart for dispersion and separation of fault gouge nanoparticles.



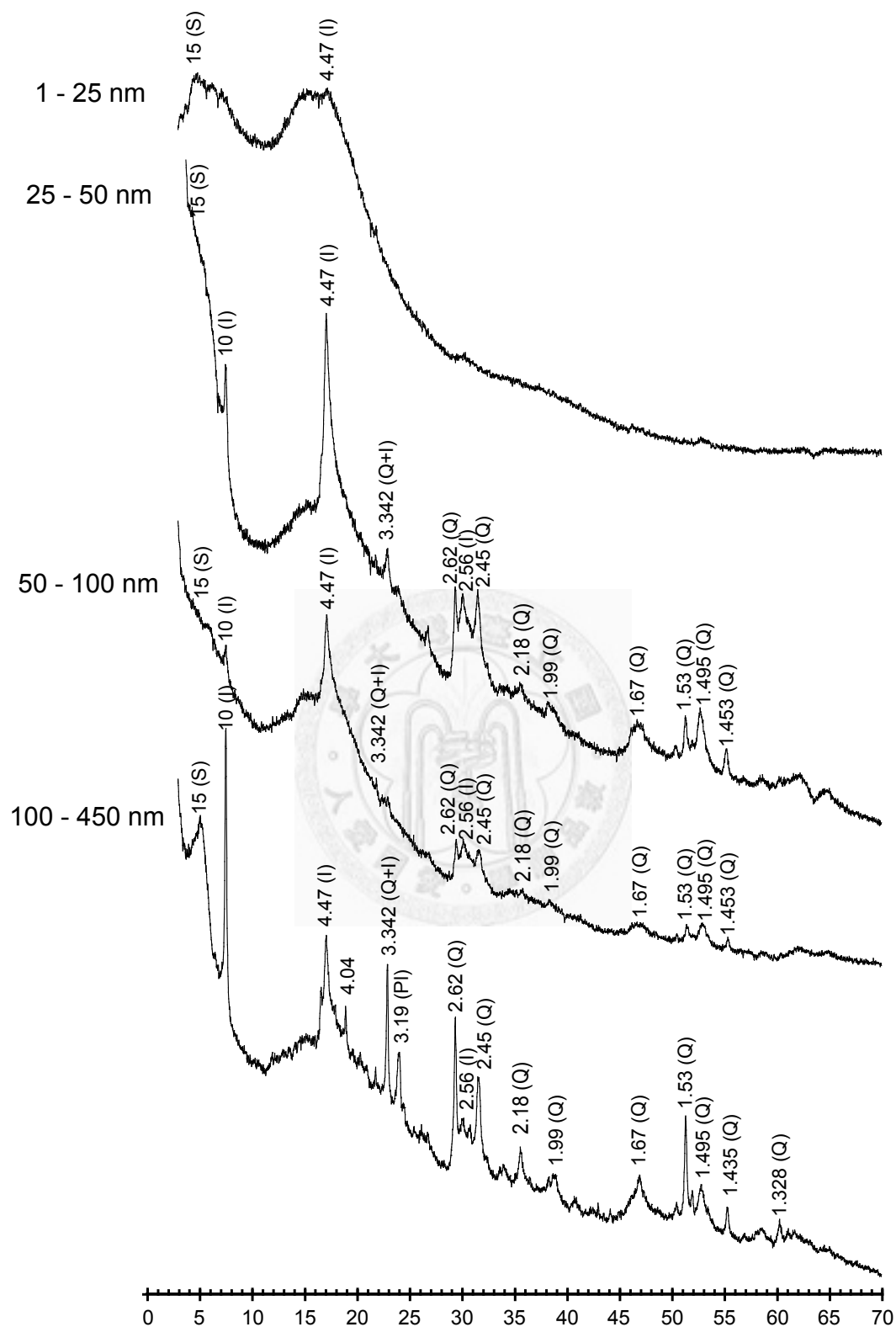


Fig. 5-6: Synchrotron XRD results of different grain size particles.

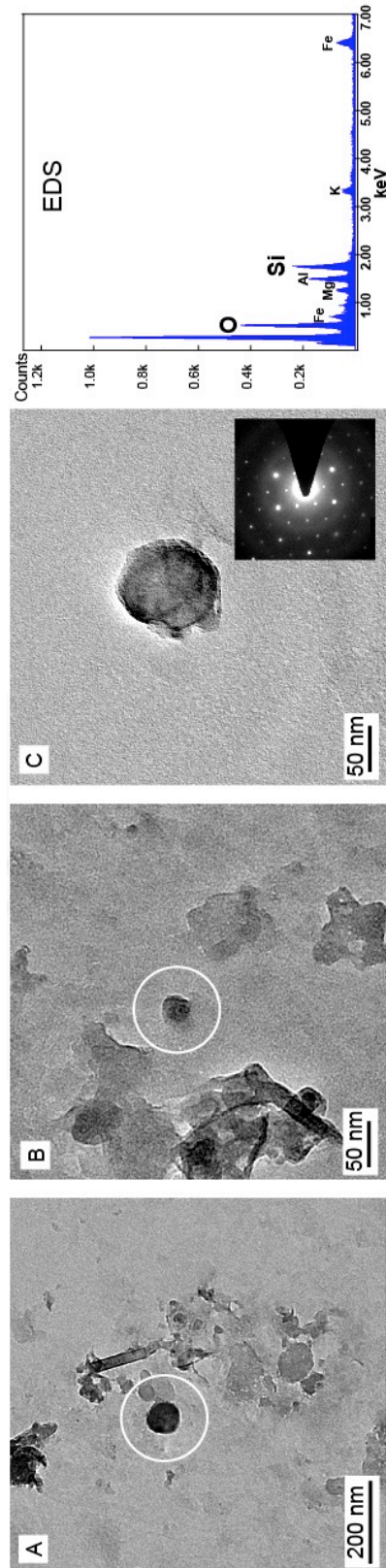


Fig. 5-7: TEM photos of <100 nm grains. (A)(B) Platy pieces, lath-like fractions, and rounded grains are observed. Some ultrafine grains (<10 nm) could be found. (C) Image of a rounded grain with electron diffraction and EDX analysis.

Table 5-1: Synchrotron XRD results of different grain size fractions.

| Grain Size         | Mineral          |
|--------------------|------------------|
| 2-50 $\mu\text{m}$ | Q, P, S, I, C, K |
| 450-2000 nm        | Q, P, S, I, C, K |
| 100-450 nm         | Q, S, I,         |
| 50-100 nm          | Q, S, I          |
| 25-50 nm           | Q, S, I          |
| 1-25 nm            | S, I             |

Q: Quartz, P: Plagioclase, S: Smectite, I: Illite, C: Chlorite, K: Kaolinite.



## Chapter 6. Preliminary result of FZB1194 and FZB1243

In the chapter 2~4, FZB1136 has been investigated substantially. At the same time, the other two fault zones have also the subject of paleomagnetic and rock magnetism investigation. In this chapter, we show some preliminary results of magnetic analyses of FZB1194 and FZB1243.

### 6.1 Analyses of FZB1194

The 22 cm-long U-channel of FZB1194 (1,194.67–1,194.89 m) contains upper fracture-damaged zone (1,194.67 – 1,194.73 m), black material disk (1,194.73 – 1,194.75 m), black fault gouge (1,194.75 – 1,194.81 m), deformed sediments (1,194.81 – 1,194.84 m), black fault gouge (1,194.84 – 1,194.87 m), deformed sediments (1,194.87 – 1,194.89 m).

The paleomagnetic record of ~15 cm-thick gouge FZB1194 is shown in Fig. 2-1, normal ( $D = 235^\circ$ ,  $I = 27^\circ$ ,  $\kappa = 110$ ,  $\alpha_{95} = 8^\circ$ ) and reversal ( $D = 154^\circ$ ,  $I = -52^\circ$ ,  $\kappa = 144$ ,  $\alpha_{95} = 5^\circ$ ) components are found. The normal record is oriented southerly, the reversal record is approximately antipodal to present day magnetic field. The deformed sediments layer between two black gouge layers separates normal and reversal records. We suggest that FZB1194 is a composite gouge and maybe record distinct seismic events within gouge zone. The magnetic cleaning was not as efficient as performed for gouge FZB1136, and magnetic components are not correctly separated, in particular the component of normal polarity. However, it is quite evident that reverse component, with correct inclination is depicted.

We measured magnetic properties of FZB1194 U-channel (Fig. 6-1). The magnetic susceptibility curve shows two humps trend with maximum values found at 1,194.79 m and at 1,194.87 m within each black gouge layer. However, the susceptibility value is ~60% less within black material disk layer. The  $IRM_{IT}$  curve of U-channel also shows two humps trend with maximum values found at 1,194.75 m and at 1,194.845 m. Note the shift between the maximum of remanence and magnetic susceptibility. The S-ratio value of upper deformed sediments and black material disk is lower (~0.93) than gouge and deformed sediments (0.97-0.98). This indicates that a hard coercive mineral is present in the black material disk.

The warming curves of LT-SIRM (Fig. 6-2) show that the Verwey transition (120 K) is well identified in all samples. The drop of LT-SIRM between 10 K and 35 K is large (>99%) for deformed sediments and is smaller for gouge. But this drop is

limited (<1%) for black material disk. This variation of drop of LT-SIRM shows an abundance decreasing of SP minerals from deformed sediments, gouge to black material disk.

The cooling curves of RT-SIRM (Fig. 6-3) also provide obvious Verwey transition (120 K) and subtle Morin transition (240 K) in all samples. The cooling increasing at about 10% from 300 K to 150 K is attributed to the presence of goethite, this increasing is found within upper deformed sediments and black material disk. The RT-SIRM increases from 100 K to 10 K as the P-behavior of SP pyrrhotite signature (*Aubourg and Pozzi, 2010; Kars et al., 2011*) could be found in all samples. However, for black material disk, the P-behavior is weak and the 35 K transition is not obvious.

The TXM observation result of FZB1194 black material disk also shows numerous elongated dense minerals (aspect ratio 2:25; maximum length 5  $\mu\text{m}$ ). These elongated minerals are likely goethite (Fig. 6-4).

In summary, the FZB1194 gouge is composite, with two gouge layers. The paleomagnetic record is different from one gouge to the other gouge. Though the components are poorly resolved, the reverse polarity is present in the record. Similarly to FZB1136, we have detected goethite in abundance within the black material disk. However some discrepancies can be listed:

- The FZB1194 gouge, when excluding the black material disk hosts SP magnetic mineral. This suggests that processes (thermal, fluid) are different, and do not destroyed the SP.
- We do not have detected pyrrhotite within the FZB1194 gouge. We interpreted the pyrrhotite as resulting from the high temperature alteration of pyrite.

We think therefore that the gouge of FZB1194 did not reached elevated temperature as FZB1136. The black material disk, however, behaves differently, and presumably, higher temperature is recorded.

## **6.2 Analyses of FZB1243**

The 18 cm-long U-channel of FZB1243 (1,243.33–1,243.51 m) contains upper deformed sediments (1,243.33 – 1,243.38 m), black material disk (1,243.38 – 1,243.40 m), black fault gouge (1,243.40 – 1,243.50 m), lower deformed sediments (1,243.50 – 1,243.51 m).

The paleomagnetic record of FZB1243 is shown in Fig. 2-1, normal ( $D = 125^\circ$ ,  $I = 11^\circ$ ,  $\kappa = 189$ ,  $\alpha_{95} = 4^\circ$ ) and reversal ( $D = 125^\circ$ ,  $I = -10.0^\circ$ ,  $\kappa = 280$ ,  $\alpha_{95} = 3^\circ$ )

components are also found. The declination of both components is the same, but the inclination is opposite and is abnormally low. Clearly AF demagnetization is not appropriate to depict the components. However, we suggest that FZB1243 record two seismic events, with dual polarities within the gouge zone.

The magnetic properties of FZB1243 U-channel are shown in Fig. 6-5. The magnetic susceptibility curve shows two humps trend with maximum values found at 1,243.40 m (black material disk) and at 1,243.49 m within gouge layer. The susceptibility value of black material disk layer is ~60% of maximum value. The  $IRM_{IT}$  curve of U-channel also shows two humps trend with maximum values found at 1,243.39 m and at 1,243.47 m. Note that the maximum of the remanence and the magnetic susceptibility curves are shifted. S-ratio value of upper deformed sediments is 0.8~0.85 and from black material disk to whole black gouge is 0.8~0.82. It is worth to note that the S-ratio is much lower than S-ratio from FZB1136 and FZB1194.

The warming curves of LT-SIRM (Fig. 6-6) show that the Verwey transition (120 K) is well identified in deformed sediments and some black gouge samples, but is not visible in black material disk and some black gouge samples. The drop of LT-SIRM between 10 K and 35 K is large (>99%) for deformed sediments and is smaller for black gouge samples (<6%). But this drop is limited (<1%) for black material disk.

The cooling curves of RT-SIRM (Fig. 6-7) provide subtle Morin transition (240 K) in all samples. The Verwey transition (120 K) is like LT-SIRM, which is not visible in black material disk and some black gouge samples. The cooling increasing at about 10% from 300 K to 150 K is attribute to the presence of goethite, this increasing is found within all samples. The RT-SIRM increases from 100 K to 10 K as the P-behavior of SP pyrrhotite signature (*Aubourg and Pozzi, 2010; Kars et al., 2011*) could be found in gray gouge and some black gouge samples. However, for black material disk and some black gouge samples, the P-behavior is weak and the 35 K transition is not obvious.

In summary, this gouge resembles to the gouge FZB1194. We have detected dual polarities, though the components are not cleaned in a proper manner. The black material disk contains less SP magnetic grains than the surrounding gouges, and goethite is detected.

## **6.3 Discussion and Conclusion**

### **6.3.1 Paleomagnetic records**



In the two fault gouges (FZB1194, FZB1243), we observed dual polarities record, but the record is here complex and the magnetic cleaning not efficient. The reverse polarity deserves important comment. The youngest geomagnetic reversal is the Bruhnes-Matuyama dated at 780 ka (*Kent and Schneider, 1995*). However, the TCDP drilling site is located at the North Chelungpu Chinshui detachment, which has a total slip of only ~0.3 km (Fig. 6-8, *Yue et al., 2005*). Consequently, the age of the fault is young (46~100 ka) (*Heermance et al., 2003; Isaacs et al., 2007*). It has to be verified that the paleomagnetic record is not the record of short-term paleomagnetic excursion (<2 ky) (e.g., Mono Lake, Laschamp; *Valet and Valladas, 2010*). This is rather unlikely because this means that two earthquakes in each gouge took place during a paleomagnetic excursion, and the inclination should be really abnormal. A second hypothesis which has to be verified is the self-reversal processes (*McElhinny and McFadden, 1999*).

### **6.3.2 Large magnitude vs. small magnitude?**

When comparing the two gouges FZB1194 and FZB1243 to the  $M_w$  7.6 Chi-Chi gouge, it appears that there are common behaviors, and significant differences.

Common behavior:

- We observe a paleomagnetic record in all gouges.
- We observe the presence of neoformed magnetic minerals such as goethite. This goethite is neoformed and developed within the ultrafine matrix of the gouge.

Difference:

- Ultrafine magnetic minerals are preserved in the gouge, while they have been altered in the FZB1136 gouge.
- Dual polarities within distinct stripes of gouge are identified.
- The black material disk has a low magnetic susceptibility, while the highest magnetic susceptibility is observed along the Chi-Chi principal slip zone.

All these observations lead us to consider that the gouges result from different processes. It is commonly accepted that a gouge layer stacks tens of earthquake slip zone (e.g. *Boullier et al., 2009*). So in theory, we must have a quite complex record. In chapter 2, we have suggested that a large magnitude earthquake erased the previous magnetic information.

In the FZB1136, only one paleomagnetic component is recovered throughout the entire gouge. This component is a ChRM (characteristic remanent magnetization)

which means that it is rather unlikely that a reverse polarity overlaps this one. By contrast, in the two other gouges, dual polarities are observed, and each component results from a probable overlapping. We hypothesize that these two gouges record smaller magnitude earthquakes, where heat generation and fluid circulation are not sufficient to erase the previous magnetic signal.

Therefore, we suggest that 1) the identification of a single paleomagnetic component, 2) the alteration of hyperfine fraction throughout the gouge, including the principal slip zone may be a diagnostic evidence for large magnitude earthquake.



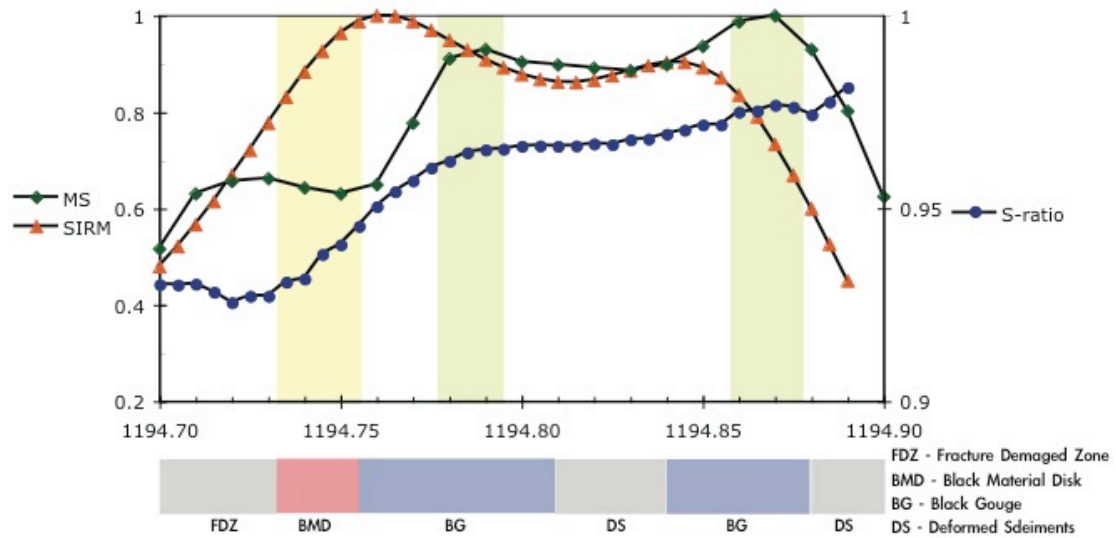


Fig. 6-1: The magnetic properties of FZB1194 U-channel show the shift between the maximum of remanence and magnetic susceptibility. The S-ratio value of upper deformed sediments and black material disk is lower (~0.93) than gouge and deformed sediments (0.97-0.98).



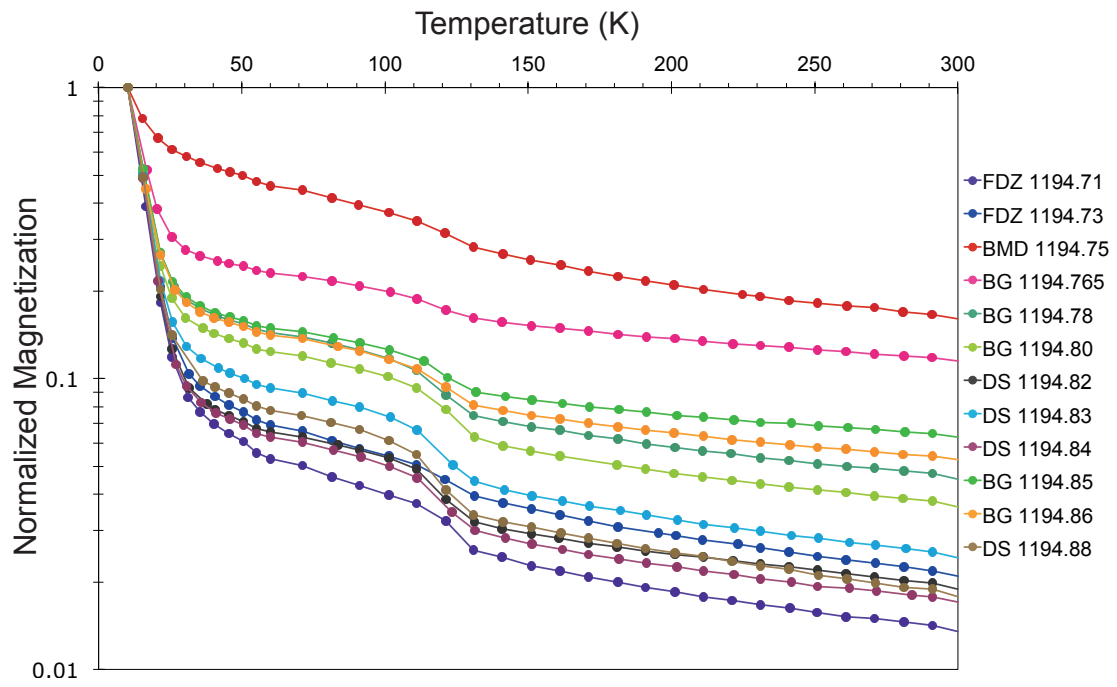


Fig. 6-2: LT-SIRM warming curves of FZB1194 samples show that the Verwey transition (120 K) is well identified in all samples. The drop of LT-SIRM between 10 K and 35 K is large (>99%) for deformed sediments and is smaller for gouge. But this drop is limited (<1%) for black material disk.

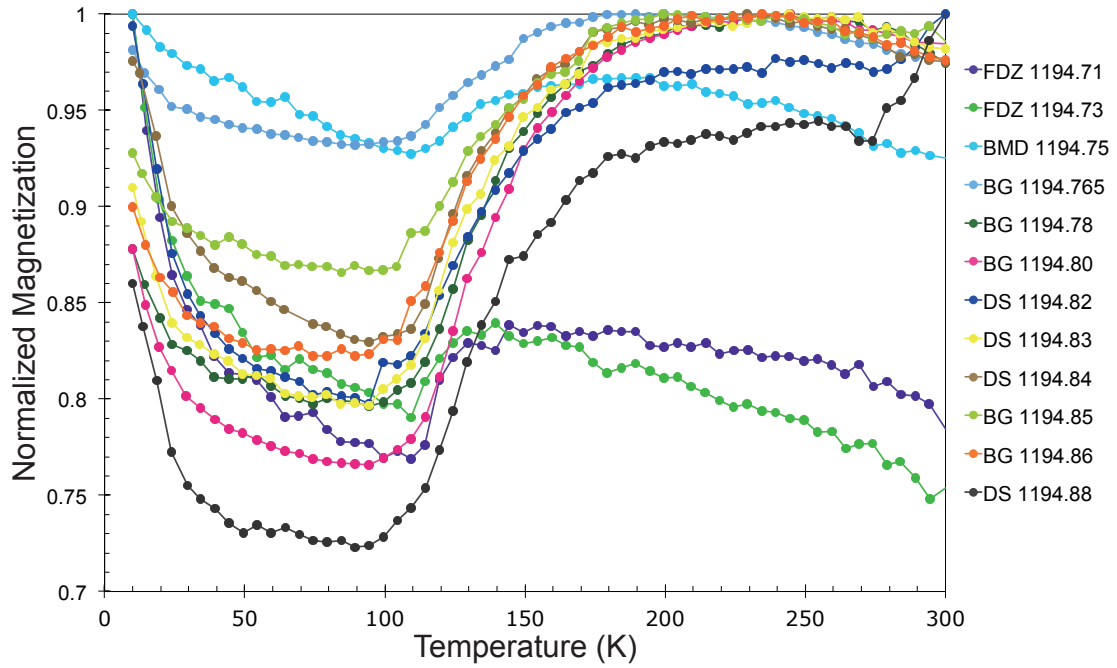


Fig. 6-3: RT-SIRM cooling curves of FZB1194 samples provide subtle Morin transition (240 K) in all samples. The Verwey transition (120 K) is not visible in black material disk and some black gouge samples. The cooling increasing at about 10% from 300 K to 150 K is attribute to the presence of goethite, this increasing is found within all samples. The increases from 100 K to 10 K as the P-behavior of SP pyrrhotite signature could be found in gray gouge and some black gouge samples. However, for black material disk and some black gouge samples, the P-behavior is weak and the 35 K transition is unclear.

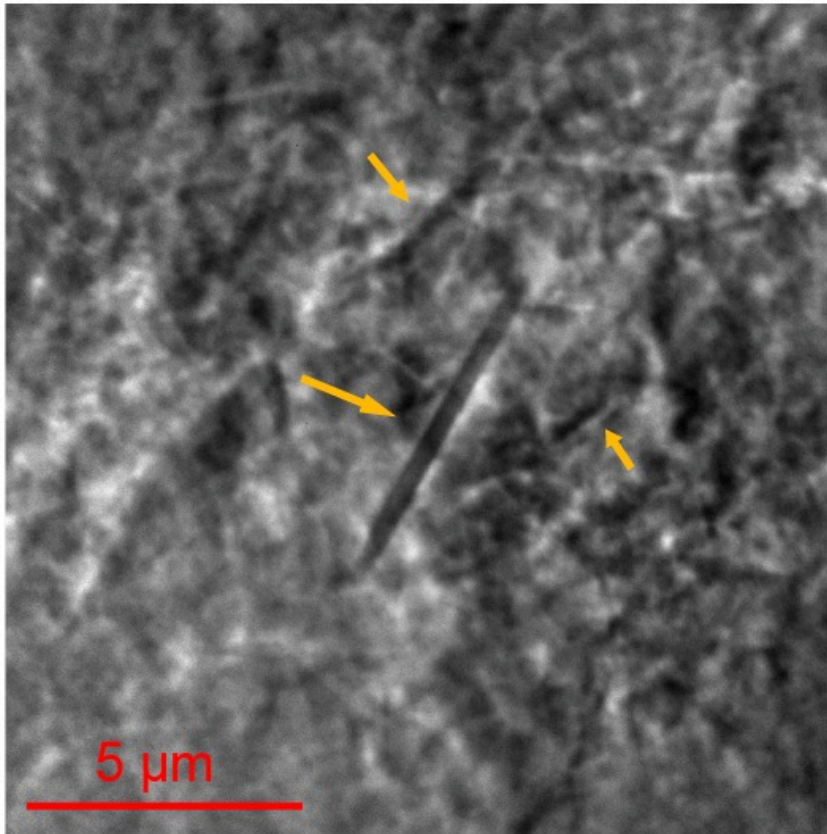


Fig. 6-4: The TXM image of FZB1194 black material disk shows numerous elongated dense minerals (aspect ratio 2:25; maximum length 5  $\mu\text{m}$ ).

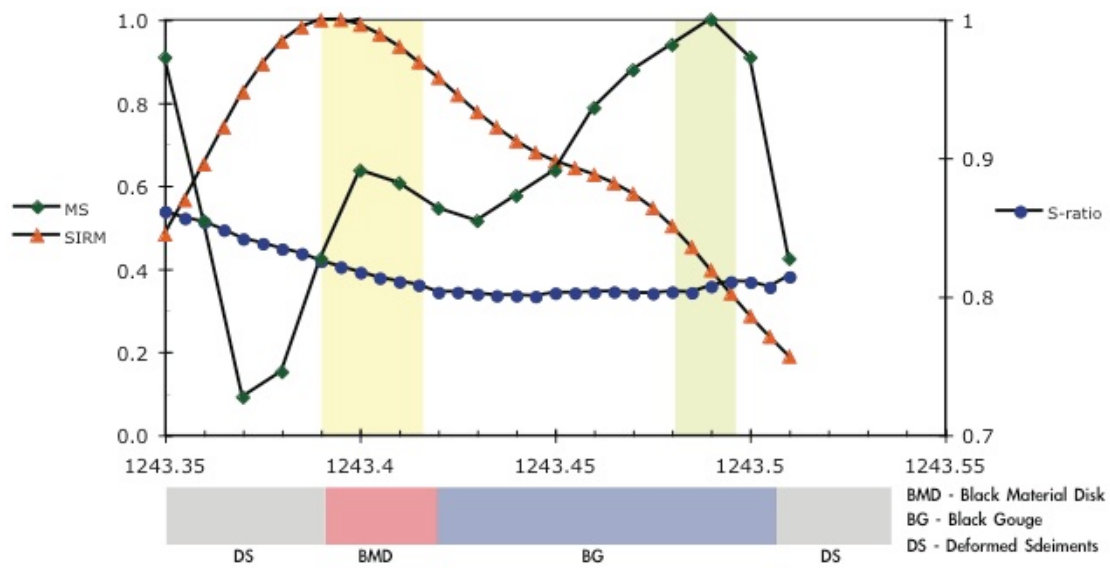
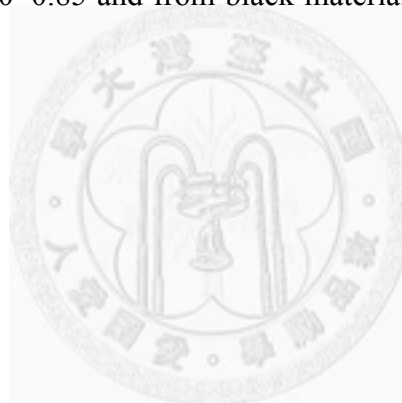


Fig. 6-5: The magnetic properties of FZB1243 U-channel show the maximum of the remanence and the magnetic susceptibility curves are shifted. S-ratio value of upper deformed sediments is 0.80~0.85 and from black material disk to whole black gouge is 0.80~0.82.



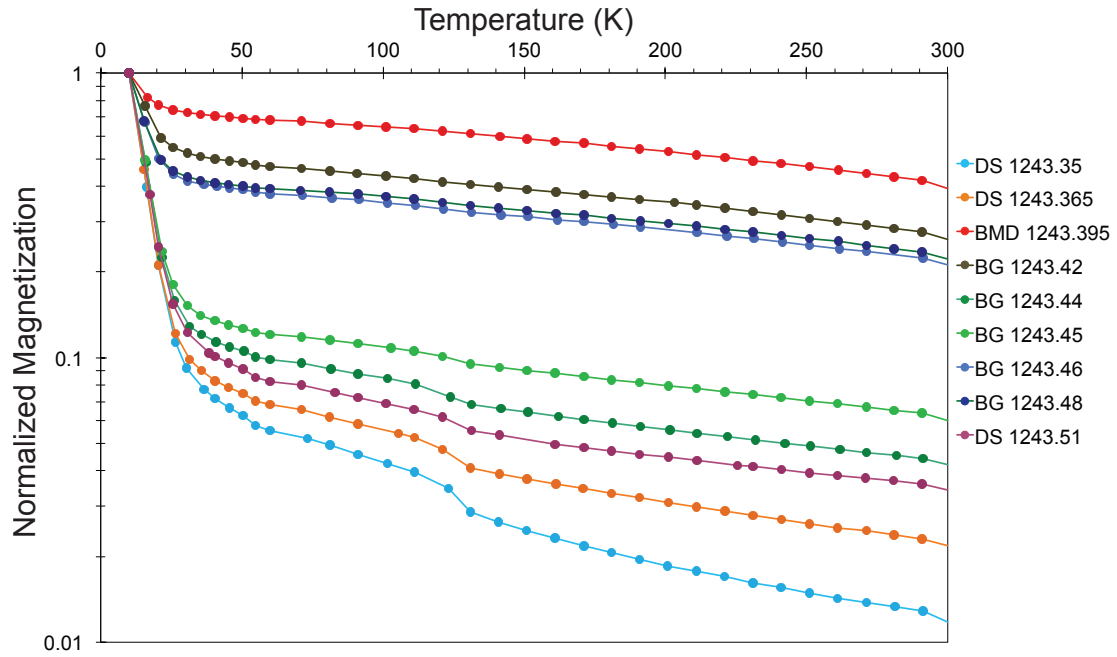


Fig. 6-6: LT-SIRM warming curves of FZB1243 samples show that the Verwey transition (120 K) is well identified in deformed sediments and some black gouge samples, but is not visible in black material disk and some black gouge samples. The drop between 10 K and 35 K is large (>99%) for deformed sediments and is smaller for black gouge samples (<6%). But this drop is limited (<1%) for black material disk.



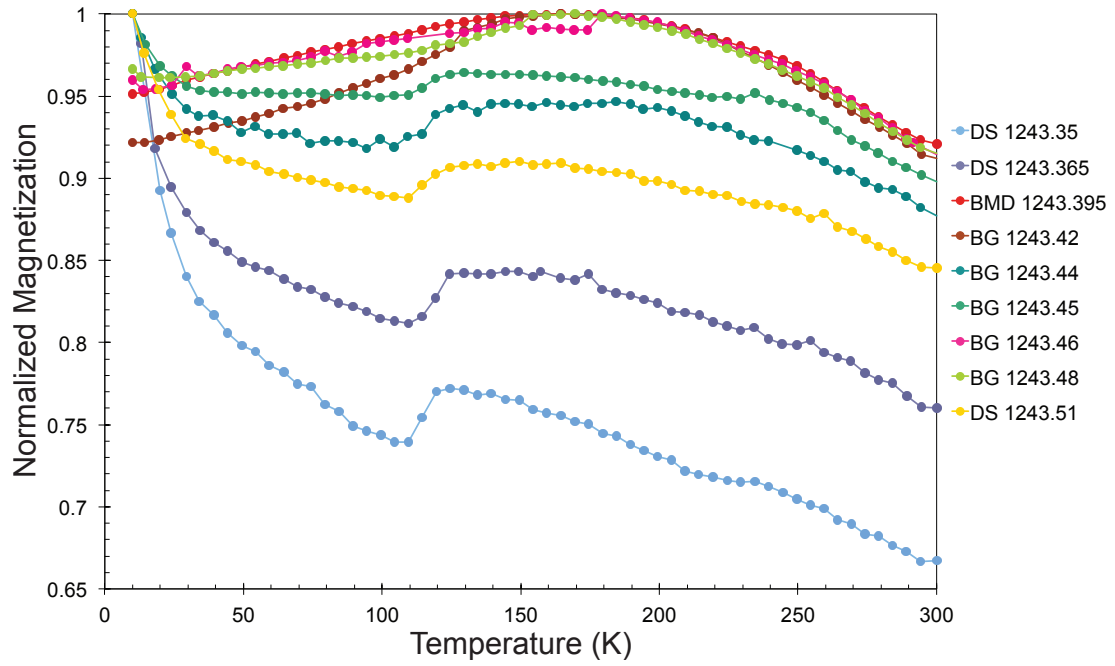


Fig. 6-7: RT-SIRM cooling curves of FZB1243 samples show subtle Morin transition (240 K) in all samples. The Verwey transition (120 K) is not visible in black material disk and some black gouge samples. The cooling increasing at about 10% from 300 K to 150 K is found within all samples. The increases from 100 K to 10 K as the P-behavior of SP pyrrhotite signature could be found in gray gouge and some black gouge samples. However, for black material disk and some black gouge samples, the P-behavior is weak and the 35 K transition is unclear.

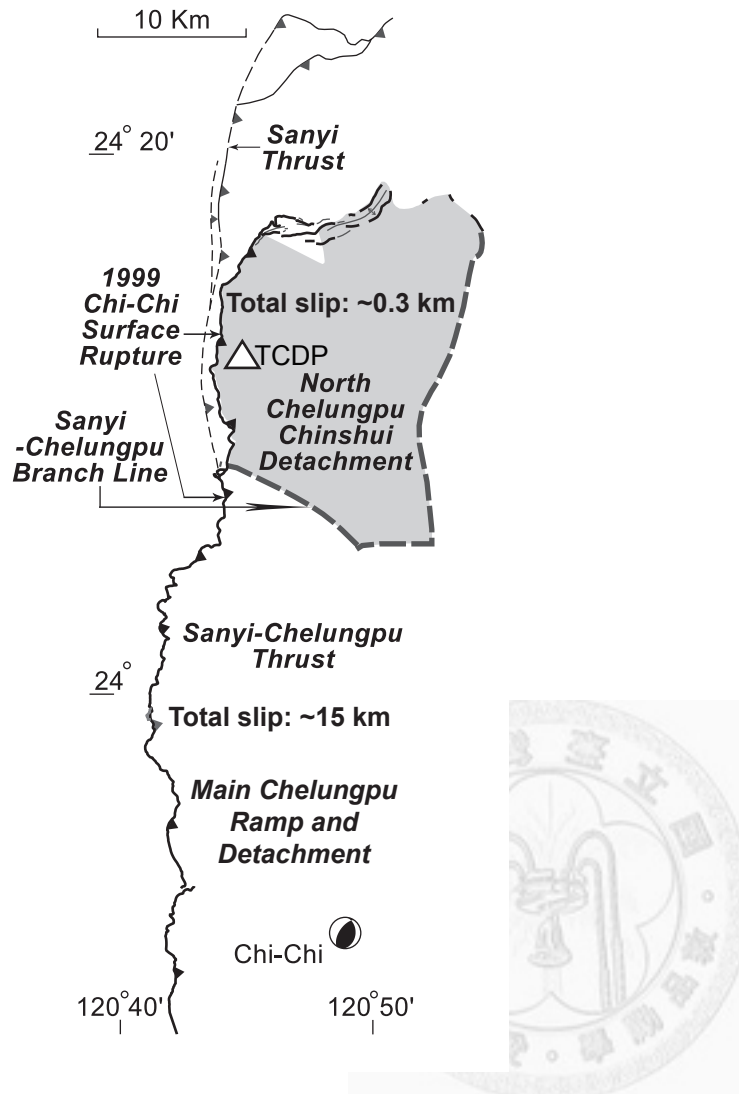


Fig. 6-8: Range and total slip (~0.3 km) of Chelungpu Chinshui detachment. (after Yue *et al.*, 2005).

## Chapter 7. Conclusions

The ensemble of mineralogy and magnetic analyses from this thesis leads us to provide a view of physical/chemical alteration of minerals within fault gouge during seismic events. Here we give a summary of the key results:

1. For the first time, we identified a magnetic record in a modern gouge, which is directly related to a large-magnitude earthquake. Generally, the paleomagnetic community tried to track earthquake lightning record (e.g. *Ferré et al.*, 2005). Here, we show that this record of the Chi-Chi gouge is due to the combination of fluid circulation and temperature elevation.
2. We discovered two magnetic minerals in the gouge that are not present in the host rock. The pyrrhotite is an iron sulfide and forms at the expense of pyrite during high temperature elevation ( $>500^{\circ}\text{C}$ ). The micron-size goethite forms on cooling of fluids that percolated within the gouge. The magnetite is oxidized in the gouge, and probably neoformed along the principal slip zone.
3. We have found that the magnetic record in the gouge is carried by magnetite within the principal slip zone and goethite in the rest of the gouge. We propose a model where magnetic record: 1) is preserved during inter-seismic time, 2) is erased during co-seismic time and 3) is imprinted during post-seismic time when fluids cooled down.
4. While the peak anomaly of magnetic susceptibility in a gouge was early identified (*Hirono et al.*, 2006a), we precised considerably this view because we correlate the maximum susceptibility to the mm-thick Chi-Chi principal slip zone within the 16 cm-thick gouge. This constitutes a potential, fast, and nondestructive way to find the most recent principal slip zone in thick gouge.
5. By using simple model of the magnetic mineral concentrations in Chi-Chi gouge, we explained satisfactorily the profiles of magnetic parameters. This modeling indicates that  $\sim 300$  ppmv of magnetite formed in the principal slip zone and its main contact area. Similarly,  $\sim 1\%$  of goethite is formed in the center of the gouge, where the fluids are more enriched in iron. This model provides us a new way to quantify magnetic mineral concentration.
6. More generally, we think that making U-channel within fault gouge is of great values because nondestructive magnetic measurement can help to focus on

specific horizons, and to estimate broadly the concentration of neoformed sediments.

7. By identification of nano-particles in Chelungpu fault outcrop gouge sample, we propose that quartz is the index mineral associated with co-seismic fracture and the minimum grain size is ~25 nm. The smectite and illite nano-particles could be associated with weathering process of gouge at shallow or surface conditions. This provides a low-cut of grain size distribution for fracture energy estimation.
8. In the FZB1194 and FZB1243, we observed dual polarities record, but the record is here complex and the magnetic cleaning not efficient. We suggest that each fault zone records two seismic events. The reverse polarity deserves important comment, the two hypotheses are: 1) record of reverse polarity period, 2) the self-reversal processes of magnetic minerals.
9. All observations of three major fault zones in TCDP hole-B lead us to consider that the gouges result from different processes. From paleomagnetic records and magnetic properties, we hypothesize that FZB1194 and FZB1243 gouge record smaller magnitude earthquakes than FZB1136 gouge, where heat generation and fluid circulation are not sufficient to erase the previous magnetic signal.

## Chapter 8. Perspectives

In this study, we reported the paleomagnetic record of FZB1136, which was acquired during 1999 Chi-Chi earthquake. For investigating the chemical/physical alteration process of Chi-Chi earthquake, we analyzed thoroughly mineralogy and rock magnetism of FZB1136. In addition, the other two major fault zones are worth to further study for understanding the Chelungpu fault system. Therefore, there are still some interesting issues that could be brought out for future research. Some issues are specific to the Chelungpu fault; some issues are of broader interest.

- 1) We have shown that dual polarities exist in fault zones FZB1194 and FZB1243. We propose to document better this reverse polarity by analysing for example additional samples from Hole A or Hole C. A particular attention is required to check whether this reverse polarity is due to a self-reversal process or is contemporaneous of magnetic excursion. If these possibilities are ruled out, the reverse polarity would indicate that the age of Chelungpu fault is older than 0.78 My. This is in contradiction by one order of magnitude with the total slip of ~0.3 km of this segment of the Chelungpu fault (Fig. 6-7, *Yue et al.*, 2005) and the proposed age of 46-100 ky (*Heermance et al.*, 2003; *Isaacs et al.*, 2007).
- 2) We observe that some rock magnetic parameters (peak of magnetic susceptibility, S-ratio, paleomagnetic record) are located precisely within the most recent earthquake principal slip zone of FZB1136. In the two other fault gouges, FZB1194 and FZB1243, a peak of magnetic susceptibility is shifted from the most evident layer: the black material disk. Thus, it is interesting to investigate the thin section where the peak of magnetic susceptibility is observed to check about possible recent earthquake record.
- 3) The findings of pyrrhotite and goethite deserve additional studies, as it may document the physical and chemical conditions in the gouge. Some experiments like flash-heating or iron-rich fluid cooling can be settled out.
- 4) The magnetic properties of FZB1194 show a higher S-ratio value (~0.95) than FZB1136 (0.75~0.85) and FZB1243 (~0.8). The MPMS results of FZB1194 also show higher SP grains and non-partial oxidation of magnetite within gouge sample. Those observations of FZB1194 are quite different to FZB1136 and FZB1243. Thus, the magnetic mineral assemblages of those three fault zones are different. This viewpoint shows that seismic

physical/chemical alteration processes of each fault zone might not be similar. The magnetic properties of fault zones could give us some valuable information for understanding the relationship and cause of those three fault zones. Further microscope observations for FZB1194 and FZB1243 are also interesting for future work.

- 5) When gouge is derived from sediments, where pyrite is naturally present (a common case), our study shows the interest to investigate the degree of alteration of pyrite in the gouge. We show for comparison a pyrite alteration from a creep gouge from the Jura mountain (Fig. 8-1, *Azaruk & Aubourg*, unpublished work). One can observe mechanical alteration, without any form of oxidation.



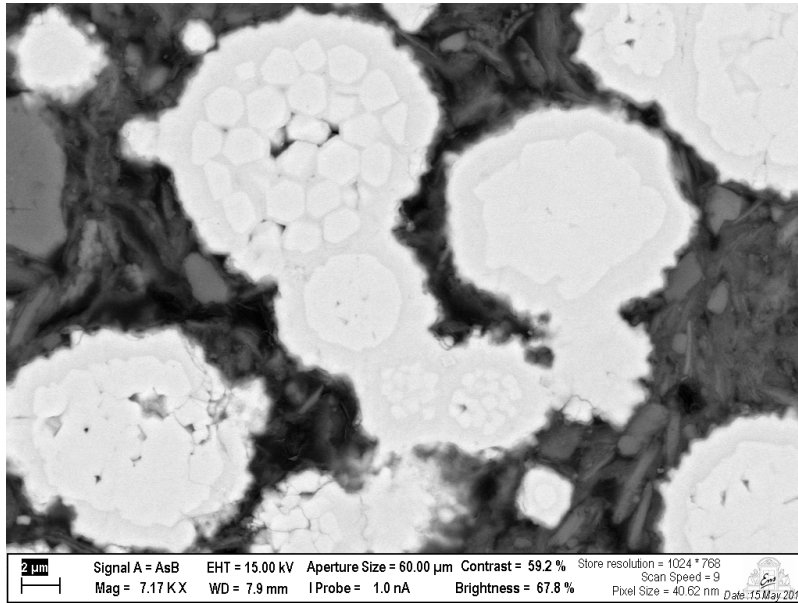


Fig. 8-1: SEM photo of pyrite alteration from a creep gouge from the Jura mountain (*Azaruk & Aubourg*, unpublished work).



## References

- Abdelmalak, M. M., C. Aubourg, L. Geoffroy, and F. Laggoun-Défarge (2012), A new oil-window indicator? The magnetic assemblage of claystones from the Baffin Bay volcanic margin (Greenland), *AAPG Bulletin*, 96(2), 205-215, doi:10.1306/07121111008.
- Abercrombie, R. E., and J. R. Rice (2005), Can observations of earthquake scaling constrain slip weakening?, *Geophys. J. Int.*, 162(2), 406-424, doi:10.1111/j.1365-246X.2005.02579.x.
- Andersen, T. B., and H. Austrheim (2006), Fossil earthquakes recorded by pseudotachylytes in mantle peridotite from the Alpine subduction complex of Corsica, *Earth Planet. Sci. Lett.*, 242, 58–72, doi:10.1016/j.epsl.2005.11.058.
- Angelier, J., J.-C. Lee, H.-T. Chu, J.-C. Hu, C.-Y. Lu, Y.-C. Chan, T.-J. Lin, Y. Font, B. Deffontaines, and Y.-B. Tsai (2001), Le séisme de Chichi (1999) et sa place dans l'orogène de Taiwan, *Earth Planet. Sci.*, 333, 5-21, Elsevier, Paris, France.
- Angelier, J., J.-C. Lee, J.-C. Hu, and H.-T. Chu (2003), Three-dimensional deformation along the rupture trace of the September 21st, 1999, Taiwan earthquake: a case study in the Kuangfu school, *J. Stru. Geol.*, 25, 351-370, doi:10.1016/s0191-8141(02)00039-1.
- Aubourg, C., and J.-P. Pozzi (2010), Toward a new <250°C pyrrhotite-magnetite geothermometer for claystones, *Earth Planet. Sci. Lett.*, 294, 47-57, doi:10.1016/j.epsl.2010.02.045.
- Berner, R. A. (1984), Sedimentary pyrite formation: An update, *Geochim. Cosmochim. Acta*, 48, 605-615.
- Bétard, F., L. Caner, Y. Gunnell, and G. Bourgeon (2009), Illite neoformation in plagioclase during weathering: Evidence from semi-arid Northeast Brazil, *Geoderma*, 152, 53-62, doi:10.1016/j.geoderma.2009.05.016.
- Bhargava, S. K., A. Garg, and N. D. Subasinghe (2009), In situ high-temperature phase transformation studies on pyrite, *Fuel*, 88, 6, 988-993, doi:10.1016/j.fuel.2008.12.005.
- Boullier, A.-M., E.-C. Yeh, S. Boutareaud, S.-R. Song, and C.-H. Tsai (2009), Microscale anatomy of the 1999 Chi-Chi earthquake fault zone, *Geochem. Geophys. Geosyst.*, 10, Q03016, doi:10.1029/2008GC002252.
- Boutareaud, S. b., D.-G. Calugaru, R. Han, O. Fabbri, K. Mizoguchi, A. Tsutsumi, and T. Shimamoto (2008), Clay-clast aggregates: A new textural evidence for



- seismic fault sliding?, *Geophys. Res. Lett.*, **35**, L05302, doi:10.1029/2007GL032554.
- Boutareaud, S., A.-M. Boullier, M. Andréani, D.-G. Calugaru, P. Beck, S.-R. Song, and T. Shimamoto (2010), Clay clast aggregates in gouges: New textural evidence for seismic faulting, *J. Geophys. Res.*, **115**(B2), B02408, doi:10.1029/2008jb006254.
- Brantut, N., A. Schubnel, J. N. Rouzaud, F. Brunet, and T. Shimamoto (2008), High-velocity frictional properties of a clay-bearing fault gouge and implications for earthquake mechanics, *J. Geophys. Res.*, **113**, B10401, doi:10.1029/2007jb005551.
- Brodsky, E., and H. Kanamori (2001), Elastohydrodynamic lubrication of faults, *J. Geophys. Res.*, **106**(B8), 16357-16374, doi:10.1029/2001JB000430.
- Chang, S.-L. (1971) Subsurface geologic study of the Taichung basin. *Petrol. Geol. Taiwan*, **8**, 21-45.
- Chen, W.-S., K. D. Ridgway, C.-S. Horng, Y.-G. Chen, K.-S. Shea, and M.-G. Yeh (2001), Stratigraphic architecture, magnetostratigraphy, and incised-valley systems of the Pliocene-Pleistocene collisional marine foreland basin of Taiwan, *Geol. Soc. Am. Bull.*, **113**, 1249-1271, doi:10.1130/0016-7606(2001)113<1249:samaiv>2.0.co;2.
- Chen, Y.-G., W.-S. Chen, Y. Wang, P.-W. Lo, J.-C. Lee, and T.-K. Liu (2002), Geomorphic evidence for prior earthquakes: Lesson from the 1999 Chichi earthquake in central Taiwan, *Geology*, **30**, 171-174, doi:10.1130/0091-7613(2002).
- Chester, J. S., F. M. Chester, and A. K. Kronenberg (2005), Fracture surface energy of the Punchbowl fault, San Andreas system, *Nature*, **437**, 133-136, doi:10.1038/nature03942.
- Chin, P. P., J. Ding, J. B. Yi, and B. H. Liu (2005), Synthesis of FeS<sub>2</sub> and FeS nanoparticles by high-energy mechanical milling and mechanochemical processing, *J. Alloys Compd.*, **390**, 255-260, doi:10.1016/j.jallcom.2004.07.053.
- Cho, H., M. A. Waters, and R. Hogg (1996), Investigation of the grind limit in stirred-media milling, *Int. J. Miner. Process.*, **44-45**, 607-615, doi:10.1016/0301-7516(95)00069-0.
- Chou, Y.-M., Song, S.-R., Aubourg, C., Lee, T.-Q., Boullier, A.-M., Song, Y.-F., Yeh, E.-C., Kuo, L.-W. & Wang, C.-Y., 2012. An earthquake slip zone is a magnetic recorder, *Geology*, doi:10.1130/g32864.1.

- Chou, Y.-M., Song, S.-R., Aubourg, C., Song, Y.-F., Boullier, A.-M., Lee, T.-Q., Evans, M., Yeh, E.-C. & Chen, Y.-M., 2012. Pyrite alteration and neoformed magnetic minerals in the fault zone of the Chi-Chi earthquake ( $M_w$  7.6, 1999): Evidence for frictional heating and co-seismic fluids, *Geochem. Geophys. Geosyst.* (in press).
- Cornell, R. M., and U. Schwertmann (2003), *The Iron oxides: structure, properties, reactions, occurrences, and uses*, Weinheim ed., 664 pp., Wiley-VCH.
- Craig, J. R., F. M. Vokes, and T. N. Solberg (1998), Pyrite: Physical and chemical textures, *Mineral. Depos.*, 34, 82-101, doi:10.1007/s001260050187.
- Cui, Y., K. L. Verosub, and A. P. Roberts (1994), The effect of low temperature oxidation on large multi-domain magnetite, *Geophys. Res. Lett.*, 21, 757-760, doi:10.1029/94GL00639.
- Dekkers, M. J. (1989), Magnetic properties of natural goethite-II. TRM behaviour during thermal and alternating field demagnetization and low-temperature treatment, *Geophys. J. Int.*, 97, 341-355, doi:10.1111/j.1365-246X.1989.tb00505.x.
- Dekkers, M. J., J. L. Mattéi, G. Fillion, and P. Rochette (1989), Grain-size dependence of the magnetic behavior of pyrrhotite during its low-temperature transition at 34 K, *Geophys. Res. Lett.*, 16, 855-858, doi:10.1029/GL016i008p00855.
- Di Toro, G., and G. Pennacchioni (2004), Superheated friction-induced melts in zoned pseudotachylites within the Adamello tonalites (Italian Southern Alps), *J. Struct. Geol.*, 26, 1783-1801, doi:10.1016/j.jsg.2004.03.001.
- Di Toro, G., T. Hirose, S. Nielsen, G. Pennacchioni, and T. Shimamoto (2006), Natural and Experimental Evidence of Melt Lubrication of Faults During Earthquakes, *Science*, 311, 647-649, doi:10.1126/science.1121012.
- Enomoto, Y., and Z. Zheng (1998), Possible evidences of earthquake lightning accompanying the 1995 Kobe Earthquake inferred from the Nojima Fault Gouge, *Geophys. Res. Lett.*, 25, 2721-2724, doi:10.1029/98GL02015.
- Enomoto, Y., F. Asuke, Z. Zheng, and H. Ishigaki (2001), Hardened foliated fault gouge from the Nojima Fault zone at Hirabayashi: Evidence for earthquake lightning accompanying the 1995 Kobe earthquake?, *Isl. Arc*, 10(3-4), 447-456, doi:10.1046/j.1440-1738.2001.00343.x.
- Evans, J. (1990), Quartz dissolution during shale diagenesis implications for quartz cementation in sandstones, *Chem. Geol.*, 84(1-4), 239-240, doi:10.1016/0009-2541(90)90224-u.

- Evans, M. A., and R. D. Elmore (2006), Fluid control of localized mineral domains in limestone pressure solution structures, *J. Struct. Geol.*, 28, 284-301, doi:10.1016/j.jsg.2005.10.004.
- Ferré, E. C., M. S. Zechmeister, J. W. Geissman, N. MathanaSekarana, and K. Kocak (2005), The origin of high magnetic remanence in fault pseudotachylites: Theoretical considerations and implication for coseismic electrical currents, *Tectonophysics*, 402, 125-139, doi:10.1016/j.tecto.2005.01.008.
- Ferré, E. C., J. W. Geissman, and M. S. Zechmeister (2012), Magnetic properties of fault pseudotachylites in granites, *J. Geophys. Res.*, 117, B01106, doi:10.1029/2011JB008762.
- Fisher, R. (1953), Dispersion on a Sphere, *Proceedings of the Royal Society of London. Series A. Mathematical and Physical Sciences*, 217(1130), 295-305.
- Fukuchi, T. (2003), Strong ferrimagnetic resonance signal and magnetic susceptibility of the Nojima pseudotachylite in Japan and their implication for coseismic electromagnetic changes, *J. Geophys. Res.*, 108(B6), 2312, doi:10.1029/2002JB002007.
- Fukuchi, T., K. Mizoguchi, and T. Shimamoto (2005), Ferrimagnetic resonance signal produced by frictional heating: A new indicator of paleoseismicity, *J. Geophys. Res.*, 110, B12404, doi:10.1029/2004JB003485.
- Gibbs, R. J. (1967), The Geochemistry of the Amazon River System: Part I. The Factors that Control the Salinity and the Composition and Concentration of the Suspended Solids, *Geol. Soc. Am. Bull.*, 78, 1203-1232, doi:10.1130/0016-7606(1967)78[1203:tgotar]2.0.co;2.
- Guatterri, M., P. Spudich, and G. C. Beroza (2001), Inferring rate and state friction parameters from a rupture model of the 1995 Hyogo-ken Nanbu (Kobe) Japan earthquake, *J. Geophys. Res.*, 106, 26511-26521, doi:10.1029/2001jb000294.
- Hailwood, E. A., R. H. Maddock, T. Fung, and E. H. Rutter (1992), Palaeomagnetic analysis of fault gouge and dating fault movement, Anglesey, North Wales, *J. Geol. Soc.*, 149(2), 273-284, doi:10.1144/gsjgs.149.2.0273.
- Hamada, Y., T. Hirono, W. Tanikawa, W. Soh, and S.-R. Song (2009), Energy taken up by co-seismic chemical reactions during a large earthquake: An example from the 1999 Taiwan Chi-Chi earthquake, *Geophys. Res. Lett.*, 36, doi:10.1029/2008GL036772.
- Harrison, R. J., and J. M. Feinberg (2008), FORCinel: An improved algorithm for calculating first-order reversal curve distributions using locally weighted

- regression smoothing, *Geochem. Geophys. Geosyst.*, **9**, Q05016, doi:10.1029/2008GC001987.
- Heaton, T. H. (1990), Evidence for and implications of self-healing pulses of slip in earthquake rupture, *Phys. Earth Planet. Inter.*, **64**, 1-20, doi:10.1016/0031-9201(90)90002-f.
- Heermance, R., Z. K. Shipton, and J. P. Evans (2003), Fault Structure Control on Fault Slip and Ground Motion during the 1999 Rupture of the Chelungpu Fault, Taiwan, *Bull. Seis. Soc. Am.*, **93**(3), 1034-1050, doi:10.1785/0120010230.
- Heider, F., A. Zitzelsberger, and K. Fabian, (1996), Magnetic susceptibility and remanent coercive force in grown magnetite crystals from 0.1  $\mu\text{m}$  to 6 mm, *Phys. Earth Planet. Int.*, **93**, 239-256, doi:10.1016/0031-9201(95)03071-9.
- Heilbronner, R., and N. Keulen (2006), Grain size and grain shape analysis of fault rocks, *Tectonophysics*, **427**, 199-216, doi:10.1016/j.tecto.2006.05.020.
- Hirono, T., W. Lin, E.-C. Yeh, W. Soh, Y. Hashimoto, H. Sone, O. Matsubayashi, K. Aoike, H. Ito, M. Kinoshita, M. Murayama, S.-R. Song, K.-F. Ma, J.-H. Hung, C.-Y. Wang, and Y.-B. Tsai (2006), High magnetic susceptibility of fault gouge within Taiwan Chelungpu fault: Nondestructive continuous measurements of physical and chemical properties in fault rocks recovered from Hole B, TCDP, *Geophys. Res. Lett.*, **33**, L19311, doi:10.1029/2006GL027329.
- Hirono, T., E.-C. Yeh, W. Lin, H. Sone, T. Mishima, W. Soh, Y. Hashimoto, O. Matsubayashi, K. Aoike, H. Ito, M. Kinoshita, M. Murayama, S.-R. Song, K.-F. Ma, J.-H. Hung, C.-Y. Wang, Y.-B. Tsai, T. Kondo, M. Nishimura, S. Moriya, T. Tanaka, T. Fujiki, L. Maeda, H. Muraki, T. Kuramoto, K. Sugiyama, and T. Sugawara (2007a), Nondestructive continuous physical property measurements of core samples recovered from hole B, Taiwan Chelungpu-Fault Drilling Project, *J. Geophys. Res.*, **112**, B07404, doi:10.1029/2006JB004738.
- Hirono, T., T. Yokoyama, Y. Hamada, W. Tanikawa, T. Mishima, M. Ikehara, V. Famin, M. Tanimizu, W. Lin, W. Soh, and S.-R. Song (2007b), A chemical kinetic approach to estimate dynamic shear stress during the 1999 Taiwan Chi-Chi earthquake, *Geophys. Res. Lett.*, **34**, L19308, doi:10.1029/2007GL030743.
- Hirono, H., M. Sakaguchi, K. Otsuki, H. Sone, K. Fujimoto, T. Mishima, W. Lin, W. Tanikawa, M. Tanimizu, W. Soh, E.-C. Yeh, and S.-R. Song (2008), Characterization of slip zone associated with the 1999 Taiwan Chi-Chi earthquake: X-ray CT image analyses and microstructural observations of the Taiwan Chelungpu fault, *Tectonophysics*, **449**, 63-84, doi:10.1016/j.tecto.2007.12.002.

- Ho, C.-S. (1986), A synthesis of the geologic evolution of Taiwan, *Tectonophysics*, *125*, 1-16, doi:10.1016/0040-1951(86)90004-1.
- Horng, C.-S., C. Laj, T.-Q. Lee, and J.-C. Chen (1992), Magnetic characteristics of sedimentary rocks from the Tsengwen-chi and Erhjen-chi sections in southwestern Taiwan, *Terr. Atmos. Ocean. Sci.*, *3*, 519-532.
- Horng, C.-S., M. Torii, K.-S. Shea, and S.-J. Kao (1998), Inconsistent magnetic polarities between greigite- and pyrrhotite/magnetite-bearing marine sediments from the Tsailiao-chi section, southwestern Taiwan, *Earth Planet. Sci. Lett.*, *164*, 467-481, doi:10.1016/s0012-821x(98)00239-8.
- Housen, B. A., S. K. Banerjee, and B. M. Moskowitz (1996), Low-temperature magnetic properties of siderite and magnetite in marine sediments, *Geophys. Res. Lett.*, *23*, 2843–2846, doi:10.1029/96GL01197.
- Huang, W.-J., Y.-H. Lin, C.-W. Lin, S.-Y. Liu, and Z.-Y. Chen (2001), Report of active faults in Taiwan – the Chelungpu fault, *Central Geological Survey*, Taipei, Taiwan,  
<http://fault.moeacgs.gov.tw/UploadFiles//files/OLD/ATSTR42/activefault/192-2.htm#23>.
- Humbert, F., P. Robion, L. Louis, D. L. Bartier, B. A. Ledésert, and S.-R. Song (2012), Magnetic inference of in situ open microcracks in sandstone samples from the Taiwan Chelungpu Fault Drilling Project (TCDP), *J. Asian Earth Sci.*, *45*, 179-189, doi:10.1016/j.jseaes.2011.10.009.
- Hung, J.-H., Y.-H. Wu, E.-C. Yeh, J.-C. Wu, and TCDP Scientific Party (2007). Subsurface structure, physical properties, and fault zone characteristics in the scientific drill holes of Taiwan Chelungpu-Fault Drilling Project, *Terr. Atmos. Ocean. Sci.*, *18*, 271-293, doi: 10.3319/TAO.2007.18.2.271(TCDP).
- Hunt, C. P., S. K. Banerjee, J. Han, P. A. Solheld, E. Oches, W.-W. Sun, and T. Liu (1995), Rock-magnetic proxies of climate change in the loess-palaeosol sequences of the western Loess Plateau of China, *Geophys. J. Int.*, *123*, 232-244, doi:10.1111/j.1365-246X.1995.tb06672.x.
- Ikehara, M., T. Hirono, O. Tadai, H. Kikuta, T. Fukuchi, T. Mishima, N. Nakamura, K. Aoike, K. Fujimoto, Y. Hashimoto, T. Ishikawa, H. Ito, M. Kinoshita, W. Lin, K. Masuda, T. Matsubara, O. Matsubayashi, K. Mizoguchi, M. Murayama, K. Otsuki, H. Sone, M. Takahashi, W. Tanikawa, M. Tanimizu, W. Soh and S.-R. Song (2007), Low total and inorganic carbon contents within the Taiwan Chelungpu fault system, *Geochem. J.*, *41*, 391-396, doi:10.2343/geochemj.41.391.

- Isaacs, A. J., J. P. Evans, S.-R. Song, and P. T. Kolesar (2007), Structural, mineralogical, and geochemical characterization of the Chelungpu thrust fault, Taiwan, *Terr. Atmos. Ocean. Sci.*, *18*, 183-221, doi:10.3319/TAO.2007.18.2.183(TCDP).
- Ishikawa, T., M. Tanimizu, K. Nagaishi, J. Matsuoka, O. Tadai, M. Sakaguchi, T. Hirono, T. Mishima, W. Tanikawa, W. Lin, H. Kikuta, W. Soh, and S.-R. Song (2008), Coseismic fluid-rock interactions at high temperatures in the Chelungpu fault, *Nature Geosci.*, *1*, 679-683, doi:10.1038/ngeo308.
- Jackson, M. L. (2005), Soil chemical analysis. Advanced course, Revised 2nd ed. Parallel Press, University of Wisconsin-Madison Libraries, Madison, WI.
- Jakobsen, F., H. Lindgreen, and N. Springer (2000), Precipitation and flocculation of spherical nano-silica in North Sea chalk, *Clay Miner.*, *35*, 175-184.
- Jiang, W.-T., C.-S. Horng, A. P. Roberts, and D. R. Peacor (2001), Contradictory magnetic polarities in sediments and variable timing of neoformation of authigenic greigite, *Earth Planet. Sci. Lett.*, *193*, 1-12, doi:10.1016/s0012-821x(01)00497-6.
- Jovanović, D. (1989), Kinetics of thermal decomposition of pyrite in an inert atmosphere, *J. Therm. Anal. Calorim.*, *35*, 1483-1492, doi:10.1007/BF01912925.
- Kanamori, H. (1994), Mechanics of Earthquakes, *Annu. Rev. Earth Planet. Sci.*, *22*, 207-237, doi:10.1146/annurev.ea.22.050194.001231.
- Kanamori, H., and T. Heaton, in GeoComplexity and the Physics of Earthquakes, J. R. Rundle, D. L. Turcotte, W. Klein, eds., *Geophysical monograph no. 120*, American Geophysical Union, Washington, DC (2000).
- Kano, Y., J. Mori, R. Fujio, H. Ito, T. Yanagidani, S. Nakao, and K.-F. Ma (2006), Heat signature on the Chelungpu fault associated with the 1999 Chi-Chi, Taiwan earthquake, *Geophys. Res. Lett.*, *33*, L14306, doi:10.1029/2006GL026733.
- Kao, H., and W.-P. Chen (2000), The Chi-Chi Earthquake Sequence: Active, Out-of-Sequence Thrust Faulting in Taiwan, *Science*, *288*, 2346-2349, doi:10.1126/science.288.5475.2346.
- Kars, M., C. Aubourg, and J.-P. Pozzi (2011), Low temperature magnetic behaviour near 35 K in unmetamorphosed claystones, *Geophys. J. Int.*, *186*, 1029-1035, doi:10.1111/j.1365-246X.2011.05121.x.
- Kendall, K. (1978), The impossibility of comminuting small particles by compression, *Nature*, *272*, 710-711, doi:10.1038/272710a0.
- Kent, D. V., and D. A. Schneider (1995), Correlation of paleointensity variation records in the Brunhes/Matuyama polarity transition interval, *Earth Planet. Sci.*

- Lett.*, 129(1-4), 135-144, doi:10.1016/0012-821x(94)00236-r.
- Keulen, N., R. Heilbronner, H. Stünitz, A.-M. Boullier, and H. Ito (2007), Grain size distributions of fault rocks: A comparison between experimentally and naturally deformed granitoids, *J. Struct. Geol.*, 29, 1282-1300, doi:10.1016/j.jsg.2007.04.003.
- Kirkpatrick, J. D., et al. (2009), Pseudotachylytes: Rarely generated, rarely preserved, or rarely reported?, *Bull. Seismol. Soc. Am.*, 99(1), 382–388, doi:10.1785/0120080114.
- Knauss, K. G., and T. J. Wolery (1988), The dissolution kinetics of quartz as a function of pH and time at 70°C, *Geochim. Cosmochim. Acta*, 52, 43-53, doi:10.1016/0016-7037(88)90055-5.
- Kuo, L.-W., S.-R. Song, E.-C. Yeh, and H.-F. Chen (2009), Clay mineral anomalies in the fault zone of the Chelungpu Fault, Taiwan, and their implications, *Geophys. Res. Lett.*, 36, L18306, doi:10.1029/2009GL039269.
- Kuo, L.-W., S.-R. Song, L. Huang, E.-C. Yeh, and H.-F. Chen (2011), Temperature estimates of coseismic heating in clay-rich fault gouges, the Chelungpu fault zones, Taiwan, *Tectonophysics*, 502, 315-327, doi:10.1016/j.tecto.2011.02.001.
- Kuo, L.-W., S.-R. Song, E.-C. Yeh, H.-F. Chen, and J.-L. Si (2012), Clay mineralogy and geochemistry investigations in the host rocks of the Chelungpu fault, Taiwan: Implication for faulting mechanism. *J. Asia. Earth Sci.*, <http://dx.doi.org/10.1016/j.jseaes.2012.07.009>.
- Lachenbruch, A. H. (1980), Frictional Heating, Fluid Pressure, and the Resistance to Fault Motion, *J. Geophys. Res.*, 85(B11), 6097-6112.
- Laidlaw, I., and M. Steinmetz (2005), Introduction to differential sedimentation. p. 270–290. In D.J. Scott et al., (ed.) *Analytical ultracentrifugation: Techniques and methods*, Royal Society of Chemistry, Cambridge, UK.
- Laj, C., and J.E.T., Channell, (2007), Geomagnetic excursions. In: Schubert, G., Bercovici, D., Dziewonski, A., Hering, T., Kanamori, H., Kono, M., Olson, P.L., Price, G.D., Romanowicz, B., Spohn, T., Stevenson, D., Watts, A.B. (Eds.), *Treatise on Geophysics, Geomagnetism*, 5, Elsevier, B.V, Amsterdam, 373–416, doi:10.1016/b978-044452748-6.00095-x.
- Lambert, J., G. Simkovich, and P. Walker (1998), The kinetics and mechanism of the pyrite-to-pyrrhotite transformation, *Metall. Mater. Trans. B*, 29, 385-396, doi:10.1007/s11663-998-0115-x.
- Lee, J.-C., H.-T. Chu, J. Angelier, Y.-C. Chan, J.-C. Hu, C.-Y. Lu, and R.-J. Rau

- (2002), Geometry and structure of northern surface ruptures of the 1999 Mw=7.6 Chi-Chi Taiwan earthquake: influence from inherited fold belt structures, *J. Stru. Geol.*, *24*, 173-192, doi:10.1016/s0191-8141(01)00056-6.
- Lin, A. (2008), *Fossil Earthquakes: The Formation and Preservation of Pseudotachylytes*, 345 pp., Springer, New York.
- Liu, Y., and Q. Liu (2004), Flotation separation of carbonate from sulfide minerals, I: flotation of single minerals and mineral mixtures, *Mineral. Eng.*, *17*, 855-863, doi:10.1016/j.mineng.2004.03.006.
- Liu, Q., Y. Yu, J. Torrent, A. P. Roberts, Y. Pan, and R. Zhu (2006), Characteristic low-temperature magnetic properties of aluminous goethite [ $\alpha$ -(Fe, Al)OOH] explained, *J. Geophys. Res.*, *111*, B12S34, doi:10.1029/2006jb004560.
- Ma, K.-F., C.-T. Lee, Y.-B. Tsai, T.-C. Shin, and J. Mori (1999), The Chi-Chi, Taiwan earthquake: Large surface displacements on an inland thrust fault, *Eos Trans. AGU*, *80(50)*, 605.
- Ma, K.-F., E. E. Brodsky, J. Mori, C. Ji, T.-R. A. Song, and H. Kanamori (2003), Evidence for fault lubrication during the 1999 Chi-Chi, Taiwan, earthquake ( $M_w$ 7.6), *Geophys. Res. Lett.*, *30*, 1244, doi:10.1029/2002GL015380.
- Ma, K.-F., H. Tanaka, S.-R. Song, C.-Y. Wang, J.-H. Hung, Y.-B. Tsai, J. Mori, Y.-F. Song, E.-C. Yeh, W. Soh, H. Sone, L.-W. Kuo and H.-Y. Wu (2006), Slip zone and energetics of a large earthquake from the Taiwan Chelungpu-fault Drilling Project, *Nature*, *444*, 473-476, doi:10.1038/nature05253.
- Maclean, L. C. W., T. Tyliczszak, P. U. P. A. Gilbert, D. Zhou, T. J. Pray, T. C. Onstott, and G. Southam (2008), A high-resolution chemical and structural study of framboidal pyrite formed within a low-temperature bacterial biofilm, *Geobiology*, *6*, 471-480, doi:10.1111/j.1472-4669.2008.00174.x.
- Magloughlin, J. F. (1992), Microstructural and chemical changes associated with cataclasis and frictional melting at shallow crustal levels: The cataclasite-pseudotachylyte connection, *Tectonophysics*, *204*, 243-260, doi:10.1016/0040-1951(92)90310-3.
- Maher, B. A., R. Thompson, and M. W. Hounslow (1999), Introduction. In: Maher, B.A., and R. Thompson (Eds.), *Quaternary Climates, Environments and Magnetism*, 1-48 pp., Cambridge University Press, Cambridge.
- Mayoral, M. C., M. T. Izquierdo, J. M. Andrés, and B. Rubio (2002), Mechanism of interaction of pyrite with hematite as simulation of slagging and fireside tube wastage in coal combustion, *Thermochim. Acta*, *390*, 103-111,



- doi:10.1016/S0040-6031(02)00075-8.
- McElhinny, W., P.L. McFadden, (1999), *Paleomagnetism: Continents and Oceans*, 139-141, Academic Press, New York.
- McFadyen, P., and D. Fairhurst (1993), High-resolution particle size analysis from nanometres to microns, *Clay Miner.*, 28, 531-537.
- Mishima, T., T. Hirono, W. Soh, and S.-R. Song (2006), Thermal history estimation of the Taiwan Chelungpu fault using rock-magnetic methods, *Geophys. Res. Lett.*, 33, L23311, doi:10.1029/2006GL028088.
- Mishima, T., T. Hirono, N. Nakamura, W. Tanikawa, W. Soh, and S.-R. Song (2009), Changes to magnetic minerals caused by frictional heating during the 1999 Taiwan Chi-Chi earthquake, *Earth Planets Space*, 61, 797-801.
- Mizoguchi, K., T. Hirose, T. Shimamoto, and E. Fukuyama (2009), High-velocity frictional behavior and microstructure evolution of fault gouge obtained from Nojima fault, southwest Japan, *Tectonophysics*, 471, 285-296, doi:10.1016/j.tecto.2008.08.009.
- Molina Garza, R. S., J. Geissman, T. Wawrzyniec, B. Weber, M. L. Martínez, and J. Aranda-Gómez (2009), An integrated magnetic and geological study of cataclasite-dominated pseudotachylytes in the Chiapas Massif, Mexico: A snapshot of stress orientation following slip, *Geophys. J. Int.*, 177(3), 891–912, doi:10.1111/j.1365-246X.2009.04046.x.
- Murad, E., and P. Rojik (2003), Iron-rich precipitates in a mine drainage environment: Influence of pH on mineralogy, *Am. Mineral.*, 88, 1915-1918.
- Music, S., S. Popović, and M. Ristić (1992), Thermal decomposition of pyrite, *J. Radioanal. Nucl. Chem.*, 162, 217-226, doi:10.1007/BF02035382.
- Nakamura, N. (2001), Changes in magnetic and fractal properties of fractured granites near the Nojima Fault, Japan, *Island Arc*, 10, 486-494, doi:10.1111/j.1440-1738.2001.00347.x.
- Nakamura, N., T. Hirose, and G. J. Borradaile (2002), Laboratory verification of submicron magnetite production in pseudotachylytes: Relevance for paleointensity studies, *Earth Planet. Sci. Lett.*, 201, 13-18, doi:10.1016/S0012-821X(02)00704-5.
- Nakamura, N., and Y. Iyeda (2005), Magnetic properties and paleointensity of pseudotachylytes from the Sudbury structure, Canada: Petrologic control, *Tectonophysics*, 402, 141–152, doi:10.1016/j.tecto.2004.10.015.
- Nakamura, N., M. Uehara, T. Mishima, T. Hirono, and TCDP team (2008), Anomalous magnetization of fault gouges recovered from Taiwan Chelungpu-fault

- Drilling Project (TCDP), *EGU, Geophysical Research Abstracts, Vol. 10*, EGU2008-A-02962.
- Néel, L., (1955), Some theoretical aspects of rock magnetism, *Adv. Phys.*, 4, 191–243.
- Oelkers, E. H., P. A. Bjørkum, O. Walderhaug, P. H. Nadeau, and W. M. Murphy (2000), Making diagenesis obey thermodynamics and kinetics: the case of quartz cementation in sandstones from offshore mid-Norway, *Appl. Geochem.*, 15, 295-309, doi:10.1016/s0883-2927(99)00047-5.
- Okubo, P. G., and J. H. Dieterich (1984), Effects of physical fault properties on frictional instabilities produced on simulated faults, *J. Geophys. Res.*, 89, 5817-5827, doi:10.1029/JB089iB07p05817.
- Olgaard, D. L., and W. F. Brace (1983), The microstructure of gouge from a mining-induced seismic shear zone, *Inter. J. Rock Mech. Min.*, 20, 11-19, doi:10.1016/0148-9062(83)91610-8.
- Otsuki, K., T. Hirono, M. Omori, M. Sakaguchi, W. Tanigawa, W. Lin, W. Soh, and S.-S. Rong (2009), Analyses of pseudotachylyte from Hole-B of Taiwan Chelungpu Fault Drilling Project (TCDP); their implications for seismic slip behaviors during the 1999 Chi-Chi earthquake, *Tectonophysics*, 469, 13-24, doi:10.1016/j.tecto.2009.01.008.
- Özdemir, Ö., D. J. Dunlop, and B. M. Moskowitz (1993), The effect of oxidation on the Verwey transition in magnetite, *Geophys. Res. Lett.*, 20, 1671-1674, doi:10.1029/93gl01483.
- Özdemir, Ö., and D. J. Dunlop (1996), Thermoremanence and Néel temperature of goethite, *Geophys. Res. Lett.*, 23, 921-924, doi:10.1029/96GL00904.
- Özdemir, Ö., and D. J. Dunlop (1999), Low-temperature properties of a single crystal of magnetite oriented along principal magnetic axes, *Earth Planet. Sci. Lett.*, 165, 229-239, doi:10.1016/S0012-821X(98)00269-6.
- Özdemir, Ö., D. J. Dunlop, and B. M. Moskowitz (2002), Changes in remanence, coercivity and domain state at low temperature in magnetite, *Earth Planet. Sci. Lett.*, 194, 343-358, doi:10.1016/S0012-821X(01)00562-3.
- Pelovski, Y., and V. Petkova (1999), Investigation on thermal decomposition of pyrite Part I, *J. Therm. Anal. Calorim.*, 56, 95-99, doi:10.1023/A:1010135425009.
- Peters, C., and M. J. Dekkers (2003), Selected room temperature magnetic parameters as a function of mineralogy, concentration and grain size, *Phys. Chem. Earth, Parts A/B/C*, 28, 659-667, doi:10.1016/s1474-7065(03)00120-7.

- Philpotts, A.R., (1964), Origin of pseudotachylites, *Am. J. Sci.*, 262, 1008–1035, doi:10.2475/ajs.262.8.1008.
- Pike, C. R., A. P. Roberts, and K. L. Verosub (1999), Characterizing interactions in fine magnetic particle systems using first order reversal curves, *J. Appl. Phys.*, 85, 6660-6667, doi:10.1063/1.370176.
- Pike, C. R., A. P. Roberts, and K. L. Verosub (2001), First-order reversal curve diagrams and thermal relaxation effects in magnetic particles, *Geophys. J. Int.*, 145, 721-730.
- Piper, J. D. A. (1981), Palaeomagnetism of pseudotachylites from the Ikertôk shear belt, and their relationship to the kimberlite-lamprophyre province, central-west Greenland, *Bull. Geol. Soc. Den.*, 30, 57–67.
- Piper, J. D. A., and T. J. Poppleton (1988), Palaeomagnetic dating of pseudotachylite formation in the Lewisian complex, *Scott. J. Geol.*, 24(3), 263–272, doi:10.1144/sjg24030263.
- Prasher, C. (1987), *Crushing and Grinding Process Handbook*, 474 pp., John Wiley, New York.
- Puretz, J. (1979), Centrifugal particle size analysis and the Joyce–Loebl disc centrifuge. p. 77–88. In J. D. Stockham and E. G. Fochtman (ed.) *Particle size analysis*, Ann Arbor Science, Ann Arbor, MI.
- Reches, Z. e., and T. A. Dewers (2005), Gouge formation by dynamic pulverization during earthquake rupture, *Earth Planet. Sci. Lett.*, 235, 361-374, doi:10.1016/j.epsl.2005.04.009.
- Reimer, T. O. (1984), Graphite in Precambrian rocks of Southern Africa: Implications on the carbon content of metamorphic rocks, *Precambrian Res.*, 26, 223-234, doi:10.1016/0301-9268(84)90002-0.
- Rice, J. R., C. G. Sammis, and R. Parsons (2005), Off-fault secondary failure induced by a dynamic slip pulse, *Bull. Seismol. Soc. Am.*, 95, 109-134, doi:10.1785/0120030166.
- Roberts, A. P., C. R. Pike, and K. L. Verosub (2000), First-order reversal curve diagrams: A new tool for characterizing the magnetic properties of natural samples, *J. Geophys. Res.*, 105, 28461-28475, doi:10.1029/2000jb900326.
- Roberts, A. P., and R. Weaver (2005), Multiple mechanisms of remagnetization involving sedimentary greigite (Fe<sub>3</sub>S<sub>4</sub>), *Earth Planet. Sci. Lett.*, 231, 263-277, doi:10.1016/j.epsl.2004.11.024.
- Roberts, A. P., Q. Liu, C. J. Rowan, L. Chang, C. Carvallo, J. Torrent, and C.-S.

- Hornig (2006), Characterization of hematite ( $\alpha$ -Fe<sub>2</sub>O<sub>3</sub>), goethite ( $\alpha$ -FeOOH), greigite (Fe<sub>3</sub>S<sub>4</sub>), and pyrrhotite (Fe<sub>7</sub>S<sub>8</sub>) using first-order reversal curve diagrams, *J. Geophys. Res.*, *111*, B12S35, doi:10.1029/2006JB004715.
- Rochette, P., G. Fillion, J.-L. Mattéi, and M. J. Dekkers (1990), Magnetic transition at 30-34 Kelvin in pyrrhotite: Insight into a widespread occurrence of this mineral in rocks, *Earth Planet. Sci. Lett.*, *98*, 319-328, doi:10.1016/0012-821X(90)90034-U.
- Rochette, P., P.-E. Mathé, L. Esteban, H. Rakoto, J.-L. Bouchez, Q. Liu, and J. Torrent (2005), Non-saturation of the defect moment of goethite and fine-grained hematite up to 57 Teslas, *Geophys. Res. Lett.*, *32*, L22309, doi:10.1029/2005GL024196.
- Rockwell, T., M. Sisk, G. Girty, O. Dor, N. Wechsler, and Y. Ben-Zion (2009), Chemical and Physical Characteristics of Pulverized Tejon Lookout Granite Adjacent to the San Andreas and Garlock Faults: Implications for Earthquake Physics, *Pure Appl. Geophys.*, *166*(10), 1725-1746, doi:10.1007/s00024-009-0514-1.
- Ross, S., and E. D. Morrison (1988), *Colloidal systems and interfaces*, 440 pp., John Wiley & Sons, New York.
- Rowan, C. J., and A. P. Roberts (2006), Magnetite dissolution, diachronous greigite formation, and secondary magnetizations from pyrite oxidation: Unravelling complex magnetizations in Neogene marine sediments from New Zealand, *Earth Planet. Sci. Lett.*, *241*, 119-137, doi:10.1016/j.epsl.2005.10.017.
- Rowan, C. J., A. P. Roberts, and T. Broadbent (2009), Reductive diagenesis, magnetite dissolution, greigite growth and paleomagnetic smoothing in marine sediments: A new view, *Earth Planet. Sci. Lett.*, *277*, 223-235, doi:10.1016/j.epsl.2008.10.016.
- Sakaguchi, A., A. Yanagihara, K. Ujiie, H. Tanaka, and M. Kameyama (2007), Thermal maturity of a fold-thrust belt based on vitrinite reflectance analysis in the Western Foothills complex, western Taiwan, *Tectonophysics*, *443*, 220-232, doi:10.1016/j.tecto.2007.01.017.
- Sammis, C. G., and G. C. P. King (2007), Mechanical origin of power law scaling in fault zone rock, *Geophys. Res. Lett.*, *34*, L04312, doi:10.1029/2006gl028548.
- Sammis, C. G., and Y. Ben-Zion (2008), Mechanics of grain-size reduction in fault zones, *J. Geophys. Res.*, *113*, B02306, doi:10.1029/2006JB004892.
- Schwertmann, U., and E. Murad (1983), Effect of pH on the formation of goethite and hematite from ferrihydrite, *Clays Clay Mineral.*, *31*, 277-284.

- Sibson, R. H. (1975). Generation of pseudotachylyte by ancient seismic faulting, *Geophys. J. R. Astr. Soc.* **43**, 775–794.
- Sibson, R. H. (2003), Thickness of the Seismic Slip Zone, *Bull. Seismol. Soc. Am.*, **93**, 1169–1178, doi:10.1785/0120020061.
- Song, S.-R., L.-W. Kuo, E.-C. Yeh, C.-Y. Wang, J.-H. Hung, and K.-F. Ma (2007a), Characteristics of the lithology, fault-related rocks and fault zone structures in TCDP Hole-A, *Terr. Atmos. Ocean. Sci.*, **18**, 243 – 269, doi:10.3319/TAO.2007.18.2.243(TCDP).
- Song, Y.-F., C.-H. Chang, C.-Y. Liu, S.-H. Chang, U.-S. Jeng, Y.-H. Lai, D.-G. Liu, S.-C. Chung, K.-L. Tsang, G.-C. Yin, J.-F. Lee, H.-S. Sheu, M.-T. Tang, C.-S. Hwang, Y.-K. Hwu, and K. S. Liang (2007b), X-ray beamlines for structural studies at the NSRRC superconducting wavelength shifter, *J. Synchrotron Rad.*, **14**, 320–325, doi:10.1107/S0909049507021516.
- Spray, J. G. (1987), Artificial generation of pseudotachylite using friction welding apparatus: Simulation of melting on a fault plane, *J. Struct. Geol.*, **9**(1), 49–60, doi:10.1016/0191-8141(87)90043-5.
- Tanikawa, W., T. Mishima, T. Hirano, W. Lin, T. Shimamoto, W. Soh, and S.-R. Song (2007), High magnetic susceptibility produced in high-velocity frictional tests on core samples from the Chelungpu fault in Taiwan, *Geophys. Res. Lett.*, **34**, L15304, doi:10.1029/2007GL030783.
- Tanikawa, W., T. Mishima, T. Hirano, W. Soh, and S.-R. Song (2008), High magnetic susceptibility produced by thermal decomposition of core samples from the Chelungpu fault in Taiwan, *Earth Planet. Sci. Lett.*, **272**, 372–381, doi:10.1016/j.epsl.2008.05.002.
- Tanikawa, W., M. Sakaguchi, T. Hirano, W. Lin, W. Soh, and S.-R. Song (2009), Transport properties and dynamic processes in a fault zone from samples recovered from TCDP Hole B of the Taiwan Chelungpu Fault Drilling Project, *Geochem. Geophys. Geosyst.*, **10**, Q04013, doi:10.1029/2008GC002269.
- Tanner, C. B., and M. L. Jackson. (1947), Nomographs of sedimentation times for soil particles under gravity or centrifugal acceleration, *Soil Sci. Soc. Am. Proc.* **12**, 60–65, doi:10.2136/sssaj1948.036159950012000C0014x.
- Tribovillard, N., O. Averbuch, A. Bialkowski, and J.-F. Deconinck (2002), Early diagenesis of marine organic-matter and magnetic properties of sedimentary rocks: The role of iron limitation and organic-matter source organisms, *Bull Soc. Geol. France*, **173**, 295–306, doi:10.2113/173.4.295.

- Tsao, T. M., M. K. Wang, and P. M. Huang (2009a), *An apparatus for collecting nanoparticles*, United States patent No. 7501, 063B2.
- Tsao, T. M., M. K. Wang, and P. M. Huang (2009b), Automated ultrafiltration device for Efficient collection of environmental nanoparticles from aqueous suspensions, *Soil Sci. Soc. Am. J.*, 73, 1808-1816, doi:10.2136/sssaj2008.0376.
- Valet, J.-P., and H. Valladas (2010), The Laschamp-Mono lake geomagnetic events and the extinction of Neanderthal: a causal link or a coincidence?, *Quat. Sci. Rev.*, 29(27-28), 3887-3893. doi:10.1016/j.quascirev.2010.09.010.
- Wang, P.-L., L.-H. Lin, H.-T. Yu, T.-W. Cheng, S.-R. Song, L.-W. Kuo, E.-C. Yeh, W. Lin, and C.-Y. Wang (2007), Cultivation-based characterization of microbial communities associated with deep sedimentary rocks from Taiwan Chelungpu Drilling Project cores, *Terr. Atmos. Ocean. Sci.*, 18, 395-412, doi:10.3319/TAO.2007.18.2.395(TCDP).
- Wang, L., Y. Pan, J. Li, and H. Qin (2008), Magnetic properties related to thermal treatment of pyrite, *Sci. China Ser. D*, 51, 1144-1153, doi:10.1007/s11430-008-0083-7.
- Wang, Y., and E. Forssberg (2006), Production of carbonate and silica nano-particles in stirred bead milling, *Inter. J. Miner. Process.*, 81, 1-14, doi:10.1016/j.minpro.2006.05.007.
- Wehland, F., A. Stancu, P. Rochette, M. J. Dekkers, and E. Appel (2005), Experimental evaluation of magnetic interaction in pyrrhotite bearing samples, *Phys. Earth Planet. Inter.*, 153, 181-190, doi:10.1016/j.pepi.2005.05.006.
- Williams, J. W., K. E. Van Holde, R. L. Baldwin, and H. Fujita (1958), The theory of sedimentation analysis, *Chem. Rev.*, 58, 715-744, doi:10.1021/cr50022a005.
- Williams, L. A., G. A. Parks, and D. A. Crerar (1985), Silica diagenesis; I, Solubility controls, *J. Sediment. Res.*, 55, 301-311, doi:10.1306/212f86ac-2b24-11d7-8648000102c1865d.
- Wilson, B., T. Dewers, Z. e. Reches, and J. Brune (2005), Particle size and energetics of gouge from earthquake rupture zones, *Nature*, 434, 749-752, doi:10.1038/nature03433.
- Wong, T.-F. (1982), Shear fracture energy of westerly granite from post-failure behavior, *J. Geophys. Res.*, 87, 990-1000, doi:10.1029/JB087iB02p00990.
- Wu, H.-Y., K.-F. Ma, M. Zoback, N. Boness, H. Ito, J.-H. Hung, and S. Hickman (2007), Stress orientations of Taiwan Chelungpu-fault Drilling Project (TCDP) Hole-A as observed from geophysical logs, *Geophys. Res. Lett.*, 34, L01303,

doi:10.1029/2006GL028050.

- Wu, Y.-H., E.-C. Yeh, J.-J. Dong, L.-W. Kuo, J.-Y. Hsu, and J.-H. Hung (2008), Core-log integration studies in hole-A of Taiwan Chelungpu-fault Drilling Project, *Geophys. J. Inter.*, *174*, 949-965, doi:10.1111/j.1365-246X.2008.03841.x.
- Yeh, E.-C., H. Sone, T. Nakaya, K.-H. Ian, S.-R. Song, J.-H. Hung, W. Lin, T. Hirono, C.-Y. Wang, K.-F. Ma, W. Soh, and M. Kinoshita (2007), Core description and characteristics of fault zones from Hole-A of the Taiwan Chelungpu-fault Drilling Project, *Terr. Atmos. Ocean. Sci.*, *18*, 327-357, doi:10.3319/TAO.2007.18.2.327(TCDP).
- Yin, G.-C., Y.-F. Song, M.-T. Tang, F.-R. Chen, K. S. Liang, F. W. Duewer, M. Feser, W. Yun, and H.-P. D. Shieh (2006), 30 nm resolution x-ray imaging at 8 keV using third order diffraction of a zone plate lens objective in a transmission microscope, *Appl. Phys. Lett.*, *89*, 221122-221123, doi:10.1063/1.2397483.
- Yu, S.-B., H.-Y. Chen, and L.-C. Kuo (1997), Velocity field of GPS stations in the Taiwan area, *Tectonophysics*, *274*, 41-59, doi:10.1016/S0040-1951(96)00297-1.
- Yue, L.-F., J. Suppe, and J.-H. Hung (2005), Structural geology of a classic thrust belt earthquake: The 1999 Chi-Chi earthquake Taiwan ( $M_w=7.6$ ), *J. Struct. Geol.*, *27*, 2058-2083, doi:10.1016/j.jsg.2005.05.020.
- Yund, R. A., M. L. Blanpied, T. E. Tullis, and J. D. Weeks (1990), Amorphous Material in High Strain Experimental Fault Gouges, *J. Geophys. Res.*, *95*, 15589-15602, doi:10.1029/JB095iB10p15589.

## Appendix

### ABSTRACT:

**Chou, Y.-M.**, T. M. Tsao, M. K. Wang and S. R. Song (2007), Preliminary Result of Clay Minerals Analysis of Chi-Chi Earthquake Fault Gouge, Wu-Feng, Central Taiwan., *Taiwan Geosciences Assembly (TGA)*, P25.

**Chou, Y.-M.**, T. Tsao, S.R. Song, E.C. Yeh, M. Wang, C. Lin, T. Lee, H. Chen, (2007), Nano-particle Analysis of Fault Gouge in the Chelungpu Fault of Taiwan, Eos Trans. *AGU*, 88(52), Fall Meet. Suppl., Abstract T43B-1330.

Yeh, E.C., T. Lee, Y. Lin, T. Chen, **Y. Chou**, C. Lu, (2007), Analysis of Magnetic and Grain Fabrics across Fault Gouge in the Chelungpu Fault of Taiwan, Eos Trans. *AGU*, 88(52), Fall Meet. Suppl., Abstract T43B-1331.

**Chou, Y. M.**, S. R. Song, E. C. Yeh, A. Boullier, Y. F. Song, Yen-Fang, T. Q. Lee, (2008), X-ray Microscopy/Tomography Research of TCDP Hole-B, 2008 Geological Annual Congress, *Geological Society of Taiwan & Chinese Geophysical Society*, T1-378.

**Chou, Y. M.**, T.-Q. Lee, C. Aubourg, A.-M. Boullier, S.-R. Song, E.-C. Yeh, (2009), Magnetic mineralogy and its correspondence with SEM observations on FZB1136 fault gouge of the Chi-Chi earthquake, Chelungpu fault, Taiwan, *EGU, Geophysical Research Abstracts*, Vol. 11, Abstract EGU2009- 5950.

**Chou, Y. M.**, S. R. Song, C. Aubourg, Y. F. Song, A.-M. Boullier, T. Q. Lee, E. C. Yeh, (2010), Pyrite alteration and neoformed magnetic minerals in the fault zone of Chi-Chi earthquake ( $M_w$  7.6, 1999), Taiwan. Eos Trans. *AGU*, Fall Meet. Suppl., Abstract T51B-2046.

**Chou, Y.-M.**, S-R., Song, C. Aubourg, T-Q., Lee, E-C., Yeh, (2010), The paleomagnetic record of Chi-Chi earthquake: ( $M_w$  7.6, 1999), Eos Trans. *AGU*, 91(26), West. Pac. Geophys. Meet. Suppl., Abstract S4.

**Chou, Y.-M.**, S-R., Song, C. Aubourg, T-Q., Lee, E-C., Yeh, (2011), Magnetic minerals as an indicator of co-seismic gouge alteration: the Chelungpu fault, Taiwan, *Asia Ocean Geos. Soc. Meet.*, Abstract SE83-A035.

**Chou, Y.-M.**, C. Aubourg, S-R., Song, T-Q., Lee, Y-F., Song, (2012), Creep versus Earthquake Slip: New insights from rock magnetic data, *EGU, Geophysical Research Abstracts*, Vol. 14, Abstract EGU2012- 6911.



## REFERED PAPERS:

- Chou, Y.-M.**, S.-R. Song, C. Aubourg, T.-Q. Lee, A.-M. Boullier, Y.-F. Song, E.-C. Yeh, L.-W. Kuo, and C.-Y. Wang (2011), An earthquake slip zone is a magnetic recorder, *Geology*, doi:10.1130/g32864.1.
- Chou, Y.-M.**, S.-R. Song, C. Aubourg, Y.-F. Song, A.-M. Boullier, T.-Q. Lee, M. Evans, E.-C. Yeh, and Y.-M. Chen (2012), Pyrite alteration and neoformed magnetic minerals in the fault zone of the Chi-Chi earthquake ( $M_w$  7.6, 1999): Evidence for frictional heating and co-seismic fluids, *Geochem. Geophys. Geosyst.*, 13, Q08002, doi:10.1029/2012GC004120.



## Geology

### An earthquake slip zone is a magnetic recorder

Yu-Min Chou, Sheng-Rong Song, Charles Aubourg, Teh-Quei Lee, Anne-Marie Boullier, Yen-Fang Song, En-Chao Yeh, Li-Wei Kuo and Chien-Ying Wang

*Geology* published online 19 April 2012;  
doi: 10.1130/G32864.1

---

#### Email alerting services

click [www.gsapubs.org/cgi/alerts](http://www.gsapubs.org/cgi/alerts) to receive free e-mail alerts when new articles cite this article

#### Subscribe

click [www.gsapubs.org/subscriptions/](http://www.gsapubs.org/subscriptions/) to subscribe to *Geology*

#### Permission request

click <http://www.geosociety.org/pubs/copyrt.htm#gsa> to contact GSA

Copyright not claimed on content prepared wholly by U.S. government employees within scope of their employment. Individual scientists are hereby granted permission, without fees or further requests to GSA, to use a single figure, a single table, and/or a brief paragraph of text in subsequent works and to make unlimited copies of items in GSA's journals for noncommercial use in classrooms to further education and science. This file may not be posted to any Web site, but authors may post the abstracts only of their articles on their own or their organization's Web site providing the posting includes a reference to the article's full citation. GSA provides this and other forums for the presentation of diverse opinions and positions by scientists worldwide, regardless of their race, citizenship, gender, religion, or political viewpoint. Opinions presented in this publication do not reflect official positions of the Society.

---

#### Notes

---

Advance online articles have been peer reviewed and accepted for publication but have not yet appeared in the paper journal (edited, typeset versions may be posted when available prior to final publication). Advance online articles are citable and establish publication priority; they are indexed by GeoRef from initial publication. Citations to Advance online articles must include the digital object identifier (DOIs) and date of initial publication.

---

# An earthquake slip zone is a magnetic recorder

Yu-Min Chou<sup>1,2</sup>, Sheng-Rong Song<sup>1,3\*</sup>, Charles Aubourg<sup>3,4\*</sup>, Teh-Quei Lee<sup>3,5</sup>, Anne-Marie Boullier<sup>3,6</sup>, Yen-Fang Song<sup>7\*</sup>, En-Chao Yeh<sup>3,8</sup>, Li-Wei Kuo<sup>1</sup>, and Chien-Ying Wang<sup>9</sup>

<sup>1</sup>Department of Geosciences, National Taiwan University, 1, Roosevelt Road Section 4, Taipei 10617, Taiwan

<sup>2</sup>Géosciences & Environnement Cergy, Université de Cergy-Pontoise, 5 mail Gay Lussac, Neuville sur Oise, 95031 Cergy-Pontoise cedex, France

<sup>3</sup>International Laboratory (LIA) ADEPT, CNRS-NSC, France-Taiwan

<sup>4</sup>Laboratoire des Fluides Complexes et Réservoirs, UMR 5150, CNRS, Université de Pau, 64013 Pau cedex, France

<sup>5</sup>Institute of Earth Sciences, Academia Sinica, 128, Section 2, Academia Road, Nangang, Taipei 115, Taiwan

<sup>6</sup>ISterre, CNRS, Université Joseph Fourier, Maison des Géosciences, BP 53, 38041 Grenoble cedex 9, France

<sup>7</sup>National Synchrotron Radiation Research Center, 101, Hin-Ann Road, Hsinchu Science Park, Hsinchu 30076, Taiwan

<sup>8</sup>Department of Earth Sciences, National Taiwan Normal University, No. 88, Section 4, Tingzhou Road, Wenshan District, Taipei 11677, Taiwan

<sup>9</sup>Department of Earth Sciences and Institute of Geophysics, National Central University, No. 300, Jhongda Road, Jhongli City, Taoyuan 32001, Taiwan

## ABSTRACT

During an earthquake, the physical and the chemical transformations along a slip zone lead to an intense deformation within the gouge layer of a mature fault zone. Because the gouge contains ferromagnetic minerals, it has the capacity to behave as a magnetic recorder during an earthquake. This constitutes a conceivable way to identify earthquake slip zones. In this paper, we investigate the magnetic record of the Chelungpu fault gouge that hosts the principal slip zone of the Chi-Chi earthquake ( $M_w$  7.6, 1999, Taiwan) using Taiwan Chelungpu-fault Drilling Project core samples. Rock magnetic investigation pinpoints the location of the Chi-Chi millimeter-thick principal slip zone within the 16 cm thick gouge at ~1 km depth. A modern magnetic dipole of Earth's magnetic field is recovered throughout this gouge, but not in the wall rocks nor in the two other adjacent fault zones. This magnetic record resides essentially in two magnetic minerals: magnetite in the principal slip zone, and neoformed goethite elsewhere in the gouge. We propose a model where the magnetic record (1) is preserved during inter-seismic time, (2) is erased during co-seismic time, and (3) is imprinted during post-seismic time when fluids cooled down. We suggest that the identification of a stable magnetic record carried by neoformed goethite may be a signature of a frictional heating process in a seismic slip zone.

## INTRODUCTION

The Chi-Chi earthquake ( $M_w$  7.6, 21 September 1999) is the largest inland earthquake to hit Taiwan during the past century. The ~85 km rupture along the Chelungpu thrust extends from the north to the south (Fig. 1A). Five years after the earthquake, two boreholes (holes A and B, 40 m apart, Taiwan Chelungpu-fault Drilling Project [TCDP]; <http://www.rcep.dpri.kyoto-u.ac.jp/~mori/ChelungpuDrilling/>) were drilled through ~2 km of alternating sandstones and siltstones of early Pliocene age. The boreholes provided fresh and unaltered material suitable for paleomagnetic investigation. In hole B, three fault zones, labeled FZB1136, FZB1194, and FZB1243 have been identified within the Chinshui Formation using core observations and physical property measurements (Hirono et al., 2007) (Fig. 1B). From an independent data set, it was proposed that the 16-cm-thick gouge of FZB1136 contained the principal slip zone (PSZ) of the Chi-Chi earthquake at 1136.38 m (Boullier et al., 2009). The Chi-Chi

PSZ accommodated a co-seismic displacement of ~8 m with a maximum 3 m/s velocity (Ma et al., 2006). To explain some characteristics of the low friction in the northern part of the fault rupture, several authors have inferred the role of fluids and thermal pressurization processes (Boullier et al., 2009; Ishikawa et al., 2008). Mishima et al. (2009) reported evidence of neoformed magnetite ( $\text{Fe}_3\text{O}_4$ ) in Chelungpu gouges possibly due to temperature elevation >400 °C. Assuming that magnetite formed by nucleation-growth process, we expect that magnetite has the capability to record durably Earth's magnetic field. To check the existence of this record, we present a paleomagnetic and rock magnetic investigation of the three major fault zones within TCDP hole B. We identify for the first time a magnetic record that is directly related to a large-magnitude earthquake. This magnetic record is carried by magnetite within the PSZ and neoformed goethite in the entire gouge.

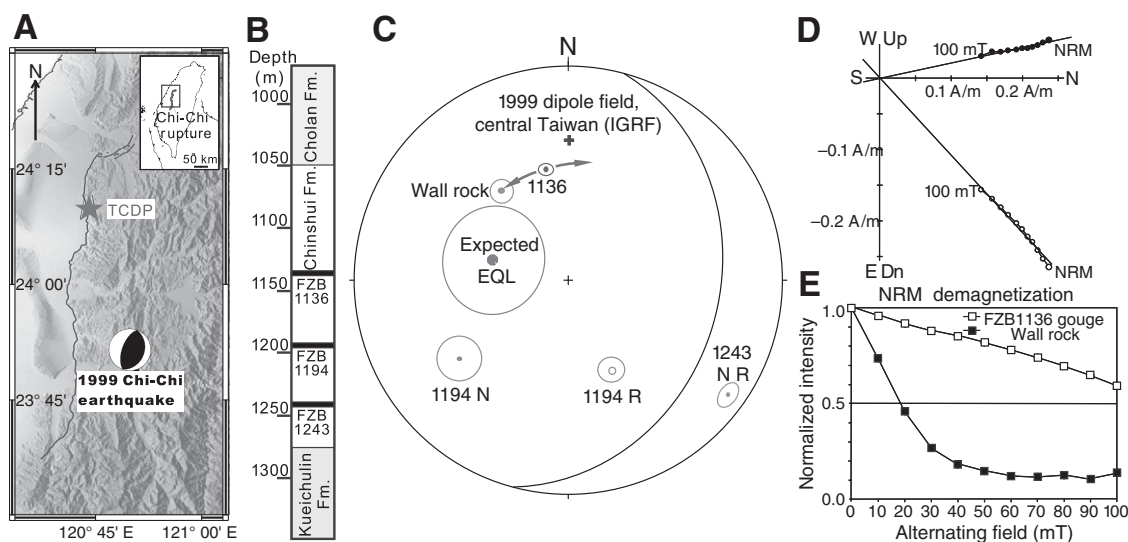
## METHODS

In 2008, U-channels (plastic boxes 2 cm × 2 cm, ~20 cm long) were used to contain core samples from the working half of TCDP hole B

within the gouge layers of the three fault zones, FZB1136 (1136.22–1136.43 m), FZB1194 (1194.67–1194.89 m), and FZB1243 (1243.33–1243.51 m). One U-channel sample was from the wall rock of the Pliocene siltstones of the Chinshui Formation (1133.55–1133.69 m). The U-channels were oriented geographically, with an error <20°, using the bedding orientation (dip 30° toward N105°E; Wu et al., 2008; Yeh et al., 2007). The natural remanent magnetization (NRM) of each U-channel was analyzed in the automated stepwise alternating-field demagnetization process (up to 100 mT) using a 755 SRM cryogenic magnetometer manufactured by 2G Enterprises. The residual field inside the shielded room was <500 nT. A principal component analysis was used to infer paleomagnetic components. The mean vector was averaged out using Fisher statistics (Fisher, 1953). The stable paleomagnetic components are characterized by declination (D), inclination (I), distribution parameter ( $\kappa$ ), and the angle of confidence at the 95% level ( $\alpha_{95}$ ). To obtain complementary information on the NRM, we performed thermal demagnetization of nonoriented core fragments (<5 mm). The S-ratio profile was measured along each U-channel. The S-ratio ( $\text{IRM}_{-0.3T}/\text{IRM}_{+1T}$ , where IRM is the isothermal remanent magnetization) is a proxy of magnetic coercivity (Thompson and Oldfield, 1986). It is measured at room temperature with a magnetic field applied first with 1 T, and second in the opposite direction with –0.3 T. In practice, an S-ratio close to 1 is an indication of magnetically soft minerals, such as magnetite. Its decrease points to the presence of magnetically hard minerals such as goethite and hematite. A transmission X-ray microscope image was obtained from a 15- $\mu\text{m}$ -thick gouge sample of FZB1136 using the Beamline 01B1 from the National Synchrotron Radiation Research Center (NSRRC) in Taiwan.

\*E-mails: srsong@ntu.edu.tw; charles.aubourg@univ-pau.fr; song@nsrrc.org.tw.

**Figure 1. A:** Geological map showing the epicenter of Chi-Chi earthquake ( $M_w$  7.6, 1999) and the Taiwan Chelungpu-fault Drilling Project (TCDP) drilling site at 120.73916° E, 24.20083° N (modified from Ma et al., 2006). **B:** Schematic log of bore-hole showing the three major fault zones of Chelungpu fault within the Chinshui Formation. FZB—fault zone of hole B. **C:** Equal-area stereoplot displaying the Chelungpu fault plane and the mean paleomagnetic components recorded in the three fault zones and wall rock. Due to the orientation of hole B, there is an error of  $\pm 20^\circ$  in declination for all paleomagnetic components. This error is indicated for the FZB1136 gouge component. We plot the orientation of an expected earthquake lightning (EQL) according to the model of Ferré et al. (2005) with  $20^\circ$  error in orientation. Solid symbols correspond to the downward hemisphere, open symbols to the upward hemisphere. Cross indicates the 1999 international geomagnetic reference field (IGRF) dipole magnetic vector ( $D = 0.2^\circ$ ,  $I = 29.7^\circ$ ). The wall rock's main component lies away from the modern magnetic field ( $D = 322^\circ$ ,  $I = 48^\circ$ ,  $\kappa = 99$ ,  $\alpha_{95} = 4^\circ$ ; range 10–80 mT). The FZB1136 gouge component ( $D = 348^\circ$ ,  $I = 48^\circ$ ,  $\kappa = 140$ ,  $\alpha_{95} = 2^\circ$ ) is closest to the modern magnetic field, and statistically different from a hypothetical EQL. Within the FZB1194 gouge, normal and reverse components are oriented southerly ( $D = 235^\circ$ ,  $I = 27^\circ$ ,  $\kappa = 110$ ,  $\alpha_{95} = 8^\circ$ , and  $D = 154^\circ$ ,  $I = -52^\circ$ ,  $\kappa = 144$ ,  $\alpha_{95} = 5^\circ$ , respectively). Within the FZB1243 gouge, normal and reverse components are also oriented southerly ( $D = 125^\circ$ ,  $I = 11^\circ$ ,  $\kappa = 189$ ,  $\alpha_{95} = 4^\circ$ , and  $D = 125^\circ$ ,  $I = -10.0^\circ$ ,  $\kappa = 280$ ,  $\alpha_{95} = 3^\circ$ , respectively). **D:** Natural remanent magnetization (NRM) orthogonal plot of FZB1136 gouge (depth 1136.33 m). Open circles represent projection of the vector along the vertical plane, solid circles along the horizontal plane. **E:** Curves of normalized NRM intensity of FZB1136 and wall rock.



Due to the orientation of hole B, there is an error of  $\pm 20^\circ$  in declination for all paleomagnetic components. This error is indicated for the FZB1136 gouge component. We plot the orientation of an expected earthquake lightning (EQL) according to the model of Ferré et al. (2005) with  $20^\circ$  error in orientation. Solid symbols correspond to the downward hemisphere, open symbols to the upward hemisphere. Cross indicates the 1999 international geomagnetic reference field (IGRF) dipole magnetic vector ( $D = 0.2^\circ$ ,  $I = 29.7^\circ$ ). The wall rock's main component lies away from the modern magnetic field ( $D = 322^\circ$ ,  $I = 48^\circ$ ,  $\kappa = 99$ ,  $\alpha_{95} = 4^\circ$ ; range 10–80 mT). The FZB1136 gouge component ( $D = 348^\circ$ ,  $I = 48^\circ$ ,  $\kappa = 140$ ,  $\alpha_{95} = 2^\circ$ ) is closest to the modern magnetic field, and statistically different from a hypothetical EQL. Within the FZB1194 gouge, normal and reverse components are oriented southerly ( $D = 235^\circ$ ,  $I = 27^\circ$ ,  $\kappa = 110$ ,  $\alpha_{95} = 8^\circ$ , and  $D = 154^\circ$ ,  $I = -52^\circ$ ,  $\kappa = 144$ ,  $\alpha_{95} = 5^\circ$ , respectively). Within the FZB1243 gouge, normal and reverse components are also oriented southerly ( $D = 125^\circ$ ,  $I = 11^\circ$ ,  $\kappa = 189$ ,  $\alpha_{95} = 4^\circ$ , and  $D = 125^\circ$ ,  $I = -10.0^\circ$ ,  $\kappa = 280$ ,  $\alpha_{95} = 3^\circ$ , respectively). **D:** Natural remanent magnetization (NRM) orthogonal plot of FZB1136 gouge (depth 1136.33 m). Open circles represent projection of the vector along the vertical plane, solid circles along the horizontal plane. **E:** Curves of normalized NRM intensity of FZB1136 and wall rock.

## RESULTS

Within the Chinshui Formation, the NRM carries multiple paleomagnetic components, with a main component of normal polarity (Fig. 1C). Its  $\sim 40^\circ$  counterclockwise deviation from the modern dipole implies that this component is not a modern record. In comparison to the wall rock, the analysis of the FZB1136 gouge reveals a stable and single characteristic remanent magnetization of normal polarity, throughout its 16-cm-thick layer (Fig. 1D). This component is close to the 1999 international geomagnetic reference field (IGRF) from central Taiwan (Fig. 1C). It resides essentially in hard coercive minerals because  $\sim 60\%$  of the NRM remains after 100 mT alternating-field demagnetization (Fig. 1E). The thermal demagnetization of core fragments reveals a linear decrease of NRM directed straight to the origin without evidence of secondary components. This is confirmed by the analysis of directional data (not shown). The analysis of the FZB1194 and FZB1243 gouges revealed multiple paleomagnetic components with both normal and reverse magnetic polarities (Fig. 1C). These components are oriented in a southern direction and away from the 1999 IGRF magnetic dipole field. After comparing the paleomagnetic results within the three fault zones and the wall rock, it is proposed that the single component observed throughout the FZB1136 gouge is the most recent magnetic

record, and more than likely contemporaneous with the 1999 Chi-Chi seismic event.

Information is provided on the magnetic carriers of the FZB1136 gouge using the unblocking temperature spectrum of NRM (Fig. 2A), transmission X-ray microscope observations (Fig. 2B), and the magnetic coercivity parameters (Fig. 2C). Within the gouge, the principal maximum unblocking temperature is close to  $120^\circ\text{C}$  (Fig. 2A) and is consistent with the Néel temperature of goethite ( $\alpha\text{-FeOOH}$ ,  $T_N = 120^\circ\text{C}$ ), a magnetically hard antiferromagnet (Hunt et al., 1995). Transmission X-ray microscopy reveals the occurrence of scattered, elongated ( $< 5\ \mu\text{m}$  long) and dense grains in the gouge, which are likely goethite (Fig. 2B). Within the Chi-Chi PSZ (1136.38 m; Boullier et al., 2009), the maximum unblocking temperature is close to  $580^\circ\text{C}$  (Fig. 2A), which is the Curie temperature of magnetite ( $\text{Fe}_3\text{O}_4$ ), a magnetically soft ferromagnet (Hunt et al., 1995). Thus, the single paleomagnetic component of Chi-Chi PSZ resides, essentially, in magnetite. The record of coercivity parameters (S-ratio) pinpoints the relative contribution of magnetite and goethite within the FZB1136 gouge (Fig. 2C). The S-ratio profile shows one relative minimum (magnetically hard) at 1136.30 m and one maximum (magnetically soft) within the Chi-Chi PSZ. The S-ratio profile is consistent with a larger distribution of goethite in the center of the gouge layer, and a larger distribu-

tion of magnetite in the Chi-Chi PSZ. It shows that the S-ratio profile is an index to identify the most recent PSZ in the Chi-Chi gouge.

## DISCUSSION AND CONCLUSIONS

From these observations, a model of the paleomagnetic record is proposed for FZB1136. We proffer three main types of magnetization that are acquired within the slip zones during an earthquake: (1) a thermoremanent magnetization (TRM) acquired post-seismically on the cooling of the slip zone (Ferré et al., 2005), (2) a chemical remanent magnetization (CRM) acquired post-seismically and carried by neoformed magnetic minerals (Nakamura et al., 2002), and (3) an isothermal remanent magnetization (IRM) acquired co-seismically during earthquake lightning (EQL) (Ferré et al., 2005). An EQL magnetization would be perpendicular to the fault plane (Ferré et al., 2005), which is not the case for the component of magnetization within the Chi-Chi gouge (Fig. 1C). Thus, we propose that EQL may be excluded as a magnetization process, and only thermal-related and chemical-related magnetic records are considered in the FZB1136 gouge. Because the magnetic carriers of the magnetic record are different, we have to distinguish scenarios in the Chi-Chi PSZ and in the rest of the gouge. A temperature elevation due to frictional heating is expected during a co-seismic slip (Rice, 2006). Frictional heating depends on the fault

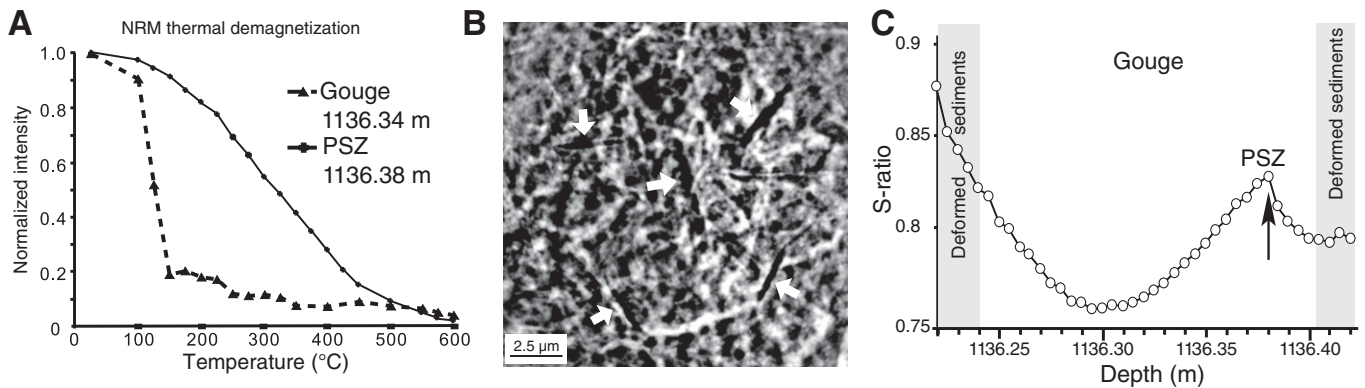


**Figure 2.** Natural remanent magnetization (NRM) thermal demagnetization, transmission X-ray microscope photo, and S-ratio. **A:** NRM thermal demagnetization for a gouge sample (depth of 1136.34 m) and the Chi-Chi principal slip zone (PSZ) (depth of 1136.38 m) within FZB1136. In the gouge, there is a break in slope near 150 °C where ~80% of the NRM is lost. The remaining part of the NRM has a maximum unblocking temperature close to 580 °C. In the Chi-Chi PSZ, the maximum unblocking temperature is close to 580 °C. **B:** Transmission X-ray microscope photo from a 15 μm thick polished section collected from a gouge within FZB1136. Scattered elongated dense minerals with a low aspect ratio of 2:25 and maximum length of 5 μm are likely to be goethite (arrows). **C:** S-ratio profile along the U-channel. The lowest value of the S-ratio (magnetically hard) is located at a depth of 1136.30 m, near the center of the gouge, and corresponds to the highest concentration in goethite. The Chi-Chi PSZ is marked by an enhancement of the S-ratio, which is consistent with a larger contribution of magnetite.

slip rate, displacement, friction coefficient, normal stress, and physical properties of the fault rocks. The ultimate phase of this process involves melting, with the formation of pseudotachylytes (Di Toro et al., 2006). The temperature peaks in the gouge and the Chi-Chi PSZ are still being debated, but generally, a lower limit of 400 °C is accepted (Boullier et al., 2009; Mishima et al., 2009). The PSZ cooling lasts only tens of seconds, and the thermal aureole extends less than the width of the PSZ (Kano et al., 2006). Upon cooling, a TRM is imprinted in the magnetic minerals contained in the PSZ and the baked contact. Within the 16 cm of gouge that carries the stable paleomagnetic component, only the millimeter-thick heated layers on both sides of the Chi-Chi PSZ have the potential to carry a friction-induced TRM. Experimental heating of the FZB1136 gouge showed that magnetite formed above 400 °C (Mishima et al., 2009). It is therefore proposed that the paleomagnetic record of the Chi-Chi PSZ and baked contact is partly a TRM carried by former magnetic minerals and partly a CRM carried by neoformed magnetite.

The paleomagnetic record in the 16 cm gouge is essentially carried by goethite, and other processes of magnetization should be viewed apart from the Chi-Chi PSZ and baked contact. To date, this is the first time that goethite has been reported in the Chelungpu fault. Nakamura and Nagahama (2001) observed similar, ~5 μm, goethite within the Nojima fault gouge (Japan). They suggested that the goethite growth postdates the grain alignment of silicate minerals. Within the FZB1136, scattered ~5 μm elongated goethite could be observed, which supports the theory that goethite growth postdates the broad texture of gouge (Fig. 2B).

In order to crystallize, goethite requires water, temperature <200 °C, and low pH and iron (Cornell and Schwertmann, 2003). Therefore, the goethite attests to the presence of water in FZB1136. Recent geochemical investigations in the FZB1136 gouge suggest the presence of pore fluids with a minimum temperature of 350 °C (Ishikawa et al., 2008). It is then possible that goethite formed upon the cooling of the pore fluids. The source of iron could possibly be brought about by the dissolution of iron sulfide in the FZB1136 gouge (Yeh et al., 2007). The dissolution of pyrite not only releases  $\text{Fe}^{2+}$  and  $\text{SO}_4^{2-}$  ions but also decreases the fluid's pH (Nakamura and Nagahama, 2001). It is therefore suggested that goethite is formed post-seismically within a few days of the earthquake's occurrence. Upon growing larger than the ~1800 nm<sup>3</sup> blocking volume (minimum volume for recording remanent magnetization; Cornell and Schwertmann, 2003), the goethite acquires a CRM. The recovery of a single-component record from within the FZB1136 gouge, unlike adjacent fault zones, implies the partial or complete removal of the magnetic records of ancient slip zones. It remains to be proven whether this behavior is related to earthquakes of large magnitudes (e.g.,  $M_w > 7$ ).

The post-seismic magnetic record is instantaneous in the geological time scale, but it has the potential to survive for millions or even billions of years (Néel, 1955). Thus, the fault gouge can retain the magnetic record during inter-seismic time. It is suggested that the fault gouge magnetic record is a record of the latest earthquake event if only a single component is recovered, as in the case of the Chi-Chi gouge. If several components are detected, as in the fault zones FZB1194 and FZB1243, it is pos-

sible that the components overlap each other due to perturbation.

Therefore, we propose the following scenario of a cycle of magnetic record during a large earthquake similar to Chi-Chi (Fig. 3).

1. During inter-seismic periods, the magnetic record of the latest large earthquake is preserved within the fault gouge.

2. During the co-seismic period, the gouge acts essentially as a magnetic eraser. Both the temperature elevation above the unblocking temperature of magnetic minerals and the chemical degradation of these minerals lead to the partial-to-complete demagnetization of the gouge. The exact mechanisms remain to be definitively determined, but in the Chi-Chi gouge, the >350 °C hot fluids (Ishikawa et al., 2008) have probably demagnetized the former goethite.

3. During the post-seismic period, the gouge acts as a magnetic recorder. The cooling of the gouge and/or fluids leads to a TRM imprint. Similarly, neoformed minerals resulting from any form of chemical process have the potential to carry a CRM. If confirmed by further studies, this proposed seismic cycle of magnetic records opens new horizons for paleoseismology as well as for PSZ identification and dating. To identify a PSZ, methods based on microscopy (Boullier et al., 2009), geochemistry (Hirono et al., 2008), or physical properties (Wu et al., 2007) are not one-to-one because several PSZs may stack together in the gouge.

In this study, the Chi-Chi gouge layer was identified using the orientation of the magnetic record; the location of the millimeter-thick Chi-Chi PSZ was pinpointed using rock magnetism characteristics. This constitutes a new, fast, and nondestructive way to find the most recent PSZ.



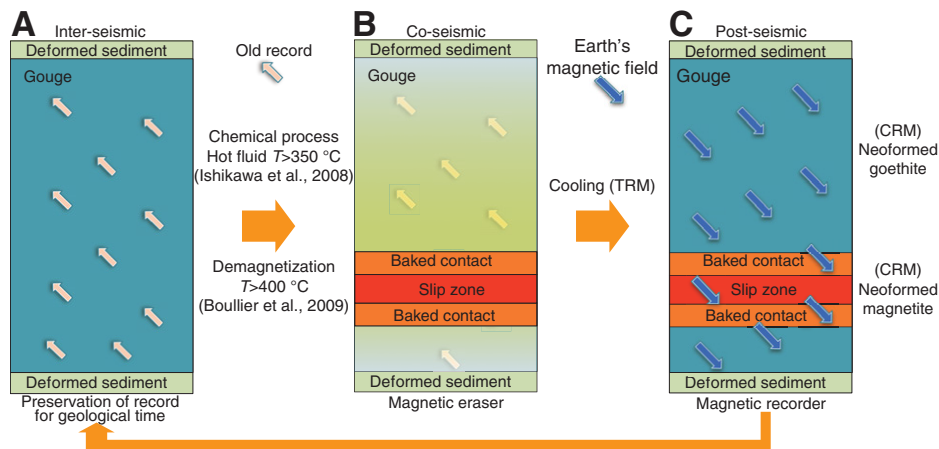


**Figure 3. Magnetic record cycle of a fault gouge.** **A:** During an inter-seismic period, the magnetic record of an old earthquake is preserved within the fault gouge through geological time. **B:** During a co-seismic period, the gouge acts as a magnetic eraser. At the principal slip zone and baked contact, the temperature elevation and chemical degradation lead to the partial-to-complete demagnetization of the gouge. The co-seismic hot fluids probably demagnetized the former goethite. **C:** During a post-seismic period, the gouge acts as a magnetic recorder. Cooling of the gouge or fluids leads to a thermoremanent magnetization (TRM) imprint. Neoformed minerals resulting from any form of chemical process, including cooling, carry a chemical remanent magnetization (CRM).

#### ACKNOWLEDGMENTS

We would like to express our gratitude to the working group of the Taiwan Chelungpu-fault Drilling Project. We thank G.-C. Yin of the National Synchrotron Radiation Research Center (NSRRC), Taiwan, for the maintenance of the transmission X-ray microscope, and Keng S. Liang of the NSRRC for his support in this project. We also thank C.-C. Chen (Academia Sinica) for his assistance when using a SQUID, and K.-C. Yeh (Academia Sinica) for helping to cut difficult gouge material into a U-channel. M.-K. Wang, T.-M. Tsao, P. Robion, C. David, L. Louis, and F. Humbert are acknowledged for their constructive criticisms. This paper benefited from constructive reviews by C. Wibberley, an anonymous reviewer, and B. Opdyke. Y.-M. Chou acknowledges the French Ministère des Affaires Étrangères for an EIFFEL doctoral grant.

#### REFERENCES CITED

- Boullier, A.-M., Yeh, E.-C., Boutareaud, S., Song, S.-R., and Tsai, C.-H., 2009, Microscale anatomy of the 1999 Chi-Chi earthquake fault zone: *Geochemistry, Geophysics, Geosystems*, v. 10, Q03016, doi:10.1029/2008GC002252.
- Cornell, R.M., and Schwertmann, U., 2003, *The iron oxides: Structure, properties, reactions, occurrences, and uses*: Weinheim, Germany, Wiley-VCH, 664 p.
- Di Toro, G., Hirose, T., Nielsen, S., Pennacchioni, G., and Shimamoto, T., 2006, Natural and experimental evidence of melt lubrication of faults during earthquakes: *Science*, v. 311, p. 647–649, doi:10.1126/science.1121012.
- Ferré, E.C., Zechmeister, M.S., Geissman, J.W., MathanaSekar, N., and Kocak, K., 2005, the Chelungpu fault: *Nature Geoscience*, v. 1, p. 679–683, doi:10.1038/ngeo308.
- Kano, Y., Mori, J., Fujio, R., Ito, H., Yanagidani, T., Nakao, S., and Ma, K.-F., 2006, Heat signature on the Chelungpu fault associated with the 1999 Chi-Chi, Taiwan earthquake: *Geophysical Research Letters*, v. 33, L14306, doi:10.1029/2006GL026733.
- Ma, K.-F., Tanaka, H., Song, S.-R., Wang, C.-Y., Hung, J.-H., Tsai, Y.-B., Mori, J., Song, Y.-F., Yeh, E.-C., Soh, W., Sone, H., Kuo, L.-W., and Wu, H.-Y., 2006, Slip zone and energetics of a large earthquake from the Taiwan Chelungpu-fault Drilling Project: *Nature*, v. 444, p. 473–476, doi:10.1038/nature05253.
- Mishima, T., Hirono, T., Nakamura, N., Tanikawa, W., Soh, W., and Song, S.-R., 2009, Changes to magnetic minerals caused by frictional heating during the 1999 Taiwan Chi-Chi earthquake: *Earth, Planets, and Space*, v. 61, p. 797–801.
- Nakamura, N., and Nagahama, H., 2001, Changes in magnetic and fractal properties of fractured granites near the Nojima Fault, Japan: *Island Arc*, v. 10, p. 486–494, doi:10.1111/j.1440-1738.2001.00347.x.
- Nakamura, N., Hirose, T., and Borradaile, G.J., 2002, Laboratory verification of submicron magnetite production in pseudotachylites: Relevance for paleointensity studies: *Earth and Planetary Science Letters*, v. 201, p. 13–18, doi:10.1016/S0012-821X(02)00704-5.
- Néel, L., 1955, Some theoretical aspects of rock magnetism: *Advances in Physics*, v. 4, p. 191–243, doi:10.1080/00018735500101204.
- Rice, J.R., 2006, Heating and weakening of faults during earthquake slip: *Journal of Geophysical Research*, v. 111, B05311, doi:10.1029/2005JB004006.
- Thompson, R., and Oldfield, F., 1986, *Environmental magnetism*: London, Allen and Unwin, 227 p.
- Wu, H.-Y., Ma, K.-F., Zoback, M., Boness, N., Ito, H., Hung, J.-H., and Hickman, S., 2007, Stress orientations of Taiwan Chelungpu-fault Drilling Project (TCDP) hole-A as observed from geophysical logs: *Geophysical Research Letters*, v. 34, L01303, doi:10.1029/2006GL028050.
- Wu, Y.-H., Yeh, E.-C., Dong, J.-J., Kuo, L.-W., Hsu, J.-Y., and Hung, J.-H., 2008, Core-log integration studies in hole-A of Taiwan Chelungpu-fault Drilling Project: *Geophysical Journal International*, v. 174, p. 949–965, doi:10.1111/j.1365-246X.2008.03841.x.
- Yeh, E.-C., Sone, H., Nakaya, T., Ian, K.-H., Song, S.-R., Hung, J.-H., Lin, W., Hirono, T., Wang, C.-Y., Ma, K.-F., Soh, W., and Kinoshita, M., 2007, Core description and characteristics of fault zones from Hole-A of the Taiwan Chelungpu-fault Drilling Project: *Terrestrial, Atmospheric and Oceanic Sciences*, v. 18, no. 2, p. 327–357, doi:10.3319/TAO.2007.18.2.327(TCDP).

Manuscript received 27 September 2011

Revised manuscript received 18 January 2012

Manuscript accepted 18 January 2012

Printed in USA



# Pyrite alteration and neoformed magnetic minerals in the fault zone of the Chi-Chi earthquake ( $M_w$ 7.6, 1999): Evidence for frictional heating and co-seismic fluids

**Yu-Min Chou**

*Department of Geosciences, National Taiwan University, 1 Roosevelt Road, Section 4, Taipei 106, Taiwan*

*Département Géosciences et Environnement, Université de Cergy-Pontoise, 5 mail Gay Lussac, Neuville sur Oise, FR-95031 Cergy-Pontoise CEDEX, France*

**Sheng-Rong Song**

*Department of Geosciences, National Taiwan University, 1 Roosevelt Road, Section 4, Taipei 106, Taiwan (srsong@ntu.edu.tw)*

*Associated International Laboratory, Active Deformation and Environment Programme for Taiwan, National Science Council, 106, Sec. 2, Heping East Road, Taipei 106, Taiwan*

**Charles Aubourg**

*Laboratoire des Fluides Complexes et Leurs Réservoirs, UMR5150, CNRS, TOTAL, Université de Pau, FR-64013 Pau CEDEX, France (charles.aubourg@univ-pau.fr)*

*Associated International Laboratory, Active Deformation and Environment Programme for Taiwan, National Science Council, 106, Sec. 2, Heping East Road, Taipei 106, Taiwan*

**Yen-Fang Song**

*National Synchrotron Radiation Research Center, 101 Hsin-Ann Road, Hsinchu Science Park, Hsinchu 30076, Taiwan (song@nsrrc.org.tw)*

**Anne-Marie Boullier**

*Associated International Laboratory, Active Deformation and Environment Programme for Taiwan, National Science Council, 106, Sec. 2, Heping East Road, Taipei 106, Taiwan*

*ISTerre, CNRS, Université Joseph Fourier, Maison des Géosciences, BP 53, FR-38041 Grenoble CEDEX 9, France*

**Teh-Quei Lee**

*Institute of Earth Sciences, Academia Sinica, 128, Section 2, Academia Road, Nankang, Taipei 115, Taiwan*

*Associated International Laboratory, Active Deformation and Environment Programme for Taiwan, National Science Council, 106, Sec. 2, Heping East Road, Taipei 106, Taiwan*

**Mark Evans**

*Department of Physics and Earth Science, Central Connecticut State University, New Britain, Connecticut 06050, USA*

## En-Chao Yeh

*Associated International Laboratory, Active Deformation and Environment Programme for Taiwan, National Science Council, 106, Sec. 2, Heping East Road, Taipei 106, Taiwan*

*Department of Earth Sciences, National Taiwan Normal University, Number 88, Section 4, Tingzhou Road, Wenshan District, Taipei 11677, Taiwan*

## Yi-Ming Chen

*National Synchrotron Radiation Research Center, 101 Hsin-Ann Road, Hsinchu Science Park, Hsinchu 30076, Taiwan*

[1] During an earthquake, physical and chemical transformations lead to alteration and formation of minerals in the gouge layer. Altered and neoformed minerals can be used as tracers of some earthquake processes. In this study, we investigate pyrite and magnetic minerals within the host Chinshui siltstone and the 16-cm-thick gouge. This gouge hosts the principal slip zone of Chi-Chi earthquake ( $M_w$  7.6, 1999). In the Chinshui siltstone, pyrite framboids of various sizes and euhedral pyrite are observed. The magnetic mineral assemblage comprises stoichiometric magnetite, greigite, and fine-grained pyrrhotite. The pyrite content is generally reduced in the gouge compared to the wall rock. The magnetic mineral assemblage in the gouge consists of goethite, pyrrhotite, and partially oxidized magnetite. The pyrrhotite, goethite and some magnetite are neoformed. Pyrrhotite likely formed from high temperature decomposition of pyrite ( $>500^\circ\text{C}$ ) generated during co-seismic slip of repeated earthquakes. Goethite is inferred to have formed from hot aqueous co-seismic fluid ( $>350^\circ\text{C}$ ) in association with the 1999 Chi-Chi event. Elevated fluid temperatures can also explain the partial alteration of magnetite and the retrograde alteration of some pyrrhotite to pyrite. We suggest that characterization of neoformed magnetic minerals can provide important information for studying earthquake slip zones in sediment-derived fault gouge.

**Components:** 9800 words, 8 figures, 1 table.

**Keywords:** Chi-Chi earthquake; TCDP; gouge; pyrite.

**Index Terms:** 3617 Mineralogy and Petrology: Alteration and weathering processes (1039); 8010 Structural Geology: Fractures and faults; 8163 Tectonophysics: Rheology and friction of fault zones (8034).

**Received** 23 February 2012; **Revised** 12 June 2012; **Accepted** 12 June 2012; **Published** 9 August 2012.

Chou, Y.-M., S.-R. Song, C. Aubourg, Y.-F. Song, A.-M. Boullier, T.-Q. Lee, M. Evans, E.-C. Yeh, and Y.-M. Chen (2012), Pyrite alteration and neoformed magnetic minerals in the fault zone of the Chi-Chi earthquake ( $M_w$  7.6, 1999): Evidence for frictional heating and co-seismic fluids, *Geochem. Geophys. Geosyst.*, 13, Q08002, doi:10.1029/2012GC004120.

## 1. Introduction

[2] High-friction fault slip zones formed during earthquakes or laboratory experiments have distinguishable textures and mineral characteristics [Nakamura *et al.*, 2002; Fukuchi *et al.*, 2005; Tanikawa *et al.*, 2007; Boullier *et al.*, 2009]. In principle, characterization of slip zones may be relevant for assessing physical processes such as frictional heating, thermal pressurization, fracture energy, redox conditions, etc. In siliciclastic sedimentary environments, faults can develop within siltstones. These detrital rocks typically contain accessory minerals like siderite, iron oxides, and iron sulfides. Among these accessory minerals, pyrite ( $\text{FeS}_2$ ) is worthy of study across slip zones

for several reasons: 1) it is common within fine-grained sediments with a concentration of about 1% [Berner, 1984]; 2) it is easy to identify using optical microscopy or electron microscopy; 3) it generally has a euhedral morphology with well-calibrated size distributions [Craig *et al.*, 1998]; 4) pyrite crystals often cluster in so-called framboids that are as large as tens of microns across [Craig *et al.*, 1998]; 5) it alters rapidly with temperature and in the presence of certain fluids; and releases  $\text{SO}_4^{2-}$  and  $\text{Fe}^{2+}$  [Jovanović, 1989; Music *et al.*, 1992; Lambert *et al.*, 1998; Pelovski and Petkova, 1999; Mayoral *et al.*, 2002]; 6) pyrite alteration lowers pH, which can result in dissolution of carbonate minerals that can then reprecipitate in the gouge [Liu and Liu, 2004].



[3] In fault zones, magnetic minerals are of interest because magnetic susceptibility anomalies have been reported in gouge and pseudotachylites [Nakamura *et al.*, 2002; Mishima *et al.*, 2009; Tanikawa *et al.*, 2007; Ferré *et al.*, 2012]. Similarly, Nakamura *et al.* [2002] and Ferré *et al.* [2005] suggested that magnetic minerals form during frictional melting associated with fault displacement during earthquakes. Generally, magnetic minerals are difficult to observe using optical or electron microscopy because of their low concentration (<0.1%) and small grain size (<1  $\mu\text{m}$ ). However, it is relatively easy to determine the nature, size and concentration of magnetic minerals using rock magnetic methods [e.g., Hunt *et al.*, 1995]. Comparison between the magnetic mineral assemblage of wall rocks and fault gouge can help to determine the nature of neoformed magnetic minerals.

[4] During the Chi-Chi earthquake ( $M_w$  7.6, 1999), a large  $\sim 80$  km rupture occurred along the Chelungpu thrust [Ma *et al.*, 1999]. The Chelungpu thrust propagates through the siliciclastic early Pliocene Chinshui Formation where pyrite framboids are initially present in the undeformed sediment [Boullier *et al.*, 2009]. However, Hirono *et al.* [2008] reported a lack of pyrite in the gouge zone. Similarly, Hirono *et al.* [2007b] and Ishikawa *et al.* [2008] observed an abundance of  $\text{SO}_4^{2-}$  in the gouge zone and related it to pyrite dissolution. The gouge zone is also marked by a magnetic susceptibility peak due to the contribution of neoformed ferrimagnetic minerals [Mishima *et al.*, 2009]. There is, therefore, an apparent correlation between the lack of pyrite and neoformed magnetic minerals that we would like to elucidate. Using unaltered samples from the Taiwan Chelungpu-fault Drilling Project (TCDP) Hole B borehole [Hirono *et al.*, 2007a; Song *et al.*, 2007a; Yeh *et al.*, 2007], we determined how pyrite alter with the gouge and established the magnetic mineralogy of the Chinshui Formation and the gouge that hosts the 1999 Chi-Chi principal slip zone. The peak temperature reached in the gouge during the Chi-Chi earthquake is still debated; however, we show that identification of neoformed magnetic minerals provides additional evidence to estimate peak temperature and the presence of co-seismic fluids.

## 2. Geologic Setting

[5] In Taiwan, one of the largest inland earthquakes ( $M_w = 7.6$ ) took place on 21 September 1999, near the town of Chi-Chi (hypocenter 120.81°E, 23.86°N, depth  $\sim 10$  km [Ma *et al.*, 1999; Kao and Chen,

2000], which caused large-scale casualties (2,321 deaths, 10,000 injured) and destruction (more than 100,000 buildings were damaged or destroyed). During the 1999 Chi-Chi earthquake, the surface rupture closely followed the  $\sim 80$  km Chelungpu fault, which is one of the most active faults in western Taiwan [Chen *et al.*, 2002]. The Chelungpu fault system is an out-of-sequence thrust (Figure 1a), which is part of the ramp of a  $\sim 20$  km fault-bend-fold that is now largely eroded [Yue *et al.*, 2005; Yeh *et al.*, 2007]. The TCDP was designed to drill two cores in DaKeng, central Taiwan (Figures 1a and 1b) [Yeh *et al.*, 2007]. Hole A (depth 2,003 m) and Hole B (depth 1,352.6 m) are separated by 40 m. At the location of the two boreholes, the estimated slip during the 1999 Chi-Chi earthquake is  $\sim 8$  m [Ma *et al.*, 2003]. Three major fault zones were identified within the Chinshui Formation [Hirono *et al.*, 2007a]. From independent data sets, different authors proposed that the fault zone at 1,111 m depth and 1,136 m depth for Hole A and B, respectively, contains the principal slip zone (PSZ) of the Chi-Chi earthquake [Kano *et al.*, 2006; Ma *et al.*, 2006; Song *et al.*, 2007a; Wu *et al.*, 2007; Chou *et al.*, 2012]. Boullier *et al.* [2009] determined the location of the Chi-Chi PSZ by identifying a  $\sim 2$  cm (Hole A) to 3 mm (Hole B) thick gouge layer. The PSZ differs from other ancient slip zones in that it has not been affected by any later compaction or deformation (veins, fractures, or shear zones). The PSZ at 1,136 m does not show evidence of melting [Boullier *et al.*, 2009].

[6] The lower Pliocene Chinshui Formation (also called the Chinshui Shale) consists of alternating siltstones and  $\sim 10$ -cm-thick sandstones. Minerals in the siltstones are quartz, clays, and accessory minerals (feldspar, calcite) [Isaacs *et al.*, 2007]. Clay minerals consist of an assemblage of illite, chlorite, and kaolinite with accessory smectite [Kuo *et al.*, 2009]. Organic matter is present at a concentration of  $\sim 1\%$  in the sediments, but its quantity is less than 0.7% in the fault zone [Ikehara *et al.*, 2007]. Iron sulfides are common in the undeformed and deformed sediments [Boullier *et al.*, 2009]. The Chinshui siltstones are unmetamorphosed with a recorded peak temperature due to modest burial of  $\sim 120^\circ\text{C}$  based on vitrinite reflectance [Sakaguchi *et al.*, 2007].

## 3. Sampling and Methods

[7] For this study, we sampled the Chinshui Formation in TCDP Hole B across the  $\sim 20$ -cm-thick

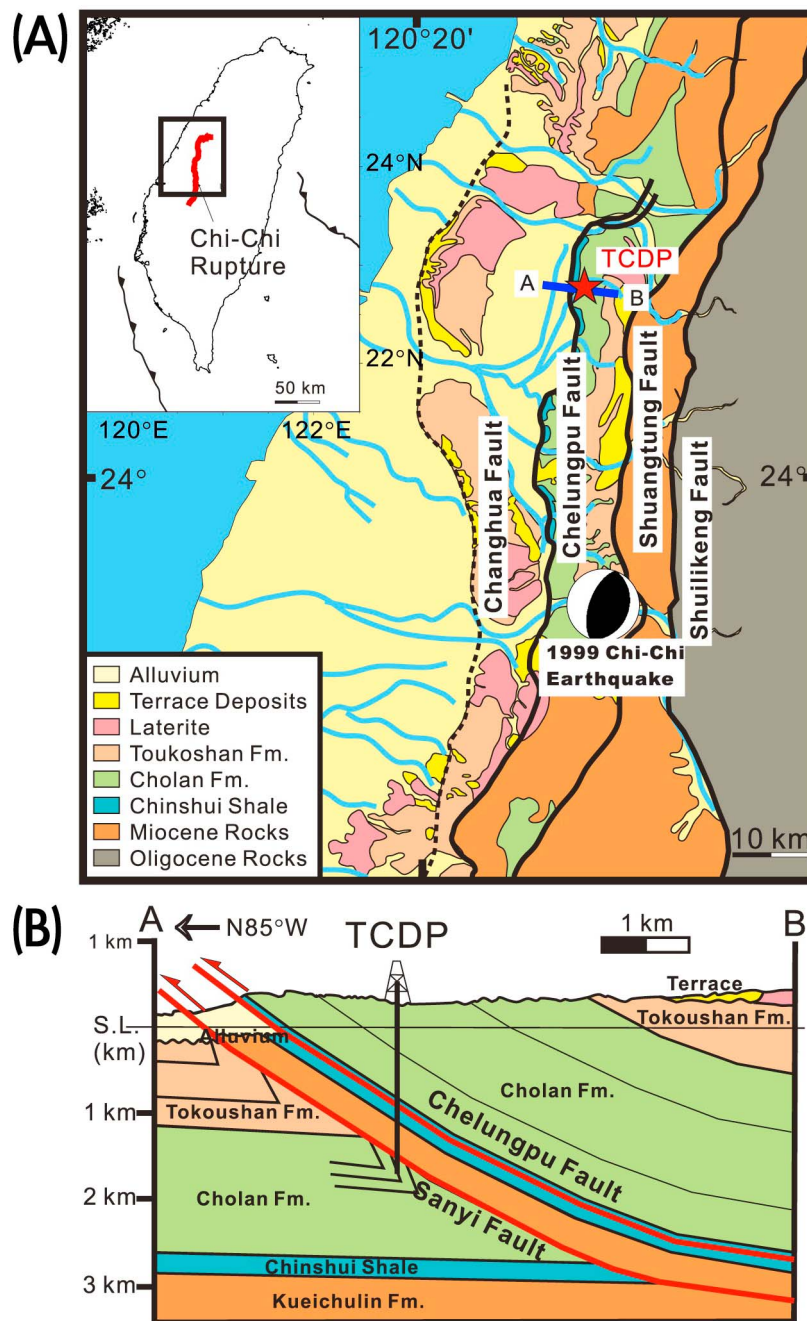


**Figure 1.** Geological setting of the TCDP borehole (modified from Yeh *et al.* [2007]). (a) Schematic geological map of western Taiwan with the location of the TCDP site (red star, 120.73916°E, 24.20083°N) on the northern part of the Chelungpu fault. The focal mechanism of the Chi-Chi main shock is located at the hypocenter of the 1999 Chi-Chi earthquake (128.81°E, 23.86°N). (b) Geological cross-section through the TCDP site. The Chelungpu fault is located within the Chinshui Formation.

fault zone (from 1,136.22 m to 1,136.43 m) together with wall rocks at different depths (Figures 2a and 2b; samples are listed in Table 1). In addition, we analyzed ten (2.5 cm × 2 cm) polished thin sections that were cut perpendicular to bedding within the fault plane (samples 1 to 10,

Figure 2c) that were thoroughly described by Boullier *et al.* [2009]. These sections contain the boundaries between the gouge, the hanging wall, and the footwall deformed sediments. The deformed sediments were initially labeled ‘gray gouge’ principally because of their color [Hirono

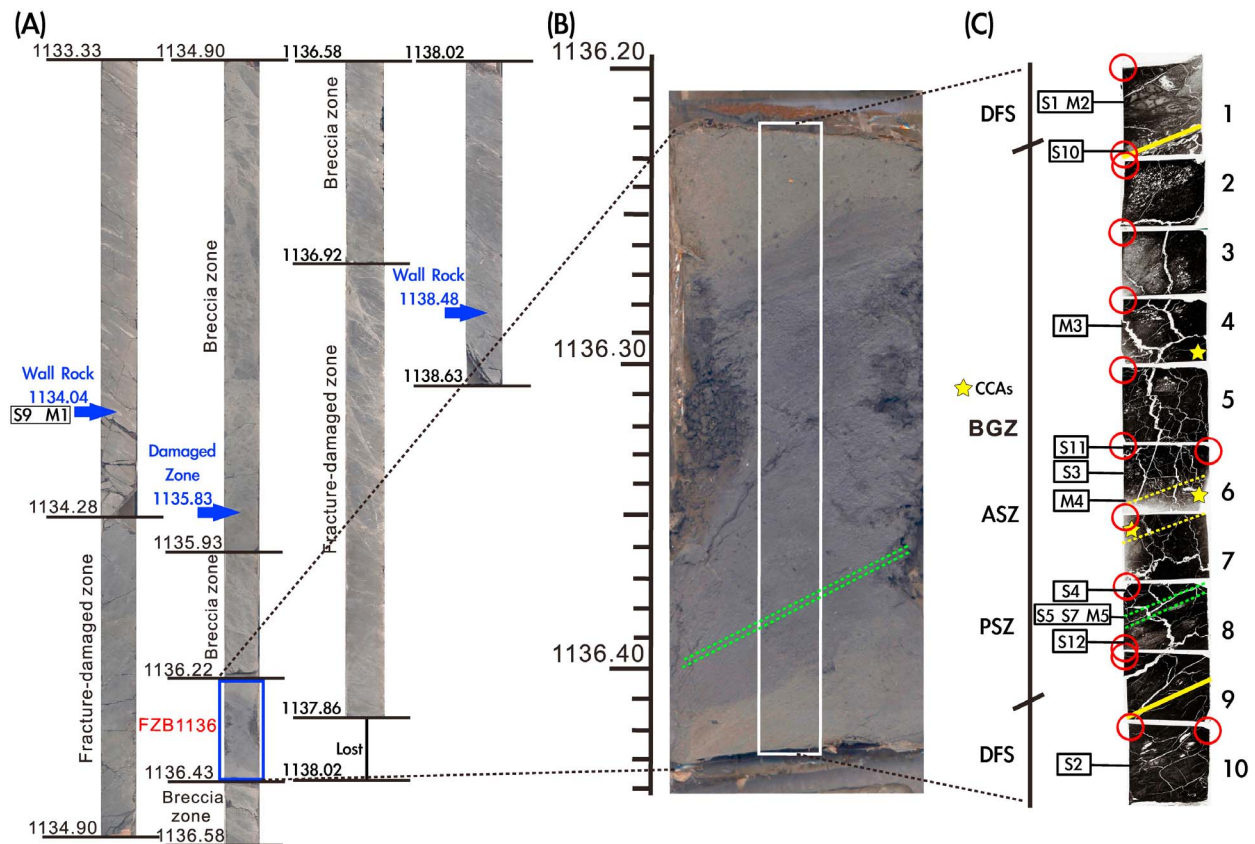


**Figure 2.** Images of the cores and samples from TCDP Hole B. (a) Half-core image for the depth interval from 1,133.33 to 1,138.63 m. The blue arrows and frame indicate the sample locations. (b) Half-core image of the FZB1136 fault zone at a depth of 1,136.22~1,136.43 m; the white frame corresponds to the locations of polished sections. The green dashed line frames the Chi-Chi principal slip zone (PSZ) [Boullier *et al.*, 2009]. (c) Collage of SEM images from the polished sections. Red circles indicate sample positions for TXM analysis. The yellow lines are the boundaries between deformed sediments (DFS) and the gouge zone (BGZ). The yellow stars indicate clay-clast aggregates (CCAs [see Boullier *et al.*, 2009]). The double yellow dashed line is an ancient slip zone (ASZ) and the double green dashed line is the Chi-Chi PSZ [after Boullier *et al.*, 2009].

*et al.*, 2007a]. However, within the ‘gray gouge’, bedding is preserved and thus the ‘gray gouge’ cannot be genetically related to gouge formation. To avoid confusion, we abandon the name ‘gray gouge’ in favor of ‘deformed sediments’ and we call gouge the ‘black gouge’ horizon. The ~16-cm-thick gouge, which is surrounded by deformed sediments, constitutes a horizon of gouges where the bedding or other sedimentary structures are no longer preserved. Some gouges are reworked and are interpreted as ancient slip zones [Boullier *et al.*, 2009]. A 3-mm-thick level of gouge in thin section 8 (Figure 2c) is not reworked and consists of alternating clay-rich and clast-rich layers. Boullier *et al.* [2009] proposed that this slip zone was generated during the 1999 Chi-Chi event. Hereafter, it is referred to as the PSZ. From the 10 thin sections, we made scanning electron microscope (SEM)

observations coupled with energy dispersive spectrometry (EDS) measurements and reflected-light polarizing microscope observations. We also made transmission X-ray microscopy (TXM) observations on 17 polished thick sections from the working section of TCDP Hole B core (Table 1). From these polished thick sections, we cut a few millimeter-long pieces and impregnated them with resin. Then, we cut each section into ~15- $\mu$ m-thick samples for TXM observation. We obtained fourteen 15- $\mu$ m-thick samples from the fault zone, and three from the two parts of the hanging wall and footwall deformed sediments (Figure 2a and Table 1). For magnetic property measurements, we sampled hundreds of milligrams of rock powder within the ~20-cm-thick fault zone, including deformed sediments and gouge.



**Table 1.** Sample Depths and Measurements Made in This Study<sup>a</sup>

| Depth (m) | Location          | Number   | Measurements              |
|-----------|-------------------|----------|---------------------------|
| 1134.04   | hanging wall rock | S9 M1    | MPMS, FORC, TXM           |
| 1135.83   | damaged zone      |          | TXM, RFM                  |
| 1136.22   | deformed sediment | S1 M2    | TXM, RFM, SEM, MPMS, FORC |
| 1136.25   | black gouge       | S10      | TXM, RFM, SEM             |
| 1136.27   | black gouge       |          | TXM, RFM                  |
| 1136.29   | black gouge       | M3       | TXM, RFM, SEM, MPMS, FORC |
| 1136.31   | black gouge       |          | TXM, RFM                  |
| 1136.33   | black gouge       | S3 S11   | TXM, RFM, SEM             |
| 1136.35   | ASZ               | M4       | TXM, RFM, SEM, MPMS, FORC |
| 1136.37   | black gouge       | S4       | TXM, RFM, SEM             |
| 1136.38   | PSZ               | S5 S7 M5 | TXM, SEM, RFM, MPMS, FORC |
| 1136.39   | black gouge       | S12      | TXM, RFM, SEM             |
| 1136.41   | deformed sediment |          | TXM, RFM, SEM             |
| 1138.48   | footwall rock     | S2       | TXM                       |

<sup>a</sup>FORC: First-order reversal curve, MPMS: Magnetic property measurement system, RFM: Reflected-light microscope, SEM: Scanning electron microscope, TXM: Transmission X-ray microscope.

[8] We used a LEO Stereoscan 440 SEM equipped with EDS (Analyzer EDX KEVEX SYGMA) for elemental analysis. The SEM was operated at 15 keV with 4 nA current. For TXM observation, we used the BL01B Beamline with 60 nm tomographic resolution at the National Synchrotron Radiation Research Center (NSRRC), Taiwan [Yin *et al.*, 2006; Song *et al.*, 2007b]. A superconducting wavelength shifter source provides a measured photon flux of  $4.5 \times 10^{11}$  photons/s/0.1% bw in the energy range 5–20 keV. X-rays generated by a wavelength shifter are primarily focused at a charge-coupled detector by a toroidal focusing mirror with a focal ratio of nearly 1:1. A double crystal monochromator that exploits a pair of Ge (111) crystals selects X-rays of energy 8–11 keV. After the focusing mirror and double crystal monochromator, a capillary condenser further shapes the X-ray beam. The condenser intercepts the impinging X-rays and further focuses them onto the sample. The image of the sample is magnified with a zone plate. The field of view of the image is  $15 \times 15 \mu\text{m}^2$  for the first-order diffraction mode of the zone plate. The phase term can be retrieved by the Zernike's phase contrast method for imaging light materials. The phase ring positioned at the back focal plane of the zone plate results in a recording of the phase contrast images at the detector. By acquiring a series of two-dimensional

(2-D) images with the sample rotated stepwise, three-dimensional (3-D) tomography data sets are reconstructed from 141 images from  $-70^\circ$  to  $+70^\circ$ . We scanned each sample over an area of  $2700 \mu\text{m}^2$ .

[9] We also conducted a non-destructive magnetic investigation at room temperature (300 K) and at low temperature (10 to 300 K) to characterize the magnetic mineral assemblage in the deformed sediments and gouge in the Chi-Chi fault zone. In a first set of experiments, we measured the low-temperature dependency of a saturation isothermal remanent magnetization (SIRM) using a Quantum Designs Magnetic Property Measurement System (MPMS) XL5 EverCool system at the Institute de Physique du Globe de Paris (IPGP), France. To impart an SIRM, a magnetic field of 2.5 T was applied, either at room temperature (RT-SIRM at 300 K) or at low temperature (LT-SIRM at 10 K). We monitored successively the cooling and the warming demagnetization curves of the RT-SIRM and the LT-SIRM. We refer to warming curves of LT-SIRM as ZFC (zero field cooled). During cooling of the RT-SIRM, a positive magnetic field of  $5 \mu\text{T}$  ( $\sim 1/10$  of the Earth's magnetic field) was applied to enable detection of a potential Néel transition. For samples M3, M4, and M5 (Table 1), we cycled the RT-SIRM during cooling and warming (cycling RT-SIRM). For this procedure, we removed the  $5 \mu\text{T}$  magnetic field, and the residual magnetic field in the MPMS was  $<0.1 \mu\text{T}$ . We measured  $\sim 400$  mg of rock powder sealed in a gel-cap. In a second set of experiments, we measured first-order reversal curves (FORCs) [Pike *et al.*, 1999; Roberts *et al.*, 2000] using a Princeton Measurement Corporation vibrating sample magnetometer located at the Institute for Rock Magnetism (Minneapolis, USA). We measured FORCs using an averaging time of 0.5 s and processed the data using the FORCinel software [Harrison and Feinberg, 2008].

## 4. Results

### 4.1. Reflected-Light Polarizing Microscopy

[10] Inspection of thin sections using reflected-light polarizing microscopy indicates the presence of numerous framboids in the undeformed and deformed sediments. Complete extinction is observed for most of the framboids under polarized reflected-light, which suggests that they are isotropic minerals. The number of framboids decreases considerably from the deformed sediments to the gouge, where only a few reflective minerals ( $<25 \mu\text{m}$ ) are observed. We

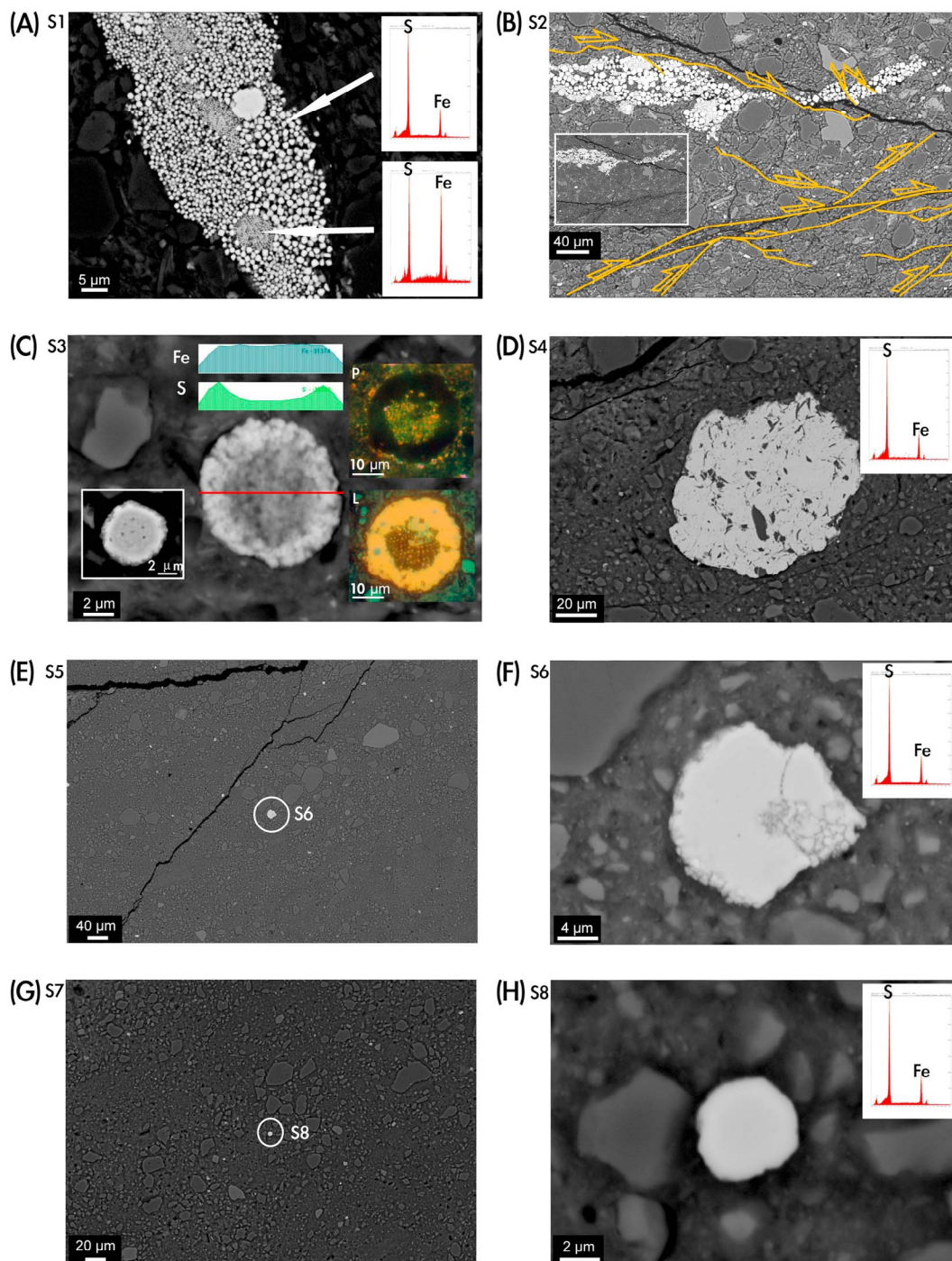


**Figure 3.** Backscattered SEM images with EDS results. (a) Large iron sulfide aggregates that contain framboidal pyrite ( $\text{FeS}_2$ ) within the deformed sediments (S1 in Figure 2c). Some parts of the aggregate are greigite ( $\text{Fe}_3\text{S}_4$ ). (b) Large iron sulfide aggregates that contain framboidal pyrite with micro-fractures and shears in the deformed sediments (S2 in Figure 2c). (c) Pyrite grain in the gouge (S3 in Figure 2c). The framboidal  $\text{FeS}$  core (pyrrhotite, which is a replacement of a framboidal pyrite) has an  $\text{FeS}_2$  rim. The photos on the right were obtained using reflected-light microscopy (P: polarized reflected; L: light reflected); pyrite is dark and pyrrhotite is light under polarized light. (d) Large cluster of pyrite grains mixed with quartz (S4 in Figure 2c). (e) Small pyrite grains (bright backscattered grains, smaller than  $5\ \mu\text{m}$ , one is  $\sim 20\ \mu\text{m}$ ) and quartz grains within the Chi-Chi PSZ (S8 in Figure 2c). (f) Detail of Figure 3e: fractured pyrite grain within the PSZ (S8 in Figure 2c). (g) Image of the Chi-Chi PSZ (S8 in Figure 2c). (h) Pyrite grain ( $3\ \mu\text{m}$ ) within the Chi-Chi PSZ (S8 in Figure 2c).



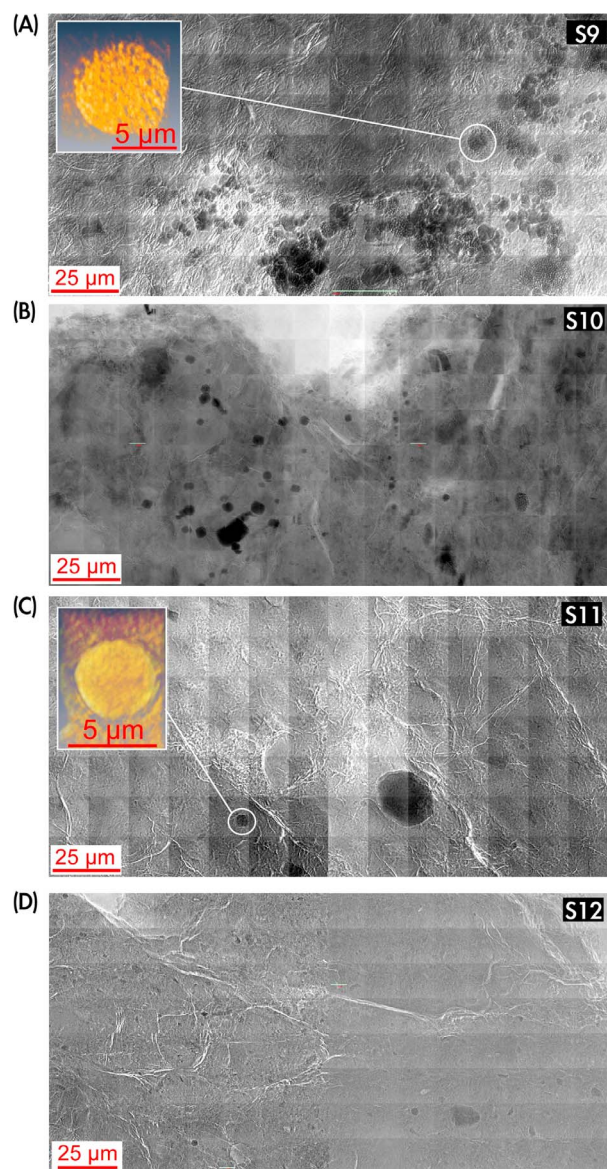


**Figure 4.** 2-D and 3-D images acquired for TXM observations. (a) Sediment at a depth of 1,134.04 m in TCDP hole B (M1 in Figure 2a). (b) Deformed sediment at a depth of 1,136.25 m (S10 in Figure 2c). (c) Gouge at a depth of 1,136.33 m (S11 in Figure 2c). (d) Gouge close to the PSZ at a depth of 1,136.38 m (S12 in Figure 2c).

did not observe magnetic minerals such as magnetite at the  $>1 \mu\text{m}$  scale.

## 4.2. SEM Observations

[11] In the deformed sediments close to the gouge, as well as in sediments from the hanging wall and footwall, numerous large iron sulfide aggregates include framboids of various sizes ( $1\text{--}5 \mu\text{m}$ )

(Figure 3a). EDS analysis reveals that euhedral crystals within the framboids consist of pyrite ( $\text{FeS}_2$ ). The size of pyrite crystals ( $\sim 1 \mu\text{m}$ ) is homogenous within framboids (Figure 3a). Isolated euhedral pyrite grains, with variable sizes, are also observed. Small framboids ( $\sim 5 \mu\text{m}$ ) consist of aggregates of  $\sim 100 \text{ nm}$  iron monosulfide grains ( $\text{FeS}$ ) (Figure 3a).  $\text{FeS}$  framboids are commonly observed from similar sediments in Taiwan and elsewhere and are interpreted as greigite ( $\text{Fe}_3\text{S}_4$ ) framboids [Jiang *et al.*, 2001; Roberts and Weaver, 2005; Rowan and Roberts, 2006]. In deformed sediments close to the gouge, some iron sulfide aggregates have been dismembered by shearing (Figure 3b). From the pattern of shear planes, we identified a sense of shear that is consistent with the thrust orientation on the Chelungpu fault (Figure 3b).

[12] In the gouge (thin sections 2 to 9), we observed framboids of two types. Some framboids, with diameter of 5 to  $\sim 25 \mu\text{m}$ , have a  $\text{FeS}$  core surrounded by a  $1\text{--}10 \mu\text{m}$   $\text{FeS}_2$  rim (Figure 3c). Under reflected-light microscopy, the core remains bright and the rim is black (Figure 3c, inset). This observation suggests that the  $\text{FeS}$  core is not cubic, which excludes the possibility that it is greigite. The second type of framboid is observed 1 mm from the PSZ (thin section 8). It consists of  $\sim 100 \mu\text{m}$  clusters of irregular-shaped pyrite crystals (Figure 3d). This resembles intensely deformed overgrown sedimentary sulfides. Within the 1999 Chi-Chi PSZ (thin section 8), we never observed framboids. Instead, small overgrown sulfide aggregates ( $<25 \mu\text{m}$ ) are identified (Figure 3h). We also observed fine ( $<3 \mu\text{m}$ ) pyrite grains scattered within the quartz and clay matrix (Figures 3g and 3h).

## 4.3. Transmission X-Ray Microscopy

[13] TXM provides three-dimensional (3-D) images of framboids that complement our two-dimensional (2-D) SEM and reflected-light microscopy observations. Within hanging wall (at a depth of 1,133.04 m) sediments, footwall (1,138.48 m) sediments, and deformed sediments (1,135.83 m) (Figure 2a), framboids are common (Figure 4a). Framboids are generally grouped in high concentrations in some parts of siltstones. This is probably a result of remineralization of large pieces of organic matter during early diagenesis [Roberts and Weaver, 2005]. Typically, the diameter of the framboids is larger than  $10 \mu\text{m}$ , and the grain size of each pyrite crystal within the framboids is close to  $1 \mu\text{m}$ .

[14] At a depth of 1,136.24 m in the borehole (thin section 2), a ~1-cm-thick layer of foliated gouge was identified by *Boullier et al.* [2009] (Figure 2c). There, TXM observations reveal the occurrence of numerous framboids together with dense spherical or cubic minerals (Figure 4b). The framboids are not aggregates and are scattered throughout the gouge. Within the gouge and near the 1999 Chi-Chi PSZ (Figures 4c and 4d), framboidal clusters are not observed. Instead, we observed 5 to 25  $\mu\text{m}$  individual spherical-like mineral aggregates (Figure 4c) that probably correspond to the pyrite that we described in the gouge using SEM (Figures 3c and 3d).

#### 4.4. Magnetic Properties

[15] Magnetic properties are comparable for the undeformed sediments (sample M1) and deformed sediments (sample M2) (Figures 5a and 5b). A Verwey transition at 120 K is detected in RT-SIRM demagnetization curves (see derivatives in insets in Figure 5) and in ZFC demagnetization curves. The Verwey transition indicates the occurrence of stoichiometric magnetite [*Özdemir and Dunlop, 1999*]. An additional magnetic transition is detected near 35 K for both ZFC and RT-SIRM demagnetization curves. This ~35 K transition is marked by a drop of one to two orders of magnitude of the LT-SIRM. The ~35 K transition is less evident in RT-SIRM demagnetization curves, with a break in slope at about 80 K followed by an enhancement of remanence (Figures 5a and 5b; see derivative). This behavior is similar to the P-behavior described by *Aubourg and Pozzi* [2010] and *Kars et al.* [2011]. The nature of P-behavior will be discussed later. We calculated the maximum concentration of magnetite by assuming that only magnetite contributes to the RT-SIRM at room temperature (300 K). The RT-SIRM at 300 K is less than  $10^{-3} \text{ Am}^2/\text{kg}$  for the different sediments that we measured. Taking the SIRM of magnetite as  $\sim 10 \text{ Am}^2/\text{kg}$  [*Maher et al., 1999*], we infer a maximum concentration of magnetite of 100 ppmv (concentration in parts per million by volume =  $1 \times 10^6 \times \text{RT-SIRM} / \text{SIRM}_{\text{magnetite}}$ ). FORC diagrams are noisy due to the small concentration of ferrimagnetic grains with respect to the paramagnetic contribution (Figures 5f and 5g), so high values of the smoothing factor (SF) were needed. The FORC diagrams are consistent with a distribution of weakly interacting single domain to superparamagnetic (SP) particles [e.g., *Pike et al., 2001*; *Rowan and Roberts, 2006*].

[16] Gouge samples M3–M5 (Table 1) have different magnetic properties (Figures 5c–5e). From

300 K to 150 K, there is a regular increase of up to ~10% of the RT-SIRM. This increase is diagnostic of goethite ( $\alpha\text{-FeOOH}$ ) [*Dekkers, 1989*; *Maher et al., 1999*; *Liu et al., 2006*]. To check for the presence of goethite, we imparted a RT-SIRM at 300 K, and warmed it up to 400 K (Figure 6), which is close to Néel temperature of goethite (120°C [e.g., *Özdemir and Dunlop, 1996*]). About ~50% of the RT-SIRM is then lost at 400 K, which indicates that goethite contributes a large part of the artificial remanence. In the host sediments, by comparison, the increase of RT-SIRM from 300 K to 150 K is limited to 1 to 2% and the drop from 300 K to 400 K is less than 25%. In the gouge, the Verwey transition is much less pronounced and is observed only during cooling of the RT-SIRM (Figures 5d and 5e). The most notable difference is observed near 35 K. The ZFC curves do not undergo the one to two order magnitude remanence decrease at 35 K that is observed in host rock sediments. In addition, there is no P-behavior during cooling of the RT-SIRM. Instead, a ~35 K transition is characterized by a remanence drop despite application of a +5  $\mu\text{T}$  magnetic field in the MPMS. This transition is similar to the magnetic transition for  $>1 \mu\text{m}$  pyrrhotite [*Dekkers et al., 1989*; *Rochette et al., 1990*]. According to *Dekkers et al.* [1989], the degree of reversibility of this transition is an indication of grain size. When cycling the RT-SIRM for sample M5 (Figure 7), we observed a reversible magnetic transition at 35 K, which indicates that pyrrhotite is fine-grained and close to 1  $\mu\text{m}$  in size ( $h/c$  ratio 0.96). We calculated the maximum concentrations of goethite, pyrrhotite, and magnetite in the studied samples. At room temperature, the RT-SIRM is  $<10^{-2} \text{ Am}^2/\text{kg}$  for the different measured gouges. We assume that the contribution of goethite is about half of this value. Taking the SIRM of goethite as  $0.05 \text{ Am}^2/\text{kg}$  [*Maher et al., 1999*], we obtain a maximum concentration of several percent goethite ( $\text{RT-SIRM} / \text{SIRM}_{\text{goethite}}$ ). Assuming that the other half of the remanence is carried by pyrrhotite or magnetite, and assuming the SIRM of pyrrhotite as  $\sim 4.5 \text{ Am}^2/\text{kg}$  and of magnetite as  $\sim 10 \text{ Am}^2/\text{kg}$  [*Maher et al., 1999*], we obtain a maximum concentration of pyrrhotite of less than 0.1% (concentration% =  $100 \times \text{RT-SIRM} / 2\text{SIRM}_{\text{pyrrhotite}}$ ) and a maximum concentration of magnetite of less than 500 ppmv (concentration ppmv =  $1 \times 10^6 \times \text{RT-SIRM} / 2\text{SIRM}_{\text{magnetite}}$ ). This suggests that there is an enhanced concentration of ferrimagnetic minerals in the gouge. FORC diagrams for gouge (M3) and PSZ (M5) have a significant high-coercivity contribution (Figures 5h and 5i). A coercivity peak at



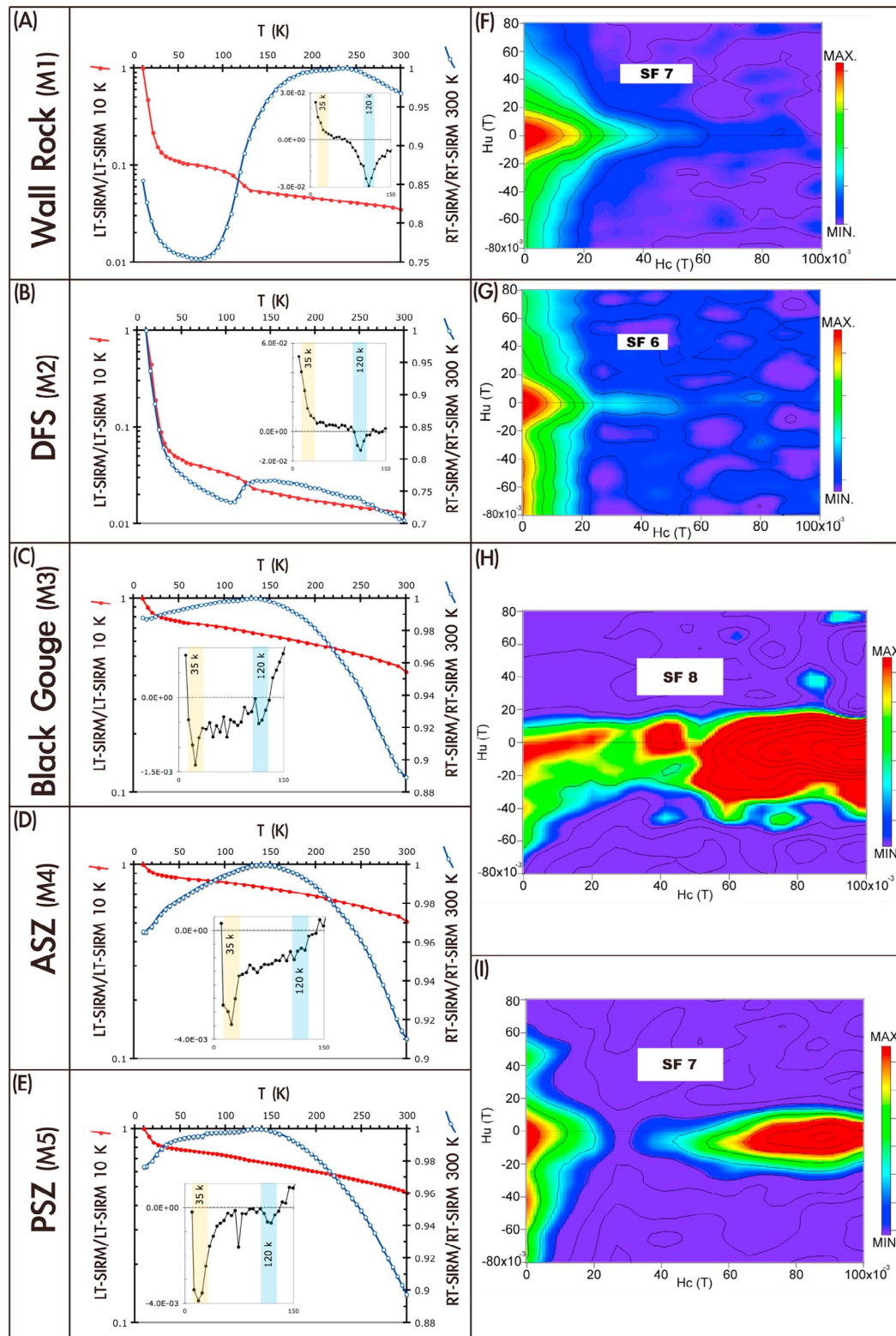


**Figure 5.** Low temperature magnetic measurements (inset: relative values of RT-SIRM) from 10 to 300 K and FORC diagrams. (a) Wall rock sample (M1 in Figure 2a). (b) Deformed sediment sample (M2 in Figure 2c). (c) Gouge sample (M3 in Figure 2c). (d) ASZ sample (M4 in Figure 2c). (e) PSZ sample (M5 in Figure 2c). (f) FORC diagram for wall rock sample (field 0–100 mT). (g) FORC diagram for deformed sediment sample (field 0–100 mT). (h and i) FORC diagrams for samples from fault gouge (field 0–100 mT).



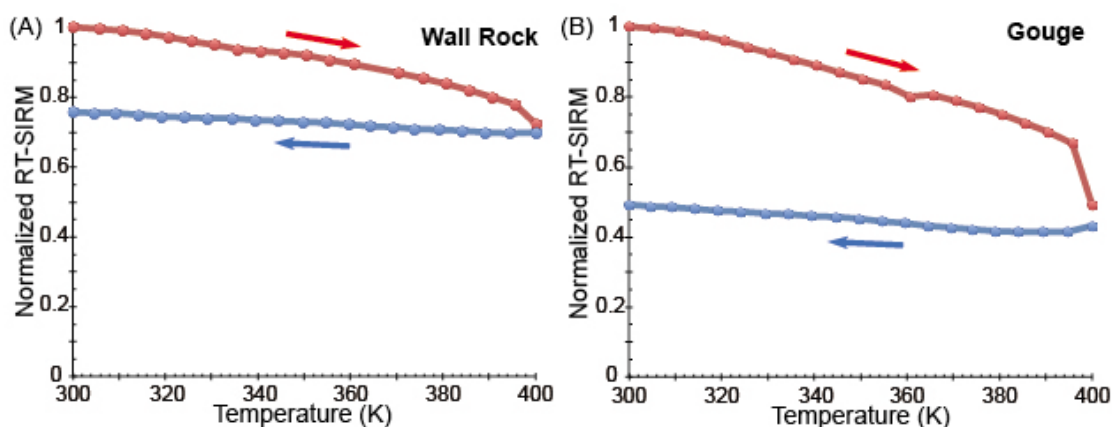


**Figure 6.** Warming-cooling RT-SIRM cycle from 300 to 400 K (127°C), which is close to the Néel temperature of goethite (120°C). (a) For a wall rock sample, less than 25% of the RT-SIRM is lost at 400 K. (b) For a gouge sample, about ~50% of the RT-SIRM is lost at 400 K. This indicates neoformation of a significant concentration of goethite in the fault gouge.

90 mT is consistent with the presence of magnetically interacting pyrrhotite [Wehland *et al.*, 2005; Roberts *et al.*, 2006]. Although goethite is identified using low-temperature remanence properties, we did not observe evidence of high-coercivities up to 500 mT in the FORC diagrams (data are not shown). We infer that the coercivity of this goethite is too high to contribute to the FORC distribution. Rochette *et al.* [2005] showed that natural goethite may not saturate even at fields up to 57 T.

## 5. Discussion

### 5.1. Iron Sulfides

[17] Iron sulfide minerals are common in organic matter rich sedimentary rocks [Reimer, 1984; Tribouillard *et al.*, 2002; MacLean *et al.*, 2008]. This is particularly true within Plio-Pleistocene sediments from Taiwan [Hornig *et al.*, 1992, 1998; Jiang *et al.*, 2001] and within the Chinshui Formation, as confirmed by our observations. In these sediments, the iron sulfides typically form as framboids (Figures 3a, 3b, and 4a), but they can also appear as individual euhedral crystals. TXM inspection indicates that the framboids are not randomly scattered but are grouped as packs of tens of framboids in the sediments (Figures 3a, 3b, and 4a). SEM observations coupled with EDS analyses indicate that the framboids consist essentially of pyrite aggregates. However, small framboids ( $<0.1 \mu\text{m}$ ) have an 'FeS' composition, and are likely greigite ( $\text{Fe}_3\text{S}_4$ ). Greigite often forms during early [Rowan *et al.*, 2009] or late [Roberts and Weaver, 2005] diagenesis and is probably preserved in the

unmetamorphosed Chinshui Formation. In deformed sediments, the only form of alteration of pyrite that we observed is the development of shear planes (Figure 3b). This is the first type of alteration of framboids that we detected in the deformed sediments. In the gouge, all micro-scale observations confirm the absence of well-preserved framboids.

[18] The pyrite content decreases drastically from the host sediments to the gouge. Hirono *et al.* [2007b] and Ishikawa *et al.* [2008] reported an

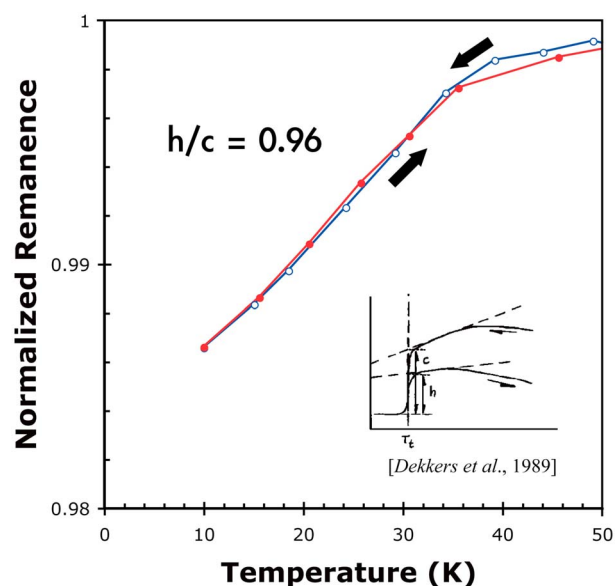


**Figure 7.** Cooling-warming RT-SIRM cycle from 10 to 50 K. A reversible magnetic transition at 35 K for the PSZ sample indicates that pyrrhotite is fine-grained and close to  $1 \mu\text{m}$  in size ( $h/c$  ratio = 0.96) [see Dekkers *et al.*, 1989].

enhanced abundance of  $\text{SO}_4^{2-}$  in the gouge zone and related it to pyrite dissolution. Pyrite dissolution would release sulfate and would lower the pH of the immediately surrounding sediment [Roberts and Weaver, 2005]. Low pH conditions in turn would favor dissolution of carbonate minerals. This could be an alternative explanation for the low inorganic carbon content in the gouge [Hirono et al., 2008; Hamada et al., 2009; Mishima et al., 2009].

[19] Hirono et al. [2008] reported a lack of pyrite in the gouge based on X-ray diffraction spectroscopy. Our observations contradict this view. In the gouge, we observe: 1) unusual small framboids ( $<25 \mu\text{m}$ ) with  $\text{FeS}_2$  as a rim and  $\text{FeS}$  as a core (Figure 3c), 2) detrital pyrite with irregular shapes (Figures 3d and 3f), and 3) individual  $<2 \mu\text{m}$  pyrite grains (Figure 3g). Individual pyrite grains are observed within the whole gouge, including the Chi-Chi PSZ (Figures 3e–3h). However, framboids have not been observed in the Chi-Chi PSZ.

[20] For the first time, we identified pyrrhotite in the gouge. This is based on the drop in remanence at  $\sim 35 \text{ K}$  in the RT-SIRM demagnetization curves (Figure 7) which is a diagnostic signature of  $>1 \mu\text{m}$  pyrrhotite [Dekkers et al., 1989; Rochette et al., 1990]. The quasi-reversible path of the pyrrhotite transition indicates that the size of pyrrhotite grains is close to  $1 \mu\text{m}$  [Dekkers et al., 1989]. The distribution of coercivities around  $\sim 90 \text{ mT}$  (Figures 5h and 5i) suggests that strongly interacting pyrrhotite dominates the magnetic assemblage of the gouge [Wehland et al., 2005; Roberts et al., 2006]. Our magnetic observations along with SEM observations reveal the occurrence of unusual framboids with rims of  $\text{FeS}_2$  (pyrite) and cores of  $\text{FeS}$  (Figure 3c). The  $\text{FeS}$  phase included in framboids is likely pyrrhotite, which is detected magnetically, because it has grain sizes between  $0.5$  and  $1 \mu\text{m}$  and is not cubic (Figure 3c). In addition, the strong magnetic interactions suggested by FORC diagrams can be explained by the tight grouping of pyrrhotite minerals enclosed in framboids. We never detected coarser  $>1 \mu\text{m}$  pyrrhotite in the Chinshui siltstones. Additional low-temperature magnetic experiments performed by Humbert et al. [2012] confirm our observations. We therefore argue that the coarser  $>1 \mu\text{m}$  pyrrhotite is not derived from the host rocks and that it was neoformed in the fault gouge.

[21] The preservation of iron sulfides like pyrite and the neoformation of pyrrhotite in the fault gouge are consistent with several observations. First, iron

sulfide neoformation attests to a reducing environment in the gouge. This is in agreement with geochemical observations in the gouge from FZB1136 [Ishikawa et al., 2008]. Second, the association of pyrite and pyrrhotite may imply heating and cooling during co-seismic and post-seismic processes. We assume that pyrrhotite formation is related to alteration of pyrite grains. Chin et al. [2005] observed that mechanical milling of pyrite under  $\text{CO}_2$ -rich conditions triggered pyrrhotite formation. This process is feasible in a gouge where milling is a common process. However, we infer the presence of large pyrrhotite grains ( $\sim 1 \mu\text{m}$ ) grains in the FZB1136 gouge, which is supported by direct observations of framboid relics that have not been completely crushed (Figure 3c). Therefore, we conclude that an additional process occurred. Wang et al. [2008] demonstrated that oxidation of pyrite to pyrrhotite or hematite can occur during short-term exposure to temperatures up to  $700^\circ\text{C}$  (heating rate:  $11^\circ\text{C}/\text{minute}$ ). With a similar heating rate, Bhargava et al. [2009] observed that heating of pyrite yields pyrrhotite at  $500^\circ\text{C}$  under inert conditions (pure  $\text{N}_2$  or  $\text{Ar}$  gas). This is consistent with the heating experiments of Mayoral et al. [2002] at  $500^\circ\text{C}$  with a higher heating rate ( $80^\circ\text{C}/\text{minute}$ ). When extrapolating these experimental results to our study, we suggest that elevated temperatures of  $>500^\circ\text{C}$  in the gouge triggered pyrrhotite formation at the expense of pyrite. The gouge is a stack of numerous slip zones, and within each slip zone elevated temperatures are likely due to frictional processes [Boullier et al., 2009]. Even if there is no evidence of melting in the FZB1136 gouge [Hirono et al., 2008; Boullier et al., 2009], temperatures above  $500^\circ\text{C}$  are nevertheless possible in parts of the gouge, including the 1999 Chi-Chi PSZ. Therefore, we suggest that pyrrhotite formed at temperatures  $>500^\circ\text{C}$  associated with repeated earthquakes.

[22] A temperature above  $350^\circ\text{C}$  in the gouge has been proposed by several authors, based on geochemistry [Ishikawa et al., 2008], carbonate alteration [Hirono et al., 2008], vaporization of water during thermal pressurization [Boullier et al., 2009], and formation of magnetic minerals [Hirono et al., 2006; Tanikawa et al., 2008; Mishima et al., 2009]. Ishikawa et al. [2008] suggested that the chemical characteristics of the gouge were produced by interaction with co-seismic aqueous fluids derived from sediment pore waters with temperatures up to  $350^\circ\text{C}$ . We calculated Eh-pH diagrams using the Geochemist's Workbench software and considered the stability of pyrite and

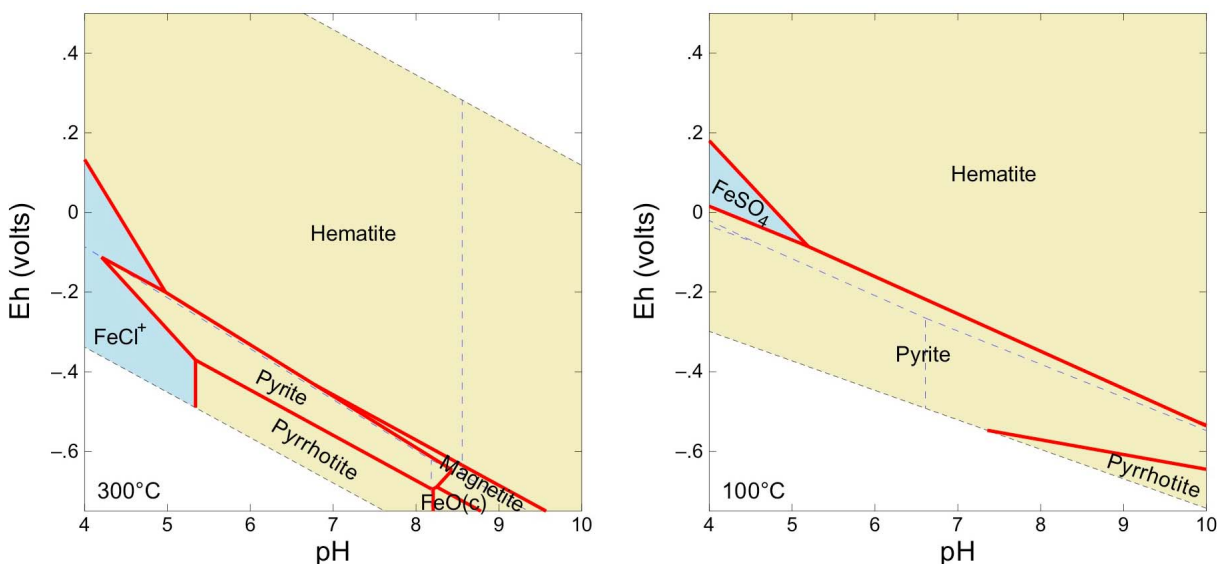


**Figure 8.** Eh-pH diagrams for fluid temperatures of 300°C and 100°C. The model parameters are:  $a_{\text{SO}_4^{2-}} = 10^{-2}$ ,  $a_{\text{Cl}^-} = 10^{-2}$ ,  $a_{\text{Fe}^{2+}} = 10^{-4}$  (higher iron concentration). The pressure used is 30 MPa, which is equivalent to lithostatic pressure at a depth of 1,100 m. Note that at higher temperatures the pyrrhotite field exists at strong reducing conditions in a pH range of 5.3–8.2. As temperature decreases, the pyrite field expands and pyrrhotite alters to pyrite.

pyrrhotite in an aqueous fluid within the gouge (Figure 8). The pyrite stability field increases from 300 to 100°C at lower Eh conditions. The gouge appears to have formed under anoxic conditions based on microbial observations at 1,000 m depth in TCDP core Hole A [Wang *et al.*, 2007]. We suggest that pyrite formed as a result of retrograde metamorphism. The presence of pyrite rims on pyrrhotite cores in the framboids (Figure 3c) supports the retrograde metamorphism hypothesis. Only pyrrhotite on the surface of framboids will be affected by retrograde metamorphism, and the core of pyrrhotite will be preserved. If correct, this suggests that most pyrite in the gouge (Figures 3e–3h) resulted from retrograde metamorphism during cooling of co-seismic fluids from above 350°C.

## 5.2. Magnetite

[23] Magnetite is present in the Chinshui Formation, and recognition of the Verwey transition (~120 K; Figure 5a) implies the occurrence of stoichiometric magnetite with a maximum concentration of 100 ppmv. Mishima *et al.* [2009] also reported a low concentration of magnetite in the Chinshui siltstones. The marked ~35 K magnetic transition observed from ZFC demagnetization curves (Figure 5), also observed by Mishima *et al.* [2009], could be explained by superparamagnetic (SP) grains, monoclinic pyrrhotite, siderite ( $\text{FeCO}_3$ ), and rhodochrosite ( $\text{MnCO}_3$ ) [Housen

*et al.*, 1996; Kars *et al.*, 2011]. It is well known that magnetite nanoparticles carry a remanence at low temperature (typically 10 K), and that they lose this remanence on warming [Hunt *et al.*, 1995]. Mishima *et al.* [2009] attributed this 35 K transition to SP grains in the Chinshui Formation. Although we agree with Mishima *et al.* [2009], from the same samples we observed development of a magnetic transition with a break-in-slope at ~35 K on RT-SIRM demagnetization curves (Figure 5). Aubourg and Pozzi [2010] and Kars *et al.* [2011] observed the same behavior in unmetamorphosed claystones. They proposed that this magnetic transition, referred to as P-behavior, is due to a combination of a fine-grained pyrrhotite transition and an induced magnetization of unknown origin. We support this interpretation because of the strong similarity of low-temperature demagnetization curves (ZFC, RT-SIRM) of Chinshui Formation sedimentary rocks with those reported by Aubourg and Pozzi [2010] and Kars *et al.* [2011]. If correct, the presence of stoichiometric fine-grained magnetite and fine-grained pyrrhotite of the Chinshui Formation is diagnostic of modest burial below 5 km [Aubourg and Pozzi, 2010; Abdelmalak *et al.*, 2012]. This is consistent with a burial temperature of about 120°C, inferred from vitrinite reflectance data ( $R_0 \sim 0.8\%$ ) [Sakaguchi *et al.*, 2007].

[24] The magnetic properties of gouge differ from those of the host sediments. In particular, we

observe a weakening of the Verwey transition (Figures 5c–5e), which suggests that magnetite is partially oxidized [Özdemir *et al.*, 1993; Cui *et al.*, 1994; Özdemir *et al.*, 2002]. The presence of co-seismic hot fluids in the gouge [Ishikawa *et al.*, 2008] constitutes a possible explanation for the partial alteration of magnetite, where magnetite could be oxidized to maghemite thereby causing weakening of the Verwey transition [Özdemir *et al.*, 1993; Cui *et al.*, 1994; Özdemir *et al.*, 2002]. The absence of a large remanence drop between 10 K and 40 K in the ZFC demagnetization curves (Figures 5a and 5b) implies that the grain size fraction of magnetite is essentially above the SP threshold size ( $\sim 20$  nm). Paradoxically, ultrafine-grained magnetic minerals present in the Chinshui Formation do not exist in the gouge, where grain size reduction by a milling process is likely. We interpret that the ultrafine fraction is altered chemically during repeated earthquakes. Aubourg and Pozzi [2010] showed that moderate heating up to 250°C promotes drastic reduction of the 35 K magnetic transition. We suggest, therefore, that the increased temperature in the gouge alters the ultrafine-grained fraction of magnetic minerals.

[25] A fraction of magnetite could have been inherited from the Chinshui Formation. However, detrital magnetite is probably unlikely in sediments that have been extensively pyritized [Rowan *et al.*, 2009]. Magnetite can form at elevated temperatures, by precipitation from frictional melts as observed in natural pseudotachylites [Ferré *et al.*, 2005, 2012] or in experimental pseudotachylites [Nakamura *et al.*, 2002]. Similar to pyrrhotite, we suggest that some magnetite formed during repeated earthquakes within the gouge.

### 5.3. Goethite

[26] The evolution of remanence on heating and cooling (Figures 5c–5e) also suggests the occurrence of goethite ( $\alpha$ -FeOOH) in the gouge. Recognition of goethite is important because it demonstrates the presence of fluid in the gouge. In a companion paper, we provided additional evidence for the occurrence of goethite [Chou *et al.*, 2012] and showed that the natural remanent magnetization in the gouge is carried essentially by goethite. We suggest that this magnetization record is contemporaneous with the 1999 Chi-Chi event. TXM tomography identified scattered 5  $\mu$ m goethite grains within the gouge. The remanence and TXM observations led Chou *et al.* [2012] to propose that goethite formed from cooling of co-seismic fluids within the gouge. Low pH conditions associated with pyrite alteration would

favor goethite formation [Schwertmann and Murad, 1983; Murad and Rojik, 2003]. In addition, Nakamura and Nagahama [2001] also observed 5  $\mu$ m goethite in the Nojima fault gouge from Japan. We therefore suggest that study of goethite in fault gouge is important to detect evidence of co-seismic fluids and could be an indicator of thermal pressurization.

### 5.4. Implications for Identification of Earthquake Slip Zones

[27] In sediment-derived fault gouge, endothermic dehydration reactions and the phase change from liquid water to steam can efficiently buffer the temperature within a fault [Brantut *et al.*, 2011]. This is consistent with the scarcity of melts in sediment-derived fault gouge, as was observed in the FZB1136 gouge [Boullier *et al.*, 2009]. Generally, recognition of clay-clast aggregates (CCA) [Boullier *et al.*, 2009] is good evidence of thermal pressurization processes, and, in turn, as a signature of earthquakes [Boutareaud *et al.*, 2008]. Identification of neoformed minerals can be an alternative indicator of limited temperature elevation and fluid interaction. In this regard, we suggest that at the time of pyrrhotite formation in the FZB1136 gouge, this implies a temperature above 500°C. Similarly, we suggest that goethite formation is an indication of thermal pressurization processes. In fold-and-thrust belts, thrusts similar to the Chelungpu fault are common and likely developed within clay-rich rocks. If pyrrhotite and goethite exist in the gouge, and not in the host rocks, then it can be inferred that temperature enhancement took place and that fluids infiltrated the gouge.

## 6. Conclusions

[28] The 16-cm-thick gouge zone intersected in the TCDP drill holes is a product of repeated earthquakes, including the Chi-Chi earthquake ( $M_w$  7.6, 1999), and has had a complex mechanical and thermal history. The wall rocks are made up of the Chinshui Formation, which contains several percent pyrite. The magnetic mineral assemblage of this formation is typical of unmetamorphosed sediments and consists essentially of nanometric stoichiometric magnetite. Micro-scale observations indicate that the concentration of pyrite framboids decreases considerably from the wall rock into the gouge. Pyrite alteration would cause a lowering of pH, and, in turn, would promote carbonate mineral dissolution. Beside pyrite alteration, we identify for the first time the occurrence of micrometric pyrrhotite in the



fault gouge. The pyrrhotite likely formed at high temperatures ( $>500^{\circ}\text{C}$ ) at the expense of pyrite. Magnetite, which is also present in the gouge, is partially altered. We propose that pyrrhotite and some of the magnetite formed at elevated temperatures during frictional heating along the slip zones. The total concentration of pyrrhotite and magnetite is therefore a result of numerous earthquakes. In the gouge, we also identify neoformed goethite, which implies the presence of hot fluids ( $>350^{\circ}\text{C}$ ). On cooling, these hot fluids altered pyrrhotite into pyrite and magnetite into partially altered magnetite. Our results demonstrate that characterization of magnetic minerals provides a useful means of studying earthquake processes in faults.

## Acknowledgments

[29] We thank the working group of TCDP for core drilling. The National Science Council of Taiwan under grants NSC 95-2745-M-002-001, NSC 96-2627-M-002-011 and NSC 97-2627-M-213-001 with a TEC contribution number supported this research. Yu-Min Chou was supported by an Eiffel excellence scholarship program (EGIDE, France) and the Graduate Student Study Abroad Program (NSC, Taiwan). We thank Guang-Chian Yin of NSRRC for maintenance of the TXM and Keng S. Liang of NSRRC for supporting this project. The MPMS XL5 EverCool used in this study was financed by the Conseil Régional d'Ile-de-France (I-06-206/R), INSU-CNRS, IPGP, and ANR. We also thank Christophe Nevado (Geosciences Montpellier) for making polished thin sections of difficult gouge material, and Olivier Romeyer (Plate-Forme d'Analyse Structurale, Université de Savoie at Chambéry) for his technical assistance when using the SEM. L.-W. Kuo, P. Robion, C. David, L. Louis, and F. Humbert are thanked for constructive discussions. This paper benefited from constructive reviews by A. P. Roberts and J. W. Geissman.

## References

- Abdelmalak, M. M., C. Aubourg, L. Geoffroy, and F. Laggoun-Defarge (2012), A new oil window indicator? The magnetic assemblage of claystones from the Baffin Bay volcanic margin (Greenland), *AAPG Bull.*, **96**, 205–215, doi:10.1306/07121111008.
- Aubourg, C., and J.-P. Pozzi (2010), Toward a new  $<250^{\circ}\text{C}$  pyrrhotite-magnetite geothermometer for claystones, *Earth Planet. Sci. Lett.*, **294**, 47–57, doi:10.1016/j.epsl.2010.02.045.
- Berner, R. A. (1984), Sedimentary pyrite formation: An update, *Geochim. Cosmochim. Acta*, **48**, 605–615, doi:10.1016/0016-7037(84)90089-9.
- Bhargava, S. K., A. Garg, and N. D. Subasinghe (2009), In situ high-temperature phase transformation studies on pyrite, *Fuel*, **88**(6), 988–993, doi:10.1016/j.fuel.2008.12.005.
- Boullier, A.-M., E.-C. Yeh, S. Boutareaud, S.-R. Song, and C.-H. Tsai (2009), Microscale anatomy of the 1999 Chi-Chi earthquake fault zone, *Geochem. Geophys. Geosyst.*, **10**, Q03016, doi:10.1029/2008GC002252.
- Boutareaud, S. B., D.-G. Calugaru, R. Han, O. Fabbri, K. Mizoguchi, A. Tsutsumi, and T. Shimamoto (2008), Clay-clast aggregates: A new textural evidence for seismic fault sliding?, *Geophys. Res. Lett.*, **35**, L05302, doi:10.1029/2007GL032554.
- Brantut, N., R. Han, T. Shimamoto, N. Findling, and A. Schubnel (2011), Fast slip with inhibited temperature rise due to mineral dehydration: Evidence from experiments on gypsum, *Geology*, **39**, 59–62, doi:10.1130/g31424.1.
- Chen, Y.-G., W.-S. Chen, Y. Wang, P.-W. Lo, J.-C. Lee, and T.-K. Liu (2002), Geomorphic evidence for prior earthquakes: Lesson from the 1999 Chichi earthquake in central Taiwan, *Geology*, **30**, 171–174, doi:10.1130/0091-7613(2002)030<0171:GEFPEL>2.0.CO;2.
- Chin, P. P., J. Ding, J. B. Yi, and B. H. Liu (2005), Synthesis of  $\text{FeS}_2$  and  $\text{FeS}$  nanoparticles by high-energy mechanical milling and mechanochemical processing, *J. Alloys Compd.*, **390**, 255–260, doi:10.1016/j.jallcom.2004.07.053.
- Chou, Y.-M., S.-R. Song, C. Aubourg, T.-Q. Lee, A.-M. Boullier, Y.-F. Song, E.-C. Yeh, L.-W. Kuo, and C.-Y. Wang (2012), An earthquake slip zone is a magnetic recorder, *Geology*, **40**, 551–554, doi:10.1130/G32864.1.
- Craig, J. R., F. M. Vokes, and T. N. Solberg (1998), Pyrite: Physical and chemical textures, *Miner. Deposita*, **34**, 82–101, doi:10.1007/s001260050187.
- Cui, Y., K. L. Verosub, and A. P. Roberts (1994), The effect of low temperature oxidation on large multi-domain magnetite, *Geophys. Res. Lett.*, **21**, 757–760, doi:10.1029/94GL00639.
- Dekkers, M. J. (1989), Magnetic properties of natural goethite—II. TRM behaviour during thermal and alternating field demagnetization and low-temperature treatment, *Geophys. J. Int.*, **97**, 341–355, doi:10.1111/j.1365-246X.1989.tb00505.x.
- Dekkers, M. J., J. L. Mattéi, G. Fillion, and P. Rochette (1989), Grain-size dependence of the magnetic behavior of pyrrhotite during its low-temperature transition at 34 K, *Geophys. Res. Lett.*, **16**, 855–858, doi:10.1029/GL016i008p00855.
- Ferré, E. C., M. S. Zechmeister, J. W. Geissman, N. Mathana-Sekaran, and K. Kocak (2005), The origin of high magnetic remanence in fault pseudotachylites: Theoretical considerations and implication for coseismic electrical currents, *Tectonophysics*, **402**, 125–139, doi:10.1016/j.tecto.2005.01.008.
- Ferré, E. C., J. W. Geissman, and M. S. Zechmeister (2012), Magnetic properties of fault pseudotachylites in granites, *J. Geophys. Res.*, **117**, B01106, doi:10.1029/2011JB008762.
- Fukuchi, T., K. Mizoguchi, and T. Shimamoto (2005), Ferromagnetic resonance signal produced by frictional heating: A new indicator of paleoseismicity, *J. Geophys. Res.*, **110**, B12404, doi:10.1029/2004JB003485.
- Hamada, Y., T. Hirono, W. Tanikawa, W. Soh, and S.-R. Song (2009), Energy taken up by co-seismic chemical reactions during a large earthquake: An example from the 1999 Taiwan Chi-Chi earthquake, *Geophys. Res. Lett.*, **36**, L06301, doi:10.1029/2008GL036772.
- Harrison, R. J., and J. M. Feinberg (2008), FORCinel: An improved algorithm for calculating first-order reversal curve distributions using locally weighted regression smoothing, *Geochem. Geophys. Geosyst.*, **9**, Q05016, doi:10.1029/2008GC001987.
- Hirono, T., et al. (2006), High magnetic susceptibility of fault gouge within Taiwan Chelungpu fault: Nondestructive continuous measurements of physical and chemical properties in fault rocks recovered from Hole B, TCDP, *Geophys. Res. Lett.*, **33**, L19311, doi:10.1029/2006GL027329.

- Hirono, T., et al. (2007a), Nondestructive continuous physical property measurements of core samples recovered from hole B, Taiwan Chelungpu-Fault Drilling Project, *J. Geophys. Res.*, **112**, B07404, doi:10.1029/2006JB004738.
- Hirono, T., et al. (2007b), A chemical kinetic approach to estimate dynamic shear stress during the 1999 Taiwan Chi-Chi earthquake, *Geophys. Res. Lett.*, **34**, L19308, doi:10.1029/2007GL030743.
- Hirono, H., et al. (2008), Characterization of slip zone associated with the 1999 Taiwan Chi-Chi earthquake: X-ray CT image analyses and microstructural observations of the Taiwan Chelungpu fault, *Tectonophysics*, **449**, 63–84, doi:10.1016/j.tecto.2007.12.002.
- Horng, C.-S., C. Laj, T.-Q. Lee, and J.-C. Chen (1992), Magnetic characteristics of sedimentary rocks from the Tsengwen-chi and Erhjen-chi sections in southwestern Taiwan, *Terr. Atmos. Oceanic Sci.*, **3**, 519–532.
- Horng, C.-S., M. Torii, K.-S. Shea, and S.-J. Kao (1998), Inconsistent magnetic polarities between greigite- and pyrrhotite/magnetite-bearing marine sediments from the Tsailiao-chi section, southwestern Taiwan, *Earth Planet. Sci. Lett.*, **164**, 467–481, doi:10.1016/S0012-821X(98)00239-8.
- Housen, B. A., S. K. Banerjee, and B. M. Moskowitz (1996), Low-temperature magnetic properties of siderite and magnetite in marine sediments, *Geophys. Res. Lett.*, **23**, 2843–2846, doi:10.1029/96GL01197.
- Humbert, F., P. Robion, L. Louis, D. L. Bartier, B. A. Ledéser, and S.-R. Song (2012), Magnetic inference of in situ open microcracks in sandstone samples from the Taiwan Chelungpu Fault Drilling Project (TCDP), *J. Asian Earth Sci.*, **45**, 179–189, doi:10.1016/j.jseae.2011.10.009.
- Hunt, C. P., S. K. Banerjee, J. Han, P. A. Solheld, E. Oches, W.-W. Sun, and T. Liu (1995), Rock-magnetic proxies of climate change in the loess-palaeosol sequences of the western Loess Plateau of China, *Geophys. J. Int.*, **123**, 232–244, doi:10.1111/j.1365-246X.1995.tb06672.x.
- Ikehara, M., et al. (2007), Low total and inorganic carbon contents within the Taiwan Chelungpu fault system, *Geochem. J.*, **41**, 391–396, doi:10.2343/geochemj.41.391.
- Isaacs, A. J., J. P. Evans, S.-R. Song, and P. T. Kolesar (2007), Structural, mineralogical, and geochemical characterization of the Chelungpu thrust fault, Taiwan, *Terr. Atmos. Oceanic Sci.*, **18**, 183–221, doi:10.3319/TAO.2007.18.2.183(TCDP).
- Ishikawa, T., et al. (2008), Coseismic fluid-rock interactions at high temperatures in the Chelungpu fault, *Nat. Geosci.*, **1**, 679–683, doi:10.1038/ngeo308.
- Jiang, W.-T., C.-S. Horng, A. P. Roberts, and D. R. Peacor (2001), Contradictory magnetic polarities in sediments and variable timing of neoformation of authigenic greigite, *Earth Planet. Sci. Lett.*, **193**, 1–12, doi:10.1016/S0012-821X(01)00497-6.
- Jovanović, D. (1989), Kinetics of thermal decomposition of pyrite in an inert atmosphere, *J. Therm. Anal. Calorim.*, **35**, 1483–1492, doi:10.1007/BF01912925.
- Kano, Y., J. Mori, R. Fujio, H. Ito, T. Yanagidani, S. Nakao, and K.-F. Ma (2006), Heat signature on the Chelungpu fault associated with the 1999 Chi-Chi, Taiwan earthquake, *Geophys. Res. Lett.*, **33**, L14306, doi:10.1029/2006GL026733.
- Kao, H., and W.-P. Chen (2000), The Chi-Chi earthquake sequence: Active, out-of-sequence thrust faulting in Taiwan, *Science*, **288**, 2346–2349, doi:10.1126/science.288.5475.2346.
- Kars, M., C. Aubourg, and J.-P. Pozzi (2011), Low temperature magnetic behaviour near 35 K in unmetamorphosed claystones, *Geophys. J. Int.*, **186**, 1029–1035, doi:10.1111/j.1365-246X.2011.05121.x.
- Kuo, L.-W., S.-R. Song, E.-C. Yeh, and H.-F. Chen (2009), Clay mineral anomalies in the fault zone of the Chelungpu Fault, Taiwan, and their implications, *Geophys. Res. Lett.*, **36**, L18306, doi:10.1029/2009GL039269.
- Lambert, J., G. Simkovich, and P. Walker (1998), The kinetics and mechanism of the pyrite-to-pyrrhotite transformation, *Metall. Mater. Trans. B*, **29**, 385–396, doi:10.1007/s11663-998-0115-x.
- Liu, Q., Y. Yu, J. Torrent, A. P. Roberts, Y. Pan, and R. Zhu (2006), Characteristic low-temperature magnetic properties of aluminous goethite [ $\alpha$ -(Fe, Al)OOH] explained, *J. Geophys. Res.*, **111**, B12S34, doi:10.1029/2006JB004560.
- Liu, Y., and Q. Liu (2004), Flotation separation of carbonate from sulfide minerals, I: Flotation of single minerals and mineral mixtures, *Miner. Eng.*, **17**, 855–863, doi:10.1016/j.mineng.2004.03.006.
- Ma, K.-F., C.-T. Lee, Y.-B. Tsai, T.-C. Shin, and J. Mori (1999), The Chi-Chi, Taiwan earthquake: Large surface displacements on an inland thrust fault, *Eos Trans. AGU*, **80**(50), 605, doi:10.1029/99EO00405.
- Ma, K.-F., E. E. Brodsky, J. Mori, C. Ji, T.-R. A. Song, and H. Kanamori (2003), Evidence for fault lubrication during the 1999 Chi-Chi, Taiwan, earthquake (Mw7.6), *Geophys. Res. Lett.*, **30**(5), 1244, doi:10.1029/2002GL015380.
- Ma, K.-F., et al. (2006), Slip zone and energetics of a large earthquake from the Taiwan Chelungpu-fault Drilling Project, *Nature*, **444**, 473–476, doi:10.1038/nature05253.
- MacLean, L. C. W., T. Tylliszczak, P. U. P. A. Gilbert, D. Zhou, T. J. Pray, T. C. Onstott, and G. Southam (2008), A high-resolution chemical and structural study of framboidal pyrite formed within a low-temperature bacterial biofilm, *Geobiology*, **6**, 471–480, doi:10.1111/j.1472-4669.2008.00174.x.
- Maher, B. A., R. Thompson, and M. W. Hounslow (1999), Introduction, in *Quaternary Climates, Environments and Magnetism*, edited by B. A. Maher and R. Thompson, pp. 1–48, Cambridge Univ. Press, Cambridge, U. K.
- Mayoral, M. C., M. T. Izquierdo, J. M. Andrés, and B. Rubio (2002), Mechanism of interaction of pyrite with hematite as simulation of slagging and fireside tube wastage in coal combustion, *Thermochim. Acta*, **390**, 103–111, doi:10.1016/S0040-6031(02)00075-8.
- Mishima, T., T. Hirono, N. Nakamura, W. Tanikawa, W. Soh, and S.-R. Song (2009), Changes to magnetic minerals caused by frictional heating during the 1999 Taiwan Chi-Chi earthquake, *Earth Planets Space*, **61**, 797–801.
- Murad, E., and P. Rojik (2003), Iron-rich precipitates in a mine drainage environment: Influence of pH on mineralogy, *Am. Mineral.*, **88**, 1915–1918.
- Music, S., S. Popović, and M. Ristić (1992), Thermal decomposition of pyrite, *J. Radioanal. Nucl. Chem.*, **162**, 217–226, doi:10.1007/BF02035382.
- Nakamura, N., and H. Nagahama (2001), Changes in magnetic and fractal properties of fractured granites near the Nojima Fault, Japan, *Isl. Arc*, **10**, 486–494, doi:10.1046/j.1440-1738.2001.00347.x.
- Nakamura, N., T. Hirose, and G. J. Borradaile (2002), Laboratory verification of submicron magnetite production in pseudotachylytes: Relevance for paleointensity studies, *Earth Planet. Sci. Lett.*, **201**, 13–18, doi:10.1016/S0012-821X(02)00704-5.
- Özdemir, Ö., and D. J. Dunlop (1996), Thermoremanence and Néel temperature of goethite, *Geophys. Res. Lett.*, **23**, 921–924, doi:10.1029/96GL00904.

- Özdemir, Ö., and D. J. Dunlop (1999), Low-temperature properties of a single crystal of magnetite oriented along principal magnetic axes, *Earth Planet. Sci. Lett.*, **165**, 229–239, doi:10.1016/S0012-821X(98)00269-6.
- Özdemir, Ö., D. J. Dunlop, and B. M. Moskowitz (1993), The effect of oxidation on the Verwey transition in magnetite, *Geophys. Res. Lett.*, **20**, 1671–1674, doi:10.1029/93GL01483.
- Özdemir, Ö., D. J. Dunlop, and B. M. Moskowitz (2002), Changes in remanence, coercivity and domain state at low temperature in magnetite, *Earth Planet. Sci. Lett.*, **194**, 343–358, doi:10.1016/S0012-821X(01)00562-3.
- Pelovski, Y., and V. Petkova (1999), Investigation on thermal decomposition of pyrite part I, *J. Therm. Anal. Calorim.*, **56**, 95–99, doi:10.1023/A:1010135425009.
- Pike, C. R., A. P. Roberts, and K. L. Verosub (1999), Characterizing interactions in fine magnetic particle systems using first order reversal curves, *J. Appl. Phys.*, **85**, 6660–6667, doi:10.1063/1.370176.
- Pike, C. R., A. P. Roberts, and K. L. Verosub (2001), First-order reversal curve diagrams and thermal relaxation effects in magnetic particles, *Geophys. J. Int.*, **145**, 721–730, doi:10.1046/j.0956-540x.2001.01419.x.
- Reimer, T. O. (1984), Graphite in Precambrian rocks of southern Africa: Implications on the carbon content of metamorphic rocks, *Precambrian Res.*, **26**, 223–234, doi:10.1016/0301-9268(84)90002-0.
- Roberts, A. P., and R. Weaver (2005), Multiple mechanisms of remagnetization involving sedimentary greigite (Fe<sub>3</sub>S<sub>4</sub>), *Earth Planet. Sci. Lett.*, **231**, 263–277, doi:10.1016/j.epsl.2004.11.024.
- Roberts, A. P., C. R. Pike, and K. L. Verosub (2000), First-order reversal curve diagrams: A new tool for characterizing the magnetic properties of natural samples, *J. Geophys. Res.*, **105**, 28,461–28,475, doi:10.1029/2000JB900326.
- Roberts, A. P., Q. Liu, C. J. Rowan, L. Chang, C. Carvallo, J. Torrent, and C.-S. Horng (2006), Characterization of hematite ( $\alpha$ -Fe<sub>2</sub>O<sub>3</sub>), goethite ( $\alpha$ -FeOOH), greigite (Fe<sub>3</sub>S<sub>4</sub>), and pyrrhotite (Fe<sub>7</sub>S<sub>8</sub>) using first-order reversal curve diagrams, *J. Geophys. Res.*, **111**, B12S35, doi:10.1029/2006JB004715.
- Rochette, P., G. Fillion, J.-L. Mattéi, and M. J. Dekkers (1990), Magnetic transition at 30–34 Kelvin in pyrrhotite: Insight into a widespread occurrence of this mineral in rocks, *Earth Planet. Sci. Lett.*, **98**, 319–328, doi:10.1016/0012-821X(90)90034-U.
- Rochette, P., P.-E. Mathé, L. Esteban, H. Rakoto, J.-L. Bouchez, Q. Liu, and J. Torrent (2005), Non-saturation of the defect moment of goethite and fine-grained hematite up to 57 Teslas, *Geophys. Res. Lett.*, **32**, L22309, doi:10.1029/2005GL024196.
- Rowan, C. J., and A. P. Roberts (2006), Magnetite dissolution, diachronous greigite formation, and secondary magnetizations from pyrite oxidation: Unravelling complex magnetizations in Neogene marine sediments from New Zealand, *Earth Planet. Sci. Lett.*, **241**, 119–137, doi:10.1016/j.epsl.2005.10.017.
- Rowan, C. J., A. P. Roberts, and T. Broadbent (2009), Reductive diagenesis, magnetite dissolution, greigite growth and paleomagnetic smoothing in marine sediments: A new view, *Earth Planet. Sci. Lett.*, **277**, 223–235, doi:10.1016/j.epsl.2008.10.016.
- Sakaguchi, A., A. Yanagihara, K. Ujiie, H. Tanaka, and M. Kameyama (2007), Thermal maturity of a fold-thrust belt based on vitrinite reflectance analysis in the Western Foothills complex, western Taiwan, *Tectonophysics*, **443**, 220–232, doi:10.1016/j.tecto.2007.01.017.
- Schwertmann, U., and E. Murad (1983), Effect of pH on the formation of goethite and hematite from ferrihydrite, *Clays Clay Miner.*, **31**, 277–284, doi:10.1346/CCMN.1983.0310405.
- Song, S.-R., L.-W. Kuo, E.-C. Yeh, C.-Y. Wang, J.-H. Hung, and K.-F. Ma (2007a), Characteristics of the lithology, fault-related rocks and fault zone structures in TCDP Hole-A, *Terr. Atmos. Oceanic Sci.*, **18**, 243–269, doi:10.3319/TAO.2007.18.2.243(TCDP).
- Song, Y.-F., et al. (2007b), X-ray beamlines for structural studies at the NSRRC superconducting wavelength shifter, *J. Synchrotron Radiat.*, **14**, 320–325, doi:10.1107/S0909049507021516.
- Tanikawa, W., T. Mishima, T. Hirono, W. Lin, T. Shimamoto, W. Soh, and S.-R. Song (2007), High magnetic susceptibility produced in high-velocity frictional tests on core samples from the Chelungpu fault in Taiwan, *Geophys. Res. Lett.*, **34**, L15304, doi:10.1029/2007GL030783.
- Tanikawa, W., T. Mishima, T. Hirono, W. Soh, and S.-R. Song (2008), High magnetic susceptibility produced by thermal decomposition of core samples from the Chelungpu fault in Taiwan, *Earth Planet. Sci. Lett.*, **272**, 372–381, doi:10.1016/j.epsl.2008.05.002.
- Tribovillard, N., O. Averbuch, A. Bialkowski, and J.-F. Deconinck (2002), Early diagenesis of marine organic-matter and magnetic properties of sedimentary rocks: The role of iron limitation and organic-matter source organisms, *Bull. Soc. Geol. Fr.*, **173**, 295–306, doi:10.2113/173.4.295.
- Wang, L., Y. Pan, J. Li, and H. Qin (2008), Magnetic properties related to thermal treatment of pyrite, *Sci. China, Ser. D*, **51**, 1144–1153, doi:10.1007/s11430-008-0083-7.
- Wang, P.-L., L.-H. Lin, H.-T. Yu, T.-W. Cheng, S.-R. Song, L.-W. Kuo, E.-C. Yeh, W. Lin, and C.-Y. Wang (2007), Cultivation-based characterization of microbial communities associated with deep sedimentary rocks from Taiwan Chelungpu Drilling Project cores, *Terr. Atmos. Oceanic Sci.*, **18**, 395–412, doi:10.3319/TAO.2007.18.2.395(TCDP).
- Wehland, F., A. Stancu, P. Rochette, M. J. Dekkers, and E. Appel (2005), Experimental evaluation of magnetic interaction in pyrrhotite bearing samples, *Phys. Earth Planet. Inter.*, **153**, 181–190, doi:10.1016/j.pepi.2005.05.006.
- Wu, H.-Y., K.-F. Ma, M. Zoback, N. Boness, H. Ito, J.-H. Hung, and S. Hickman (2007), Stress orientations of Taiwan Chelungpu-fault Drilling Project (TCDP) Hole-A as observed from geophysical logs, *Geophys. Res. Lett.*, **34**, L01303, doi:10.1029/2006GL028050.
- Yeh, E.-C., et al. (2007), Core description and characteristics of fault zones from Hole-A of the Taiwan Chelungpu-fault Drilling Project, *Terr. Atmos. Oceanic Sci.*, **18**, 327–357, doi:10.3319/TAO.2007.18.2.327(TCDP).
- Yin, G.-C., Y.-F. Song, M.-T. Tang, F.-R. Chen, K. S. Liang, F. W. Duewer, M. Feser, W. Yun, and H.-P. D. Shieh (2006), 30 nm resolution x-ray imaging at 8 keV using third order diffraction of a zone plate lens objective in a transmission microscope, *Appl. Phys. Lett.*, **89**, 221,122–221,123, doi:10.1063/1.2397483.
- Yue, L.-F., J. Suppe, and J.-H. Hung (2005), Structural geology of a classic thrust belt earthquake: The 1999 Chi-Chi earthquake Taiwan ( $M_w = 7.6$ ), *J. Struct. Geol.*, **27**, 2058–2083, doi:10.1016/j.jsg.2005.05.020.